NTNU
Norwegian University of Science and Technology

Dynamic Load Effects on a Submerged Floating Tube Bridge with emphasis on Vortex-induced Vibrations

Maria Hapnes von Schack

MASTEROPPGAVE VÅREN 2017

Maria Hapnes von Schack

DYNAMISK LASTVIRKNING I RØRBRU
MED SÆRLIG VEKT PÅ EFFEKT AV VORTEXINDUSERTE VIBRASJONER

Dynamic Load Effects on a Submerged Floating Tube Bridge with emphasis on Vortex Induced Vibrations

De tre firmaer Dr. Tech. Olav Olsen AS, Norconsult AS og Reinertsen AS har på oppdrag for Statens vegvesen utviklet et konsept på neddykket rørbru knyttet til veiprosjektet E39. Brua skal krysse over Bjørnafjorden sør for Bergen og vil ha en total lengde på rundt 5000 meter. Den består av to parallelle betongrør i en horisontal bue med radius 6400 meter. Broen ligger med overkant på 30 meter under vannoverflaten for å tillate skipstrafikk over.

Det er utviklet to konsepter, en løsning med strekkstag til bunnen og en med pongtonger i vannlinjen. Oppgaven knyttes til strekkstag-løsningen.

Studenten skal undersøke ulike former for dynamisk lastvirkning i brua, med særlig vekt på effekt fra saktevarierende VIV. Oppgaven omfatter følgende hovedpunkter:

1. Litteraturstudium. Gjennomgang av konseptet som er utviklet og beskrivelse statisk og dynamisk lastvirkning som opptrer. Studenten vil få tilgang på noen prosjektrapporter inklusive Design Basis fra hovedprosjektet, dette må avklares med Statens vegvesen.
2. VIV effekt. Det skal gis en oversikt av hvilke VIV genererte responser som kan forekomme på grunn av virvelavløsning under operasjon. Dette knyttes mot eksisterende veileder for VIV, så som DNV GL-RP-F105, og dokumenteres med enkle overslag. Her kan studenten fremskaffe egenperioder basert på egne overslag for de aktuelle svingemoder.
3. Modellering av brua i Sima-Riflex i operasjonstilstand, det vil si med endeforankring på plass. Modellen evalueres og tilnærmelser i modellering diskuteres. Fremskaffelse av egenmoder og sammenligning av disse med resultater fra prosjektering. Det utføres så analyse av dynamisk lastvirkning fra et utvalg av tilstander av vind-sjø og dønning, som igjen sammenholdes med tidligere prosjektering. Resultater fremskaffes i form av snittkrefter langs brua og bevegelser. En viktig kontroll er slakke i stag som også skal vurderes.
4. VIV-analyse. Brua modelleres i programmet Vivana og det gjøres analyse av VIV for hoved-brua og for stagene. Forutsetninger for Vivana og tilnærmelser i modellen diskuteres, herunder effekt av to nabo-rør. Resultat kontrolleres mot RP105. Betydningen av VIV i forhold til øvrige lastvirkninger for dimensjonering diskuteres.

Oppgaven utføres i nært samarbeide med Dr. Techn. Olav Olsen AS. Tilgjengelig litteratur fra deres prosjekt skal avklares med veileder. I perioder kan det være aktuelt å sitte hos firmaet.
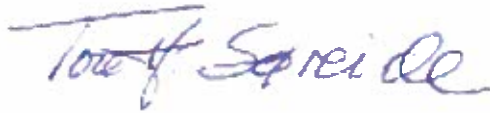
Hovedveileder NTNU:

Prof. Bernt Leira

Co-veileder NTNU:

Prof. Svein Sævik

Veileder Dr. Techn. Olav Olsen AS:

Tore Søreide

Preface

This report is a Master Thesis in marine structural engineering. The thesis was written at the Department of Marine Technology at The Norwegian University of Science and Technology (NTNU) in Trondheim, during the spring 2017.

The task has been very interesting and challenging. Much time was spent on creating the model and on computing the eigenfrequencies of the model. Lessons were learnt and after this the rest of the analysis and processing could be done. It has been a busy semester with a lot of work on the thesis. Some results thought irrelevant for the report is included in the appendix.

I would like to thank my supervisor Bernt Johan Leira for answering all questions and giving support during the work. Also I want to thank Tore Helge Søreide from Dr. techn. Olav Olsen for proposing the task, providing documents on the assessment study and for support during the process. Elizabeth Passano and Andreas Amundsen from SINTEF Ocean need to be thanked for answering my questions on Vivana software. Also the student assistant in the software used Yuna Zhao and PhD candidate Thomas Viuff deserve acknowledgements for their help. Last but not least, I want to thank the ladies at office A1.019 - Kontorrypene - for support and loads of fun during five years at NTNU.

Maria Hapnes von Schack
Trondheim, June 9, 2017

Summary

A ferry-free highway is under planning of the Norwegian Public Roads Administration on the south-west coast of Norway. Many of the fjords are characterized as very deep and wide, resulting in a need for innovative, new technology for todays bridges and tunnels. Submerged Floating Tube Bridges (SFTBs) are an alternative solution for fjord crossing and have been considered for some of these crossings.

The objective of this thesis has been to survey the different forms of dynamic load effects on a proposed tether-stabilized SFTB-concept for the 5 km long Bjørnafjord. The concept is made by the design group Dr.techn. Olav Olsen, Reinertsen and Norconsult during an Assessment Study. Vortex-induced Vibrations (VIV) have been analysed by the software Vivana and compared with empirical models provided by DNV GL. A model of the SFTB was created in Sima/Riflex. A few dynamic analyses have been performed in order to compare response with response from analyses done by the design group.

The reliability of results from VIV-analyses are limited by the used software Vivana. The bridge consist of tubes and tethers in tandem, and in reality the inflow current velocity of the second tube will be affected by the first tube. This is not included in Vivana, and hence one tube and one tether were analysed individually.

It was found that the onset for in-line VIV for the tube was at a return period of 7 years with an amplitude of 23 cm. The amplitudes of a 100 year current were found to be 0.86 m and the resulting maximum moment was estimated to be about 25 % of moments from the wave analyses of a 100 year return period. Horizontal accelerations for the bridge are within requirements. No cross-flow VIV was found for both tube and tether. VIV was not found to be of a concern for tethers due to low amplitudes and high fatigue life. However, the response amplitude for the tethers is seen to increase with with the decrease in tension and this may be critical for smaller tensions. The DNV GL in-line model is in general conservative compared to the amplitudes found from Vivana.

Dynamic wave analyses were conducted for both wind-sea, and for wind-sea and swell. It was observed that swell is important to include in the analysis, as on this depth, it is the dominant wave. Envelopes of the maximum and minimum response was compared to results from the analysis done by the design group. The tension in the tethers were found to be positive for all performed dynamic analyses, always maintaining the vertical stability of the bridge.

Sammendrag

Statens Vegvesen planlegger ferjefri E39 langs sørvestkysten av Norge. Mange av fjordene som skal krysses karakteriseres som veldig dype og brede. På grunn av dette, er det et behov for ny teknologi til broer og tuneller. Flytetunneler, også kalt rørbruer, er blitt sett på som en alternativ løsning for fjordkryssningene.

Målet med denne masteroppgaven har vært å undersøke de forskjellige dynamiske lastvirkninger som oppstår på en stag-stabilisert rørbru prosjektert for den 5 km lange Bjørnafjorden. Konseptet som er studert er laget av designgruppen Dr.techn. Olav Olsen, Reinertsen og Norconsult gjennom et mulighetsstudie. Vortexinduserte vibrasjoner (VIV) er analysert i Vivana og sammenlignet med empiriske modeller gitt av DNV GL. En modell av broen er laget i Sima/Riflex. Et utvalg dynamiske analyser ble utført for å sammenligne respons med respons fra analyser utført av designgruppen.

Påliteligheten i VIV-resultatene er begrenset av programmet Vivana. Flytetunnelen består av rør og stag i en tandem-konfigurasjon hvor strømhastigheten på nedstrømsrøret vil påvirkes av oppstrømsrøret. Dette er ikke inkludert i Vivana, og dermed er et rør og et stag analysert hver for seg for å oppnå førstegangsestimater av VIV-opptreden.

Det ble funnet at oppstartshastigheten hvor strøm gav VIV for røret hadde en returperiode på 7 år, med en amplitude på 23 cm. Amplituder fra an 100 års returperiode ble funnet til å være 0.86 m og tilhørende momenter var estimert til å være ca 25 % av momenter fra en 100 års bølgeanalyse. Horisontale akselerasjoner av broen er innenfor regelverk, og cross-flow VIV ble ikke funnet for verken rør eller stag. VIV er ikke sett på som et problem for stagene, på grunn av lave amplituder samt høye utmattingsliv. Likevel er det observert at responsamplituden for stag øker med minkende strekk i stag, og dette kan være kritisk ved små strekk. Totalt sett gir DNV GL in-line modellen konservative amplituder sammenlignet med resultater funnet fra Vivana.

Dynamisk bølgeanalyse ble utført med vindsjø, samt med vindsjø og dønning. Det ble observert at dønning er viktig å inkludere i en analyse, da denne er en dominerende bølge på dypet til rørbruen. Enveloper av maksimal og minimal respons er sammenlignet med resultater fra analyser gjort av designgruppen. Strekket i stagene er positivt for alle analyser utført, dermed er den vertikale stabiliteten til broen beholdt.

Contents

List of Figures

List of Tables

Glossary

A cross-sectional area.

A Amplitude.

a$_i$ Acceleration component along i-axis (x,y or z).

A$_{kj}$ Added mass coefficient in degree of freedom j from motion in degree of freedom k.

A$_{outer}$ Outer area.

A$_{projected}$ Projected area.

A$_y$ / D Maximim in-line VIV response amplitude.

A$_z$ / D Maximim cross-flow VIV response amplitude.

B Buoyancy.

B$_{kj}$ Damping coefficient in degree of freedom j from motion in degree of freedom k.

C the total circumference of the bridge.

C$_A$ added mass coefficient.

C$_D$ Drag coefficient.

C$_{kj}$ Restoring force coefficient in degree of freedom j from motion in degree of freedom k.

D Cylinder diameter.

$\frac{d^2}{dx^2}$ Second derivative.

ds Infinitesimal piece of curve.

$\frac{d^2w}{dx^2}$ Curvature.

E Elasticity modulus.

F Force.

F$_C$ Current force.

F$_{exc}$ Wave excitation force.

f$_{osc}$ Oscillating frequency.

f$_{non}$ Non-dimensional frequency.

f$_p$ Preak frequency.

F$_{rad}$ Wave radiation force.

f$_n$ Natural frequency for a given vibration mode.

f$_s$ The vortex-shedding frequency.

f$_w$ the (significant) wave frequency.

g Gravitational constant.

H Sagitta of an arch.

h Time step length.

Hs significant wave height.

I Second moment of area.

$\mathbf{I_y}$ Second moment of area about y-axis.

$\mathbf{I_z}$ Second moment of area about z-axis.

$\boldsymbol{K}$ Stiffness matrix.

k Wave number.

k Modulus of subgrade reaction.

KC Keulegan-Carpenter number.

$\mathbf{k_f}$ Foundation modulus.

$\boldsymbol{K_I}$ Incremental stiffness.

j,k 1,2,...6, Six degrees of rigid body moves.

$\mathbf{k_{nl}}$ Nonzero roots for a fixed beam.

$\mathbf{K_S}$ the stability parameter.

k data for the SN-curve.

L Length of a given structure.

l Length.

logC constant for the SN-curve.

$\boldsymbol{M}$ Mass matrix.

m Mass.

$\mathbf{m_a}$ Added mass.

m data for the SN-curve.

$\mathbf{m_{dry}}$ Dry mass.

$\mathbf{m_e}$ Effective mass.

$\mathbf{m_s}$ Mass per unit length including structural, added mass and internal fluid mass.

$\mathbf{M_y}$ Moment about y-axis.

$\mathbf{M_z}$ Moment about z-axis.

$\boldsymbol{n}$ Unit vector.

$\mathbf{N_{\Delta\sigma}}$ the number of stress ranges.

$\mathbf{N_i}$ the number of cycles to failure for stress cycle i.

n_i the number of occurrences for each cycle.

p Pressure.

R Load.

$\ddot{r}$ Acceleration of object.

R^D Damping force vector.

$\dot{r}$ Velocity.

Re Reynolds number.

R^I Inertia force vector.

R^S Structural force vector.

St The Strouhal number.

$S(\omega)$ Spectrum.

T Wave period.

T Pre-tension in tether.

T_p peak period.

t_{ref} the wall thickness for the cross section.

U_C Current velocity.

U_w Current in the wake of a cylinder.

$\dot{v}$ Fluid particle acceleration.

V_R Reduced velocity.

v_r Relative velocity between wave particels and object.

V_{Rd} Design value for reduced velocity.

W Weight.

w Deflection.

x Centre-to-centre distance between two cylinders.

x_n Displacement of step n.

x_{n+1} Displacement of step n+1.

α_m Mass proportional damping coefficient.

α_s Stiffness proportional damping coefficient.

α current flow velocity ratio.

$\alpha(n)$ Parameter for generalized modal analysis.

β_w Parameter for Newmark β-family technique.

β_0 the degree of the first supernode position.

β_{end} the polar angle for the end point.

$\beta(n)$ Parameter for generalized modal analysis.

$\beta_{neighbour}$ the polar angle of the neighbouring point.

$\Delta\sigma_i$ the stress range.

$\Gamma()$ Gamma function.

γ peak shape parameter.

γ_f Safety factor for DNV GL VIV Models.

γ_k Safety factor for DNV GL VIV Models.

$\kappa(n)$ Parameter for generalized modal analysis.

λ Wave length.

λ_n Modal damping ratio.

∇ Displaced volume in water.

ν Kinematic viscosity.

ω Wave frequency.

ω_{bt} Frequency of a beam in tension.

ω_n Angular eigenfrequency n.

ω_p angular spectral peak frequency.

ω_{sn} Frequency of a straight bridge.

$\phi(s)$ Assumed mode shape satisfying boundary conditions.

ρ_w Water density.

σ Spectral width parameter.

θ_p Wave direction.

θ_{rel} the flow angle relative to the pipe.

ζ_T Total modal damping ratio.

Acronyms

DNV GL Det Norske Veritas GL.

NPRA Norwegian Public Roads Administration (Statens Vegvesen).

SFTB Submerged Floating Tube Bridge.

VIV Vortex-induced Vibrations.

Chapter 1

Introduction

1.1 Motivation and Background

Along the south-west coast of Norway there are many fjords, and some are very deep and wide. Today, the 1100 km coastal highway between Kristiansand and Trondheim has eight ferry crossings over these fjords, see figure 1.1. The ferry crossings increases the travel time significantly along the coast. A ferry free coastal highway is under planning by the Norwegian government and the travel time is estimated to decrease to 11 hours from todays 21 hours.

The Norwegian Public Roads Administration (Statens Vegvesen) is commissioned by the Norwegian Ministry of Transport and Communications to develop the plans. Challenges arises due to the extremity of the fjords and conventional bridges or tunnels will require very large investments. An alternative to conventional bridges or tunnels are Submerged Floating Tube Bridges (SFTBs).

One of the fjords to be crossed is the 5 km long Bjørnafjord, between Reksteren and Os in Hordaland. An assessment study for an SFTB has been performed by the design group Reinertsen, Dr. techn. Olav Olsen and Norconsult. During the assessment study, little consideration has been given to the effect of Vortex-induced Vibrations (VIV) on the bridge, and the investigations are left for further work(Reinertsen et al., 2016b). This is of interest for the design group and is the basis for this thesis. The task is proposed by Tore H. Søreide from company Dr. techn. Olav Olsen.

1.2 Objective

The objective of this thesis is to survey the different forms of dynamic load effects on the proposed SFTB, and especially effects from VIV are to be considered. A model is to be established in Riflex. The VIV-related software Vivana is to be used and results compared with the general rules for VIV provided by Det Norske Veritas GL (DNV GL). Effects from wind-sea and swell will be checked and compared with results from the original analysis performed previously by the design group in a different software.

Figure 1.1: The costal highway between Kristiansand and Trondheim. The black lines mark the current ferry crossings (Statens Vegvesen, d).

This original model and results are in this thesis later referred to as "the reference model and results".

1.3 Limitations

The results herein will be limited by the capabilities of the software Vivana. Some relevant theories are not included in the program. For instance, the effect of two cylinders in tandem and the resulting velocity in the wake of the first cylinder is not included. Therefore, only the first tube will be checked when analysing the bridge for VIV. Accordingly for VIV-check of the tethers, only one of the tethers in each tether group will be modelled. This will give limited results, as the real interference between the structure as a whole and sea water will not be modelled. The use of the default curve in Vivana for the relationship between the Strouhal number and Reynolds number will also limit the reliability of the results. This is used since no such curve is given for the actual cross-section.

Recommended practice given by DNV GL is intended for steel pipelines, and may not give sufficient guiding for slender structures made of concrete. However, this is the

guideline available today, and will be used in the evaluation of the SFTB.

As most of the focus in the thesis is to be done on VIV, only a few dynamic wave analysis will be performed. Therefore, the results from the wave condition may not be representative, as not enough data is made available for it to represent the real condition.

Some parameters are not specifically given in the technical reports provided by the design group. Therefore some simplifications and assumptions are done when establishing the model in Riflex. Weight variation such as water absorption in concrete, marine growth and traffic, are ignored in this thesis.

1.4 Outline of the Thesis

The thesis includes the following chapters:

- *Chapter 1 - Introduction.*
- *Chapter 2 - General SFTB Technology.* Introduces the concept of Submerged Floating Tube Bridges and gives a review of what research is done on the subject in Norway.
- *Chapter 3 - Developed Concept and its Environment.* Gives information about the SFTB-design that will be studied and about the environment at the specific location.
- *Chapter 4 - Theory.* Necessary theory is presented.
- *Chapter 5 - Modelling the SFTB.* How the model is created in Riflex and related assumptions are explained.
- *Chapter 6 - Method and Setup of Analyses.* Explanation of what methods are used and how the different analyses are performed in Sima.
- *Chapter 7 - Results.* Pure results are given and explained.
- *Chapter 8 - Discussion.* Results are discussed.
- *Chapter 9 - Conclusive Remarks*
- *Chapter 10 - Recommendations for Further Work*

Chapter 2

General SFTB Technology

2.1 Ferry Free E39 Project

The Norwegian Parliament confirmed when adopting the National Transport Plan for 2014-2023, that the E39 coastal highway route is to be realized as a continuous road without ferries within 20 years. An investment cost of NOK 340 billion is estimated. To realize the ambition within 2035, new fjord crossing technology is needed, and extreme structures and building projects will be a reality. Innovative solutions that combine known bridge technology with offshore technology must be developed. Especially the Bjørnafjord, Sognefjord and Sulafjord need new and unproven technology. A pilot project for an SFTB is considered for the Halsafjord.

In May 2017, the crossing of the Boknafjord was adopted by the Parliament. The solution will be a 27 km long underground tunnel and will be the worlds longest and deepest, according to Statens Vegvesen (a). Updated information on development of the concept for the Bjørnafjord can be found at Statens Vegvesen (c).

2.2 Introduction to SFTBs

The following is adapted from the author's Project thesis. A Submerged Floating Tube Bridge is a tunnel tube floating at a given water depth beyond sea surface. It works as an alternative to conventional bridges and is of special interest if a crossing is very wide or deep, see figure 2.1. The tunnel is also called an Archimedes bridge, as it uses its buoyancy to float neutrally in the water.

The submergence depth is restricted by ship traffic on the sea surface and pressure on the sea bottom. Usually the depth of a submerged floating tube bridge is set to around 25 meter. This guarantees no ship collision in the water surface and avoids the need of very thick walls to withstand the high hydrostatic pressure in deeper waters. Advantages of the use of an SFTB in extreme cases are that it would be a cheaper alternative due to use of less materials and lower installation costs than a deep mined rock tunnel and a high level bridge (Wallis). In addition it is isolated from the atmosphere, resulting in low impact on the environment, and low weather dependence. Compared to an

underground tunnel it has a low inclination, resulting in a safer driving environment for vehicles.

At the present day, an SFTB has never been built. Nevertheless there has been performed an extensive amount of research and given proposals since the end of the 19th century in for instance Turkey, England, Italy and Norway.
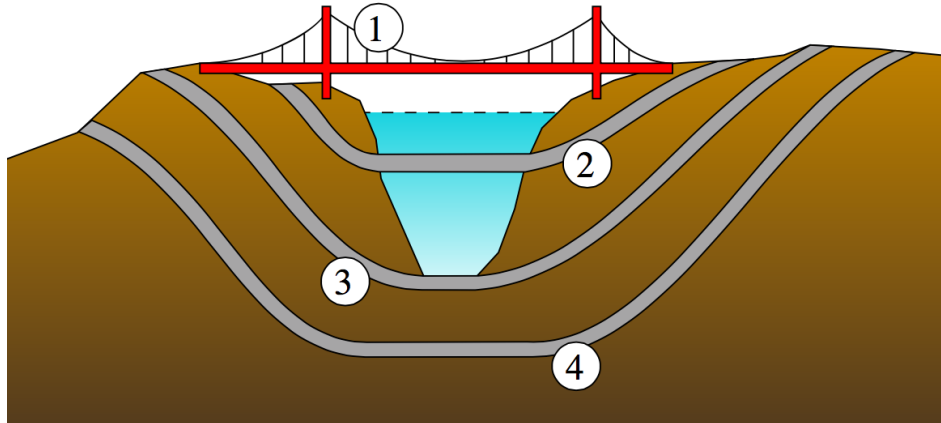
Figure 2.1: Crossing Concepts. 1: Suspension bridge. 2: SFTB. 3: Immersed tunnel. 4: Underground tunnel. Photo taken from (User:Waldir) at [`https://commons.wikimedia.org/w/index.php?curid=3238712`].

2.3 Research on SFTBs in Norway

In Norway, the SFTBs have been seen as a potential for fjord crossing in deep or wide fjords. A great amount of research has been done during the last hundred years. The first SFTB patent dates from 1923 (U. Evang, 1996). In the 1960s, the NPRA appointed a committee to report on the possibility of submerged floating tube bridges. The final report was completed in 1971 and concluded that the use of SFTBs was feasible and that they would also offer an economical advantage to the conventional bridges (U. Evang, 1996).

Until 1985 many proposals were introduced on the use of SFTBs. At last, Høgsfjord, on the south-west coast was approved by the Norwegian Parliament to be the site of a pilot project. During the 1980s and the 1990s, four different concepts were considered. One anchored to the seabed and three with pontoons in the surface as illustrated in figure 2.2 (Skorpa, 2013). The length of the fjord is 1400 m and the depth is 155 m. Due to heavy ship traffic in the area, anchors to the seabed were preferred opposed to pontoons in the surface. This concept, provided by Selmer, was approved as a way of crossing, but was in the very last moment not realized due to political reasons and resistance.

The Sognefjord is the most extreme fjord in Norway with the combination of an extreme width of 3.7 km and en extreme depth of 1250 m. It is considered one of the longest fjord crossings in the world, and brings large challenges. The research on SFTBs in
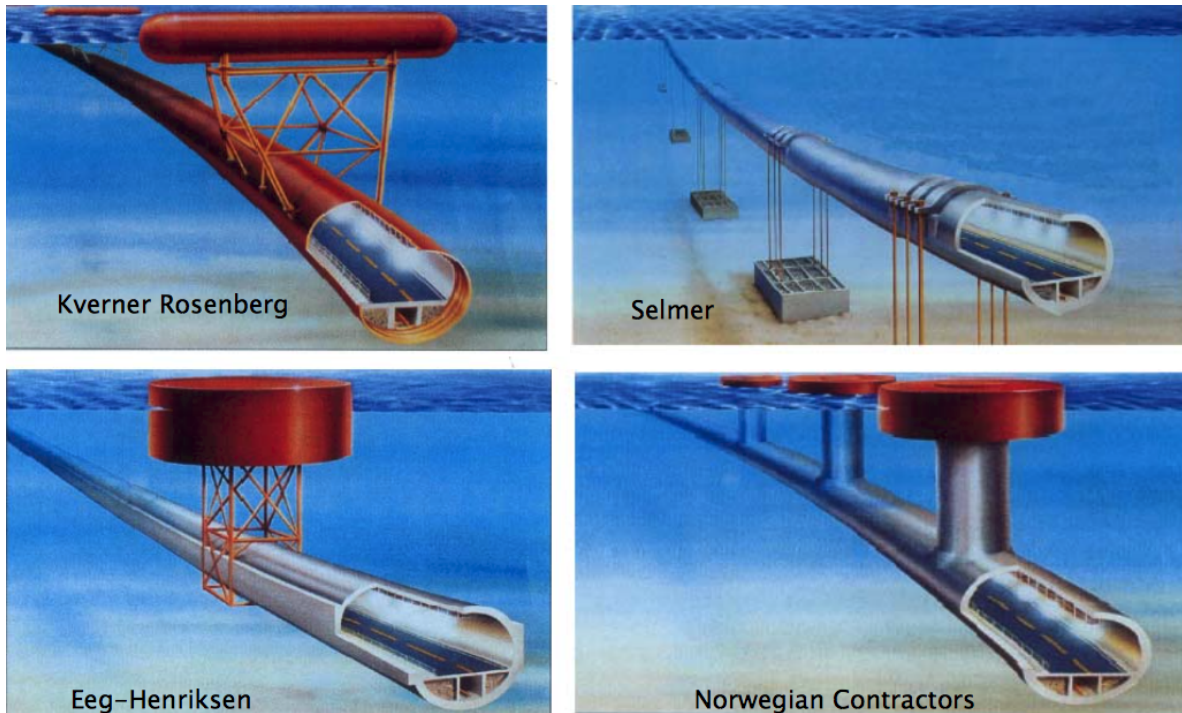
Figure 2.2: Concepts for Høgsfjord (Statens Vegvesen, b).

this fjord was started in 2012. A feasibility study was conducted with the objective of demonstrating the technical feasibility of an SFTB for this fjord (Reinertsen and Dr. techn. Olav Olsen, 2013). Due to the extreme water depth, the SFTB proposed by Reinertsen/Olav Olsen consisted of two tubes with sixteen pontoons in the surface, as seen in figure 2.3 and 2.4. A passage for ships between the pontoons were included in the design. The two tubes were interconnected with truss-work to give required horizontal stiffness, but also to give the possibility for escape routes between the tubes. The results from the study are that this SFTB is technically feasible, and that it meets all requirements from the Public Roads Administration, Eurocode, NORSOK and DNV GL.
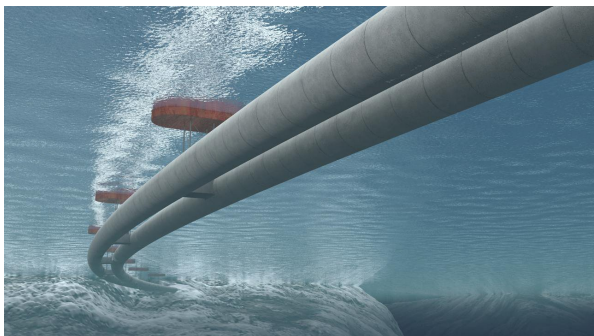
Figure 2.3: Concept for Sognefjord crossing (Reinertsen and Dr. techn. Olav Olsen, 2013).

Figure 2.4: Pontoons on the surface of Sognefjord (Reinertsen and Dr. techn. Olav Olsen, 2013).

An SFTB concept is also created for the Bjørnafjord, and is the basis for this thesis. It is made by Reinertsen, Olav Olsen and Norconsult. Solutions with both tethers and pontoons are considered. It is reported that the motions for both concepts are within comfort and driving limits, also for a 100 year return condition (Reinertsen et al., 2016b). More information on the concept will be given in later chapters.

2.4 The Concept of SFTBs

2.4.1 Types of SFTBs

There are in general four different concepts that can be used in order to support the SFTB from unwanted displacement. These are illustrated in figures 2.5 to 2.8. Depending on the depth and soil of the area to be crossed, one can either use support moored to the ground or floating pontoons.
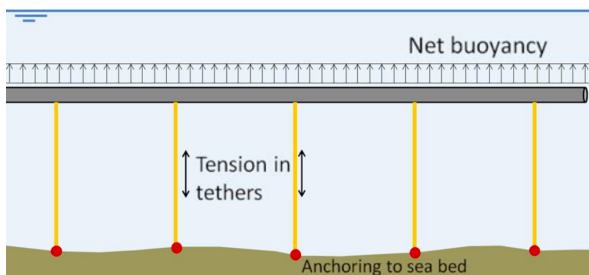
Figure 2.5: Tension leg support. Adapted from (Reinertsen et al., 2016b).
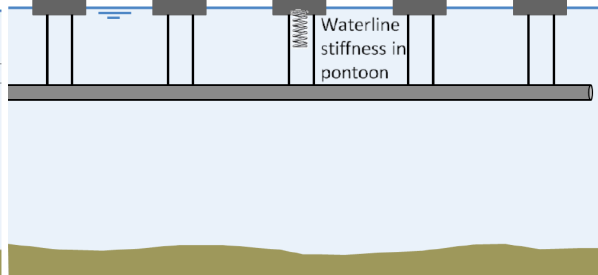
Figure 2.6: Pontoon support. Adapted from (Reinertsen et al., 2016b).
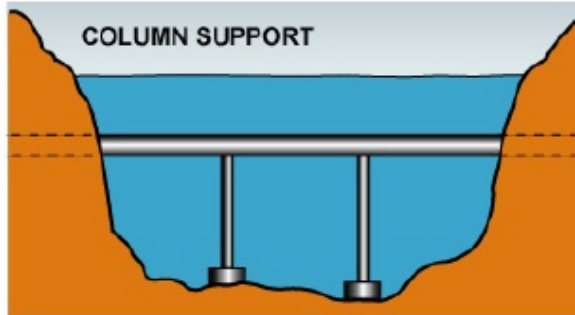
Figure 2.7: Column support (Kawade and Meghe).
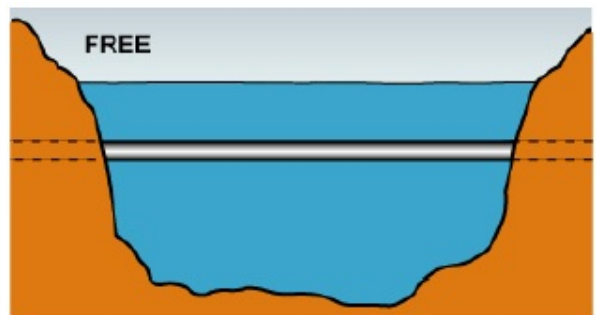
Figure 2.8: Free (Kawade and Meghe).

Comparisons between a tether- and a pontoon-stabilized SFTB is taken from the study for the Bjørnafjord, Reinertsen et al. (2016b). SFTBs with mooring to the ground gives no visual impact from shore and free ship passage, but restricted submarine passage. It needs a positive net buoyancy giving a pre-tension in the tethers. The major part of the wave excitation is eliminated due to the submergence, giving small environmental impact (Reinertsen et al., 2016b), see figure 2.5.

A pontoon-stabilized SFTB is vertically supported by the water plane stiffness of the pontoons. The pontoons will be subject to risks of ship collisions but give free submarine

passage below the tube. This concept can be useful when depths are too large for practical anchoring or when the soil is soft. The pontoons interact with the waves in the surface, and will transfer more motions to the tube, compared to a tether-stabilized tube. A visualization of the concept is seen in figure 2.6. No modern cases of column support is found. Non-stabilized tube can be acceptable over smaller spans, as for longer spans it would demand a very high stiffness.

2.4.2 Important Features of SFTBs

The general advantages of SFTBs are several. Large draft eliminates the major part of the wave loads, leading to the traffic in the tube never being affected by weather conditions. It also makes it impossible for ship collisions with the tube, but this must be considered for the pontoons. Submarine collisions may be a threat and the tube should be designed accordingly. The pontoons need sufficient freeboard, so that extra loads can be carried by them without the risk of water entry on the pontoons.

By use of tethers it is important that they are designed with a pre-tension and never will obtain slack during a dynamic environment as this can cause high stresses in the transition from slack to tension. In addition, the tube looses its vertical and horizontal stabilization. It is important that the SFTB is designed to have eigenfrequencies different from those of the waves, especially in heave and roll, to ensure tether tension (Reinertsen et al., 2016b).

2.4.3 Design Challenges

In addition to the usual loads from dead weight, buoyancy and traffic, the SFTB has to resist the following special load situations:

- Buckling as an arch

- Ship and submarine impact

- Vortex-induced Vibrations

- First order wave forces

- Slowly varying second order wave forces

Thermal expansion can lead to buckling. To avoid this, it is important to include a high safety factor for buckling in design. The risk of buckling can be decreased by increasing the stiffness of the tube. Designing the bridge in the shape of an arch, decreases the risk of buckling.

The feasibility study for the Sognefjord, by Reinertsen and Dr. techn. Olav Olsen (2013), states that a ship impact would be in the magnitude of 1500 MNm. Designing a pontoon that can resist such a load is judged impossible. A solution can be to design a "weak link" between the tube and the pontoon that will break before the forces are transmitted further in the tubes. After this, the tubes would have to survive with the loss of one pontoon, until a new pontoon is installed.

Vortex-induced Vibrations (further explained in section 4.3.3) leads to tube vibrations due to it being subject to a current. In the design of an SFTB it would be important to make sure the eigenfrequencies of the SFTB are not in the same range as the vortex shedding frequency, as this can cause resonance. Vibrations will lead to fatigue damage over time and can cause large vibrations endangering the driving environment. Also the effect of two cylinders in tandem would have to be considered. Galloping (see Faltinsen (1990)) may be a problem in this case.

Wind in the fjord will induce waves. As the decrease of first order waves is exponential with depth, the effects of such waves on the depth of a tube may be negligible. Further, incoming waves from the outside ocean (swell) have very low amplitudes and periods when they reach into the fjords, and are also not expected to give any critical response. However, waves with large periods decrease slower than wind-sea, and may be of a higher importance at the depth of the SFTB than wind-sea.

Slowly varying wave forces (explained in section 4.3.1) may be a threat to slender structures like an SFTB, if resonance occur. These wave effects may origin from second order wave drift forces and internal waves due to layering in the water from salinity differences. The effects of wave drift forces are not expected to be problematic if the eigenperiods of the structure are less than 30 seconds. If the eigenperiods are larger than this, the response can be critical (Skorpa, 2013).

Even though the forces will give significant response on the system, it is not necessarily critical as it will be possible to design the SFTB with a corresponding strength. This must be considered in the design process (Jakobsen et al., 2013).

2.5 General Understanding of the Safety of an SFTB

There is a scepticism regarding crossing a fjord in a "floating" tunnel, with this large draft. The concept has never been built before and people are afraid it will not work as planned. This is probably some of the reasons it has never been realized, even though an extensive amount of studies has been done. Similar thoughts were found to underground tunnels, before they were built. In reality, the SFTBs are based on known technology and dimensioned to withstand loads that are of a 100 year dimension, meaning they will have the same order of safety as an ordinary bridge or underground tunnel. However, like for underground tunnels, there will always be risks of explosions within the tube (U. Evang, 1996).

2.6 Floating Bridges

The concept of using buoyancy of structures in design, is also seen in floating bridges. Floating bridges are supported by pontoons that rest on the water surface. The following bridges exist in Norway.

Bergøysund Bridge in Møre og Romsdal, was officially opened in 1992. It is a curved truss bridge in steel only supported to land in the ends. The bridge is resting on 7 oval

concrete pontoons and the total length is 931 m. With Nordhordalands Bridge it is the only one of its kind. The longest span is of 106 meters and it has a sailing lead of 6 m (Store Norske Leksikon).

Nordhordalands Bridge in Hordaland opened in 1994. It is a curved cable-stayed bridge, with a total length of 1614 m. It has a sailing lead of 32 meters and a floating bridge of 1243 meter resting on 10 oval concrete pontoons (Bergen Byleksikon). Photos of both bridges can be seen in figures 2.9 and 2.10.

Figure 2.9: Bergøysund Bridge (Broer.no).

Figure 2.10: Nordhordalands Bridge (Underskog).

Chapter 3

Developed Concept and its Environment

The developed concept proposed for the Bjørnafjord by the design group Reinertsen, dr. techn. Olav Olsen and Norconsult is a curved SFTB submerged at a 30 m depth of two main tubes, one for each driving direction, see figure 3.1. The two tubes are interconnected with cross-over tubes and diagonal bracings. The cross-over tubes transfers vertical support forces, provides stability between the main tubes, accommodates escape ways, and room for technical installations and ballast tanks. 26 tether groups, consisting of four tethers each are mooring the tubes to the seabed. Information about the SFTB is taken from the provided technical report, Reinertsen et al. (2016b), which is the result of the assessment study.
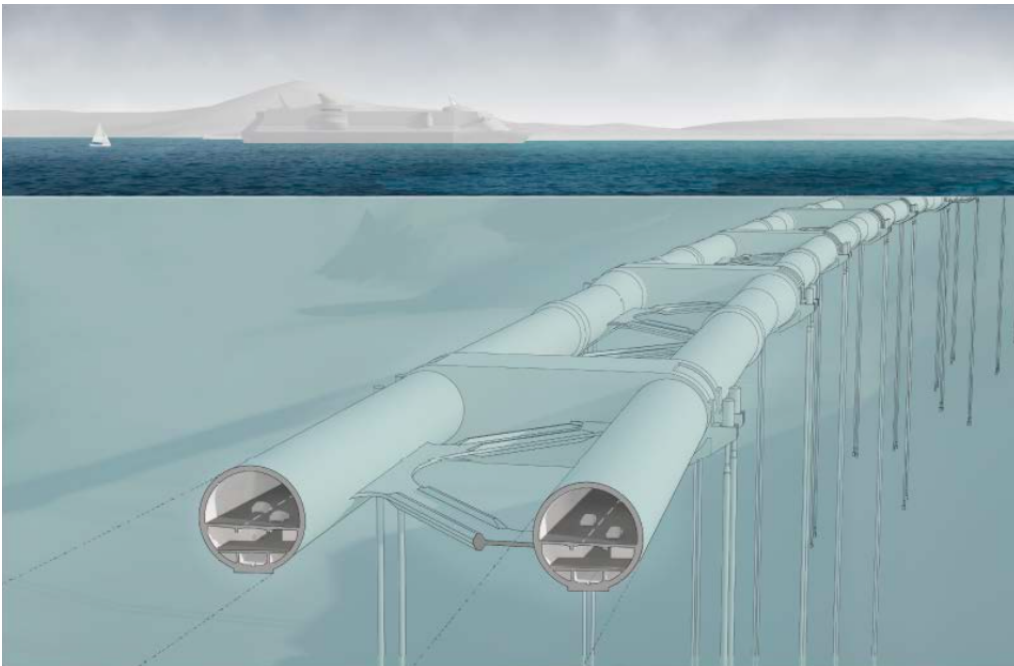
Figure 3.1: The tether-stabilized Submerged Floating Tube Bridge proposed for the Bjørnafjord (Statens Vegvesen, 2016a).

3.1 Dimensions

The SFTB has a length in centerline of 5495 m and a radius of curvature of 6400 m, see figures 3.2 and 3.3. Due to requirements about minimum ship passage clearance and hydrodynamical considerations, the free water clearance above the tube bridge is set to 30 m (Reinertsen et al., 2016b).

Figure 3.2: The horizontal alignment of the SFTB. The length of the bridge is arranged in a north-south orientation. The left side is the south end and the right side is the north end. Magnified figure in appendix A.1. (Reinertsen et al., 2016b).
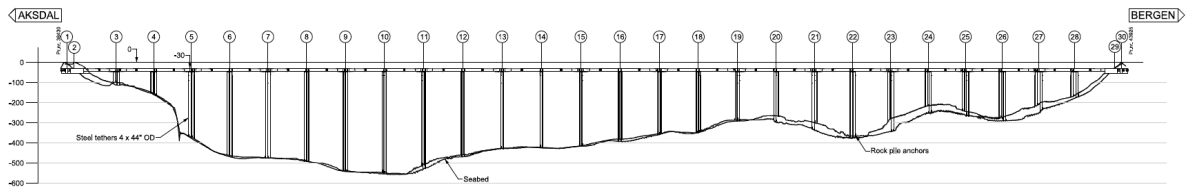
Figure 3.3: The vertical alignment of the SFTB, showing the depth of the seabed. Magnified figure in appendix A.1. (Reinertsen et al., 2016b).

3.1.1 Main Tubes

The main cross-section of the two tubes is designed as the tunnel profile T9.5, as standardized by the NPRA. It is seen to the left in figure 3.5. The tubes are made of concrete and has a spacing of 40 m between the center points. A traffic deck and three separate compartments below the traffic deck are the main rooms. The middle compartment is dedicated to bicycle lane and service, while the other compartments are meant for ballasting.

Emergency escape routes are required by the NPRA every 200 m, and this is found in the cross-over tubes. Emergency lay-bys of 3 m are required every 500 m, hence, a larger tube cross-section with the required lay-by, is applied at every other cross-over tube, i.e. every 400 m. A lay-by, illustrated in figure 3.4 is a transverse extension of the drive path, giving room for parking during an emergency stop. The standard tunnel profile with lay-by is called T12.5. Both the cross-sections are seen in figure 3.5. The pattern with transitions between the two cross-sections T9.5 and the T12.5 is seen in figure 3.6.
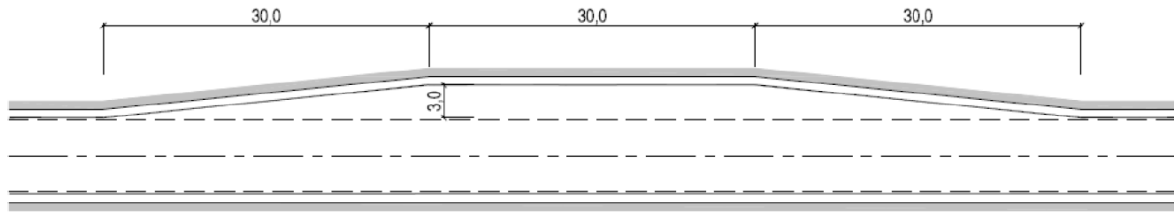
Figure 3.4: The required lay-by every 500m. The lay-by has a net length of 30 m, the merge and diverge lengths the same. (Reinertsen et al., 2016b).

Note the alternating width of the tubes, altering between the T9.5 and the T12.5 with the required lay-by, approximately 400m apart. The cross-sectional properties of the two cross-sections are summarized in table 3.1. For magnified figures, see appendix A.1.
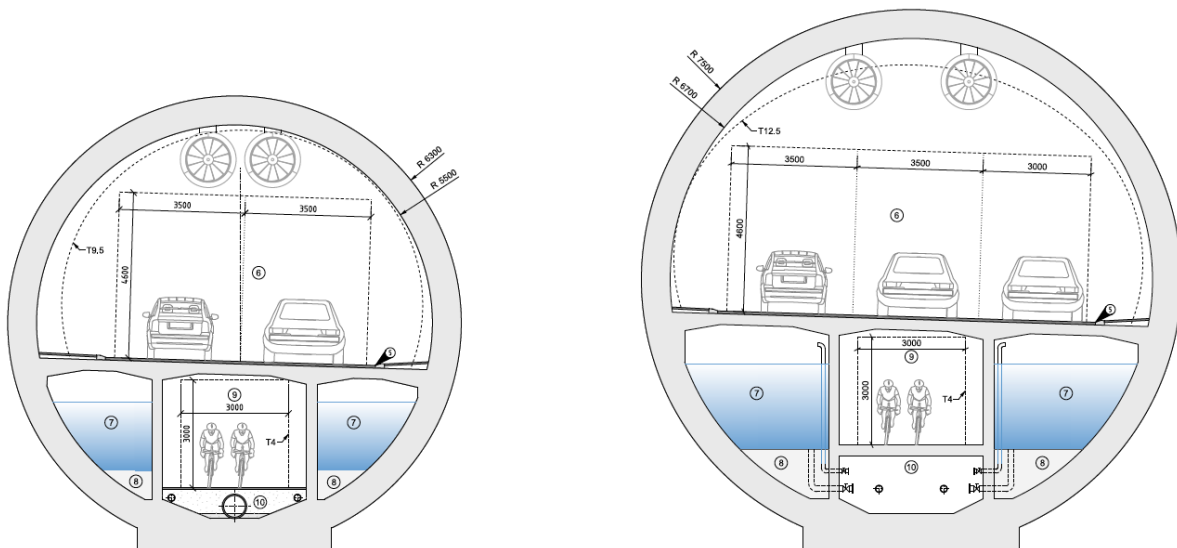
Figure 3.5: Left: Cross-section T9.5. Right: Cross-section T12.5 with the required lay-by. Magnified figure in appendix A.1 (Statens Vegvesen, 2016b).
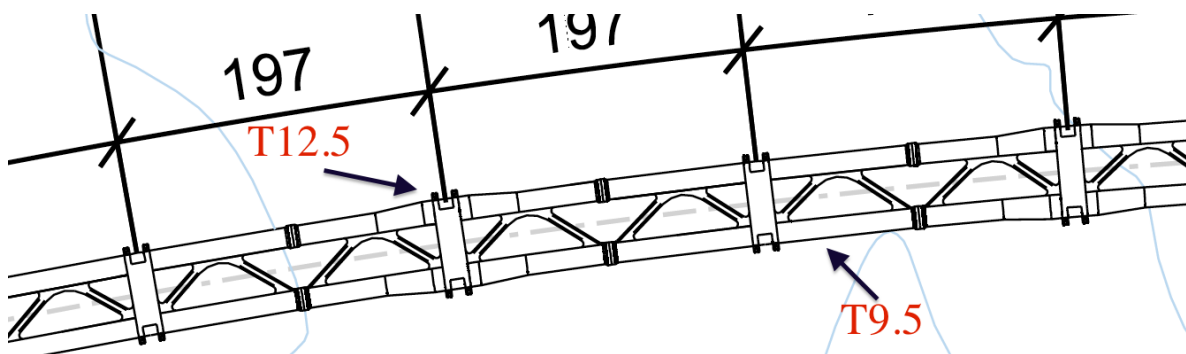
Figure 3.6: The repetitive pattern for the SFTB, alternating between the T9.5 and the T12.5. Adapted from (Statens Vegvesen, 2016b).

Table 3.1: Properties of the two cross-sections for the main tubes.

Parameter	Unit	General (T9.5)	With lay-by (T12.5)
Outer diameter	m	12.6	15.0
Thickness	m	0.8	0.8
Cross sectional area	m^2	37.3	46.7
Outer area	m^2	125.7	177.9
Vertical offset COG	m	0.55	0.76
Moment of inertia Iy	m^4	574	1002
Moment of inertia Iz	m^4	592	1059
Ballast compartment area	m^2	13.5	26.7

3.1.2 Cross-over Tubes

Cross-over tubes are found at every support position and provides escape routes and technical room and also incorporates the mooring connections. To avoid unnecessary loading of the main tubes, the excess buoyancy needed to prevent slacking of the tethers, is set at the cross tubes. A mean net pre-tension of 42-44 MN per mooring is needed to prevent the slacking. The size of the cross-over tubes are governed by demands regarding buoyancy and ballast (Reinertsen et al., 2016b). Illustrations and dimensions are seen in figure 3.7 and 3.8. For magnified figures, see appendix A.1.
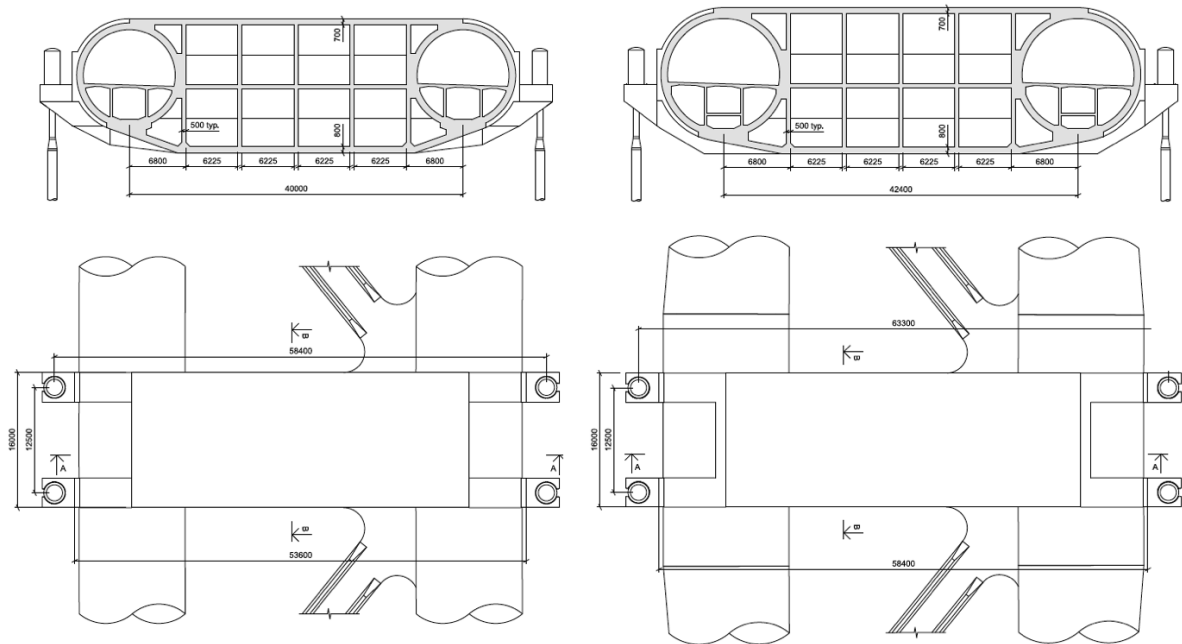
Figure 3.7: Cross-tubes seen from along bridge (upper) and above (lower). Magnified figure in appendix A.1 (Statens Vegvesen, 2016b).

3.1.3 Bracings

To limit the lateral, wave induced flexural response of the main tubes, horizontal bracings are required. Diagonal bracings have been identified as the most structural efficient
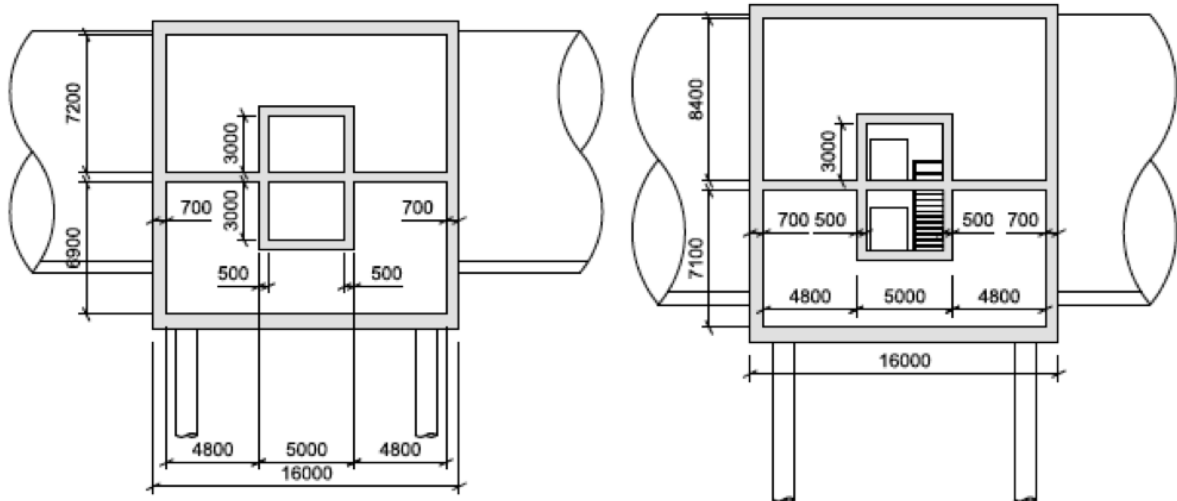
Figure 3.8: Cross-over tube seen from along cross-tube. Magnified figure in appendix A.1 (Statens Vegvesen, 2016b).

system (Reinertsen et al., 2016b). The bracings are composed of four diagonals with a 40 degree inclination in the bay between the adjacent cross tubes, see figure 3.9. For magnified figures, see appendix A.1.
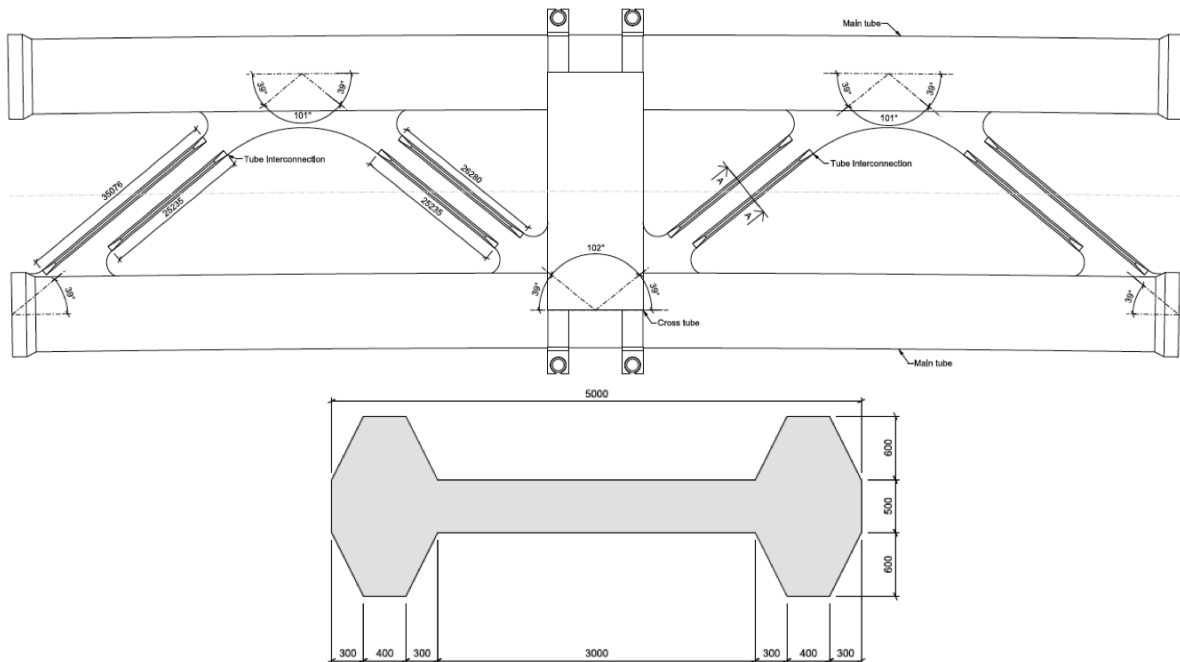
Figure 3.9: Arrangement of and cross-section of bracings. Magnified figure in appendix A.1 (Statens Vegvesen, 2016b).

3.1.4 Tether Mooring

The tethers are moored to the ground and stabilize the SFTB vertically from dynamic loads. Stabilization of the tube bridge horizontally is not done by the tethers, as this

is taken care of by the arch shape (Reinertsen et al., 2016b). It is important to have sufficient tension in the tethers when installed, to prevent the time varying loads lead to tether slack. The tethers are made of steel and installed with a nominal tension of $\approx$ 10 MN per tether (Reinertsen et al., 2016b). With four tethers in each tether group, this gives the needed $\approx$ 40 MN pre-tension. Parameters are found in table 3.2. A detailed drawing and further details of the total tether configuration is found in appendix A.1. More information can be found in Reinertsen et al. (2016b).

Table 3.2: Properties of tethers. The magnitude of the nominal pre-tension is given for the support points without and with lay-by, respectively.

Parameter	Unit	Magnitude
No. of tethers per group	-	4
Tether outer diameter	m	1.118
Wall thickness	m	0.038
Cross-sectional area	m^2	0.129
Tether resistance	MN	27 (Grade S235)
Nominal pre-tension	MN	10.5/11

3.1.5 Landfalls

The transition from the bridge to land is through a hard-rock tunnel. This transition is supported by a caisson in each end. Further details are found in appendix A.1, and more information is found in Reinertsen et al. (2016b).

3.2 Materials

The material suggested for the tubes, cross-over tubes and bracings is concrete grade B55 M40. For the tethers, steel grade S235 is suggested. Material parameters are found in table 3.3. The concrete is pre-stressed with steel of type Y1860S7 15.3 with values as in table 3.4. The pre-stressing allows for more tension stresses in the material than what the pure concrete does with its initial 3 MPa.

Table 3.3: Material Parameters

Parameter	Unit	Concrete B55 M40	Steel S235
Elasticity Modulus	GPa	30	207
Poissons ratio	-	0.2	0.3
Shear Modulus	GPa	12.5	79.62
Density	kg/m^3	3160.04	7850
Yield Strength	MPa	-	235
Tensile Strength	MPa	3.0	-
Compressive Strength	MPa	55	-

Table 3.4: Properties of pre-stressing steel type Y1860S7 15.3

Parameter	Unit	Value
Characteristic proof stress	MPa	1640
Ultimate tensile strength	MPa	1080
Elasticity Modulus	GPa	195

3.3 Damping

According to the NPRA handbook *Håndbook N400 Bruprosjektering*, a structural damping ratio of 0.8 % for uncracked concrete shall be applied for analysis. The wave range of interest used in the reference model is between 4s and 31s.

3.4 Design Process

According to Reinertsen et al. (2016b), the governing strategy for concept definition to avoid resonant response was tailoring the eigenperiods and mode shapes for heave and roll motions. The key parameters for tuning of dynamic performance were mooring spacing and tether group configuration. The arc shape gives flexibility to thermal expansion, favourable roadway layout and horizontal stabilization.

3.5 Some Functional Requirements

The NPRA has required the operational design life to be 100 years (Reinertsen et al., 2015a). Because of this, the bridge is designed to withstand a 100 year extreme storm condition in the analysis. The limits for accelerations from vibrations are set to 0.5 m/s^2 for vertical and 0.3 m/s^2 for horizontal vibrations, by the NPRA.

3.6 Environment Conditions at Site

3.6.1 Wave Conditions

Design values for significant wave height and spectral peak period, are based on offshore wave and wind data, as no on-site environmental information is known (Reinertsen et al., 2015a).

The relevant wave spectrum, S(ω) to be used for calculations according to Det Norske Veritas (2014), is the 3-parameter Jonswap spectrum (Reinertsen et al., 2015a). The three parameters are significant wave height Hs, peak period Tp (or peak frequency $f_p = 1/Tp$) and the peak shape parameter γ. The spectre is given in equation 3.1. γ is calculated from equation 3.2. A higher γ gives a higher spectrum peak, i.e. wave energy is more concentrated around Tp (Reinertsen et al., 2015a). Wave spreading is

taken according to the directional spectrum given in equation 3.3, where θ_p is the wave direction and $\Gamma()$ is the gamma function.

$$S(\omega) = \frac{5}{16}(1 - 0.287 ln\gamma)H_s^2\omega_p^4\omega^{-5}exp(-\frac{5}{4}(\frac{\omega}{\omega_p})^{-4})\gamma^{exp(-0.5(\frac{\omega-\omega_p}{\sigma\omega_p})^2)} \tag{3.1}$$

ω_p = angular spectral peak frequency
γ = non-dimensional peak shape parameter
σ = spectral width parameter
  σ = 0.07 for $\omega \leq \omega_\mathrm{p}$
    = 0.09 for $\omega > \omega_\mathrm{p}$

$$\gamma = exp(5.75 - 1.15\frac{Tp}{\sqrt{Hs}}) \text{ for } 3.6 < \frac{Tp}{\sqrt{Hs}} < 5 \tag{3.2}$$

$$D(\theta) = \frac{\Gamma(1 + \frac{n}{2})}{\sqrt{\pi}\Gamma(\frac{1}{2} + \frac{n}{2})}cos^2(\theta - \theta_p) \tag{3.3}$$

Recommendations from Det Norske Veritas (2014) regarding the constant n:

n, wind-sea   = 4 < n < 6
n, swell   > 7

Wind-sea

The NPRA has specified a 100y wind-sea wave condition to be used in the analysis. This is given in the design basis in Reinertsen et al. (2016a). Important parameters are found in table 3.5. Highest significant wave height Hs with corresponding lowest peak period (Tp,min) and maximum peak period (Tp,max) is given. The peak period shall be varied between the minimum and maximum value in a dynamic analysis. The significant wave height is considered constant along the length of crossing and coming from east. Note that the n-value for the spread is outside the recommended range. It is chosen to maintain this value because it is the value used in the reference analyses.

Table 3.5: 100y wind-sea given by the NPRA.

Hs [m]	**Tp,min** [s]	**Tp** [s]	**Tp,max** [s]	γ [-]	**Spread** [n]	**Direction** [deg]
3.0	4.0	-	6.0	3.2	9	270

Swell

Likewise, the 100 year sea state for swell is taken from Reinertsen et al. (2016a). The significant wave height is considered constant along the length of crossing. Swell condition is described:

Tp = 6-11 s: Hs increases linearly from 0.1 m to 0.3 m
Tp = 11-16 s: Hs = 0.3 m
Tp = 16-20 s: Hs decreases linearly from 0.3 m to 0.1 m
Tp = 20-30 s: Hs = 0.1 m
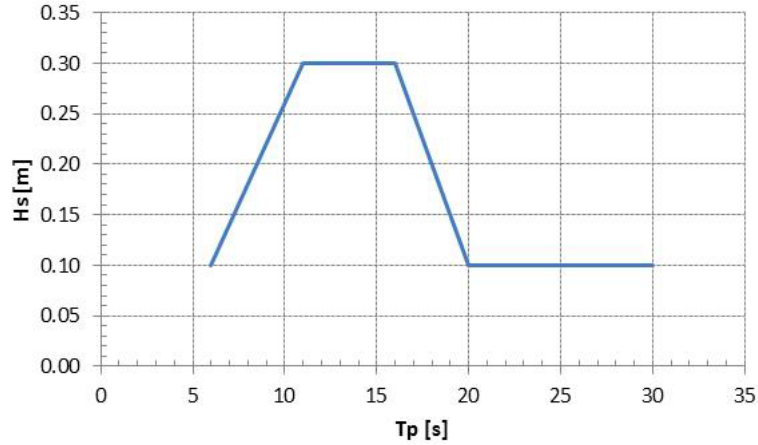
Figure 3.10: Relationship between Hs and Tp under a 100y swell condition (Reinertsen et al., 2016a).

Table 3.6: Parameters for 100y swell given by the NPRA.

γ [-]	**Spread** [n]	**Direction** [deg]
5	8	300

3.6.2 Current

A 100 year return period for the current is used and taken from Reinertsen et al. (2015a). Its surface current velocity is given as 0.7 m/s. The vertical current profile can be found by the scale values in table 3.7, and resulting current velocities are listed. Between the locations, linear interpolation can be used(Reinertsen et al., 2015a). Current surface velocities and velocities at tube depth for different return periods are given in table 3.8. The center of the tube is considered as the depth of the tube, which is -37.5 m.

Table 3.7: Scaling factors to be used with surface current at given depths, and resulting velocities at given depths.

Depth [m]	**0-3**	**10**	**30**	**50**	**>100**
Scale factor [-]	1.0	0.64	0.41	0.34	0.21
Current speed [m/s]	0.7	0.448	0.287	0.238	0.147

Table 3.8: Current velocities at depth of tube (-37.5 m) for different return periods

Return period [year]	1	10	50	100	10000
Current speed in surface [m/s]	0.50	0.60	0.65	0.70	0.90
Current speed at tube depth [m/s]	0.19	0.23	0.25	0.27	0.34

3.7 Results from the Reference Analyses

The SFTB is analysed by Dr. techn. Olav Olsen using the software SOFiSTiK for the static analysis and 3D Float for the dynamic analysis. Resulting eigenvalues are listed in table 3.9. The first 9 modes are horizontal modes, while the first vertical mode is mode number 10.

Tables with the stress extremals calculated within the cross-sections and envelopes of the dynamic translation and tether forces can be found in the appendix B. The results are found in Reinertsen et al. (2016b) and Dr. techn. Olav Olsen (2016).

Table 3.9: Resulting frequencies and periods from the reference modal analysis.

Mode	Frequency [Hz]	Period [s]
1	$1.55 \cdot 10^{-2}$	64.68
2	$2.97 \cdot 10^{-2}$	33.63
3	$4.4 \cdot 10^{-2}$	22.72
4	$4.91 \cdot 10^{-2}$	20.36
5	$7.17 \cdot 10^{-2}$	13.95
6	$9.81 \cdot 10^{-2}$	10.2
7	0.13	7.89
8	0.16	6.29
9	0.19	5.22
10	0.21	4.8
11	0.21	4.69
12	0.22	4.62
13	0.23	4.38
14	0.23	4.37
15	0.23	4.3
16	0.24	4.2
17	0.24	4.16

3.8 Wind Tunnel Tests

Wind tunnel test and analyses were performed for the NPRA and the project in 2015. The objective was validation of the SFTB in-line amplitude response and to predict the flow-induced forces on the low-density structures considered for the Bjørnafjord crossing.

A steady low turbulent flow is used on a series of close to neutrally buoyant models.

The results are static coefficients, such as the drag coefficient, the lift coefficient and the moment coefficient, and the Strouhal number for the fixed structure. Circular cross-sections with and without fins are tested. Adding fins to the models is seen to increase the drag. In-line response oscillations have also been measured. A comparison between the measured in-line vibration response of a circular cross-section is done to the DNV GL in-line response model. Results show that the DNV GL model correspond well with measured response.

For the tube cross-section with fins, the Strouhal number is 0.18 at a Reynolds number of $4x10^4$ (Hansen, 2015). Also, two similar tubes in tandem are tested for different center-to-center/diameter ratios. For the relevant ratio (3.33), the Strouhal number is $\tilde{0}.15$ for a Reynolds number of $4x10^4$.

The wind tunnel experiments have shown that the in-line vortex-induced vibrations of neutrally buoyant structures in air are very similar to equivalent experiments in water (Hansen, 2015).

Chapter 4

Theory

4.1   General Loads

The following is adapted from the author's Project thesis. The loads acting on an SFTB consist of permanent and time-varying loads. Permanent or static loads are summarized as

- Self-weight

- Buoyancy

- Current

Time-varying loads are summarized as

- Wave loads

- Wind loads

- Marine growth

- Water absorbed by the structure

- Traffic loads

- Tidal loads

- External water pressure

- Accidental loads and impacts

Wind loads are only relevant for SFTBs that are supported by pontoons in the surface, as they will be exposed to wind in the atmosphere. In accidental loads, earthquake loads, and ship and submarine impacts are included. In this report, the loads considered are self-weight, buoyancy, current and wave loads.

4.2 Static Actions

4.2.1 Permanent Loads

Self weight of the structure includes the weight of the tubes, equipment, asphalt, ballast etc. A tether-stabilized tube should be designed to have a net buoyancy, to always maintain a positive tension in the supporting tethers. The equilibrium equation can be seen in equation 4.1.

$$F = W - B = mg - \rho_w g \nabla \tag{4.1}$$

F is the force, W is the weight, B is the buoyancy, m is the mass, g is the gravitational constant, ρ_w is the water density and ∇ is the displaced volume in water by the tube.

The magnitude of the net buoyancy must be considered in relation to the stress that will be at the end supports of the bridge. A large buoyancy in the bridge, will give larger stresses and moments to the supports. This need to be balanced, and careful design where the whole static system is considered must be performed in order to save the bridge from unwanted and unnecessary stresses.

4.2.2 Current Actions

The mean drag force, F_C from a current stream can be calculated according to equation 4.2 (Reinertsen et al., 2015b).

$$F_C = \frac{1}{2} \rho_w C_D D U_c^2(z) \tag{4.2}$$

ρ_w is the water density, C_D is the 2D drag coefficient for a single tube, D is the tube diameter and $U_C(z)$ is the current velocity at depth z. The drag coefficient depends on the Reynolds number and the roughness of the surface. According to Reinertsen et al. (2015b), the Reynolds number for a 100 year current flow past the tube is estimated to $5x10^6$. Consequently, the roughness for a circular concrete tube can be taken at k/D = $3x10^{-3}$, where k is the characteristic dimension of the roughness on the body surface, giving a steady drag coefficient of 1.0 (Det Norske Veritas, 2014).

When two tubes are placed in tandem, there will be a reduced inflow velocity on the second tube, see figure 4.1. Equation 4.3 is taken from Blevins (2005). $U_w(x)$ is the average velocity in the wake at point x, which is the centre-to-centre distance between the two cylinders, when the vertical offset between the cylinders is set to zero (y = 0). The equation can be expected to be valid when x exceeds a few cylinder diameters. For this case, x = 3.17D, and the equation is assumed to be valid.

$$U_w(x) = U_C \left(1 - 1.2 \sqrt{C_D \frac{D}{x}} \right) \tag{4.3}$$
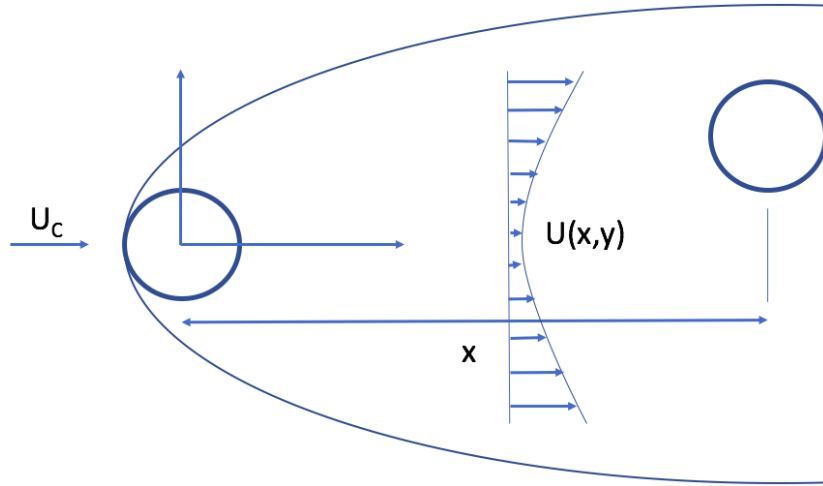
Figure 4.1: The wake of a cylinder. The current velocity in the wake of the upstream cylinder is reduced.

$U_C(z)$ is the inflow current velocity of the first cylinder. Thus, in the case of a 12.6m tube in an x = 40m distance, with a drag coefficient of 1, the equation simplifies to

$$U_w(x = 40) = U_C \left(1 - 1.2\sqrt{1\frac{12.6}{40}} \right) = 0.327 U_C \tag{4.4}$$

and the expected inflow current of the second tube is reduced to ~ 0.33 of the initial current velocity.

Huse (1993) gives the formula for the current velocity at the downstream cylinder, close to the upstream cylinder (when the vertical offset between the cylinders is set to zero) as in equation 4.5.

$$U_w = U_C \left(1 - \sqrt{\frac{C_D D}{\frac{4D}{C_D} + x}} \right) \tag{4.5}$$

With the same inserted values as in equation 4.4, this gives

$$U_w = U_C \left(1 - \sqrt{\frac{1 * 12.6}{\frac{4*12.6}{1} + 40}} \right) = 0.627 U_C \tag{4.6}$$

~ 0.63 of the initial current velocity is almost 2x the value found in equation 4.4. Obviously the estimation of currents in wakes, are subject to much uncertainties. A lower current velocity will give a lower drag force on the structure. In terms of dynamic loads, it will give a lower reduced velocity, resulting in a lower risk of vibrations, according to Det Norske Veritas (2006), as will be further explained in section 4.4.

4.3 Dynamic Actions

4.3.1 Wave Actions

Morisons Equation

For slender structures, where the cross-sectional dimensions are smaller than the wave length, the Morisons equation can be used to calculate wave actions, if the condition in equation 4.7 is satisfied, i.e. if the wave length is larger than five times the diameter.

$$\lambda > 5D \tag{4.7}$$

λ is the wave length and can be calculated using the three equations 4.8 - 4.10. Equation 4.8 is the relation between the wave number k and the wave length, equation 4.9 is the dispersion relation for deep water, and equation 4.10 is the relation between the angular frequency and the period, T. Deep water is assumed since the depth is larger than half the wave length (Pettersen, 2007).

$$k = \frac{2\pi}{\lambda} \quad (4.8) \qquad\qquad \omega^2 = kg \quad (4.9) \qquad\qquad \omega = \frac{2\pi}{T} \quad (4.10)$$

Using relevant values from the environment in the Bjørnafjord, a wave period of 15 s for swell and 4.5 s for wind-sea, it is seen that the condition in equation 4.7 is satisfied for swell conditions. Therefore, the Morisons equations are applicable for the swell waves that the SFTB is experiencing. Comparing the value for the exponential decay for both the wind-sea and swell, it is seen that swell is also the governing wave type at the depth of the SFTB, as seen in figure 4.2. In this decay, the assumption of deep water is used in the dispersion relation.
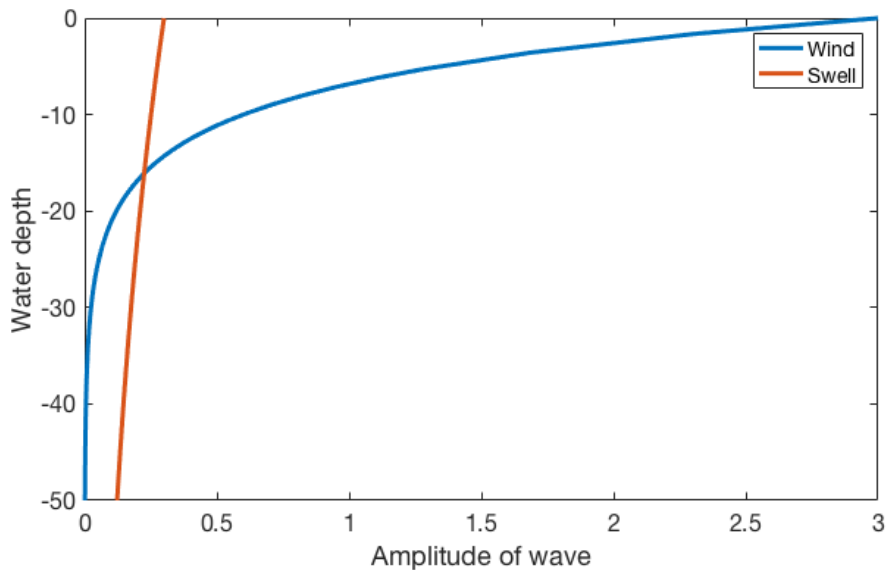
Figure 4.2: Wave decay for wind-sea and swell waves in the Bjørnafjord.

Morisons equation valid for a moving tube is given in equation 4.11.

$$F = -\rho_w C_A A\ddot{r} + (1 + C_A)\rho_w A\dot{v} + \frac{1}{2}\rho_w C_D D v_r^2 \qquad (4.11)$$

C_A is the added mass coefficient, A is the cross-sectional area, $\ddot{r}$ is the acceleration of the tube, $\dot{v}$ is the fluid particle acceleration and v_r is the relative velocity between the wave particles and the tube (Reinertsen et al., 2015b). The equation consist of an inertia force and a drag force, where the latter is the equivalent of the current force. The first term is the added mass force acting in opposite direction to the tube acceleration.

Wave Induced Loads on Large-volume Structures

For extreme wind-sea conditions, the condition in equation 4.7 is no longer satisfied for tubes with diameters above 12m. In this case, wave diffraction effects become important. The structure is thus categorized as a large-volume structure, and wave loads must be calculated from 3D diffraction theory. Waves and current on three different time scales are relevant for a floating, moored structure.

- Wave frequency motions

- Low frequency motions

- High frequency motions

Wave frequency causes the largest wave loads and take place at the same frequency as the waves. Offshore structures are often designed such a way that the natural frequencies of the structure are kept well off from the wave frequency range. This is to avoid large resonant effects from the waves (Det Norske Veritas, 2014).

Due to non-linearities in the ocean surface waves and non-linear interactions between the waves and tubes, the SFTB will be excited also by second order wave loads. Low frequency motions, also named slow-drift motions, are caused by slowly-varying wave and wind loads (with high periods). High frequency motions are caused by higher-order (sum) frequency wave loads (with low periods).

The sum-frequency dynamic pressure decays slower than the first order pressure. Therefore, this non-linear wave load may be of importance for a tether-supported tube bridge. This is because the tether-supported bridge may have eigenperiods of the vertical modes in the order of 6-8 seconds and lower (Reinertsen et al., 2015b). For the SFTB in the Bjørnafjord, second order loads are neglected according to Reinertsen et al. (2016b).

Diffraction Theory

The wave induced loads in an irregular sea can be found by linearly superimposing the loads from regular wave components. Within a linear analysis, the hydrodynamic problem is divided into two sub-problems, the radiation problem and the diffraction problem (Det Norske Veritas, 2014). The wave force can be written as a sum of the wave excitation force F_{exc} and the wave radiation force F_{rad}, as seen in equation 4.12 (Reinertsen et al., 2015b).

$$F(x, t) = F_{exc}(x, t) + F_{rad}(x, t) \qquad (4.12)$$

The radiation forces are the forces originating from the added mass, damping and restoring terms, as seen in equation 4.13.

$$F_{rad} = -A_{kj}\frac{d^2\eta_j}{dt^2} - B_{kj}\frac{d\eta_j}{dt} - C_{kj}\eta_j \tag{4.13}$$

A_{kj}, B_{kj} and C_{kj} are the added mass, damping and hydrostatic restoring coefficients, respectively. j,k = 1,2,...6, for the six degrees of rigid body modes. A_{kj} and B_{kj} are functions of the wave frequency ω (Det Norske Veritas, 2014), further explained in the next section.

The wave excitation load is a sum of respectively, the Froude-Kriloff forces/moments and the diffraction forces/moments represented by the acceleration terms as in equation 4.14.

$$F_{exc} = \iint p n_{iS} ds + A_{i1}a_1 + A_{i2}a_2 + A_{i3}a_3 \tag{4.14}$$

where p is the pressure in the undisturbed wave field, $\boldsymbol{n} = $(n$_1$, n$_2$, n$_3$) is the unit vector normal to the body surface, defined positive into the fluid. The integration is done over the average wetted surface of the body. a$_i$ for i = 1, 2 and 3, is the acceleration component along the x- y and z-axes of the undisturbed wave field (Faltinsen, 1990).

4.3.2 Added Mass and Damping

Added mass and damping are dependent on frequency and body shape. The added mass goes to an asymptotic finite value for high frequencies in heave, while damping goes to zero. For low frequencies, the 2D added mass goes to infinity, while the damping also here goes to zero.

According to Pettersen (2007), we have frequency-independent added mass for a circular cylinder, at a submergence of three times the radius. The added mass for a line with a circular cross-section fully submerged is calculated according to equation 4.15.

$$A_{kj} = C_A \rho_w A \tag{4.15}$$

Coefficients can be found from (Det Norske Veritas, 2014).

4.3.3 Current Actions

VIV

Vortex-induced Vibrations are oscillations of slender structures due to being exposed to currents. When a fluid particle flows along a cylinder in a real flow, the pressure in the fluid will force the particle to separate from the cylinder at some point near the widest section of the cylinder, as seen in figure 4.3. This is due to viscous effects.

This separation point depends on the Reynolds number and the shape of the structure. The Reynolds number gives information about the flow type. For a fixed cylinder, the

COMPLETE VORTEX PAIR SHEDDING CYCLES -
WITH CROSS-FLOW RESPONSE

CROSS - FLOW
RESPONSE
DIRECTION

CURRENT
FLOW

IN - LINE
RESPONSE
DIRECTION

SINGLE VORTEX SHEDDING CYCLES -
ASSOCIATED WITH IN-LINE RESPONSE
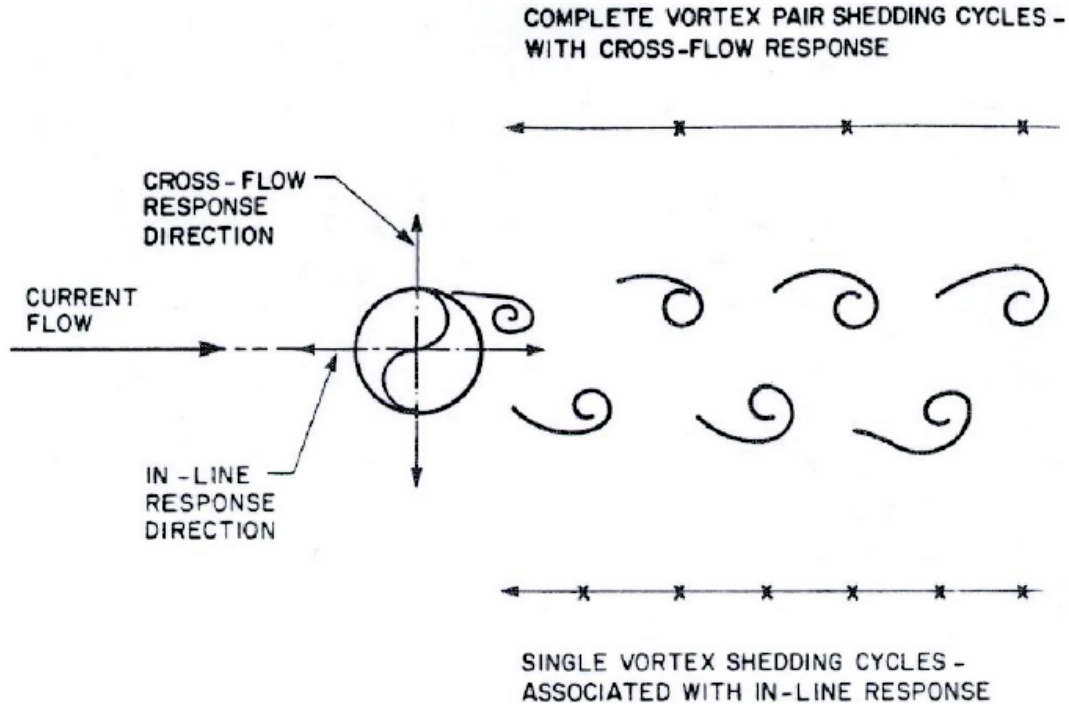
Figure 4.3: In-line and cross-flow response of vortex shedding. Flow separation on top of the cylinder illustrated by the shedding of a vortex (Kenny and Ltd, 1993).

Reynolds number Re, defines the vortex pattern and is given by

$$Re = \frac{UcD}{\nu} \tag{4.16}$$

were ν is the kinematic viscosity (Larsen, 2016).

From the separation point, the fluid inside the boundary layer will reverse and create a vortex. These vortices will be shed alternatingly from the top and bottom of the cylinder. The vortices create an oscillating drag force on the cylinder in the in-line (IL) direction and an oscillating lift force in the cross-flow (CF) direction, see figure 4.3. The cross-flow force will have a period identical to the shedding period, while the in-line force will have a period half the shedding period. The vortex shedding frequency f_s can be found from the Strouhal number, St, seen in equation 4.17.

$$f_s = \frac{StUc}{D} \tag{4.17}$$

The Strouhal number is a function of the geometry and the Reynolds number (Blevins, 1977).

VIV is a resonance problem. When the vortex shedding frequency for the fixed cylinder approaches the cylinders natural frequency (in still water), the vortex shedding suddenly locks onto the natural frequency (Blevins, 1977). This phenomena is called lock-in, and may induce resonance. The resulting frequency is a compromise between the vortex shedding frequency and the natural frequency, and is called the oscillation or the response frequency (Larsen, 2016).

For a dry structure, the vibrations will occur at the eigenfrequency of the structure. However, the frequency in water is also dependent on the hydrodynamic (added) mass, see equation 4.18. The oscillating frequency, f_{osc}, is influenced by the mass so that it is adjusted in the direction of the vortex shedding frequency (Larsen, 2016), see equation 4.18.

$$f_{osc} = \frac{1}{2\pi}\sqrt{\frac{k}{m}} = \frac{1}{2\pi}\sqrt{\frac{k}{m_{dry} + m_a}} = \frac{1}{2\pi}\sqrt{\frac{k}{m_{dry} + \rho_w C_A \frac{\pi D^2}{4} L}} \quad (4.18)$$

k is the stiffness, m_{dry} is the dry mass, m_a is the added mass, C_A is the added mass coefficient, and L is the length of the cylinder.

The region where lock-in may occur is defined by the dimensionless number, the reduced velocity, V_R(Reinertsen et al., 2015b), as defined in equation 4.19

$$V_R = \frac{U_C}{f_n D} \quad (4.19)$$

f_n is the natural frequency and D is the projected dimension normal to the flow, often the diameter. More information given in section 4.4.

4.4 DNV-RP-F105 - VIV Guidelines

Det Norske Veritas GL has provided the most relevant guideline for VIV, DNV-RP-F105 (2006). The guideline is meant for subsea steel pipelines, but may also be used for non-circular cross-sections and concrete structures, as long as other hydrodynamic phenomena are accounted for, according to Reinertsen et al. (2015b). Ranges of reduced velocities where lock-in may occur are given. For the present case, in-line VIV is relevant for the tubes and tethers, and cross-flow VIV is relevant for the tethers only. Since the tubes are held down by the tethers, this will limit the cross-flow motion and consequently only in-line is of interest. The steel tethers will perhaps have a more similar behaviour to the empirical VIV response model, because of its more similar dimensions and material to steel pipelines.

Important for the SFTB is also the tandem effect between the two tubes and between the four tethers in groups. This effect is not included in the current guideline.

4.4.1 DNV GL Response Models

The response amplitudes depend on the reduced velocity, V_R, the Keulegan-Carpenter number, KC, the current flow velocity ratio α, the turbulence intensity I_c, the flow angle relative to the pipe θ_{rel} and the stability parameter, K_S. The Keulegan-Carpenter number is defined as

$$KC = \frac{U_w}{f_w D} \quad (4.20)$$

where U_w is the significant mean wave-induced flow velocity and f_w is the (significant) wave frequency. The stability parameter is given by

$$K_S = \frac{4\pi m_e \zeta_T}{\rho_w D^2} \quad (4.21)$$

and represents the damping for a given modal shape. The effective mass, m_e is defined by

$$m_e = \frac{\int_L m_s \phi(s)^2 ds}{\int \phi(s)^2 ds} \quad (4.22)$$

where $\phi(s)^2$ is the assumed mode shape satisfying the boundary conditions and m_s is the mass per unit length including the structural mass, added mass and mass of internal fluid (Det Norske Veritas, 2006). The total damping ratio, ζ_T, comprises structural damping, soil damping and hydrodynamic damping.

4.4.2 In-line Response Model

The in-line response model applies for all in-line vibration modes. It is dependent on the reduced velocity, V_R, and the stability parameter, K_S. A_y / D is defined as the maximum in-line VIV response amplitude (normalised with D), as a function of V_R and K_{Sd}. This is illustrated in figure 4.4. K_{Sd} is found by the use of a safety factor, explained in section 4.4.4.
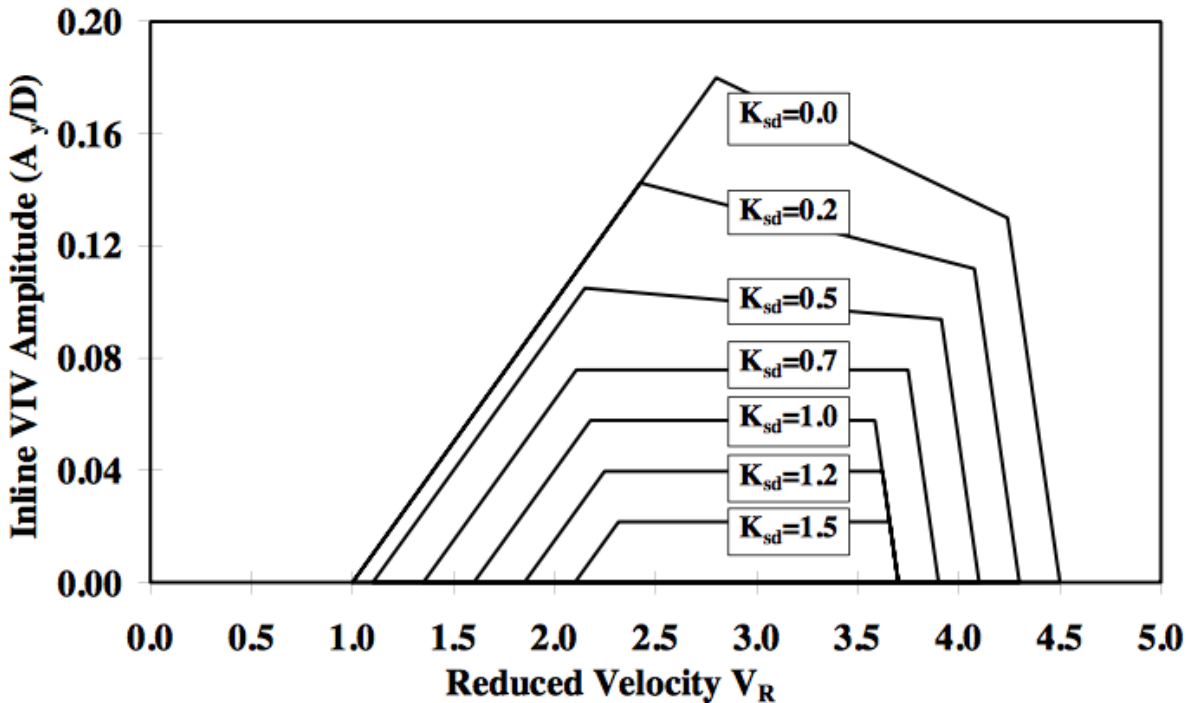
Figure 4.4: The in-line response model provided by DNV GL (Det Norske Veritas, 2006).

It can be noted from the figure that in-line VIV is generated with a minimum reduced velocity of 1, where the stability parameter K_{Sd} is 0.

4.4.3 Cross-flow Response Model

Cross-flow VIV depend on the reduced velocity V_R, the Keulegan-Carpenter number, KC and the current flow velocity ratio α. The cross-flow VIV amplitude A_z / D as a function of V_R, KC and α is seen in figure 4.5. It is observed that in-line VIV may
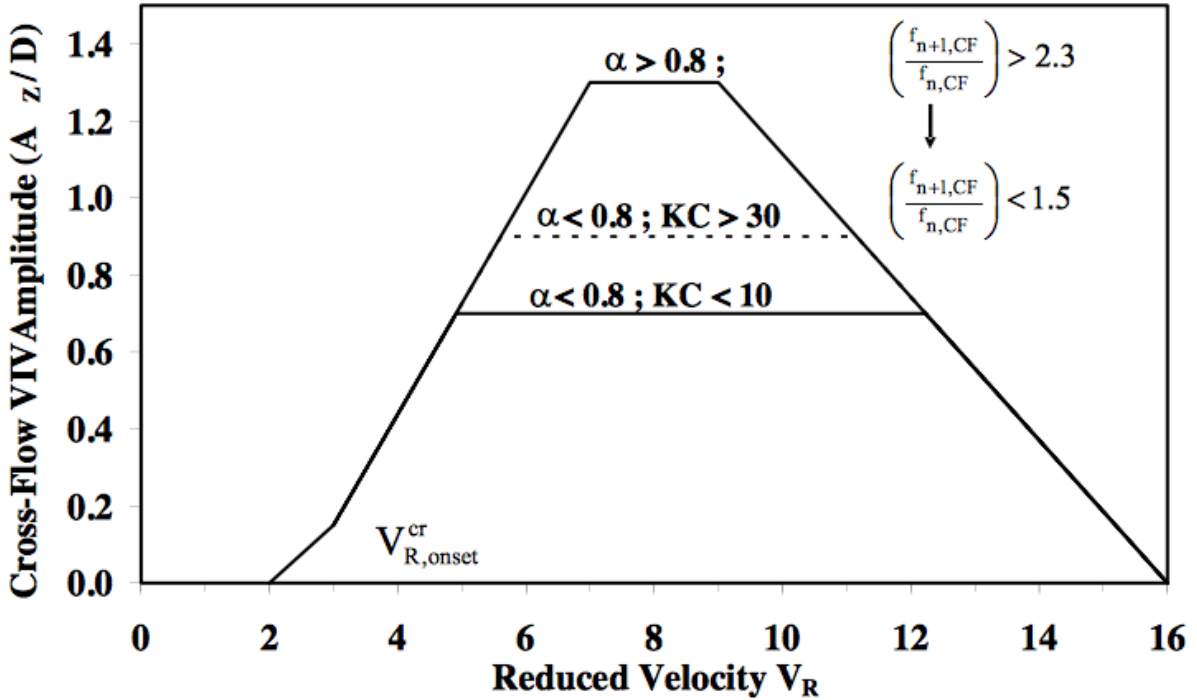
Figure 4.5: The cross-flow response model provided by DNV GL (Det Norske Veritas, 2006).

occur for lower current velocities than for cross-flow, as the reduced velocity onset is lower than for cross-flow. Also, the range where cross-flow may occur is larger.

4.4.4 Safety Factors

DNV GL recommends that design values for the reduced velocity, V_{Rd}, and stability parameter, K_{Sd}, shall be applied for both in-line and cross-flow. The design values are obtained by use of safety factors, as in the equations below.

$$V_{Rd} = V_R \gamma_f \qquad (4.23)$$

$$K_{Sd} = \frac{K_S}{\gamma_k} \qquad (4.24)$$

γ_f and γ_k are safety factors related to the natural frequency and damping respectively and are given for class *very well defined spans* in table 4.1.

The free span category giving related values for γ_k is chosen as *very well defined* spans, i.e. spans where important span characteristics like span length, gap and effective axial force are determined with a high degree of accuracy, because the span for the tubes and tethers are well known. Conditions for soil and environment along the route are

Table 4.1: Safety factors to be used with VIV models

Safety Class	Low	Normal	High
γ_f	1.0	1.0	1.0
γ_k	1.0	1.15	1.30

well known, and the safety factors are chosen from Safety Class "normal" since no other specification is given.

4.4.5 Accelerations

From the in-line vibration amplitudes, the horizontal accelerations, a, can be calculated from equation 4.25.

$$a = A\omega^2 = A(f_n 2\pi)^2 \tag{4.25}$$

A is the amplitude, ω is the angular natural frequency and f_n is the natural frequency.

4.5 Modal Analysis

Modal analysis is the study of dynamic properties of systems in the frequency domain. The stiffness and mass of a structure is used to find the periods in seconds at which the structure will naturally resonate. These periods are important to note, to make sure that the natural frequency of the structure is not the same as the frequency of an expected load in its environment. If this resonance occur, the structure may experience damage as large deflections and large moments will be induced. Methods for estimating the eigenfrequencies of a structure is presented in section 4.6 and 4.7. If the angular eigenfrequency in rad/s is known, the eigenfrequency in hertz can be found by equation 4.26, and the eigenperiod in seconds can be found by 4.27.

$$f_n = \frac{\omega_n}{2\pi} \tag{4.26} \qquad\qquad T_n = \frac{2\pi}{\omega_n} \tag{4.27}$$

4.6 Analytical Solution for Eigenfrequencies

4.6.1 Stretched Wire

For a stretched wire with a tension, T, that is fixed in both ends, the angular eigenfrequency, ω_{sn} in rad/s is given by

$$\omega_{sn} = \frac{n\pi}{l}\sqrt{\frac{T}{m}} \tag{4.28}$$

where n = 1,2,... ∞ is the frequency and mode number and l is the length (Timoshenko et al., 1974).

4.6.2 Simple Beams

For a straight beam with a constant cross-section, the angular eigenfrequency ω_n can be found by equation 4.29. The eigenvalues, $\bar{\omega}_n$ for a beam with fixed ends, needed for the straight beam equation, are listed in table 4.2 (Larsen, 2015). According to (Søreide and Brekke, 1989), equation 4.30 is valid if the beam is curved. E is the elasticity modulus, I is the area moment of inertia, A is the cross-sectional area and H is the sagitta of the circular arch. The equation for curved beams is valid for the first frequency. For the further frequencies, the bow effect can be neglected (Søreide and Brekke, 1989).

$$\omega_{n,straight} = \bar{\omega}_n \sqrt{\frac{EI}{ml^4}} \tag{4.29}$$

Table 4.2: Eigenvalues, $\bar{\omega}_n$, to be used with equation 4.29.

n=1	n=2	n=3	n>3
22.37	61.67	120.9	$\left(\frac{2n+1}{2}\pi\right)^2$

$$\omega_{1,curved} = \sqrt{\frac{\pi^4 EI}{ml^4}\left(1 + \frac{AH^2}{2I}\right)} \tag{4.30}$$

For a simply supported beam in tension, the eigenfrequency, ω_{bt} is defined by equation 4.31 (Larsen, 2015). This equation is especially relevant for the tethers. It is observed that the frequency is dependent on the axial tension in the beam as well as the bending stiffness of the beam. It can also be noted that for long lengths, the beam will be more and more dependent on the tension and the bending stiffness will contribute less.

$$\omega_{bt} = \frac{n\pi}{l}\sqrt{\frac{T}{m} + \frac{n^2\pi^2}{l^2}\frac{EI}{m}} \tag{4.31}$$

4.6.3 Beams on Elastic Foundations

Timoshenko et al. (1974) states that the angular frequencies of a straight beam on an elastic foundation is

$$\omega_n = k_n^2 \sqrt{\frac{EI}{m}}\sqrt{1 + \frac{k_f}{EIk_n^4}} \tag{4.32}$$

where k_f is the foundation modulus, defined as the load per unit length necessary to produce a displacement of the foundation equal to unity. It is noted that the frequency is a sum of the frequency of the beam and the foundation stiffness. The nonzero roots k_{nl} for a beam with fixed ends may be approximated by

$$k_n l \approx \left(i + \frac{1}{2}\right)\pi \tag{4.33}$$

The resulting equation will then look like

$$\omega_n = \sqrt{\frac{((n+\frac{1}{2})\pi)^4}{l^4}\frac{EI}{m} + \frac{k_f}{m}}$$

(4.34)

Winkler Foundation Model

According to Kerr (1964), Winkler released in 1867 a way to model an elastic foundation. The model is based on the assumption that the foundation consist of closely spaced discrete independent linear springs and is a one-parameter model. The vertical displacement of a point is proportional to the pressure at that point. The model neglects interaction between the springs, and leads therefore to a discontinuous displacement field. The pressure-deflection relation at any point is given by the equation 4.35, where p is the pressure and w is the deflection (Kerr, 1964). k is the modulus of subgrade reaction and will in this case be the foundation modulus, k_f.

$$p = kw$$

(4.35)
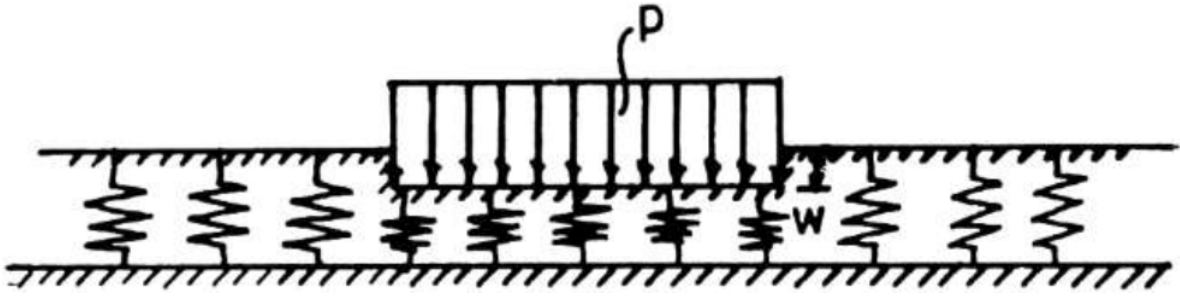
Figure 4.6: The one-parameter Winkler Foundation Model (Kerr, 1964).

Model of Tether Foundation

From this theory, a model to represent the tethers as the Winkler springs can be made. The foundation modulus in horizontal and vertical direction is thus modelled as a sum of the stiffness in all tethers in the horizontal and vertical direction respectively, divided by the total length of the bridge. This is to achieve the right form of the foundation modulus of Timoshenko.

For the horizontal motion, the stiffness is dependent on the tension in the tethers and the bending stiffness

$$k_{f,hor} = \frac{\sum_j \sum_i k_{tether}}{L_{bridge}} = \frac{\sum_j \sum_i \frac{T}{l_{teth}} + \frac{E_{teth}I_{teth}}{l_{teth}}}{L_{bridge}}$$

(4.36)

For the vertical motion, the stiffness is dependent on the axial stiffness of the tethers.

$$k_{f,vert} = \frac{\sum_j \sum_i k_{tether}}{L_{bridge}} = \frac{\sum_j \sum_i \frac{E_{teth}A_{teth}}{l_{teth}}}{L_{bridge}}$$

(4.37)

where j is the number of tether groups, and i is the number of tethers per group (Leira, 2017). In this model it is assumed that the tethers are equally spaced and the effect of a curved bridge is not included.

4.7 Generalized Modal Analysis

A generalized modal analysis can be used to find the natural frequencies and periods of the bridge. The method explained here is found in Reinertsen et al. (2015b) and is simplified since it assumes a straight bridge. The modal mass and stiffness in sway and heave can be found from equations 4.38 - 4.41. A shape function for the displacement is assumed as equation 4.42, from where the curvature is found. Displacement and curvature for the first two modes are seen in figures 4.7 and 4.8. The angular frequencies are found from 4.46.

$$M_{sway,n} = \int_0^L m_{tube}\phi(x,n)^2 dx + \frac{1}{3}m_{teth}\sum_i \phi(j_i,n)^2 \tag{4.38}$$

$$K_{sway,n} = \int_0^L EI_z \frac{d^2}{dx^2}\phi(x,n)^2 dx + k_{teth,hor}\sum_i \phi(j_i,n)^2 \tag{4.39}$$

$$M_{heave,n} = \int_0^L m_{tube}\phi(x,n)^2 dx + m_{teth}\sum_i \phi(j_i,n)^2 \tag{4.40}$$

$$K_{heave,n} = \int_0^L EI_y \frac{d^2}{dx^2}\phi(x,n)^2 dx + k_{teth,vert}\sum_i \phi(j_i,n)^2 \tag{4.41}$$

$$\phi(x,n) = e^{-\beta(n)x} - cos(\beta(n)x) + \alpha(n)sin(\beta(n)x) - (-1)^n \frac{e^{\beta(n)(x-L)} - e^{\beta(n)(x+L)}}{1 + e^{2\kappa(n)}} \tag{4.42}$$

$$\alpha(n) = \frac{sin(\kappa(n))}{(-1)^n - cos(\kappa(n))} \tag{4.43}$$

$$\beta(n)x = \kappa(n)\frac{x}{L} \tag{4.44}$$

$$\kappa(n) = (n + \frac{1}{2})\pi - \frac{(-1)^n}{cosh((n+\frac{1}{2})\pi)} \tag{4.45}$$

$$\omega(n) = \sqrt{\frac{K(n)}{M(n)}} \tag{4.46}$$

$\frac{d^2}{dx^2}\phi(s)$ is the second derivative of the mode shape, $k_{teth, vert}$ is the vertical stiffness that comes from the axial stiffness in the tether multiplied with the number of tethers in one group. $k_{teth, hor}$ is the horisontal stiffness that comes from the tension in all tethers in one tether group. $\alpha(n)$, $\beta(n)$ and $\kappa(n)$ are parameters dependent on the mode number to be used in the shape function $\phi(s)$.

$$k_{teth,vert} = N_{teth}\frac{EA}{l} \tag{4.47}$$

$$k_{teth,hor} = N_{teth}\frac{T}{l} \tag{4.48}$$
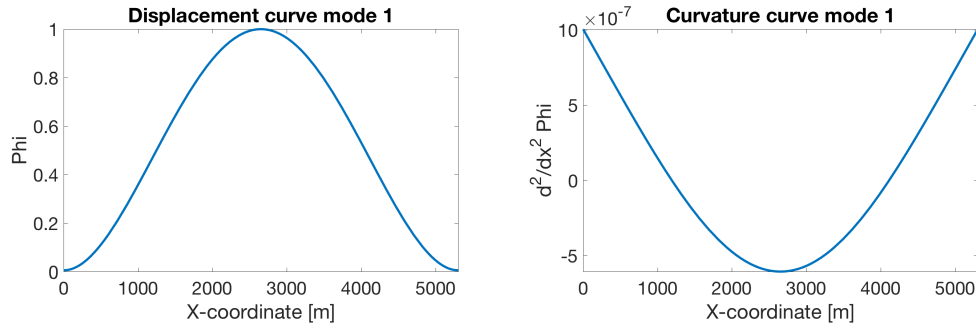
Figure 4.7: Displacement and curvature of mode 1.
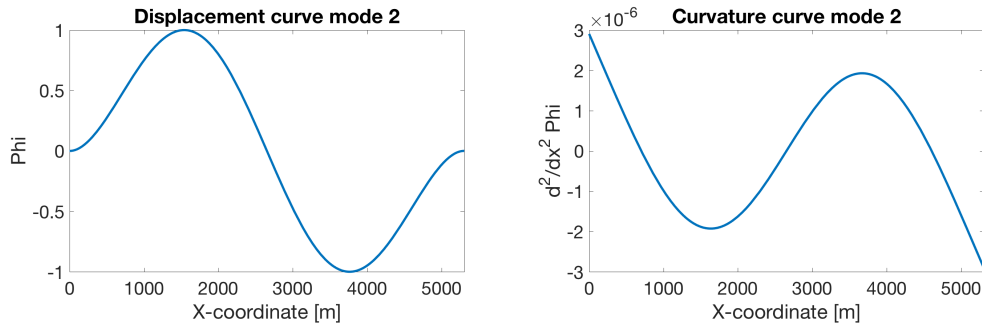
Figure 4.8: Displacement and curvature of mode 2.

4.8 Stress Calculation within Cross-section

The stress, σ at any point, defined by (y,z), of a cross-section, illustrated in figure 4.9, can be calculated from

$$\sigma = \frac{F}{A} + \frac{M_y}{I_y}z + \frac{M_z}{I_z}y \tag{4.49}$$

F is the axial force, A is the cross-sectional area, M_y and M_z are the moments about the y- and the z-axis and I_y and I_z are the second moment of area about the y- and z-axis.
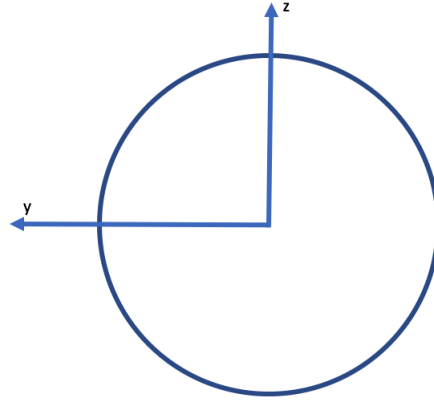
Figure 4.9: Cross-section definition.

4.9 Computing Moments from Curvature

The differential equation for an elastic beam in the horizontal plane is given by

$$\frac{d^2 w}{dx^2} = \frac{M_z}{EI_z} \tag{4.50}$$

where w is the horizontal deflection, M_z is the moment about the z-axis. $\frac{d^2 w}{dx^2}$ is the curvature of the displacement. By finding the displacement field w for a given load, the curvature can be found by double differentiation of the displacements. Then the moment can be calculated from the equation by use of the elasticity modulus, E and the second moment of area, I_z.

By assuming the deflection of the tube to be of a sinus curve, see equation 4.51, the curvature can be found by double derivation of the function. The maximum moment is then found where the deflection is largest, i.e. sin() = 1.

$$y = sin\left(\frac{n\pi x}{L}\right) \tag{4.51}$$

n is the number of half waves that the mode shape shall represent. For a mode shape with one half wave and also accounting for end/stiffening effects, equation 4.52 can be used (Reinertsen and Dr. techn. Olav Olsen, 2013).

$$M_{viv,1} = A\left(\frac{2\pi}{L(1 - \frac{0.33}{2})}\right)^2 EI_z \tag{4.52}$$

4.10 Computational Software

4.10.1 Sima/Riflex

The following is adapted from the author's Project Thesis. Sima is a simulation and analysis tool for marine operations and floating systems, developed by SINTEF Ocean. It covers the whole process from modelling to results, built on software for non-linear

time-domain analysis. Sima gives the graphical representation for many computer programs, two of them being Riflex and Vivana.

Riflex is a computer program for analysis of slender structures, often applied to risers (Marintek, a). Slender structures are characterized by small bending stiffness, large deflection, large upper end motion excitation, nonlinear cross-section properties and complex cross-section structure.

When modelling the cross-section of a structure in Riflex, usually a global cross-section is applied. This means that the properties such as axial, bending- and torsional stiffness must be calculated and specified as input. Therefore only global deformations and stresses will be calculated, not considering local response in the different cross-section layers and materials. Riflex computes static and dynamic characteristics of the structure. The dynamic analysis comprises eigenvalue analysis and response to both harmonic and irregular wave- and motion excitation. The structural analysis part of Riflex is based on a nonlinear finite element formulation (Marintek, b).

In Riflex, the main building blocks relevant for this case are supernodes and lines. Each line is designated a line type and each line type is designated a cross-section. A line can have several segments with different line types. An illustration of the system definition is seen in figure 4.10. Every line meeting at a connection need to be connected to the same supernode for the connection to be rigid.
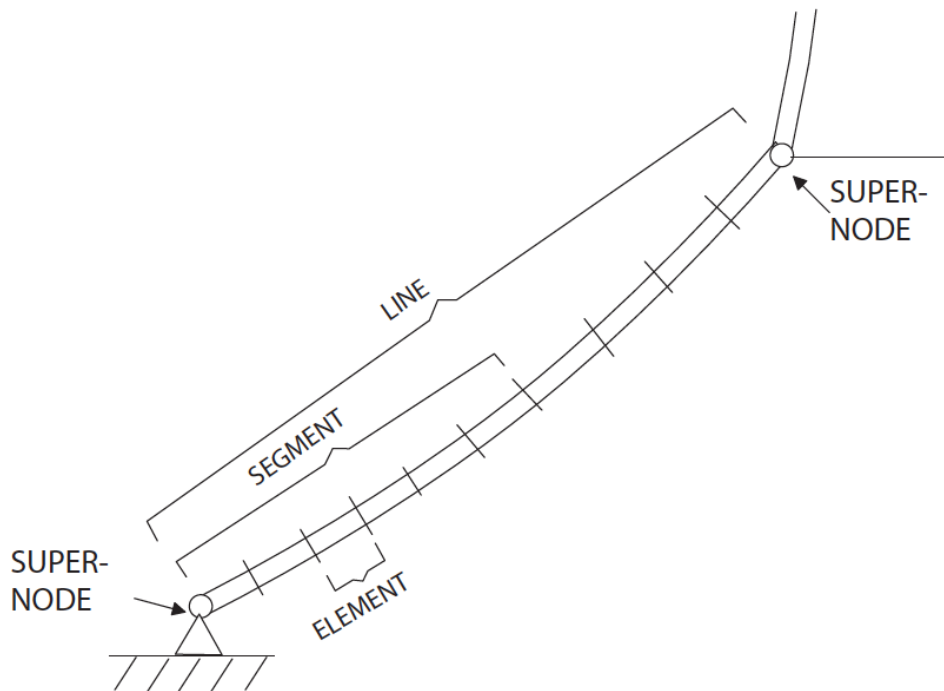
Figure 4.10: System definition in Riflex (Marintek, b).

The program system consist of five modules, namely IMPMOD, STAMOD, DYNMOD, FREMOD and OUTMOD. IMPMOD reads the input data, such as node coordinates, line topology and information about cross-sections. STAMOD performs the static analysis and is also used to find the initial equilibrium configuration before a dynamic analysis. DYNMOD performs the time domain dynamic analysis based on the static
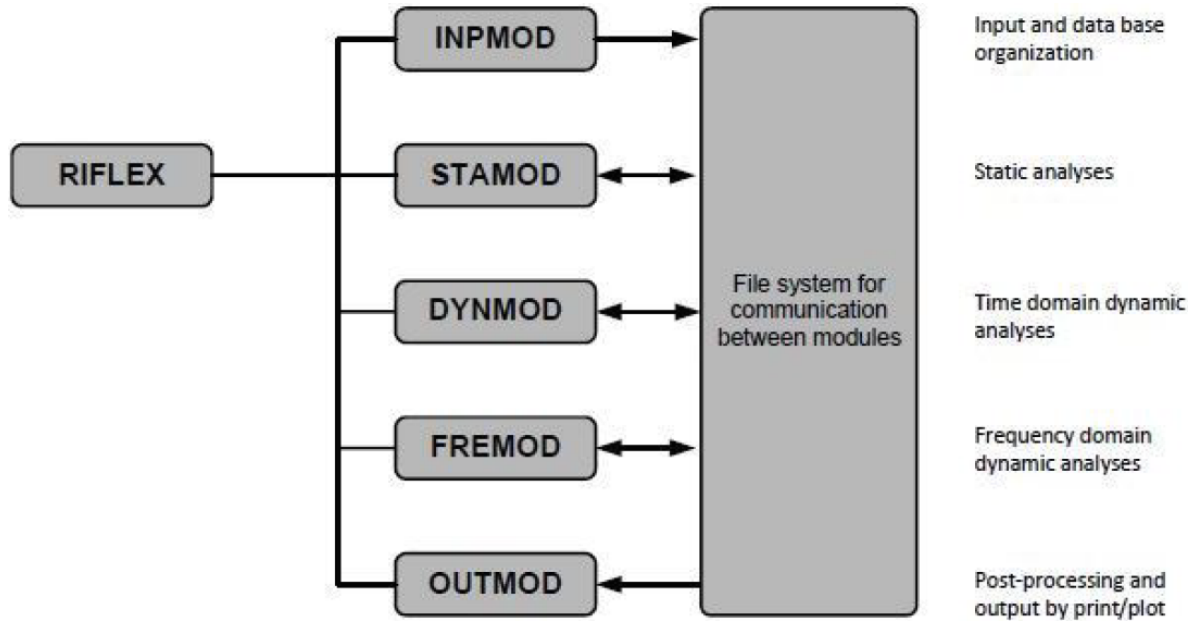
Figure 4.11: System definition in Riflex (Marintek, b).

equilibrium and environmental data. The natural frequencies and mode shapes are also calculated by DYNMOD. OUTMOD performs the post-processing of results generated by STAMOD and DYNMOD (Marintek, b).

4.10.2 Static Analysis in Riflex

The static analysis gives the response or the nodal displacements when the structure is in equilibrium with the applied loads. An initial configuration is used as a starting point and Riflex uses an iteration process to find the equilibrium position by applying a nonlinear finite element analysis (Marintek, b). The loads are assumed to be applied in a slow manner, so that inertia and damping is not considered.

Incremental and Iterative Methods

Euler-Cauchy Method
Static equilibrium is found numerically by application of an incremental loading procedure. The incremental-iterative procedure used by Riflex is the Euler-Cauchy incrementation. Internal and external forces will in general be nonlinear functions of the nodal displacement vector, and the nonlinear problem is solved by an iterative application of the external loading. The loading $\boldsymbol{R}$ is divided into small load increments. Increments of the displacement Δr are found by applying the loading increments stepwise by equation 4.53 and the total displacement, $\mathbf{r}$ is found by summing all the displacement increments. $\boldsymbol{K}_{\mathrm{I}}$ is the incremental stiffness (Moan, 2003).

$$\mathbf{K_I}(r)d\mathbf{r} = d\mathbf{R} \tag{4.53}$$

$$r_1 = \Delta r_1 \approx K_1(0)^{-1} \Delta R_1$$

$$r_2 = r_1 + \Delta r_2 = r_1 + K_1(r_1)^{-1} \Delta R_2$$

$$r_3 = r_2 + \Delta r_3 = r_2 + K_1(r_2)^{-1} \Delta R_3$$

$$\vdots$$
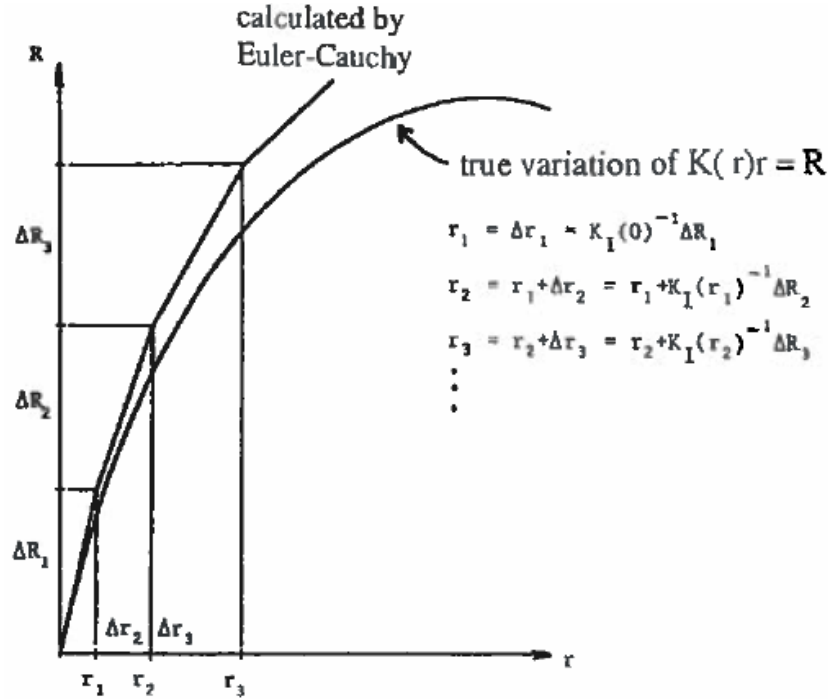
Figure 4.12: Euler Cachy incrementing (Moan, 2003).

Newton-Raphson Method

Iteration techniques can be used to improve the original solution. The Newton-Raphson approach is adopted in Riflex. The algorithm is as in equation 4.54, and the iteration is stopped when the accuracy is acceptable. This acceptance is in this case found from a modified Euclidean displacement norm and is as in equation 4.55, where ϵ is a specified tolerance requirement (Moan, 2003). x_n is the displacement at step n, x_{n+1} is the displacement at step n+1. For more information, see Marintek (a).

$$x_{n+1} = x_n - \frac{f(x_n)}{f'(x_n)} \tag{4.54}$$

$$\frac{\|\Delta r_k^j\|}{\|r_k^j\|} < \epsilon \tag{4.55}$$

4.10.3 Dynamic Response Analysis in Riflex

The purpose of this type of analysis is to study the influence of direct wave induced loads on the system. In the case of a support vessel to a riser, the influence of these vessel motions and the coupling, would be included. A static analysis to define equilibrium condition should initially be carried out (Marintek, b).

In a dynamic analysis, also mass and damping will be of importance, as the loads no longer are applied in a very slow manner. The dynamic equilibrium is therefore dependent on these terms, in addition to coupling between the external load and structural displacement and velocity. As for the static case, there is also for the dynamic case, a
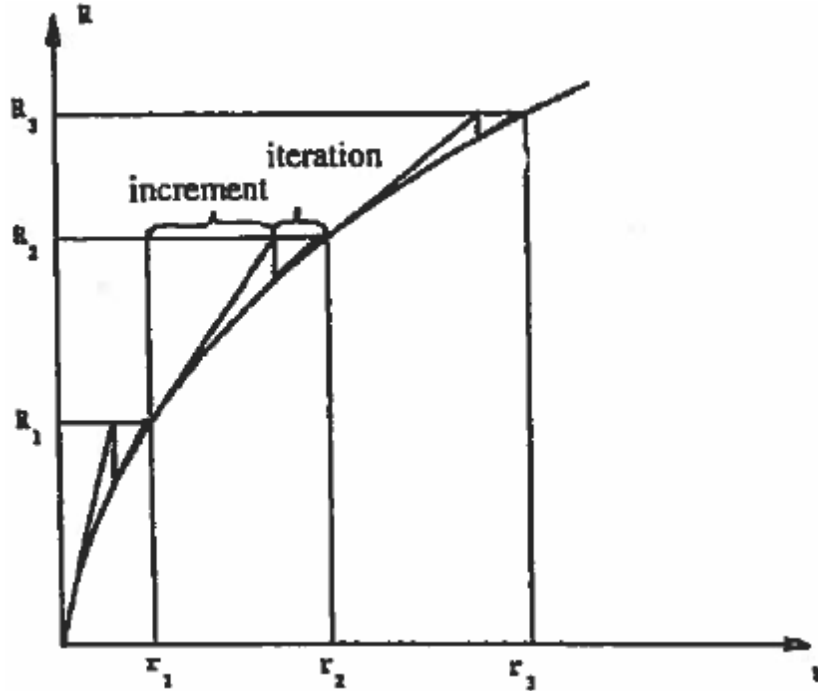
Figure 4.13: Euler Cachy with modified Newton-Raphson iteration (Moan, 2003).

nonlinear relationship between the internal forces and displacements. For a spatially, discretized finite element system model, the dynamic equilibrium equation is given as

$$\mathbf{R^I}(r, \ddot{r}, t) + \mathbf{R^D}(r, \dot{r}, t) + \mathbf{R^S}(r, t) = \mathbf{R^E}(r, \dot{r}, t) \qquad (4.56)$$

where R^I, R^D, R^S and R^E are inertia, damping, internal structural reaction and external force vectors. And r, $\dot{r}$ and $\ddot{r}$ are structural displacement, velocity and acceleration vectors, respectively.

The external force vector accounts for weight and buoyancy, forced displacement due to support vessel motions, drag and wave particle acceleration terms in the Morison equation, given in equation 4.11 and specified discrete nodal point forces. The inertia force vector includes structural mass, internal fluid mass and hydrodynamic mass accounting for the structural acceleration terms in the Morison equation as added mass contributions in local directions. The damping force vector includes internal structural damping, hydrodynamic damping and specified discrete dashpot dampers.

Time Integration

A solution to an equation like 4.56 can be given in the time domain and in the frequency domain. The equation is an initial-value problem where the solution is given by the start values. Next, the practical numerical integration method for such problems can be described as a stepwise process. The studied time domain is divided into sub-time domains and the solution is found by using the obtained values from the current calculation as initial values for the next time step calculation. The smaller the time

steps, the more accurate solution. For the numerical integration method, velocity and displacement are found at each new time step by integrating the acceleration twice. Different methods based on the assumptions on how the acceleration will vary can be applied. Here, the Newmark β-family is used. The equations are obtained by a Taylor-series expansion and given as

$$\dot{r}_{k+1} = \dot{u}_{k+1} = \dot{u}_k + (1 - \lambda)h\ddot{u}_k + \lambda h\ddot{u}_{k+1} \tag{4.57}$$

$$r_{k+1} = u_{k+1} = u_k + h\dot{u}_k + (\frac{1}{2} - \beta_w)h^2\ddot{u}_k + \beta_w h^2\ddot{u}_{k+1} \tag{4.58}$$

where h is the time step length and λ and β_w are parameters determined by requirements related to stability and accuracy. λ depends on whether the method has artificial damping, but is normally set to 0.5 to obtain a second order accuracy (Langen and Sigbjörnsson, 1979; Marintek, a). β_w is given according to the time integration technique used. For more details see Langen and Sigbjörnsson (1979).

Rayleigh Damping Model

The damping model used is the Rayleigh, or proportional damping model, which is a linear combination of the mass and stiffness matrices. By using this, a proportionality to the velocity of each mass point, and to the the strain velocity at each point is assumed. α_m and α_s are denoted the mass- and stiffness proportional damping coefficients.

$$\mathbf{C} = \alpha_m\mathbf{M} + \alpha_s\mathbf{K} \tag{4.59}$$

The orthogonality of the structural damping matrix to the eigenvectors can be used to express the modal damping for a linear dynamic system as a function of the damping coefficients, as in equation 4.60.

$$\lambda_n = \frac{1}{2}(\frac{\alpha_m}{\omega_n} + \alpha_s\omega_n) \tag{4.60}$$

where λ_n is the modal damping ratio relative to critical damping, and ω_n is the angular eigenfrequency (Langen and Sigbjörnsson, 1979; Marintek, a).

4.10.4 Eigenvalue Analysis

Eigenvalues are of high importance for any structure as they characterize how the structure will respond to dynamic loading. The solution to this problem requires a special reduced form of the equation of motion. No damping and no loading applied gives a system that can oscillate freely and the dynamic equation reduces to the equation for undamped free vibration, see equation 4.61.

$$\mathbf{M}\ddot{\mathbf{r}} + \mathbf{K}\mathbf{r} = 0 \tag{4.61}$$

M and K is the mass and stiffness matrix. The solution to this problem is found by assuming a harmonic motion described by

$$\mathbf{r} = \boldsymbol{\phi}sin(\omega t) \tag{4.62}$$

And the solution after simplifying becomes

$$(\mathbf{K} - \omega^2 \mathbf{M})\boldsymbol{\phi} = 0 \qquad (4.63)$$

$\boldsymbol{\phi}$ is the eigenvector which determines the mode of vibration and ω is the eigenvalue (circular frequency). There is an eigenvector which satisfies the equation and corresponds to each eigenvalue.

The mass matrix will be dependent on the frequency, as the hydrodynamic mass is frequency-dependent (Langen and Sigbjörnsson, 1979).

4.10.5 Recommendations Regarding Analysis

When performing an analysis, it is in general hard to give quantitative advice for specification of an incremental loading procedure that ensures a stable, efficient numerical solution. The order of application of loading need to be chosen, and should be chosen to have the highest stability. Instability problems of compression or "snap-through" (see Moan (2003)) must be avoided. Each load condition is applied in a user-defined number of incremental load steps. The required number of load steps to obtain a stable numerical solution depends on the sensitivity to the actual load condition. Fewer load steps are normally required for application of volume forces. The load conditions should be applied with the corresponding number of load steps, in the sequence given in table 4.3.

For the equilibrium iteration procedure, the true Newton-Raphson iteration scheme is preferred. The required accuracy measured by the displacement norm should for beam elements be $1 \cdot 10^{-6}$. The number of equilibrium iterations is normally selected in the range 5 - 15 (Marintek, a).

Table 4.3: Recommended number of load steps for beam and bar elements

Load conditions	Number of load steps (beam/bar element)
Volume forces	5-10
Prescribed displacements	50-200
Current	1-10

4.10.6 Vivana

Vivana is a semi-empirical program for prediction of Vortex-induced Vibrations of slender marine structures subjected to ocean current. (Passano et al.). The program is developed by SINTEF Ocean and NTNU Department of Marine Technology. Vivana is linked to Riflex by the two modules IMPMOD and STAMOD, as seen in figure 4.14, while the other modules are not needed for Vivana. Riflex performs the structure description and static analysis, and stores these in files given as input to Vivana. Vivana consist of the modules VIVEIG, INIVIV, VIVRES, VIVFAT and VIVDRG. A complete VIV analysis follows the list below.
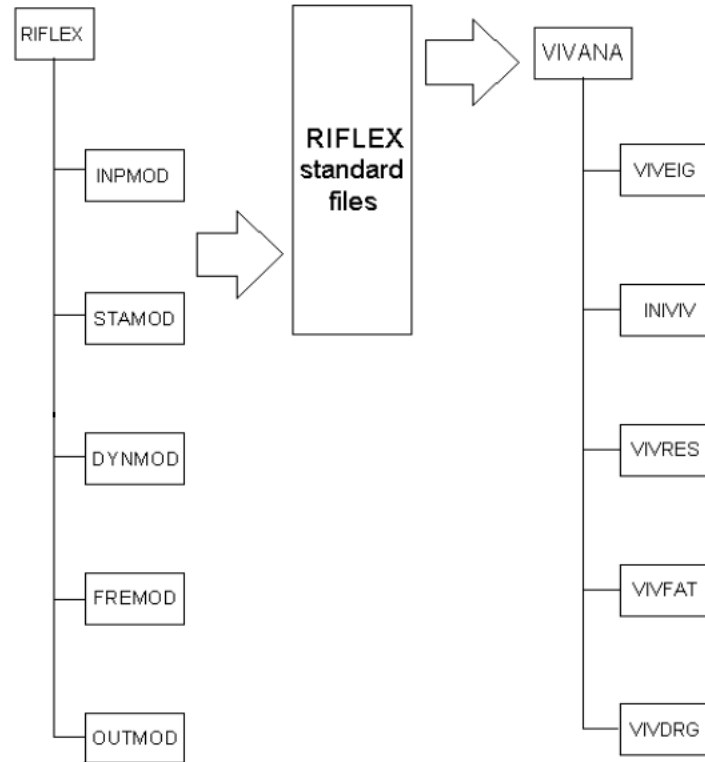
Figure 4.14: System of modules in Riflex and Vivana and the communication between. IMPMOD and STAMOD are given from Riflex as input to Vivana. Adapted from (Passano et al.).

- An initial Riflex analysis using the INPMOD and STAMOD modules.

- VIVEIG: Computes normal modes and eigenfrequencies.

- INIVIV: Calculates some initial key parameters.

- VIVRES: Carries out the dynamic response analysis according to the method described below. Cross-flow and/or in-line response is calculated.

- VIVFAT: Calculates fatigue damage based on the results from VIVRES

- VIVDRG: Calculates VIV magnified drag coefficients.

Some relevant dimensionless parameters used by Vivana are the Strouhal number, the Reynolds number and the non-dimensional frequency.

Strouhal number

The Strouhal number can represent the non-dimensional vortex shedding frequency, f_s, for a fixed cylinder as in equation 4.64 (Faltinsen, 1990). It is used for an initial evaluation of possible response frequencies. The Strouhal number varies with the Reynolds number (Larsen, 2016). Vivana uses a specific relationship between the Strouhal number and the Reynolds number, which is seen in figure 4.15. This relationship is valid

for a circular cylinder with some roughness (Passano et al.).

$$St = \frac{f_s D}{U_c} \tag{4.64}$$
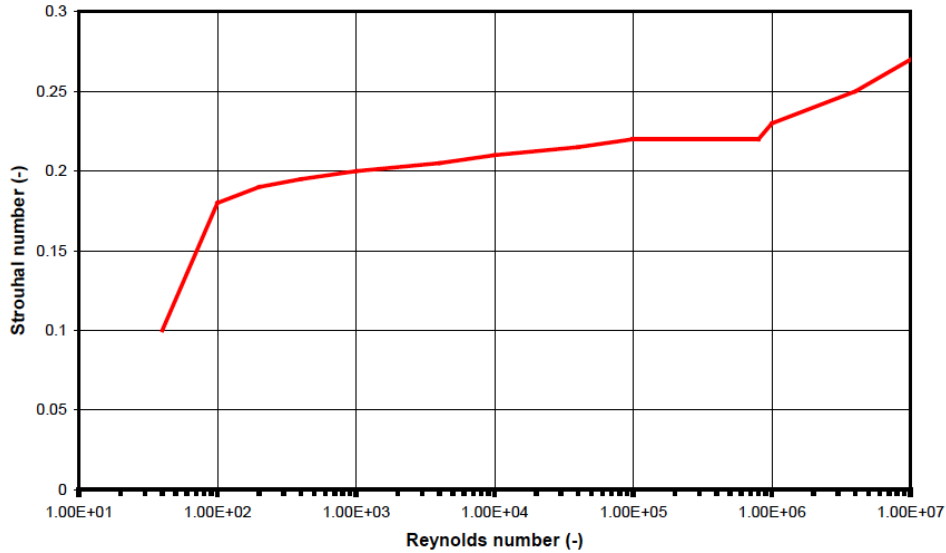
Figure 4.15: The default Strouhal curve used in Vivana (Passano et al.).

The figure shows the St for a fixed cylinder. An oscillating cylinder may have a significantly different "effective" St, also affecting the oscillation frequency to be different from the vortex shedding frequency for the fixed cylinder (Larsen, 2016).

Analysis Procedure

An explanation on how Vivana computes Vortex-induced Vibrations is given (Passano et al.).

1. Static Analysis Vivana uses Riflex to calculate the static shape of the structure.

2. Eigenvalue Analysis, Still Water Thereafter, the eigenfrequencies and mode shapes are found, satisfying equation 4.65, where M and K are the mass and stiffness matrices. Added mass is a constant from the user input to Riflex. Results are given as eigenvectors and eigenfrequencies. The eigenvectors are sorted into groups of cross-flow and in-line, depending on the relative magnitude of the norms. More information in Passano et al..

$$(\mathbf{M_0} - \omega_i^2 \mathbf{K_0})\boldsymbol{\varphi}_i = 0 \tag{4.65}$$

3. Identification of Possible Excitation Frequencies Out of the eigenfrequencies found in step 2, some of these will be response frequencies, i.e. will become active under

the given flow condition (Larsen, 2016), and must be identified. The procedure applies the non-dimensional frequency f$_{non}$ as a controlling parameter.

$$f_{non} = \frac{f_{osc}D}{U_c} \tag{4.66}$$

The added mass constant given by the user will now need to be updated, as in reality, added mass is dependent on frequency. Also, the added mass will vary along the length of the structure, exposed to a sheared current. The response frequency will then appear as an eigenfrequency influenced by the added mass distribution. Since the added mass and the frequency depend on each other, iterations need to be carried out for each response eigenfrequency candidate. Candidate-frequencies are those considered candidates for being excited by vortex shedding. When there is consistency between the added mass and eigenfrequency, the iteration stops. The new frequency becomes a compromise between the original eigenfrequency and the vortex-shedding frequency for a fixed cylinder. Vivana applies models for cross-flow and in-line added mass provided by Gopalkrishnan (1993) and Aronsen (2007), respectively. More information is found in Passano et al..

The result of the iteration is a set of possible response frequencies, with associated added mass distributions and the corrected non-dimensional frequency distribution along the structure. It is now possible to identify active response frequencies, since excitation requires values of the non-dimensional frequency within an interval that gives positive excitation coefficients (Passano et al.). Thus the frequencies will give excitation if the excitation coefficient is positive. When the excitation coefficient is positive can be found from contour plots for cross-flow or in-line excitation coefficients in an amplitude/frequency map, illustrated in figure 4.16.

For cross-flow, the default values used in Vivana are found in figure 4.16. The red lines marks the start and end for the excitation range for cross-flow response, as $0.125 < f_{non} < 0.3$.
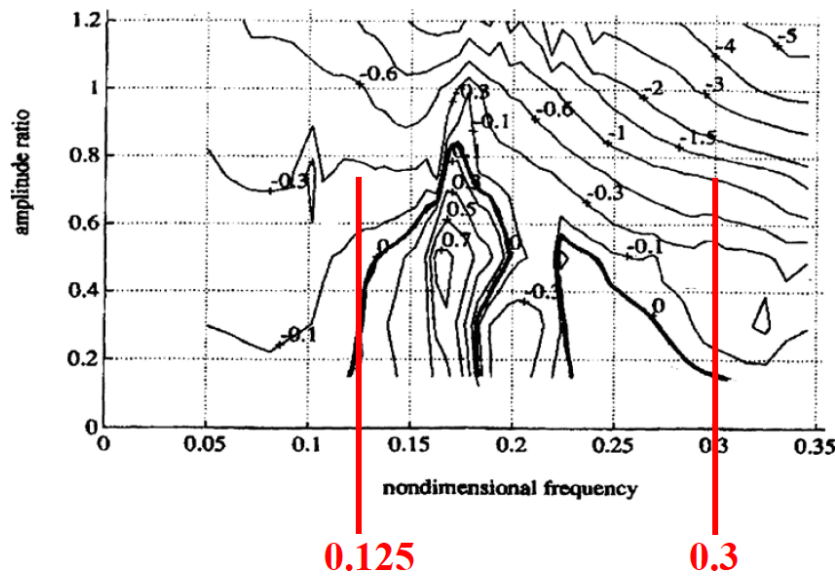
Figure 4.16: Cross-flow amplitude/ nondimensional frequency map giving the excitation range for CF response. (Passano et al.).

4. Allocation of Excitation Zones Ranges for the non-dimensional frequency, seen in figure 4.16, define the excitation zones for each response frequency. Within this range, each frequency will have its own zone, as illustrated in figure 4.17. As seen, overlapping may occur, and this implies that the vortex shedding may act at more than one frequency at a specific part of the structure, simultaneously. However, since it is observed that the response almost always is dominated by one frequency, it is reasonable to assume that one of them will dominate. This frequency will then occupy its entire excitation zone. Outside this zone, on the rest of the structure, other frequencies may control the vortex shedding. The response frequencies can be ranked to define their excitation zones (and importance), to avoid overlaps.
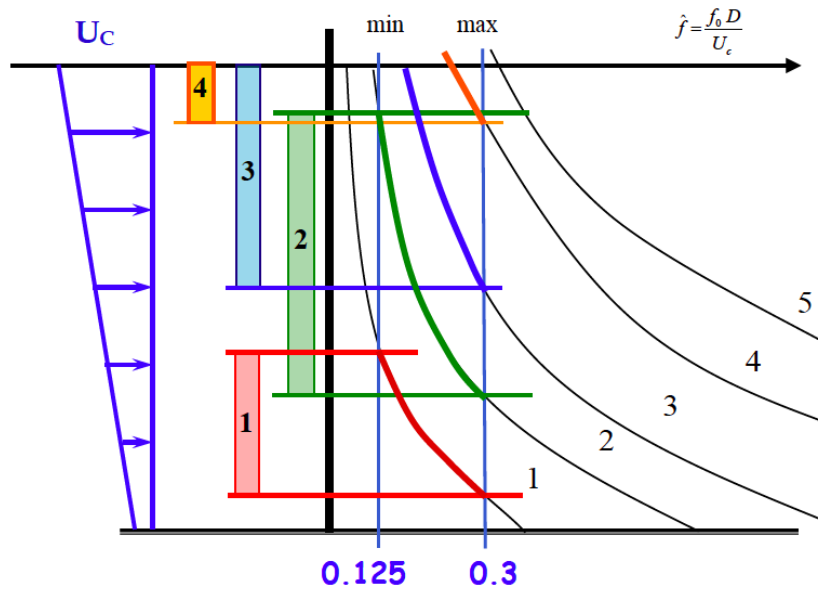
Figure 4.17: Overlapping excitation zones on riser with uniform cross-section, exposed to sheared current. (Numbers 0.125-3 are the CF non-dimensional frequency interval) The nondimensional frequencies, dependent on the current velocity, are shown in black from 1 to 5. Within the CF motion interval, each of these frequencies are excited in its excitation zone, illustrated by the coloured zones (Passano et al.).

Two definitions for the zones can be applied

- Space sharing: The frequencies act simultaneously on different parts of the structure. This is default in Vivana.

- Time sharing: One frequency is excited for the whole structure at one period of time, and is replaced by another frequency the next time.

5. Calculation of Cross-flow and In-line Response The dynamic response at the response frequencies (from step 3) is calculated by the frequency response method. The excitation zones from step 4 are used. An iteration is needed to get the response in accordance with the non-linear models for excitation and damping forces.

The in-line response is calculated in the same way as for cross-flow, but with different hydrodynamic coefficients. More information about this is found in Passano et al..

Fatigue Analysis

Vivana calculates stresses for fatigue damage on the outer surface of the cross-section. The user specifies calculation options and data to be used in the calculation of the SN curve. The accumulated damage is calculated from equation 4.67 and the accumulated fatigue life is found as the inverse of the accumulated damage.

$$D = \sum_{i=1}^{N_{\Delta\sigma}} \frac{n_i}{N_i} \tag{4.67}$$

where n_i is the number of occurrences for each cycle, N_i is the number of cycles to failure for stress cycle i, found from equation 4.68, and $N_{\Delta\sigma}$ is the number of stress ranges.

$$logN_i = logC + mlog\left(\Delta\sigma_i \frac{t_{iel}}{t_{ref}}^k\right) \tag{4.68}$$

logC, m, t_{ref} and k are data for the SN-curve to be specified by the user. m and logC are material parameters, t_{ref} is the wall thickness for the cross section and $\Delta\sigma_i$ is the stress range (Passano et al.). For more information on how Vivana calculates fatigue, see Passano et al..

Chapter 5

Modelling the SFTB

The SFTB is modelled in SIMA/Riflex as close to the original drawings as possible. As mentioned in section 4.10.1, a Riflex model is built of supernodes, lines, line types and cross-section types. Six different cross-sections are used in the model. The two cross-sections for the main tubes, are referred to as the T9.5 and the T12.5. There are two types of cross-over tubes between the two tubes, one with the required emergency lay-by, used with the larger T12.5 and one without lay-by used with the smaller T9.5. In addition, there is one cross-section used for the diagonal bracings between the tubes and one cross-section used for the tethers attached to the bridge, anchored down to the seabed.

As the bridge consist of two tubes in an arch, the two tubes are referred to as the inner and outer tube, respectively. Coordinates for inner and outer tube in the horizontal curve is found by geometrical considerations by use of a MATLAB script. It can be found in appendix E.1. The method used is described here.

Coordinates are found considering the circular geometry and using polar coordinates. The two tubes have their respective inner and outer radius and length in centerline, locally. The length in centerline of the total bridge, i.e. between the two tubes, is set to 5304 m. When the span between the two tubes is known to be 40m, their respective centerline lengths and radius can be found. The following is done for both the inner and outer tube coordinates.

5.1 Middle Part

Reference to the cross-over points are done to the drawing of the bridge in appendix A.1. A cross-over point is a point where the bridge has a cross-over tube. The pattern of the model is considered constant between cross-over point 3 and cross-over point 28 with respect to supernode configuration. Therefore, the node coordinates for the two tubes between these two points are found first, using the following equations. Reference are made to the illustration in figure 5.1. α, the number of degrees of a circle occupied in the bridge curvature is found by equation 5.1. L is the arc length of the bridge, i.e. the length in centerline for the bridge. It is set to 197*25 = 4925m, because there are 25
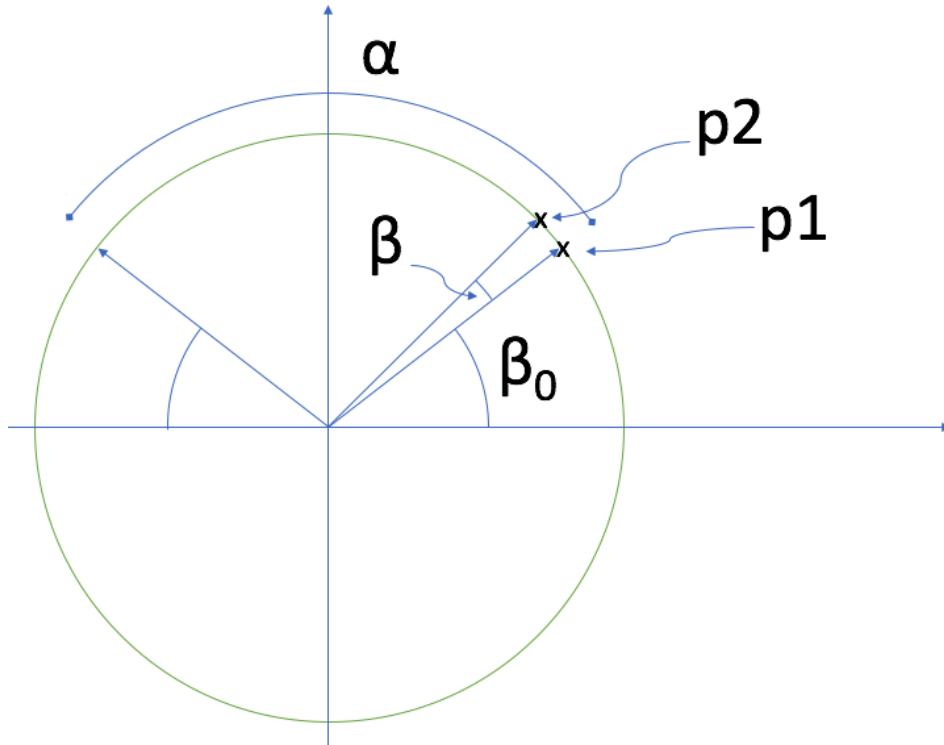
Figure 5.1: Definition of parameters for supernode calculation.

spans between cross-over points 3 and 28, each of 197m. C is the total circumference of the bridge.

β_0, the degree of the first supernode position, cross-over point 28, is found with equation 5.2. Thereafter the number of degrees between each coordinate, β, is found by equation 5.3. At last, the x- and y- coordinate to be used for input to Riflex, are found by conversion from polar to Cartesian coordinates by equations 5.4 and 5.5. i is the number of the coordinate point, from 1 to 26, and r is the respective radius for the inner and outer tube. Note that, coordinate point number 1 (p1 in the figure) is the cross-over point number 28, coordinate point number 2 is the cross-over point number 27, and so on.

$$\alpha = \frac{L}{C} * 360 \tag{5.1}$$

$$\beta_0 = 90 - \frac{\alpha}{2} \tag{5.2}$$

$$\beta = \frac{\alpha}{\text{number of nodes needed} - 1} \tag{5.3}$$

$$\text{X-coord} = r * cosd(\beta_0 + \beta * (i - 1)) \tag{5.4}$$

$$\text{Y-coord} = r * sind(\beta_0 + \beta * (i - 1)) \tag{5.5}$$

5.2   End Parts

The coordinate points for the ends, β_{end}, for cross-over point 2 and cross-over point 29, see appendix A.1, is found by using the arc length and arc angle between the end point and the neighbouring point. As they are symmetric, this arc length and arc angle will be equal. We find the polar coordinate of the end point, β_{end}, by adding this angle to the polar coordinate angle of the neighbouring point, $\beta_{\text{neighbour}}$, as in equation 5.7. Thereafter the Cartesian coordinate is easily found by conversion, as in equations 5.8 and 5.9. Length of end spans are set to be 189.5m, and is measured from the mid point of the cross-overs to the point where the tube goes into the concrete box at the landfalls.

$$\beta_{\text{neighbouring point}} = acosd(\frac{\text{X-coord}_{\text{neighbouring point}}}{r}) \tag{5.6}$$

$$\beta_{\text{end}} = \beta_{\text{neighbouring point}} + \text{arc angle} \tag{5.7}$$

$$\text{x-coord}_{\text{end point}} = r * cosd(\beta_{\text{end}}) \tag{5.8}$$

$$\text{y-coord}_{\text{end point}} = r * sind(\beta_{\text{end}}) \tag{5.9}$$

In Riflex, a direct transition from the T9.5 to the T12.5 cross-section is used, and not a gradual, as is designed in the reference concept. Global response is the aim in this thesis, so the model choice is thought to be sufficient.

5.3   Bracings Points

To find the points for the diagonal bracings, the same equations are used. as previously described. Since there are 25 spans in the middle part of the bridge, and four bracings per span, the number of nodes needed in equation 5.3, is set to 101. Then, again there is a need to adapt for the end nodes, as these are different than for the middle part.

The bracings are modelled using a 39 degree angle between the tube and the bracing. No difference are made on the outer or inner angle, and they are modelled with an equal length for all the bracings, going both ways.

5.4   Node Points for Tethers

The supernodes for the tether configuration are found by assuming the distance between the supernode of the cross-over and the supernode for the tether intersection, to follow the arch as well, instead of being along the tangent to the point. This is an approximation to enlighten the calculations and will come with a small, insignificant error. The same method as described previously is used to find these points.

To verify the calculated coordinates, a graphical visualization of the relevant coordinates are made in Matlab, and found in figure 5.2. A zoomed plot of the supernodes at the

south end is seen in figure 5.3. In the figures, the dots are supernodes to be given as input to the Riflex model. The blue are for the outer tube and the red are for the inner tube. Main tubes will be connected between each supernode of the same color. Where three dots are arranged closely, the middle dot is the point for the cross-over bar, and the two adjacent dots are the supernodes for connection of the tethers on each side. From the node for the cross-over tube, a bracing will be connected to the next diagonal dot, at the opposite main tube.
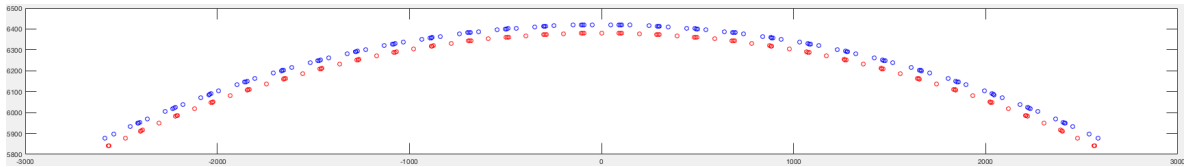
Figure 5.2: Plot of the supernodes used to model the bridge. For comparance, the reader can see figure 3.2.
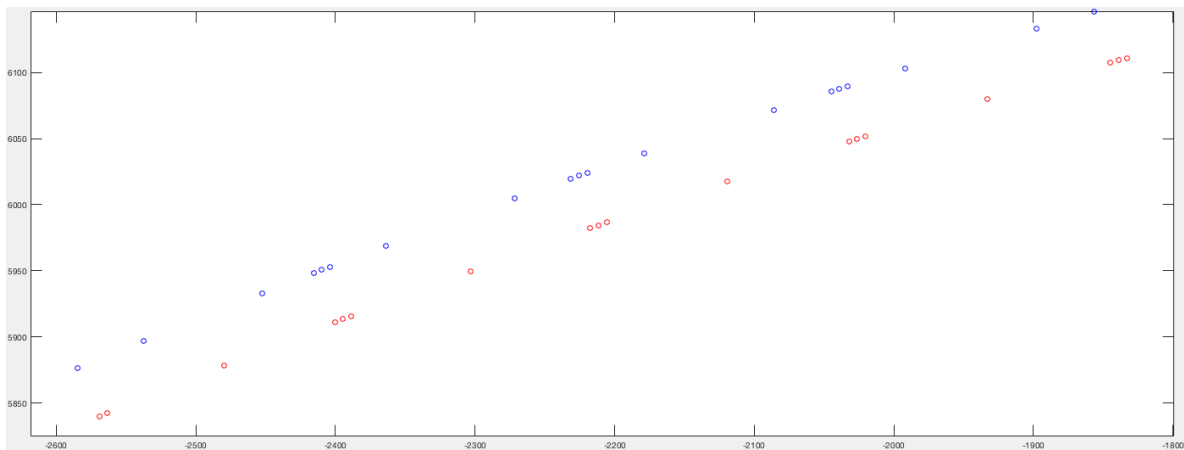
Figure 5.3: Zoomed plot of the South end showing the supernodes.

5.5 Assumptions for Modelling

At the crossing site, the seabed is not constant, and has a maximum depth of -550m. For the Riflex model, the seabed depth is considered constant, at -550m. The bottom of the tethers are assumed as fixed in the seabed with no specific seabed stiffness applied.

The fins on the bottom of the main cross-sections, as seen in 3.5, are neglected from the T9.5 and T12.5 cross-sections when calculating stiffness and mass. Neglecting the fin, gives a smaller drag coefficient to the circular cross-section, as it is more streamlined. It also leads to a different value for the stiffness and mass. Constant cross-sections over the segments in each line are assumed. This leads to all interior rooms and walls giving contribution to stiffness and mass are neglected.

Referring to the drawing of the bridge in appendix A.1, the bridge is modelled between the caissons at the landfalls. This leads to point 1 and 30 being left out of the model. The ends are modelled as fixed to all translations and rotations.

Regarding the bracing, a simplification is made with respect to calculation of the stiffness. As seen in figure 3.9, the flanges of the bracings have triangular ends. In the calculation of the stiffnesses, the flanges are considered rectangular, not including the triangular part of the flanges. This leads to a reduction of the stiffness for the bracings, as less area is included. The same assumption is used for the determination of the drag coefficient.

5.6 Rigid Supernode Connections

In Riflex, a supernode has to be connected to the end of a line to be dependent on the motion of the line. When a new supernode close to another is modelled, it can sometimes be inconvenient to split the line up in two, to make the new supernode dependent on the motion of the line. Rigid connections can be modelled between supernodes, allowing for an establishing of a rigid connection between two supernodes. This is convenient for instance when modelling the tethers to a supernode very close to the main connector node for the area. To do this, one have to define a master node and a slave node. The theoretical formulation is a special application of linear constraints between degrees of freedom (Marintek, b).

The top nodes for the tethers intersections to the tubes are slaved to their respective midnode of the cross-over. This is to ensure that the tethers are affected by the motion of the main horizontal tubes. A motion in the midnode of the cross-over will be the same as the motion in the tether top.

The positive effect of this, is being able to include less lines in the model, as all lines going past a supernode, has to be connected to that respective supernode, to be fixed with respect to the node. In other words, if a supernode exists on a line segment, but the line end is not connected to the supernode, this supernode will be independent on the motion of the line. As we want the tether to be dependent on the movement of the tube, and want to save time not modelling a line between the tether supernode and the cross-over supernode, the rigid supernode connections are efficient.

5.7 Material

The materials used are the same as listed for the reference model in the introduction, section 3.3. The reinforcement and pre-stressing in the concrete is not included in the analysis. Hence, the E-modulus given to the program will give a larger deformation of the structure than in reality, as the material will behave softer than what will be expected after reinforcement and pre-stressing is added.

5.8   Damping

A damping ratio of 0.8 % is required by the NPRA. The Rayleigh damping parameters are calculated from an upper and lower bound for the wave period area between 4s and 10s., recommended by supervisor, Bernt Leira. The parameters are found to be 0.072 and 0.073 for the mass and stiffness proportional damping factors, respectively. This is added as global damping to the structure in Riflex.
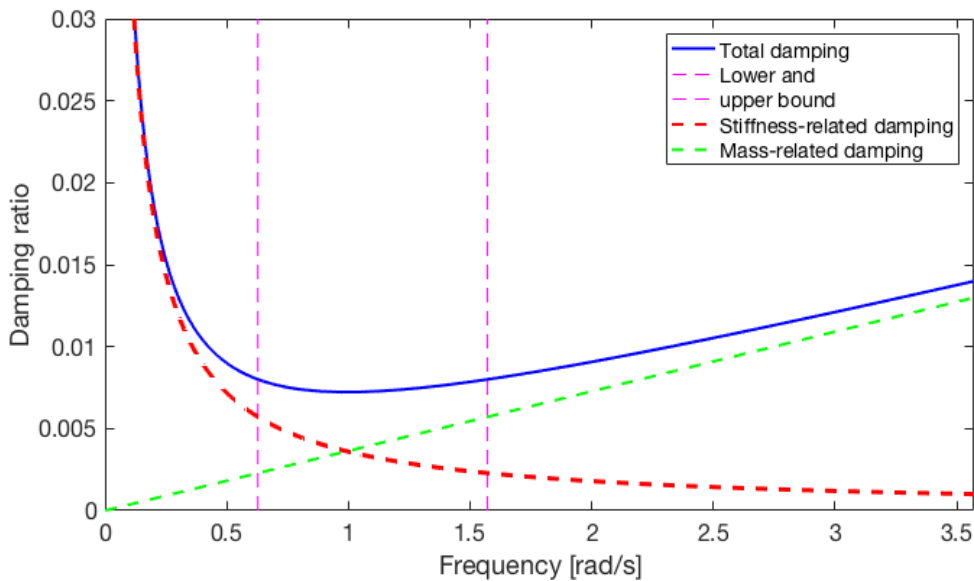
Figure 5.4: Rayleigh Damping. Dotted vertical lines show lower and upper limit for frequency range.

5.9   Cross-sectional Parameters for Model

The reference model has a pre-tension in the two different tethers of 10.5 MN and 11 MN. This comes from the positive net buoyancy and this is the governing design factor for the model in this thesis. The simplest way in varying the net buoyancy is varying the structural mass. The concrete density thus becomes the main design variable. The concrete density is varied to obtain a static pre-tension of the tethers to be approx 10 MN. Excel is used in order to calculate the total mass and buoyancy, line-wise of the bridge. From a parameter analysis in Riflex, the effective tension in the tethers can be easily obtained. The global density of the concrete is then set to 31.7 kN/m³. This gives the total bridge a buoyancy of 6.97 % with respect to the mass.

The parameters for the cross-sections, as the moment of inertia, torsional stiffness, and more, are calculated using Matlab scripts and Excel. The scripts and equations used can be found in the appendix E.2 and D.

5.9.1 Main Tubes

As mentioned, the fins for both the T9.5 and the T12.5 cross-section are neglected. Due to the walls inside the cross-section, they will have different stiffnesses in the two planes. The added mass coefficient and the drag coefficient is set to 1 for the main tubes., as given in Reinertsen et al. (2016b). The drag coefficient used for the main tubes in the analysis, is the same as the one used for the reference model in the technical report for the Bjørnafjord. One can discuss the value of this coefficient with respect to the load scenario needed. Higher current velocities gives higher Reynolds numbers, and the drag coefficient will vary with this. Thus for a 100y current, an extreme current, the drag coefficient may be higher than for a not less extreme load case.

For information about formulas used in the calculations of the cross-sectional parameters for input to Riflex, see appendix D.

5.9.2 Cross-over Tubes

For the two cross-over tubes, coefficients for added mass are found in Faltinsen (1990). For the cross-over tube with lay-by the coefficients are set to be 1.5 for sway, and 1.6 for heave. For the cross-over tube without lay-by, both are set to 1.5 due to the relatively equal height and width. Coefficients for drag are found from Det Norske Veritas (2014) to be 2.2 for both sway and heave.

While calculating the torsional constant, see appendix D, the cross-sections are assumed rectangular with no inner walls. The drag coefficients are taken from Det Norske Veritas (2014), and set to 2.2 for both directions.

5.9.3 Bracings

Added mass for the bracings are found in Faltinsen (1990) to be 2.2 for sway, and 1.5 for heave. The cross-section is assumed rectangular to simplify the establishing of a coefficient, and a drag coefficient for sway is set to 0.9 and 2.1 for heave (Det Norske Veritas, 2014).

When calculating the torsional constant, see appendix D, the cross-sections are assumed rectangular with no inner walls.

5.9.4 Tethers

Added mass and drag coefficients are set to 1 due to the circular shape of the cross-section, as in Reinertsen et al. (2016b).

5.9.5 Summary of Cross-sectional Parameters

A summary of the parameters for each cross-section is given in table 5.1.

Table 5.1: Cross-sectional parameters to be used for Riflex model

Parameter	Unit	T9.5	T12.5	Bracing
Outer area	m^2	125.7	177.9	4.18
Inner area	m^2	88.4	131.2	0
CS area	m^2	37.3	46.7	4.18
Iz	m^4	572.58	993.45	11.94
Iy	m^4	551.40	970.15	0.59
Torsional constant	m^4	1123.98	1963.60	12.53
Mass	t/m	120.5	150.9	13.21
Buoyancy	t/m	128.84	182.35	4.28
Net buoyancy	%	6.90	20.83	-67.56
Axial stiffness	N	$1.12 \cdot 10^{12}$	$1.4 \cdot 10^{12}$	$1.25 \cdot 10^{11}$
Bending stiffness, z	Nm^2	$1.72 \cdot 10^{13}$	$2.98 \cdot 10^{13}$	$3.58 \cdot 10^{11}$
Bending stiffness, y	Nm^2	$1.65 \cdot 10^{13}$	$2.91 \cdot 10^{13}$	$1.77 \cdot 10^{10}$
Torsional stiffness	Nm^2/rad	$1.41 \cdot 10^{13}$	$2.45 \cdot 10^{13}$	$1.83 \cdot 10^{10}$
Added mass coeff, y	-	1	1	2.2
Added mass coeff, z	-	1	1	1.5
Drag coefficient, y	-	1	1	0.9
Drag coefficient, z	-	1	1	2.1
Outer diameter	m	12.6	15	-
Thickness	m	0.8	0.8	-
Outer Height	m	-	-	1
Outer Width	m	-	-	5
Elasticity modulus	GPa	30	30	30
Shear modulus	GPa	12.5	12.5	12.5
Dry density	kN/m^3	31.7	31.7	31.7
Parameter	**Unit**	**Cross-over w/lb**	**Cross-over n/lb**	**Tether**
Outer area	m^2	280	257.6	0.98
Inner area	m^2	215.3	194.86	0.85
CS area	m^2	64.7	62.74	0.13
Iz	m^4	1615.50	1534.40	0.0188
Iy	m^4	2122.80	1828.30	0.0188
Torsional constant	m^4	3275.5	2816.38	0.0376
Mass	t/m	209.07	202.74	1.01
Buoyancy	t/m	287.0	264.04	1.01
Net buoyancy	%	37.27	30.24	0.71
Axial stiffness	N	$1.94 \cdot 10^{12}$	$1.88 \cdot 10^{12}$	$2.67 \cdot 10^{10}$
Bending stiffness, z	Nm^2	$4.85 \cdot 10^{13}$	$4.60 \cdot 10^{13}$	$3.89 \cdot 10^{9}$
Bending stiffness, y	Nm^2	$6.37 \cdot 10^{13}$	$5.48 \cdot 10^{13}$	$3.89 \cdot 10^{9}$
Torsional stiffness	Nm^2/rad	$4.09 \cdot 10^{13}$	$3.52 \cdot 10^{13}$	$2.99 \cdot 10^{9}$
Added mass coeff, y	-	1.5	1.5	1
Added mass coeff, z	-	1.6	1.5	1
Drag coefficient, y	-	2.2	2.2	1
Drag coefficient, z	-	2.2	2.2	1
Outer diameter	m	-	-	1.1176
Outer Height	m	17.5	16.1	-
Outer Width	m	16	16	-
Elasticity modulus	GPa	30	30	207
Shear modulus	GPa	12.5	12.5	207
Dry density	kN/m^3	31.7	31.7	77.0

5.10 Different Models

The reference model is asymmetric, as the cross-over tubes are applied asymmetrically over the bridge, as seen from figure 3.2. To better understand the effect of this asymmetry, two models are made in Riflex, one symmetric and one asymmetric. The only difference between those two, are the order of appearance of the emergency lay-bys. For the symmetric model the two middle cross-over tubes are with lay-by. The start and end point cross-over tubes are also with lay-by. For the asymmetric model, the start and end point cross-overs are one of each, creating an asymmetric distribution of mass and buoyancy. Both models are created and performed static analysis upon. The static results are found in appendix C.1. Further, only the symmetric model is used for the analysis A screen shot of the Riflex model is shown in figure 5.5.

In Vivana, only axi-symmetric cross-sections are allowed. A third model is therefore made for this analysis. When giving information to Riflex about the new axi-symmetric cross-sections, the parameters used for sway motion in the original models is used. This leads to a larger net buoyancy for the bridge. This is accounted for by increasing the concrete density used in the cross-sections. Analyses are run with a varying concrete density, to find the density that gives the wanted buoyancy. Resulting concrete density is set to 4200 kg/m^3 (41.202 kN/m^3). The new cross-sections defined are given in table 5.2.
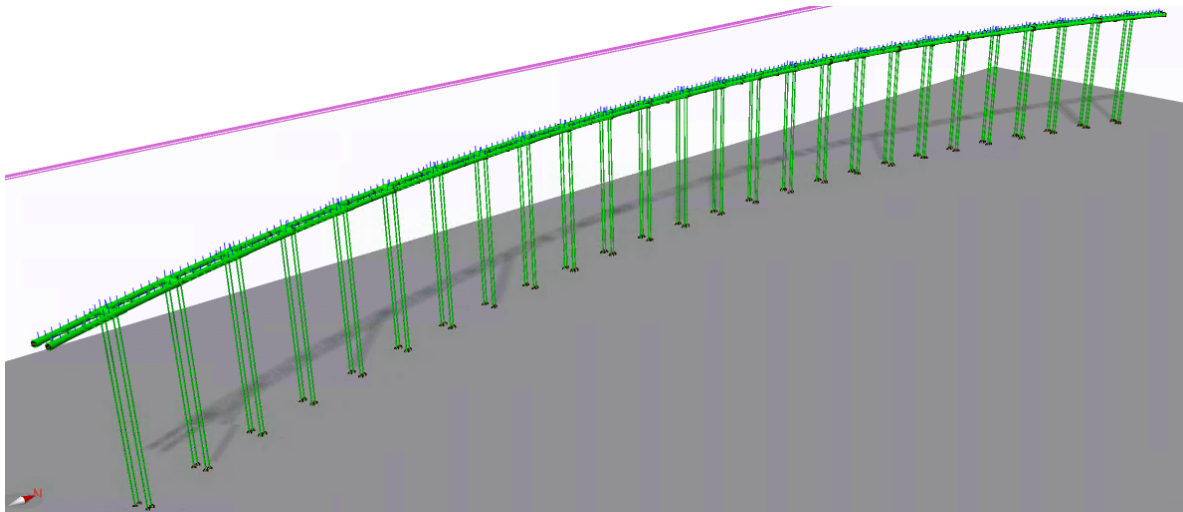
Figure 5.5: Riflex Model.

In Riflex, added mass is defined by weight per unit length, and not by the coefficient. The same added mass is defined for the Vivana model as for the main model, even though the submerged volumes will differ. This is also done for the drag.
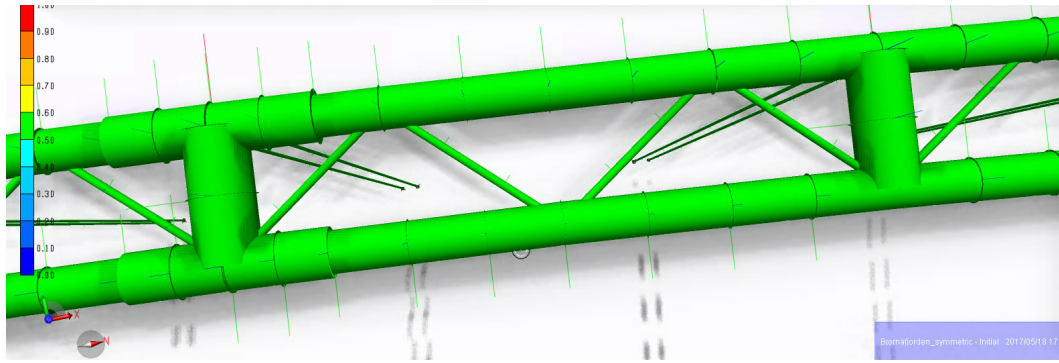
Figure 5.6: Close-up of bridge configuration in Riflex.

Table 5.2: Cross-sectional parameters to be used for Vivana-analysis.

Parameter	Unit	T9.5	T12.5	Bracing
Outer diameter	m	12.5	15	1
Thickness	m	0.8	0.8	0.4999
Drag force coefficient	-	1	1	0.9
Added mass coefficient	-	1	1	2.2
Area	m^2	29.7	35.7	0.785
Second moment of area	m^4	518.5	902.4	0.049
Parameter	**Unit**	**Cross-over w/lb**	**Cross-over n/lb**	**-**
Outer diameter	m	17.5	16.1	-
Thickness	m	0.8	0.8	-
Drag force coefficient	-	2.2	2.2	-
Added mass coefficient	-	1.5	1.5	-
Area	m^2	41.97	38.45	-
Second moment of area	m^4	1389.04	1128.26	-

5.11 Calculated Parameters for use in DNV GL Formulas

To check whether in-line VIV should occur, the necessary parameters to be applied in the DNV formulas are calculated. A constant T9.5 cross-section for one tube is assumed. Equations 4.21, 4.22 and 4.24 are used for the calculations. Effective mass is calculated as a sum of structural mass and hydrodynamic mass. For the damping ratio, the structural damping ratio of 0.8 % is used.

Table 5.3: Parameters to be used with DNV GL model, in equation 4.21.

Parameter	Unit	T9.5	Tether
m_e	kg/m	265082.84	2018.16
ζ_T	-	0.008	0.008
K_{sd}	-	0.142	0.138

It is seen from figure 4.4, that with a Ksd of 0.14, the in-line VIV has an onset of 1 for the reduced velocity. The maximum in-line response amplitude for the tube is

approximately Ay/D = 0.18. This gives an in-line amplitude of Ay = 0.18·12.6 = 2.27m. The maximum in-line response amplitude for the tether is approximately Ay/D = 0.18, Ay = 0.18·1.12 = 20.1cm, according to the calculations and the DNV GL model..

From figure 4.5, the maximum cross-flow response amplitude for the tether is found by assuming a current flow velocity ratio of 1. This implies that only current velocity is included, and not the wave-induced flow velocity. The maximum Az/D-ratio is approximately 1.3, giving an amplitude Az = 1.3·1.12m = 1.46m. Expected amplitudes before evaluating the reduced velocity, are summarized in table 5.4.

Table 5.4: Expected response amplitudes according to DNV GL.

Component	Unit	In-line	Cross-flow
1 Tube	m	2.27	-
1 Tether	m	0.20	1.46

64

Chapter 6

Method and Setup of Analyses

6.1 Riflex Analysis

In Riflex, one have to pay attention to the type of matrix used in the calculations. Two options are available, namely sparse and skyline matrix. Skyline is a consistent matrix that is more time-consuming to use in calculations, hence sparse matrix is preferred in general. For the static and dynamic calculations, sparse is available. On the other hand, for the free vibration option in DYNMOD, i.e. eigenvalue analysis and Vivana-analysis, skyline matrix is required (Marintek, b).

The version of Sima/Riflex used, does not automatically sort lines after appearance. For many of the results, it sorts the lines like they are defined in the input list of lines. Therefore, it is important that the user sorts the lines in order of physical appearance to more explicitly be able to view the result in the post-processor of Sima.

To verify that the Riflex-model does not contain any errors and that results are realistic, both the asymmetric and the symmetric model is run in a static analysis, without current applied. From the symmetric model results, an error or an asymmetry in the model can easily be observed. After this, the further analysis is run on the symmetric model.

6.2 Modal Analysis

Analytical Calculations

The eigenfrequencies of the bridge is found analytically using two methods. Generalized modal analysis, section 4.7, is used, as well as the formula for beams on elastic foundation using a Winkler approach, section 4.6.3. Matlab is used for the calculations and the scripts are found in appendices E.3 and E.4. In the calculations, the bridge is assumed consisting of two tubes with a constant cross-section of the T9.5 type.

The eigenfrequency for one tether is found using equations 4.28, 4.29 and 4.31. Values used for the tether are given in table 6.1. By comparing the different equations, one

Table 6.1: Parameters used for calculation of tether analytical frequencies.

Parameter	Unit	Value
Mass	kg/m	2018.2
Tension	N	$14.5 \cdot 10^6$
Length	m	512.5
Elasticity Modulus	GPa	$207 \cdot 10^9$
Area moment of inertia	m^4	0.0188

can observe how the bending stiffness term and the tension term varies and dominates over the different modes. A plot with varying mode number is created in Matlab and seen in the results.

Computing by Riflex

The eigenfrequencies for the bridge are found using 1 element for the tethers. This is the same way as the eigenfrequencies were found for the reference model in 3D Float. This is to obtain frequencies of the bridge while held down of the tethers, and not include coupling of local frequencies of tethers.

Sensitivity Studies

To see how the length of one tether affects the first eigenfrequency found, analysis is done with a varying submergence, i.e varying length of the tethers. The analysis is run on the asymmetric model. From the equation seen in 4.28, the eigenfrequency should increase for decreasing lengths.

To see how the tension in the tethers affects the eigenfrequency, analysis is done with a varying tension. The varying of the tension is done by varying the buoyancy. This is easily done by varying the density of the concrete. From the equation seen in 4.28, the eigenfrequency should increase for increasing tension.

To see how the number of elements for the tether affects the number of frequencies and modes found, the eigenvalue analysis is run with a different number of tether elements. One with 1 element for each tether, and one with ten elements for each tether.

6.3 Dynamic Analysis

12 dynamic analyses are performed with the JONSWAP spectrum. Four analyses with only wind-sea with a varying Tp. The same four analyses are repeated with a swell wave with a constant Tp of 14s and thereafter with a constant Tp of 15s. The set of analyses are summarized in table 6.2.

The direction is kept constant at 90 degrees onto the bridge from east. A visualization of the wave direction applied is seen in figure 6.1. The base runs with the wind-sea condition are chosen to correspond to the wave conditions used in 3D Float, referred to
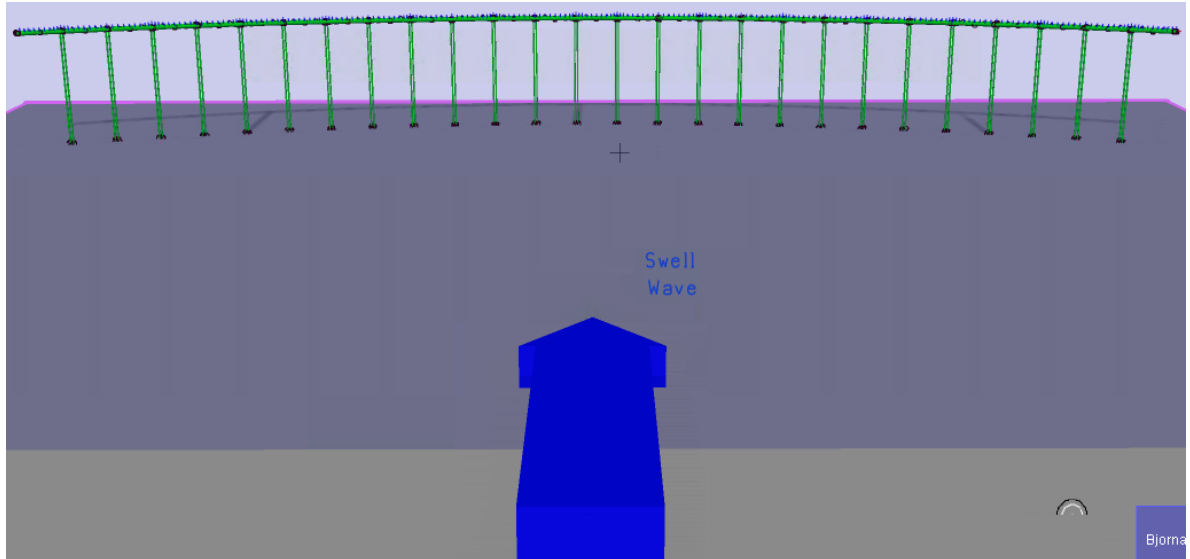
Figure 6.1: Wave direction used for dynamic analysis.
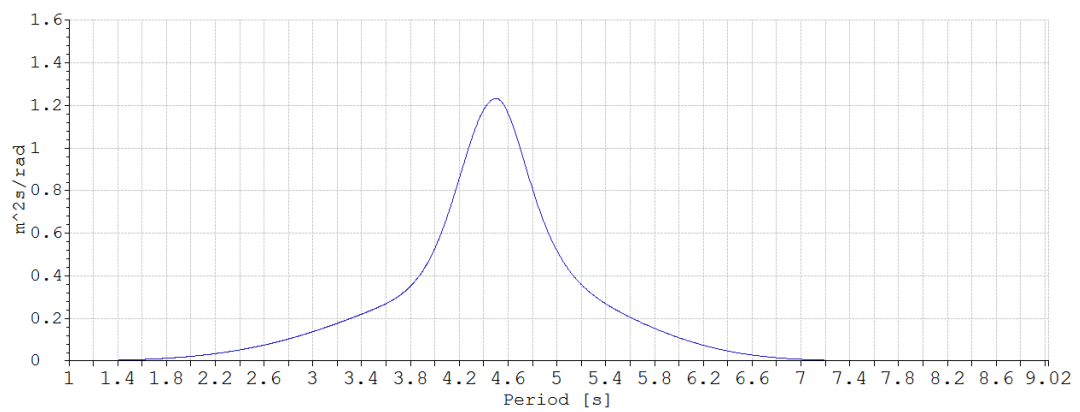
Figure 6.2: Plot of the wind-sea spectrum used.

Table 6.2: Environment used for the 12 runs of dynamic analysis.

Run	Wind-sea				Swell			
	Hs[m]	Tp[s]	γ[-]	Spread[n]	Hs[m]	Tp[s]	γ[-]	Spread[n]
1	3	4.5	3.2	9	-	-	-	-
2	3	5	3.2	9	-	-	-	-
3	3	5.5	3.2	9	-	-	-	-
4	3	6	3.2	9	-	-	-	-
5	3	4.5	3.2	9	0.3	14	5	17
6	3	5	3.2	9	0.3	14	5	17
7	3	5.5	3.2	9	0.3	14	5	17
8	3	6	3.2	9	0.3	14	5	17
9	3	4.5	3.2	9	0.3	15	5	17
10	3	5	3.2	9	0.3	15	5	17
11	3	5.5	3.2	9	0.3	15	5	17
12	3	6	3.2	9	0.3	15	5	17

as ULS17 - ULS20. The swell-conditions correspond to ULS09 and ULS10 (Dr. techn. Olav Olsen, 2016).

The time domain procedure is nonlinear with Newmark parameters of $\beta = 0.25$ and $\gamma = 0.5$. Airy linear wave theory is applied. The simulation length is set to 3 hours and the time step is set to 0.1. Wave seed is set to 1. Global damping of 0.8 % is applied.

Envelope curves showing the maximum and minimum response along the bridge of all runs are presented in the results. The axial bending stress is calculated by Riflex at eight points of the outer circumference of the circular cross-sections, see figure 6.3. By choosing this option in Riflex, the tube cross-sections are considered axi-symmetric. The specified point of calculation is set to end 1 at element 1 in each line of the main tubes. For the stress calculation, it is specified an external pressure of $\rho \cdot g \cdot h = 9.81 \cdot 1.025 \cdot 37.5 = 377.1$ N/m^2.

6.4   VIV Analysis

6.4.1   VIV on Main Bridge

The Vivana-model of the SFTB with global damping is applied for the Vivana analysis. The space-sharing method is used. A 100y current velocity, as specified in section 3.6 is applied. It is applied 90 degrees onto the bridge, from east. Results are presented as amplitudes, accelerations and moments.

The default St-Re relationship in Vivana is used. The wind tunnel testing on the actual cross-section, gives a St number of 0.8 at the Re of 1x10^4, which is slightly lower than the default curve at the same Reynolds number. However, as no relationship curve for other Reynolds numbers are given, it is chosen to use the default curve in Vivana. Also, in Vivana, cross-sectional parameters are given per cross-section, and the information
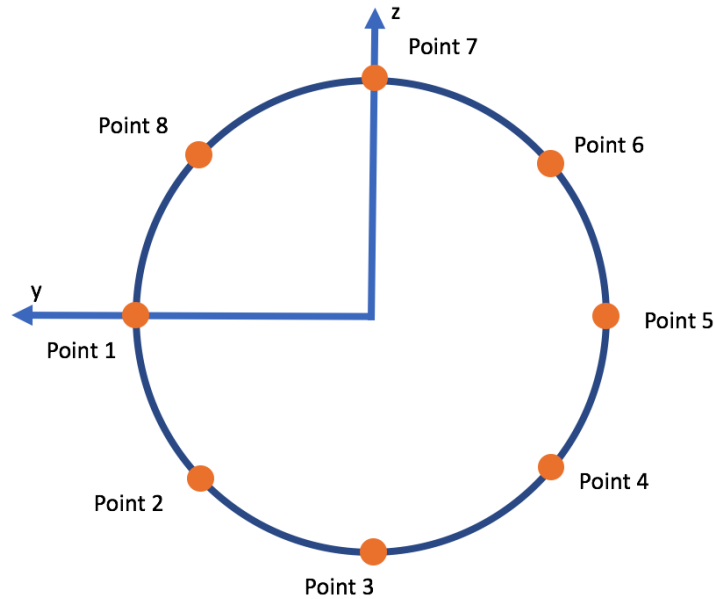
Figure 6.3: Points for calculation of stress throughout cross-section during the dynamic analyses.

from the wind-tunnel tests about the tandem configuration can not be further used in the program.

From Vivana, the moment or curvature is not given explicitly. In order to calculate the moment induced by the vibrations, two methods are used to gain knowledge about the uncertainty in estimating the moment. From the curvature, the moment can be calculated, according to equation 4.52. From the amplitude stresses, moments can be found by manipulation of equation 4.49. The moment about the y-axis, is assumed zero because the main motion from VIV is in the horizontal plane, resulting in the moment about the z-axis being the dominant term. Estimating the axial force is explained further in chapter 7.3.1.

6.4.2 VIV on Single Tether

A single tether with an axial tension is analysed in Vivana. Both cross-flow and in-line is calculated separately in two analysis. Global damping of 0.8 % is used. The top node of the tether is considered fixed to translation in horizontal direction, but free in the vertical direction. This is to allow for the simulation of the buoyancy of the bridge, creating the tension. All rotations are considered fixed. The bottom node is considered fixed. 80 elements are used for the tether, to allow for a detailed analysis.

The VIV analysis is run with a specified force in degree of freedom no. 3 at the upper node. This is specified under "Load components" under "Static Calculation". The SN-curve specified for fatigue calculation is the same as from an example calculation in Vivana. This has specified an m = 4 and logC = 15.01. As these material parameters are used for a riser made of steel, the material parameters are considered to be sufficient also for a steel tether. Rainflow counting is used for calculation of fatigue.

The average value for the tension for the supports with emergency lay-by is approxi-

mately 14.5 MN. This tension is specified for the analysis for a tether with lay-by. The average value for the tension for the supports without lay-by is approximately 10.5 MN. This tension is specified for the analysis for a tether without lay-by.

6.4.3 Variable Reduced Velocity

To verify that the Vivana results correspond with the DNV GL models for in-line and cross-flow, analyses are performed with a varying current velocity to achieve a varying reduced velocity. The current velocity is scaled from 0.5 to 2.5 for the in-line motion. This is done for both the tubes and the tether. Only the tether with a tension of 14.5 MN is analysed. The current is scaled from 2 to 6 for the cross-flow motion of the tether. Damping is applied to both the isolated tether and the bridge. Only response in mode 1 is considered and the reduced velocity is calculated from the first natural eigenperiod.

6.4.4 Methodology and Limitations of Vivana

Current need to be included in the "Static Calculation" toolbox. Skyline matrix technology is needed in the "Static Calculation" toolbox to do the Vivana-analysis. For analysis of large structures, it is of interest to increase the number of arrays used by Vivana from the default value.

In Vivana, the downstream current of a cylinder in the wake of another cylinder is not included. The program is meant for free spans, and does not include the tandem effect of two cylinders. Therefore, only the amplitude of the first tube of the bridge is looked into, as this is equal to the results of the second tube.

6.5 Post-processing in Matlab and Excel

The plots of the eigenmodes and envelopes are created in Matlab. Values are normalized within each eigenvector. The plots of tether tension, the tables of stress extremals and the tables and figures from the variable VIV analyses are created in Excel.

Chapter 7

Results

This chapter gives all relevant results found from the work. Discussion of results are found in chapter 8.

7.1 Modal Analysis

7.1.1 Bridge

Analytical solutions

Calculated horizontal and vertical frequencies and periods are found in tables 7.1 and 7.2. Both methods explained in sections 4.6.3 and 4.7 are used. The frequencies are found by equations 4.34 and 4.46.

Table 7.1: Analytical horizontal eigenfrequencies and periods.

Mode	Generalized modal approach		Beam w/ elastic foundation	
	Frequency [rad/s]	Period [s]	Frequency [rad/s]	Period [s]
1	0.056	111.590	0.043	147.633
2	0.101	62.097	0.096	65.759
3	0.185	34.050	0.182	34.577
4	0.299	20.990	0.298	21.063
5	0.445	14.117	0.445	14.132
6	0.620	10.132	0.620	10.127
7	0.825	7.617	0.826	7.610
8	1.059	5.933	1.060	5.926
9	1.322	4.751	1.324	4.744
10	1.615	3.890	1.618	3.884

It is seen that the horizontal eigenperiods are very similar. Only the first period is significantly different between the two methods. In modes from 2 to 10, they coincide well, and the largest difference is seen at mode no 2 with a difference percentage of 6 %.

Table 7.2: Analytical vertical eigenfrequencies and periods.

	Generalized modal approach		Beam w/ elastic foundation	
Mode	Frequency [rad/s]	Period [s]	Frequency [rad/s]	Period [s]
1	2.231	2.816	1.398	4.494
2	2.120	2.964	1.398	4.493
3	2.125	2.957	1.399	4.492
4	1.983	3.168	1.399	4.490
5	2.126	2.955	1.401	4.486
6	1.992	3.155	1.403	4.478
7	1.994	3.151	1.407	4.466
8	1.998	3.144	1.412	4.448
9	2.004	3.136	1.420	4.424
10	2.011	3.124	1.431	4.390

It is seen that the analytic vertical frequencies in table 7.2 are more different between the two methods. The eigenfrequencies resulting from the generalized modal approach (from equations 4.46) are not found in the usual increasing order, and they have a "random" appearance of frequencies.

Computed from Riflex

The found frequencies for the symmetric model, run with 1 element per tether, are listed in table 7.3. The first 13 eigenmodes of the total bridge are shown in figures 7.1 - 7.13 below. The blue horizontal line is illustrating the bridge, and the different coloured vertical lines are illustrating the tethers. Only one tether from each tether group is included in the plot. The modes are seen from three planes, the XY-plane (bridge seen from above), the XZ-plane (bridge seen from the side, with a view of the whole length) and the YZ-plane (bridge seen from the north end). The ratio for the axis are the same, for easy comparance of relative magnitude of mode shapes. When looking at the YZ-plane (left figure), it is important to note the arch shape of the bridge. The left end of the figure is the two ends of the bridge, and the right end of the figure is the middle part of the bridge.

It is seen from the figures that the ten first frequencies are horizontal modes and the first vertical mode is seen as mode no 11.

By comparing the ten first analytical horizontal frequencies in table 7.1 with the ten first computed horizontal frequencies, table 7.3, it is seen that the first period is a lot larger analytically. For the rest of the frequencies, there are smaller differences between analytical and computed frequencies (below 40 %), and the difference is decreasing with the frequency.

Table 7.3: Eigenfrequencies computed from Riflex.

Mode	Frequency [Hz]	Period [s]	Mode	Frequency [Hz]	Period [s]
1	0.014	72.123	26	0.202	4.947
2	0.023	43.851	27	0.208	4.808
3	0.041	24.495	28	0.209	4.785
4	0.044	22.803	29	0.213	4.699
5	0.061	16.286	30	0.214	4.684
6	0.080	12.521	31	0.221	4.534
7	0.103	9.687	32	0.228	4.395
8	0.127	7.857	33	0.228	4.386
9	0.153	6.522	34	0.228	4.385
10	0.180	5.549	35	0.237	4.228
11	0.189	5.301	36	0.239	4.178
12	0.190	5.265	37	0.245	4.081
13	0.190	5.264	38	0.246	4.067
14	0.190	5.263	39	0.257	3.893
15	0.190	5.262	40	0.264	3.782
16	0.190	5.260	41	0.265	3.775
17	0.190	5.255	42	0.268	3.725
18	0.191	5.237	43	0.281	3.555
19	0.191	5.224	44	0.285	3.514
20	0.193	5.179	45	0.292	3.423
21	0.194	5.156	46	0.294	3.398
22	0.194	5.153	47	0.307	3.261
23	0.199	5.028	48	0.307	3.260
24	0.201	4.983	49	0.325	3.078
25	0.202	4.962	50	0.327	3.058
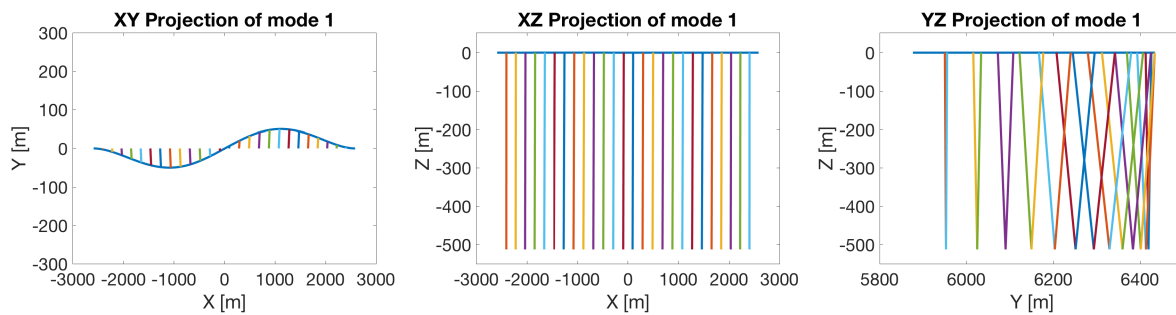
Figure 7.1: Eigenmode 1, T = 72.123 (horizontal mode).
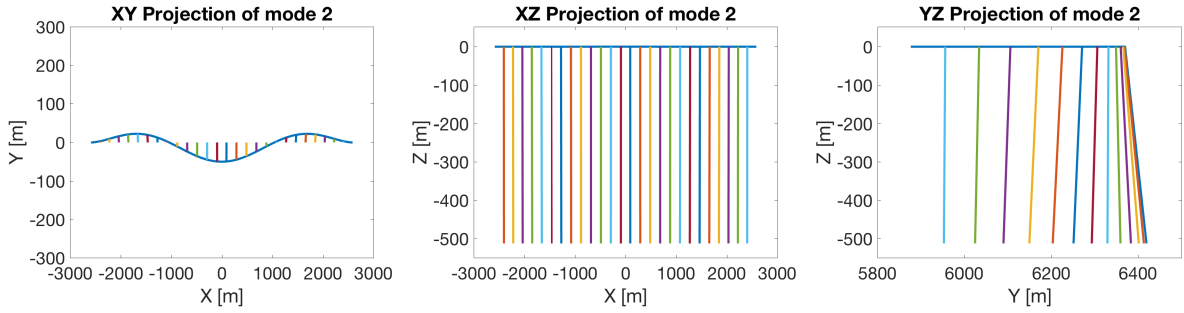
Figure 7.2: Eigenmode 2, T = 43.851 (horizontal mode).
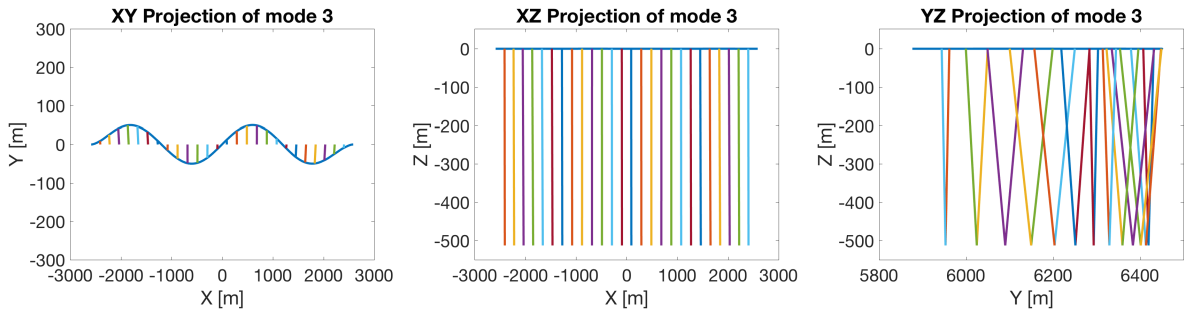
Figure 7.3: Eigenmode 3, T = 24.495 (horizontal mode).
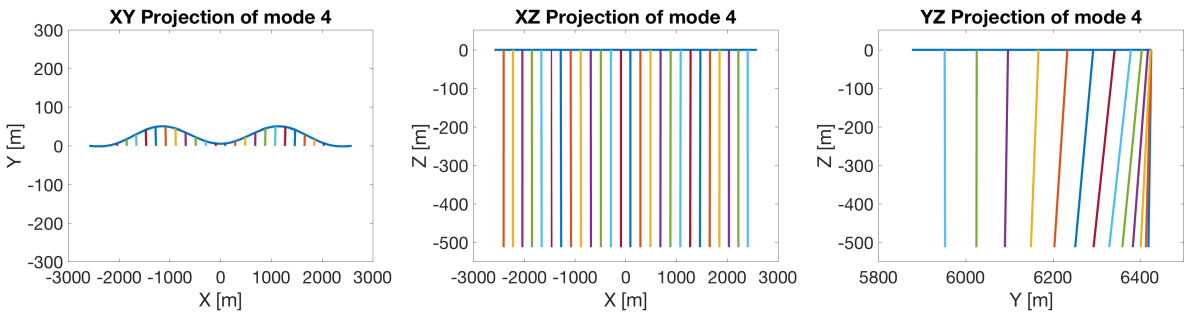
Figure 7.4: Eigenmode 4, T = 22.803 (horizontal mode).
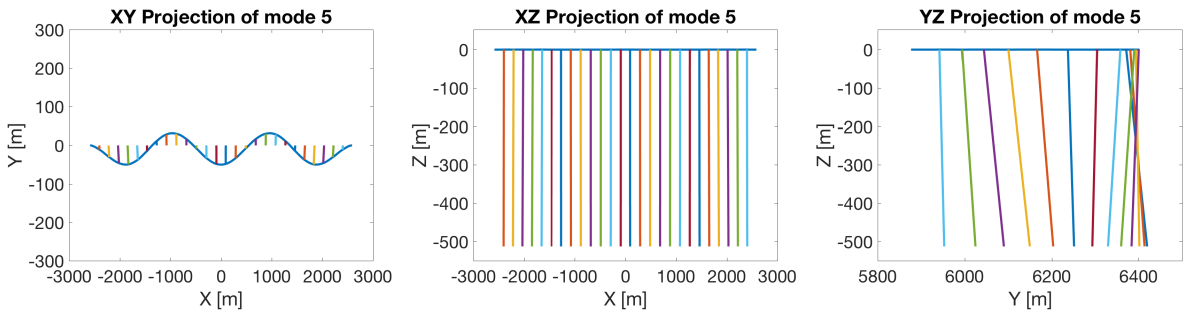
Figure 7.5: Eigenmode 5, T = 16.286 (horizontal mode).
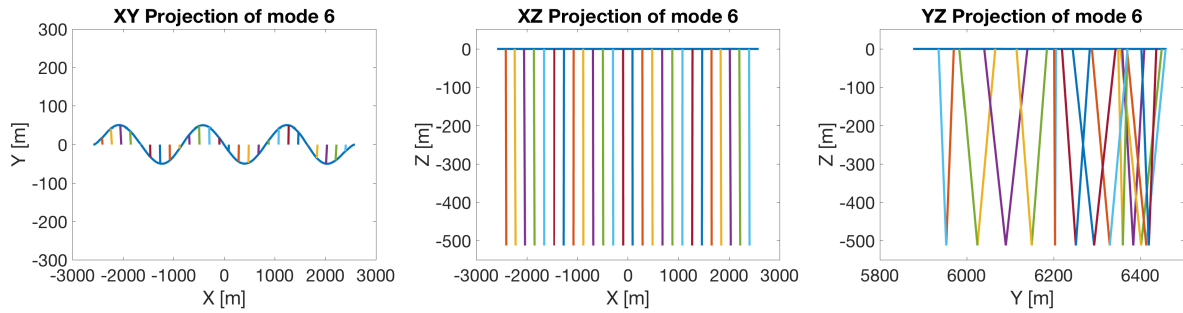
Figure 7.6: Eigenmode 6, T = 12.521 (horizontal mode).
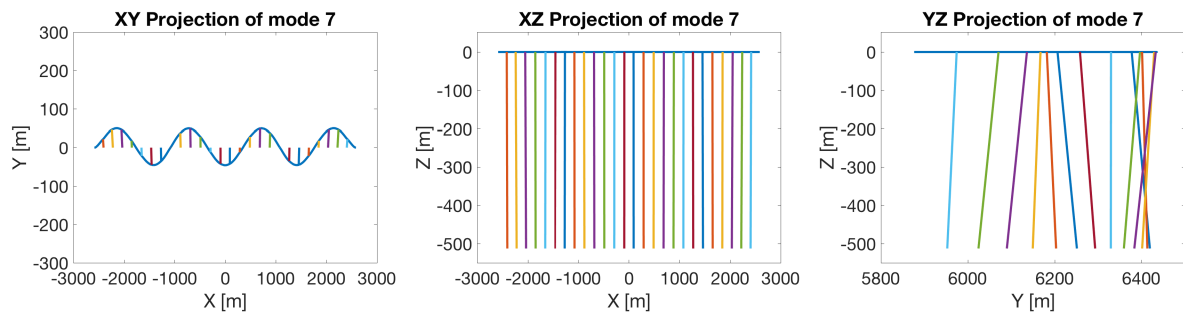
Figure 7.7: Eigenmode 7, T = 9.687 (horizontal mode).
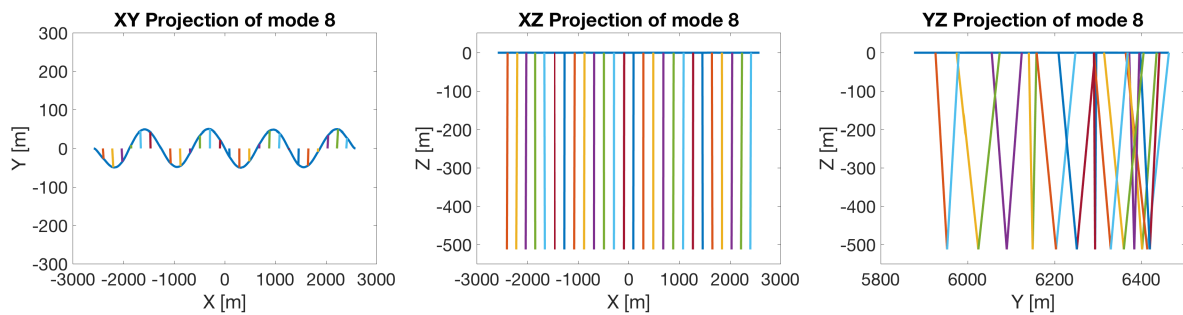
Figure 7.8: Eigenmode 8, T = 7.857 (horizontal mode).
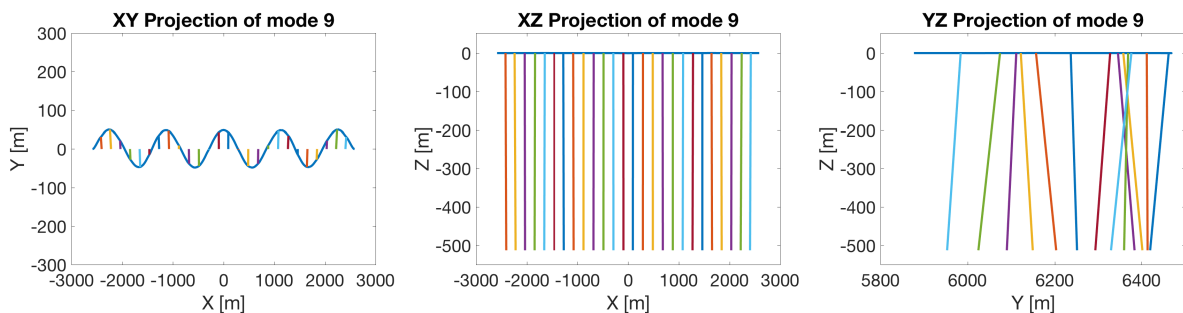
Figure 7.9: Eigenmode 9, T = 6.522 (horizontal mode).
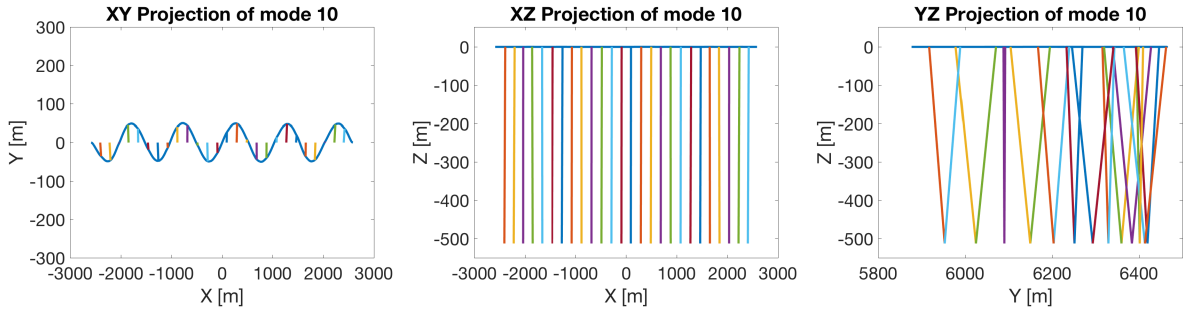
Figure 7.10: Eigenmode 10, T = 5.549 (horizontal mode).
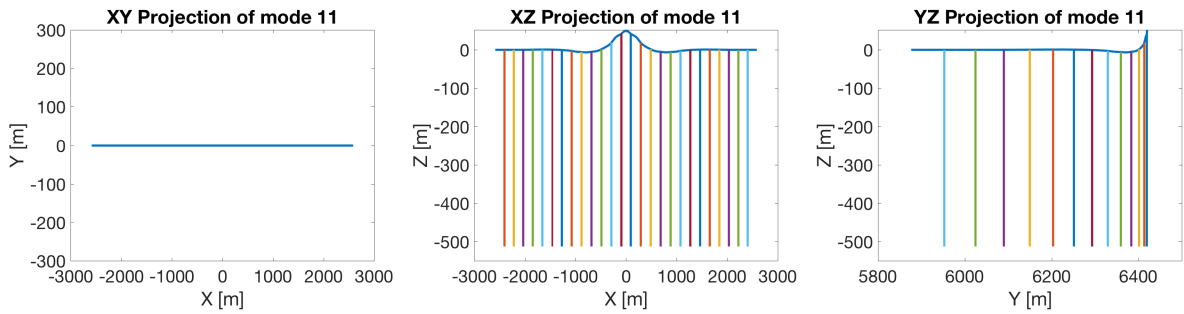
Figure 7.11: Eigenmode 11, T = 5.301 (vertical mode).
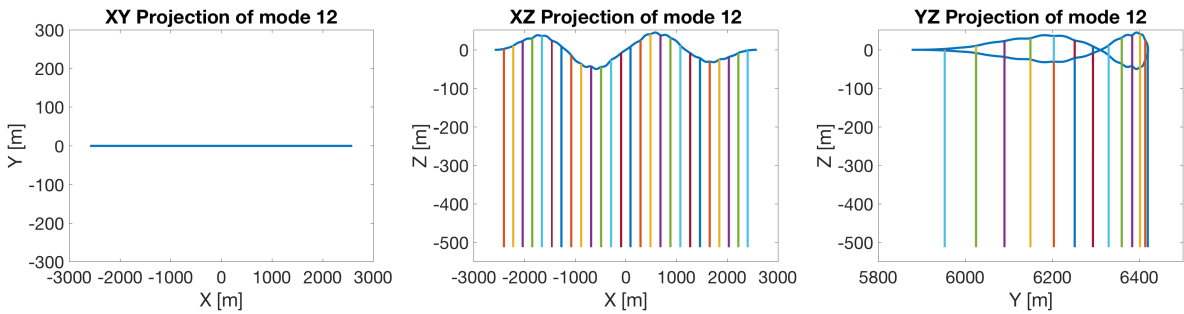
Figure 7.12: Eigenmode 12, T = 5.265 (vertical mode).
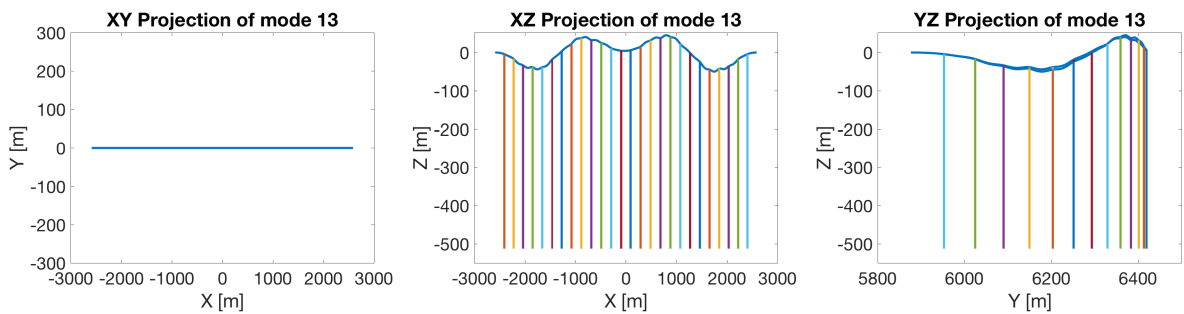
Figure 7.13: Eigenmode 13, T = 5.264 (vertical mode).

7.1.2 Tether

Analytical solutions

The first 20 eigenfrequencies for the tether with a tension of 14.5 MN accounting for the buoyancy, are found by equation 4.31, and given in table 7.4. These frequencies are the same for the horizontal and vertical motion, as the tether is axisymmetric.

Table 7.4: Anlytical horizontal and vertical eigenfrequencies for a tether with a tension T = 14.5 MN.

Mode	Frequency [Hz]	Period [s]
1	0.083	12.032
2	0.169	5.928
3	0.259	3.859
4	0.356	2.805
5	0.463	2.161
6	0.579	1.726
7	0.708	1.413
8	0.849	1.178
9	1.003	0.997
10	1.172	0.853
11	1.355	0.738
12	1.554	0.644
13	1.768	0.566
14	1.997	0.501
15	2.243	0.446
16	2.504	0.399
17	2.781	0.360
18	3.075	0.325
19	3.385	0.295
20	3.711	0.269

The first 20 eigenperiods found by equations 4.28, 4.29 and 4.31, are plotted and given in the figure 7.14. By studying the plot, it is seen that for the first periods, the equation for a beam with no tension (orange line) gives very high periods. The result of the equation for beam with tension (yellow line) gives very similar results to the equation for a stretched wire with tension (blue line).
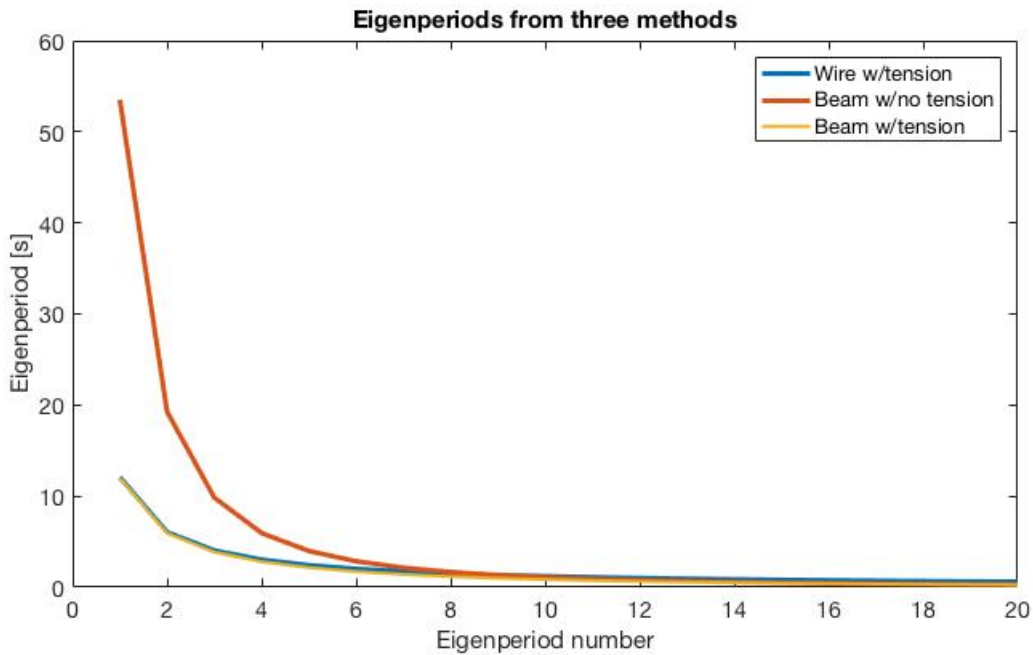
Figure 7.14: Resulting eigenfrequencies from equations 4.28, 4.29 and 4.31.

Computed from Riflex

The eigenfrequencies for a simple tether is found from Riflex. An equivalent vertical tension load of 14.5 MN is applied, to account for the buoyancy. Eigenfrequencies for tether are given in table 7.5.

The analytically calculated frequencies for a tether, table 7.4, correspond well with the frequencies from Riflex, table 7.5. The first period has a difference of 6.4 %. In the plots of the modes from Riflex in figures 7.15 - 7.18, it is seen that two and two frequencies are of same value and mode shape, but one appear in in-line motion and one appear in cross-flow motion.

Table 7.5: Computed eigenfrequencies for a tether with a tension T = 14.5 MN.

Mode	Frequency [Hz]	Period [s]
1	0.089	11.265
2	0.089	11.265
3	0.180	5.549
4	0.180	5.549
5	0.277	3.613
6	0.277	3.613
7	0.381	2.626
8	0.381	2.626
9	0.494	2.024
10	0.494	2.024
11	0.618	1.618
12	0.618	1.618
13	0.754	1.326
14	0.754	1.326
15	0.903	1.107
16	0.903	1.107
17	1.066	0.938
18	1.066	0.938
19	1.243	0.804
20	1.243	0.804
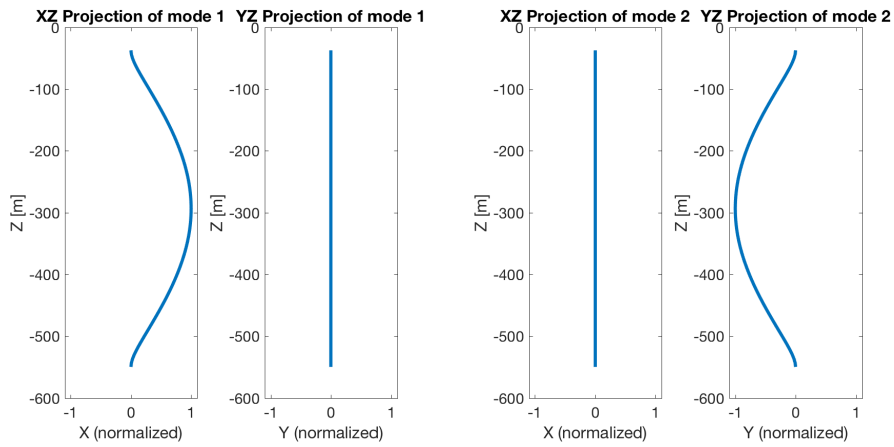
Figure 7.15: Eigenmode no 1 (left) and 2 (right) of tether. T = 11.265s.
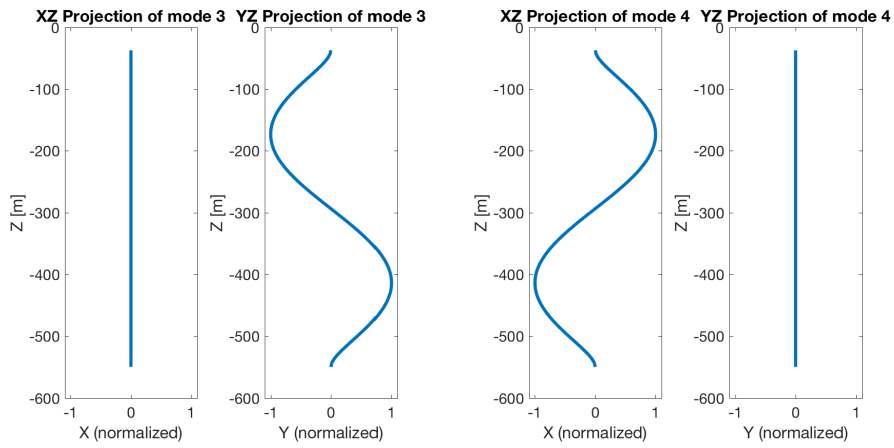
Figure 7.16: Eigenmode no 3 (left) and 4 (right) of tether. T = 5.549s.
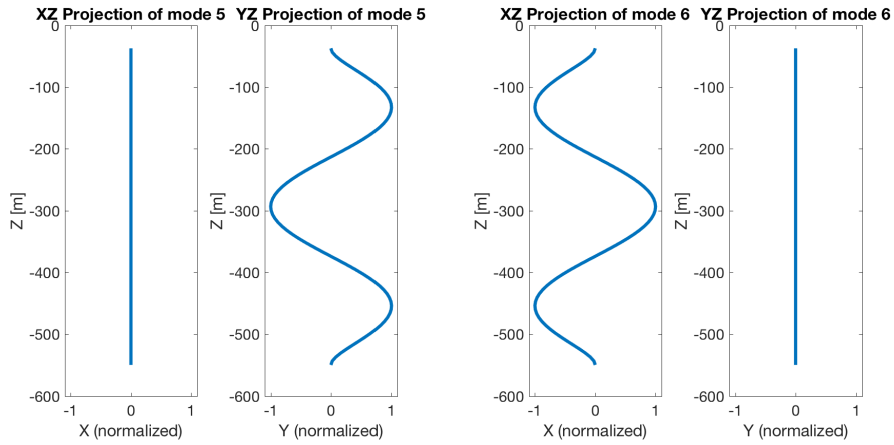
Figure 7.17: Eigenmode no 5 (left) and 6 (right) of tether. T = 3.613s.
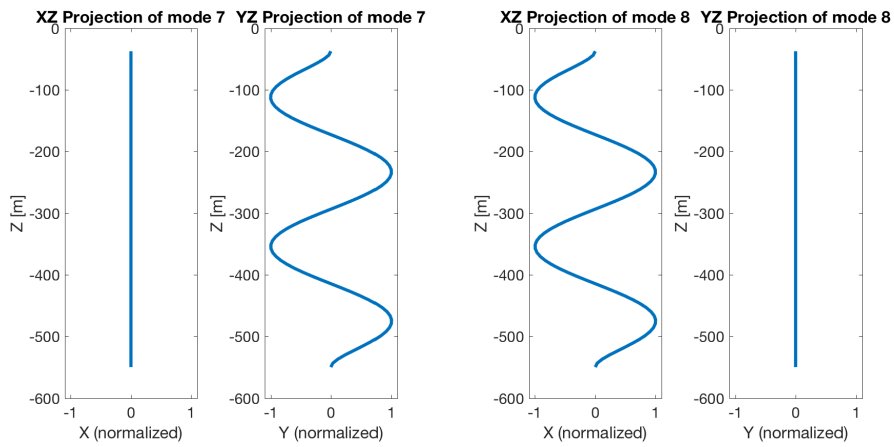
Figure 7.18: Eigenmode no 7 (left) and 8 (right) of tether. T = 2.626s.

7.1.3 Sensitivity to Tension in Tether and Length of Tether

Sensitivity studies with respect to the frequency is performed. Results from varying the tension in the tethers and varying the length of the tethers, when analysing the whole SFTB, are found in figures 7.19, 7.20 and 7.21. From the analysis varying the tension illustrated in both figures 7.19 and 7.20, it can be seen that the first frequency decreases with increasing concrete density and increases with increasing tension.

From the analysis varying the length of the tether illustrated in figure 7.21,it is seen that the eigenfrequency decreases with an increasing length. When the length of the tether becomes very large, a unit increase in length is less significant in the change of frequency.
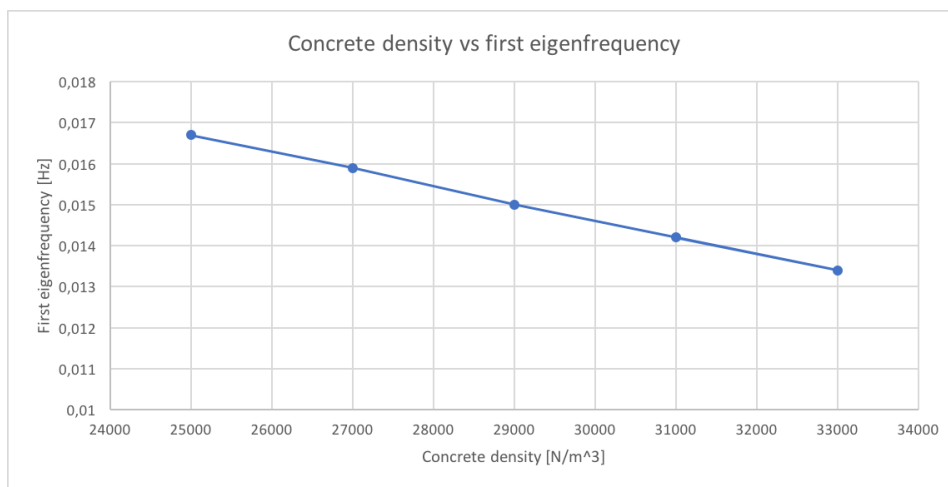
Figure 7.19: Concrete density against the first eigenfrequency.
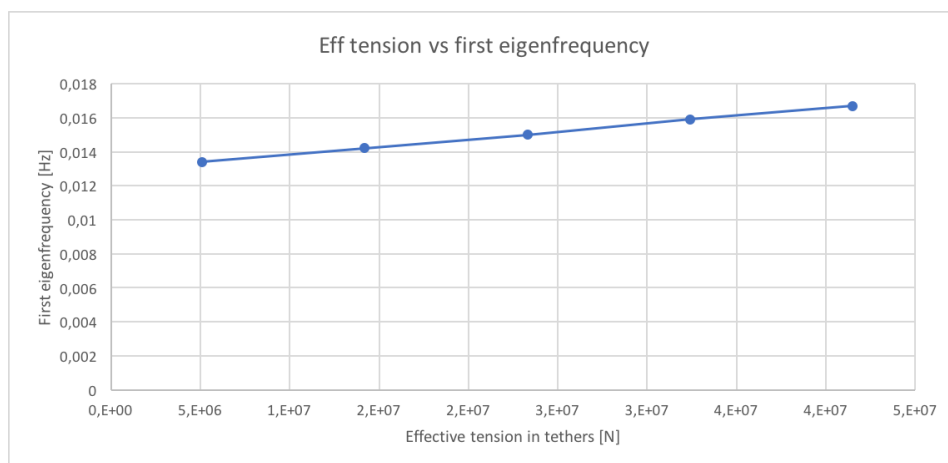
Figure 7.20: Effective tension in one tether against the first eigenfrequency.
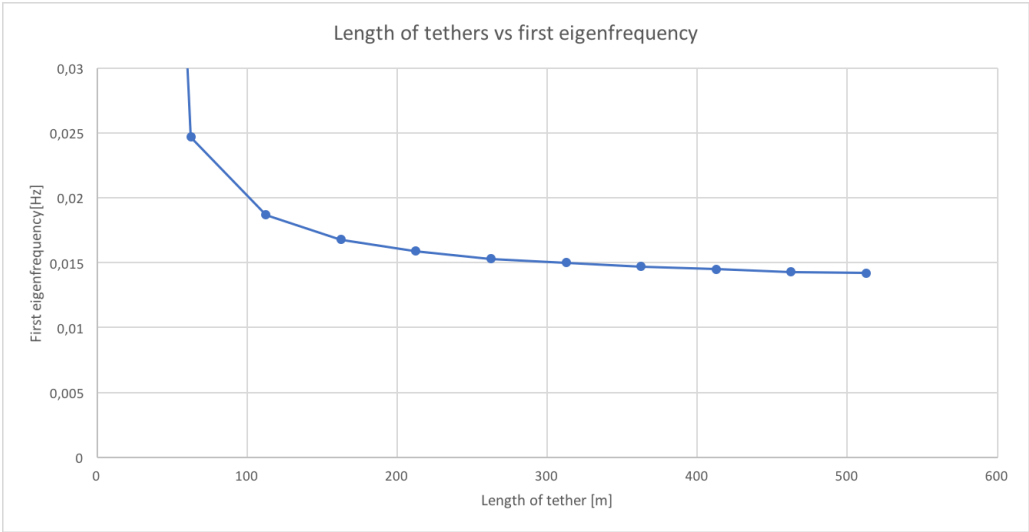
Figure 7.21: Length of tether against the first eigenfrequency.

7.2 DNV GL Expected VIV Response Amplitudes

7.2.1 First Estimate of Maximum Response Amplitudes

The in-line maximum amplitude is estimated from the DNV GL IL response model from section 4.4.2 by use of the stability parameter calculated in section 5.11. The CF maximum amplitude is estimated from the DNV GL CF response model from section 4.4.3, by use of the current flow velocity ratio, explained in section 5.11. This is done before taking into account the reduced velocity. Results are seen in table 7.6.

It is seen that according to Det Norske Veritas (2006), the maximum amplitude the tube can experience is 2.27 m in the in-line direction, while the maximum amplitude the tether can experience is 1.46 m in the cross-flow direction.

Table 7.6: Stability parameter, current flow velocity ratio and amplitudes estimated from Det Norske Veritas (2006).

Parameter	Unit	T9.5	Tether
K_{sd}	-	0.142	0.138
α	-	-	1
Amplitude IL	m	2.27	0.20
Amplitude CF	m	-	1.46

7.2.2 Second Estimate of Maximum Response Amplitudes for Tube T9.5

The reduced velocity for the tube T9.5 is calculated for the 10 first horizontal eigenfrequencies found from Riflex. From the DNV GL diagrams, the in-line amplitude can be estimated when the reduced velocity is known. The results are shown in table 7.7. The onset for in-line VIV is a reduced velocity larger than 1. With the current for the relevant depth, only the first eigenfrequency gives a reduced velocity larger than 1 for one tube of the bridge. Therefore only the first eigenfrequency is at risk for onsetting VIV, according to Det Norske Veritas (2006). However, for higher currents, also the second and maybe the third and fourth may give VIV. Hence, it is of relevance, checking for VIV in Vivana.

The maximum response amplitude for in-line was estimated from the DNV GL model to be 1 m at the first frequency, seen in table 7.7.

Table 7.7: The reduced velocity and the maximum expected IL amplitude of bridge according to Det Norske Veritas (2006).

Mode	Frequency [Hz]	Reduced Velocity [-]	Max Expected Ay/D [-]	Max expected amplitude [m]
1	0.014	1.643	0.06	1.01
2	0.023	0.999	0	0
3	0.041	0.558	0	0
4	0.044	0.519	0	0
5	0.061	0.371	0	0
6	0.080	0.285	0	0
7	0.103	0.221	0	0
8	0.127	0.179	0	0
9	0.153	0.149	0	0
10	0.180	0.126	0	0

7.2.3 Second Estimate of Maximum Response Amplitudes for Tether

With lay-by - Tension = 14.5 MN

The in-line reduced velocities are calculated from the in-line frequencies from Riflex for the tether with a 14.5 MN tension, and the cross-flow reduced velocities are calculated from the cross-flow frequencies. Max expected amplitudes predicted by Det Norske Veritas (2006) are found and results are given in table 7.8 and 7.9 As the onset for cross-flow VIV is a reduced velocity at about 2, no cross-flow VIV is expected at this current velocity.

For the tether with a tension of 14.5 MN, it was estimated from Det Norske Veritas (2006) that only the first frequency would yield VIV in-line response. The maximum response amplitude was estimated to be 5.6 cm.

Table 7.8: The reduced velocities and corresponding maximum expected IL amplitudes of tether according to Det Norske Veritas (2006). Tension = 14.5 MN.

Mode	Frequency [Hz]	Reduced Velocity [-]	Max Expected Ay/D [-]	Max expected amplitude [m]
1	0.0888	1.48	0.05	0.056
3	0.1802	0.73	0	0
5	0.2768	0.475	0	0

Without lay-by - Tension = 10.5 MN

The in-line reduced velocities are calculated from the in-line frequencies from Riflex for tethers with a tension of 10.5 MN. The cross-flow reduced velocities are calculated from the cross-flow frequencies. Maximum expected amplitudes predicted by Det Norske Veritas (2006) are found and the results are given in table 7.10 and 7.11. As the onset

Table 7.9: The reduced velocities and corresponding maximum expected CF amplitudes of tether according to Det Norske Veritas (2006). Tension = 14.5 MN.

Mode	Frequency [Hz]	Reduced Velocity [-]	Max Expected Az/D [-]	Max expected amplitude [m]
2	0.0888	1.48	0	0
4	0.1802	0.73	0	0
6	0.2768	0.475	0	0

for cross-flow VIV is a reduced velocity of about 2, no cross-flow VIV is expected at this current velocity.

For the tether with a tension of 10.5 MN, it was estimated that only the first frequency would yield VIV in-line response, according to Det Norske Veritas (2006). The maximum response amplitude was estimated to be 8.4 cm.

Table 7.10: The reduced velocities and corresponding maximum expected IL amplitude of tether according to Det Norske Veritas (2006). Tension = 10.5 MN.

Mode	Frequency [Hz]	Reduced Velocity [-]	Max Expected Ay/D [-]	Max expected amplitude [m]
1	0.0766	1.7171	0.075	0.084
3	0.1563	0.842	0	0
5	0.2421	0.543	0	0

Table 7.11: The reduced velocities and corresponding maximum expected CF amplitude of tether according to Det Norske Veritas (2006). Tension = 10.5 MN.

Mode	Frequency [Hz]	Reduced Velocity [-]	Max Expected Az/D [-]	Max expected amplitude [m]
2	0.0766	1.7171	0	0
4	0.1563	0.842	0	0
6	0.2421	0.543	0	0

7.3 Vivana Analyses

7.3.1 Bridge

The maximum in-line response amplitude of the main bridge for the current, calculated by Vivana is 0.86 m. Snapshots of the outer tube can be seen in figure 7.22. Only the first natural frequency is excited. The response frequency is 0.013 Hz and the response natural period, T = 78.43s. The results and the calculated horizontal acceleration to be checked with limit requirements from the NPRA are found in table 7.12. The maximum IL moment (about the z-axis) is evaluated.
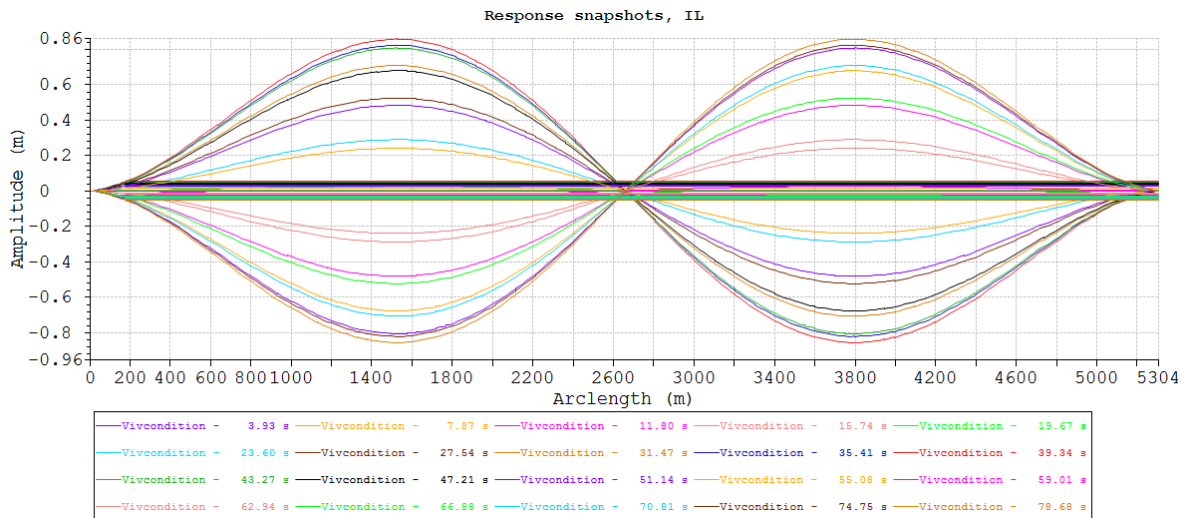
Figure 7.22: Snapshot of the tube for 1 period. The IL frequency is 0.013. The coloured lines represent displacement at time increments during on period.

Table 7.12: Results from IL VIV-analysis of bridge.

Response frequency [Hz]	Response period [s]	Amplitude [m]	Horizontal Acceleration [m/s^2]
0.013	78.43	0.86	5.67·10^{-3}

The moment on the bridge is not given explicitly from Vivana and can be estimated from the stress amplitudes by two methods, from equation 4.52 and from equation 4.49. From the latter, equation 7.1 can be derived by assuming the moment about the y-axis to be zero in the case of pure in-line motion. Since the force is not explicitly given by Vivana, a relative factor between the force and the moment about the z-axis can be assumed in the estimation of the moment from VIV. The equation is then solved with respect to Mz. By studying resulting force and moments from the dynamic analysis, the relative stress resulting from the force and moment can be calculated. At the point of max deflection from VIV, it is estimated that the force gives a stress of 1.88 MPa in equation 7.2 and the moment gives a stress of 1.10 MPa in equation 7.3. The force and moment is taken from figures 7.33 and 7.35 at a length of bridge ≈ 1540 m, to get the value where maximum IL occur at the bridge. At this point, the T9.5 cross-section

is the present cross-section for the tube, hence the corresponding values found from table 5.1 are used.

$$M_{viv,2} = \frac{\sigma A I_z}{1.71 I_z + Ay} \tag{7.1}$$

The relative factor is then calculated to be 1.71 in equation 7.4.

$$\sigma_F = \frac{F}{A} = \frac{70MN}{37.3m^2} = 1.88MPa \tag{7.2}$$

$$\sigma_{M_z} = \frac{M_z}{I_z}y = \frac{100MNm}{572.6m^4}6.3 = 1.10MPa \tag{7.3}$$

$$Relative factor = \frac{1.88}{1.10} = 1.71 \tag{7.4}$$

The moment in equation 7.1 is then calculated to be 36.6 MNm by equation 7.5. In this calculation, the cross-sectional parameters from the Vivana model is used, found in table 5.2.

$$M_{viv,2} = \frac{2.5MPa \cdot 29.7m^2 \cdot 518.5m^4}{1.71 \cdot 518.5m^4 + 29.7m^2 \cdot 6.3} = 36.6MNm \tag{7.5}$$

From equation 4.52, the maximum moment is calculated to be 106.5 MNm in equation 7.6.

$$M_{viv,1} = 0.86 \left(\frac{2\pi}{\frac{5304}{2}\left(1 - \frac{0.33}{2}\right)} \right)^2 30 \cdot 10^9 \cdot 518.5m^2 = 106.45MNm. \tag{7.6}$$

If compared to each other, these methods give significantly different moments.

7.3.2 Tethers

With lay-by - Tension = 14.5 MN

The excited in-line frequency for a tether with a tension of 14.5 MN is 0.089 Hz. This is the first frequency. Snapshots of the whole period can be seen in figure 7.23. Amplitude is found to be 3.6 cm. No cross-flow excited at this current velocity, also as expected from the estimates in section 7.2.3. The results with the accumulated damage and the corresponding fatigue life are summarized in table 7.13.
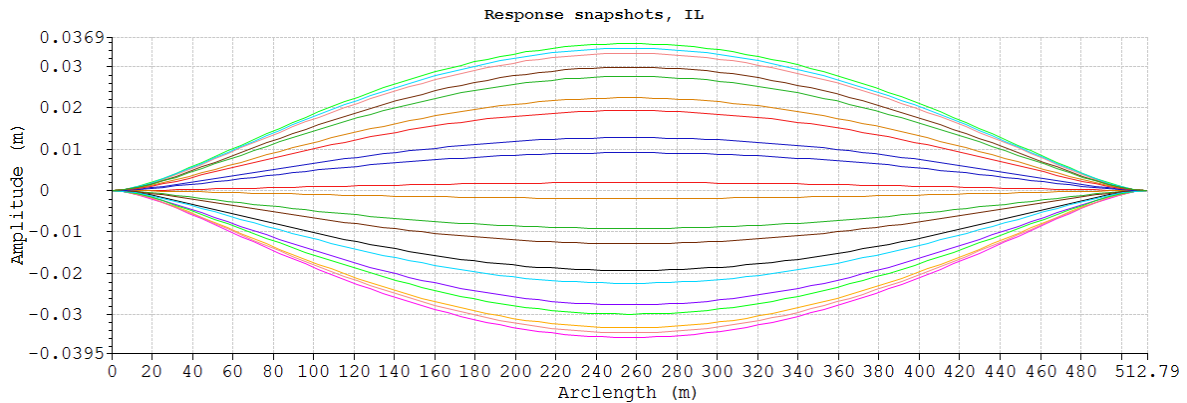
Figure 7.23: Snapshot of the tether for 1 period. The IL frequency is 0.089. The coloured lines represent displacement at time increments during on period.

Table 7.13: Results from IL VIV-analysis of tether with a tension of 14.5 MN.

Response frequency [Hz]	Response period [s]	Amplitude [m]	Accumulated Damage [1/y]	Fatigue life [y]
0.089	11.23	0.036	$0.31713 \cdot 10^{-6}$	$0.31533 \cdot 10^{7}$

Without lay-by - Tension = 10.5 MN

The excited in-line frequency for a tether with a tension of 10.5 MN is 0.077 Hz. This is the first frequency. Snapshots of the whole period can be seen in figure 7.24. Amplitude is found to be 7.5 cm. No cross-flow excited at his current velocity, also as expected from the estimates in section 7.2.3. The results with the accumulated damage and the corresponding fatigue life are summarized in table 7.14.
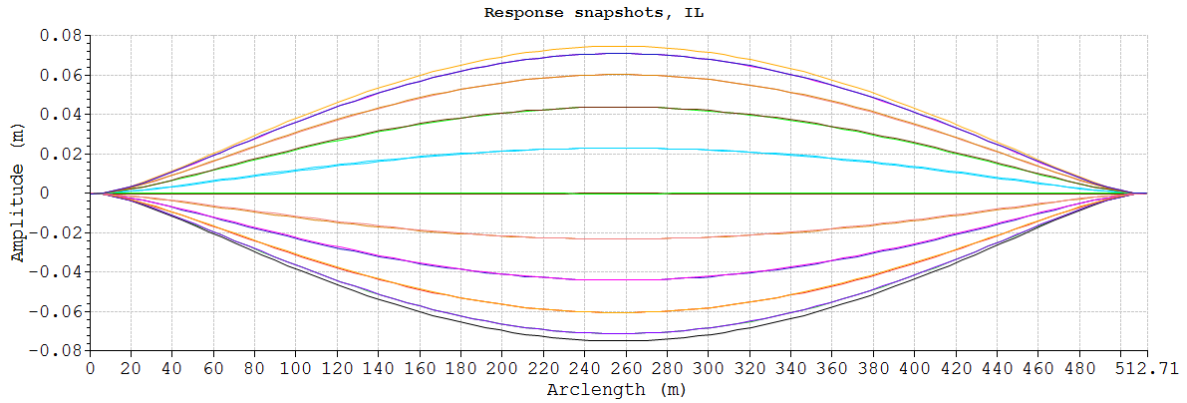
Figure 7.24: Snapshot of the tether for 1 period. The IL frequency is 0.077. The coloured lines represent displacement at time increments during on period.

Table 7.14: Results from IL VIV-analysis of tether with tension of 10.5 MN.

Response frequency [Hz]	Response period [s]	Amplitude [m]	Accumulated Damage [1/y]	Fatigue life [y]
0.077	12.98	0.075	$0.30114 \cdot 10^{-5}$	$0.33207 \cdot 10^{6}$

7.3.3 Varying Current - Correspondence with DNV GL

To check how the amplitudes will vary for different scales of the current velocity, the Vivana analysis is run for different velocities and compared with predictions by DNV GL. Results from analysis with scaling the current is shown for the bridge and the tether. Only in-line motion is analysed for the bridge, while both in-line and cross-flow are analysed for the tether with a tension of 14.5 MN.

Bridge IL

Table 7.15 gives results for the in-line motions of the main tube. It can be seen that at a current scale of 0.7, no in-line VIV is excited. At a current scale of 2.1, the second mode is excited. Therefore, no higher scaling is performed. In figure 7.25, the results from table 7.15 is plotted with the response model from DNV GL.

Table 7.15: Vivana IL results for the main tube with a current scaling from 0.7 to 2.1.

Current scaling	Mode no.	Response frequency [Hz]	Amplitude [m]	Ay/D [-]	Reduced velocity [-]
0,7	No significant VIV occur		0,000	0,000	1,214
0,8	1	0,013	0,227	0,018	1,387
1	1	0,013	0,858	0,068	1,734
1,1	1	0,013	0,963	0,076	1,907
1,2	1	0,013	1,082	0,086	2,081
1,3	1	0,013	1,304	0,103	2,254
1,4	1	0,013	1,293	0,103	2,427
1,5	1	0,014	1,248	0,099	2,601
1,6	1	0,014	1,292	0,103	2,774
1,7	1	0,014	0,941	0,075	2,948
1,8	1	0,015	0,927	0,074	3,121
1,9	1	0,015	1,165	0,092	3,294
2	1	0,015	1,246	0,099	3,468
2,1	2	0,021	1,506	0,120	3,641

The in-line response amplitudes for the bridge increase with increasing current velocity up to a current scale of 1.3. This is seen as the amplitudes are increasing with increasing reduced velocities up to 2.3, which is a function of the current. After this, the amplitudes are held approximately constant for increasing reduced velocity. This correspond well the in-line model from DNV GL.

The results seem the follow the lines for K_{Sd} quite well, but for a higher K_{Sd} than predicted in table 7.6, giving a lower amplitude than predicted. The response follows the ksd of 0.5, which is over 2x of the predicted value.

The results stops around a reduced velocity of 3.5, as after this only higher modes were excited. There is a decrease in the amplitude around a reduced velocity of 3.
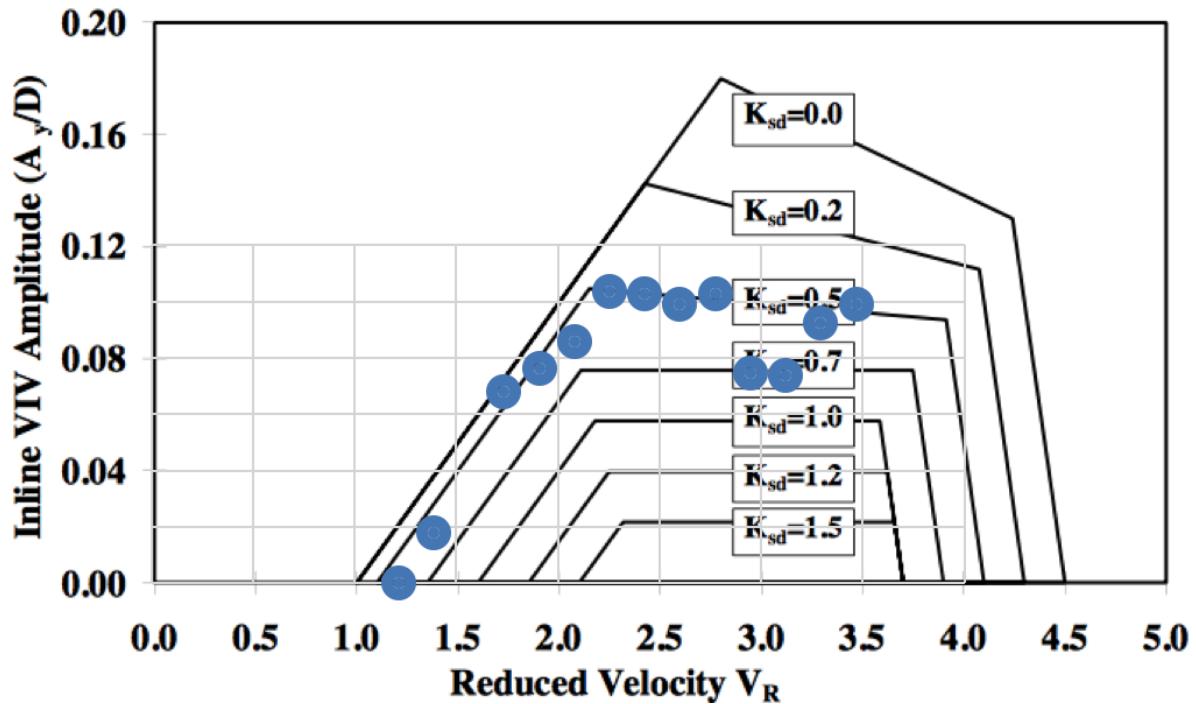
Figure 7.25: IL VIV-results for the main tube compared to the DNV GL IL model. Only first frequency included.

Tether IL

Table 7.16 gives results for the in-line motions of the tether. It can be seen that at a current scale of 0.5, no in-line VIV is excited. At a current scale of 2.4, the second mode is excited. Therefore, no higher scaling is performed. In figure 7.26, the results from table 7.16 is plotted with the response model from DNV GL.

Table 7.16: Vivana IL results for tether with a current scaling from 0.5 to 2.4.

Current scaling	Mode no.	Response frequency [Hz]	Amplitude [m]	Ay/D [-]	Reduced velocity [-]
0,5	Excitation zone too smal		0	0	0,741
1	1	0,089	0,036	0,032	1,481
1,5	1	0,092	0,111	0,099	2,222
1,6	1	0,093	0,128	0,115	2,370
1,8	1	0,098	0,148	0,132	2,666
2	1	0,101	0,142	0,127	2,962
2,2	1	0,104	0,141	0,126	3,259
2,4	2	0,181	0,084	1,744	3,555

The in-line response amplitudes for the tether increase with increasing current velocity up to a current scale of 1.8. This is seen as the amplitudes are increasing with increasing reduced velocities up to 2.7, which is a function of the current. After this, the amplitudes are held approximately constant for increasing reduced velocity. This correspond well the model from DNV GL.
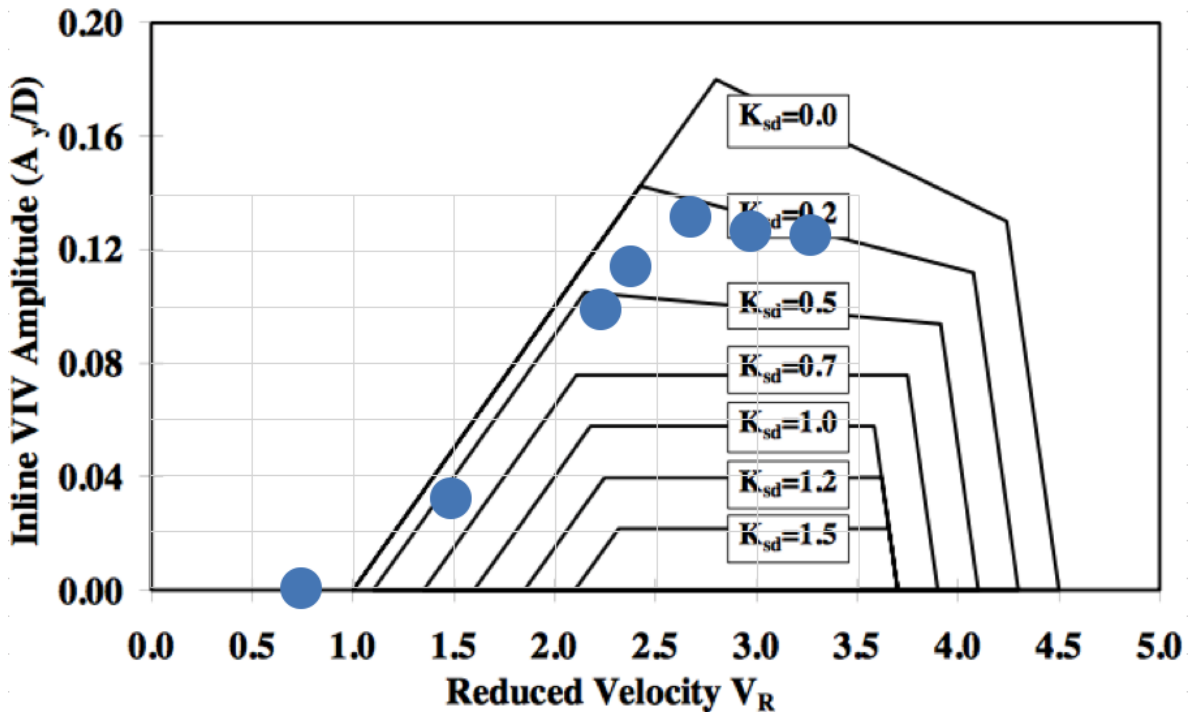
Figure 7.26: IL VIV-results for the tether compared to the DNV GL IL model. Only first frequency included.

The results for the tether IL seem the follow the lines for K_{Sd} of 0.5 quite well for the increasing part. This is a higher ksd than predicted by 4.21, giving a lower amplitude than predicted. The ksd seem to lay around 0.25 at the stabilized region, which is around 2x of the predicted value. The results stops around a reduced velocity of 3.5, as after this only higher modes where excited.

Tether CF

Table 7.17 gives results for the cross-flow motions of the tether. It can be seen that at a current scale of 2, no cross-flow VIV is excited. At a current scale of 4.5 and 5, both the first and the second mode is excited. Therefore, no higher scaling is performed. In figure 7.27, the results from table 7.17 is plotted with the response model from DNV GL.

The cross-flow response amplitudes for the tether increase with increasing current velocity up to a current scale of 4. This is seen as the amplitudes are increasing with increasing reduced velocities up to 5.9, which is a function of the current. After this, the amplitudes decrease for increasing reduced velocity. This is unexpected compared to the DNV GL CF model.

The results for the tether CF are not inside the maximum prediction for the given reduced velocities. The amplitudes are higher than predicted for the same reduced velocities.

The results stops around a reduced velocity of 8, as after this only higher modes where excited. Also for this case, there is a decrease in the amplitude around a reduced

Table 7.17: Vivana CF results for tether with a current scaling from 2 to 5.5.

Current scaling	Mode no.	Response frequency [Hz]	Amplitude [m]	Az/D [-]	Reduced velocity [-]
2	No significant VIV occur		0	0	2,963
2,5	1	0,076	0,570	0,510	3,704
3	1	0,072	0,956	0,855	4,445
3,5	1	0,078	1,113	0,996	5,186
4	1	0,088	1,129	1,010	5,927
4,5	1	0,096	0,744	0,666	6,668
4,5	2	0,162	0,017	0,015	3,288
5	1	0,108	0,646	0,578	7,409
5	2	0,154	0,020	0,018	3,654
5,5	1	0,117	0,850	0,760	8,149
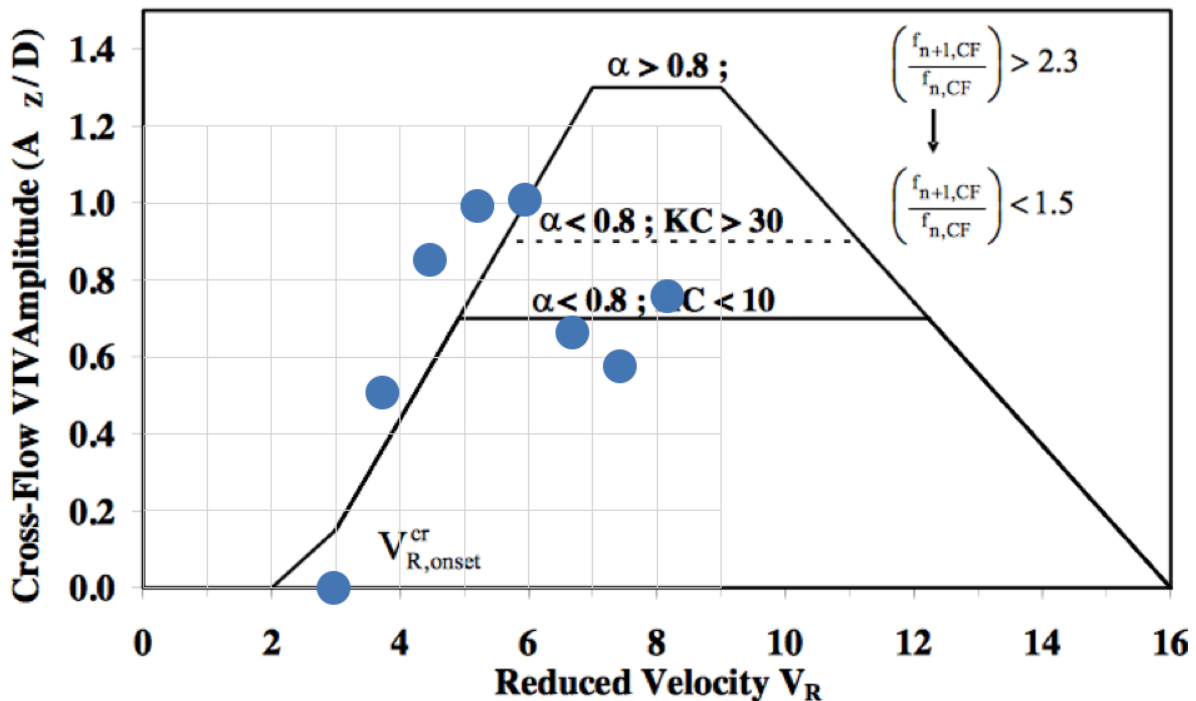
Figure 7.27: CF VIV-results for the tether compared to the DNV GL CF model. Only first frequency included.

velocity of 7. From the results it is seen that at this value of reduced velocity, more than one frequency is excited. This may be the reason for the decrease in amplitude for the first frequency as the other excited frequencies are disturbing the response.

The cross-flow relationship found between the reduced velocity and the amplitude for the tether is not as corresponding as the in-line. The onset for VIV for the tether seem to be at a reduced velocity of a little over 3.

7.4   Dynamic Analyses

The envelopes for maximum and minimum response for each point of the bridge is shown. The plots are made by extracting files with information from Riflex and making a script that plots in Matlab. The envelope plots are a representation of the overall maximum and minimum values found at each integration point of the bridge, for all the conditions run. They do not give information on the simultaneous occurrence of forces/etc. The red lines represent results from analysis when wind-sea only is applied, while the blue lines represent results from analysis with both wind-sea and swell applied.

7.4.1   Displacements
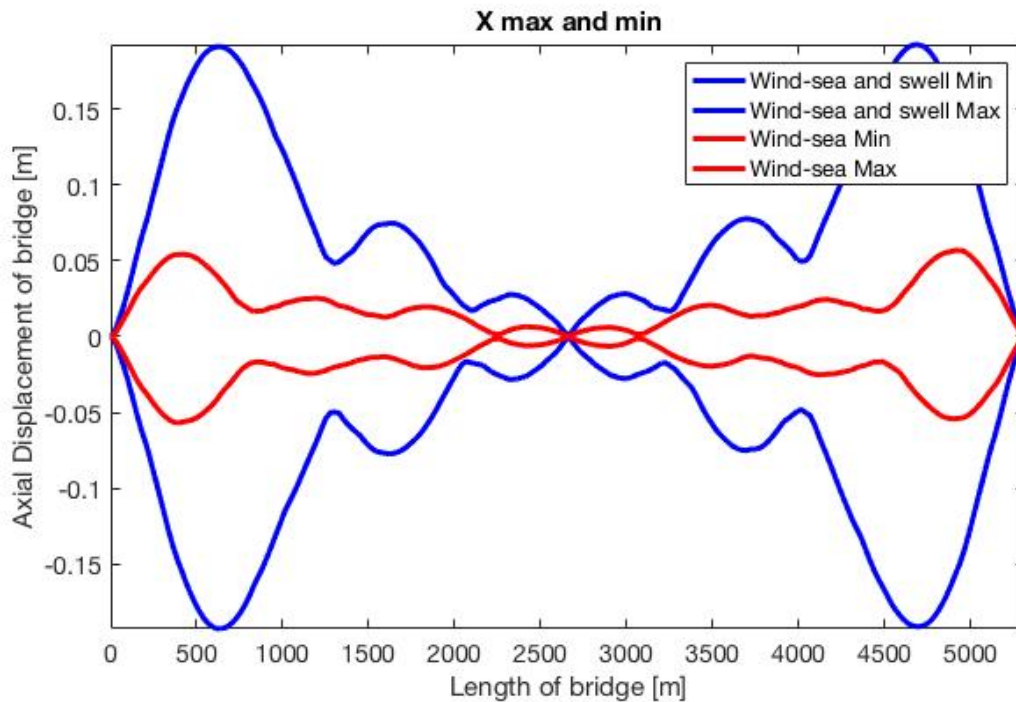
Figure 7.28: Maximum and minimum envelopes of axial displacement for 3h wind-sea (red lines) and 3h wind-sea and swell (blue lines).

It can be seen from figures 7.28 and 7.29 that for axial and horizontal motion, the swell wave is very dominant. For vertical motions, figure 7.30, the swell does not contribute so much to the displacement.
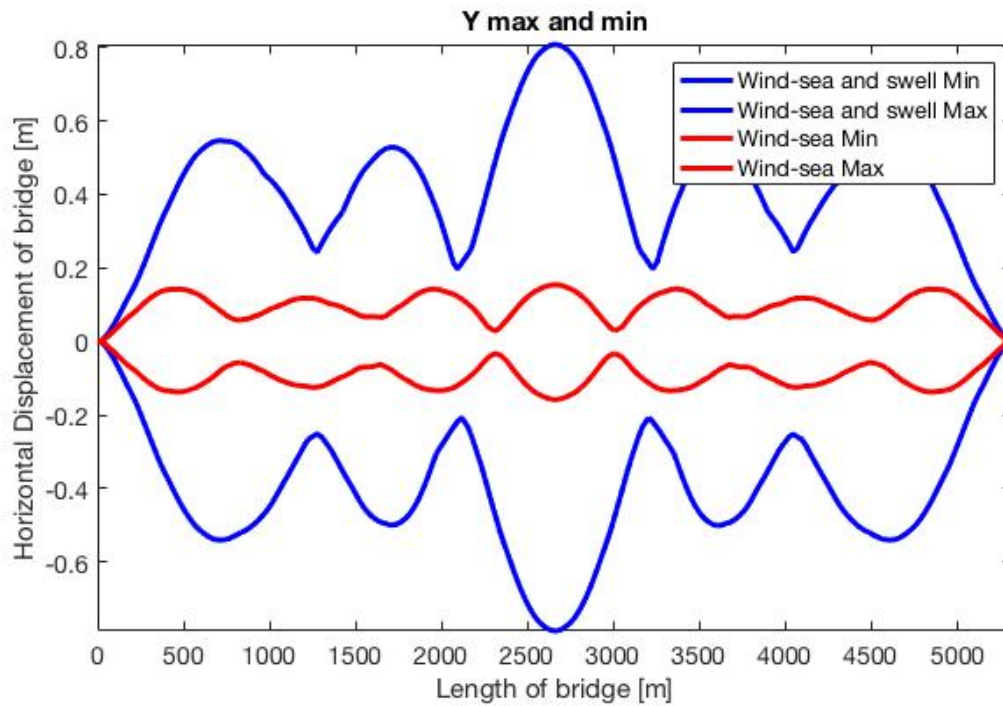
Figure 7.29: Maximum and minimum envelopes of horizontal displacement for 3h wind-sea (red lines) and 3h wind-sea and swell (blue lines).
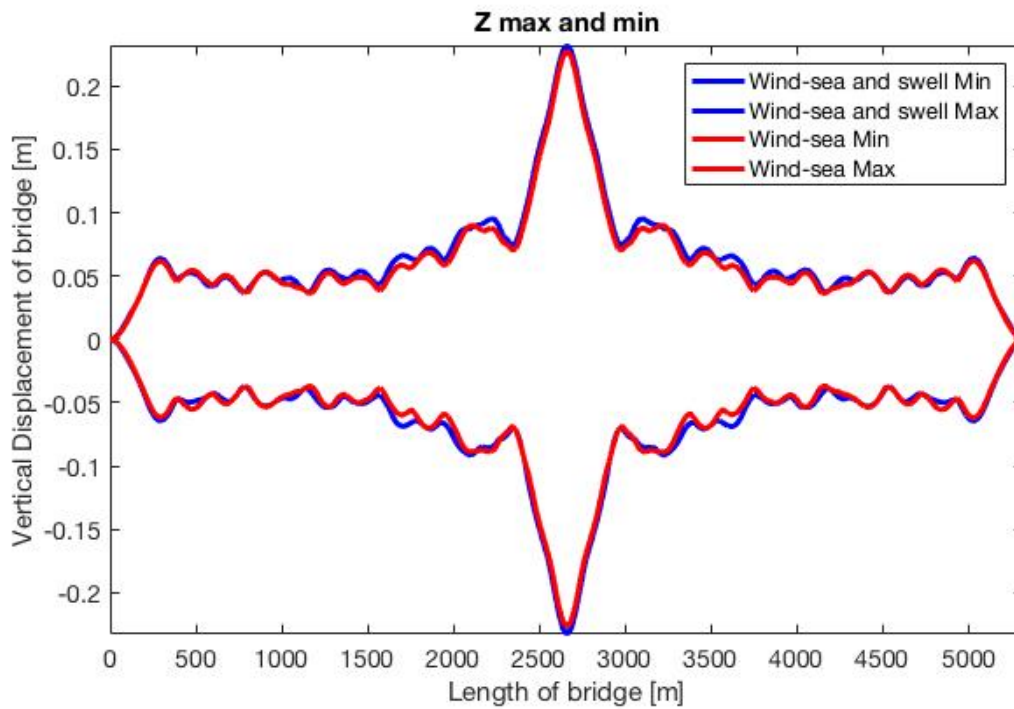
Figure 7.30: Maximum and minimum envelopes of vertical displacement for 3h wind-sea (red lines) and 3h wind-sea and swell (blue lines).

7.4.2   Tether Tension

The tether tension for all tethers are plotted by use of Excel. Figure 7.31 shows response of only wind-sea applied, while figure 7.32 shows response from wind-sea and swell applied. The plot shows the tension per tether. The mooring groups are represented by four tether dots.
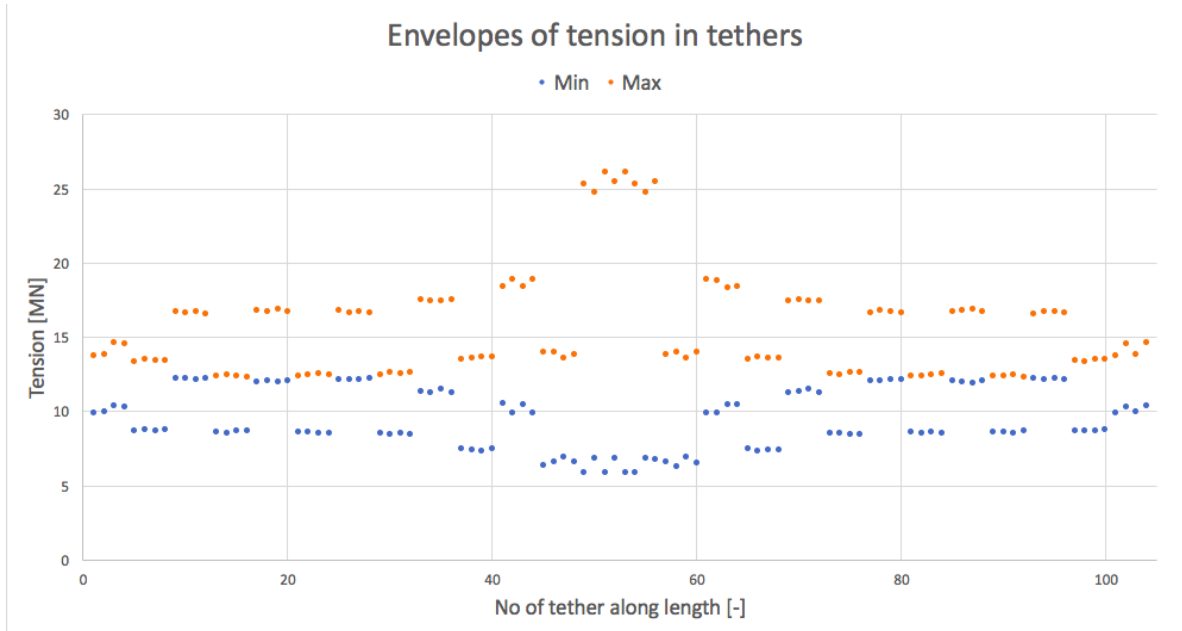
Figure 7.31: Maximum and mimimum tension in each tether from 3h wind-sea condition.
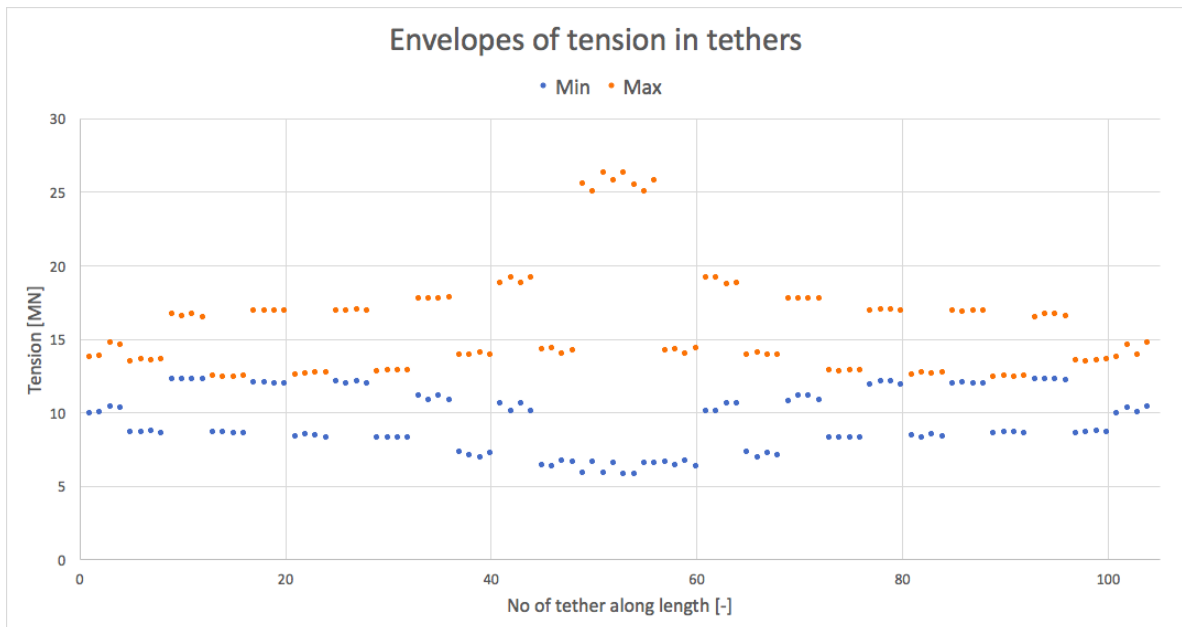
Figure 7.32: Maximum and mimimum tension in each tether from 3h wind-sea and swell condition.

It can be seen that the swell wave does not make a significant difference for the tether tension. The tension varies between 5 MN and 27 MN, and is seen to be a little larger for

some tethers (about 0.5 MN) with swell. Also here one can see the result of having two cross-over tubes with a larger net buoyancy in the middle, as this gives more tension in the tethers of the middle tethers. The small variation of the symmetry in the plots 7.31 and 7.32, is due to misreferencing between the four tethers in each mooring group and their corresponding number along the x-axis of the plot.

7.4.3 Forces and Moments

The axial force and the moment about y and z-axis are shown in figures 7.33, 7.34 and 7.35. The axial force is very dominated by the swell wave, as seen in figure 7.33. In the plot for the moment about the y-axis, figure 7.34, a small swell-dependence is seen, as there are small difference between results from the two conditions. The plot for the moment about the z-axis, figure 7.35, again illustrates the importance of swell waves for horizontal motions, as there is a large difference between max and min for the two types.
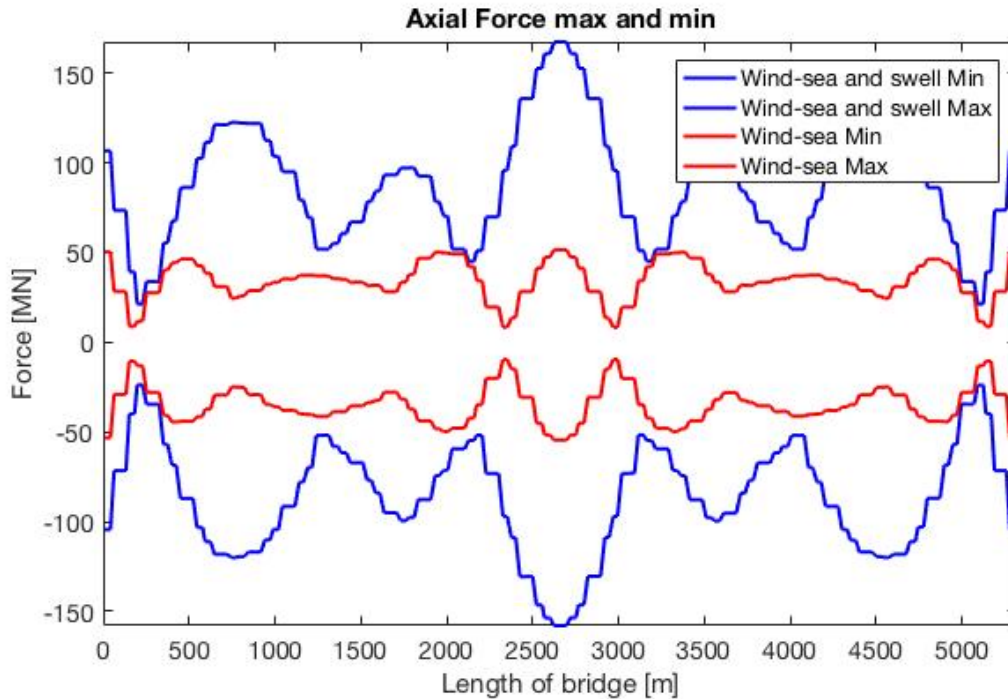
Figure 7.33: Maximum and minimum envelopes of axial force for 3h wind-sea (red lines) and 3h wind-sea and swell (blue lines).
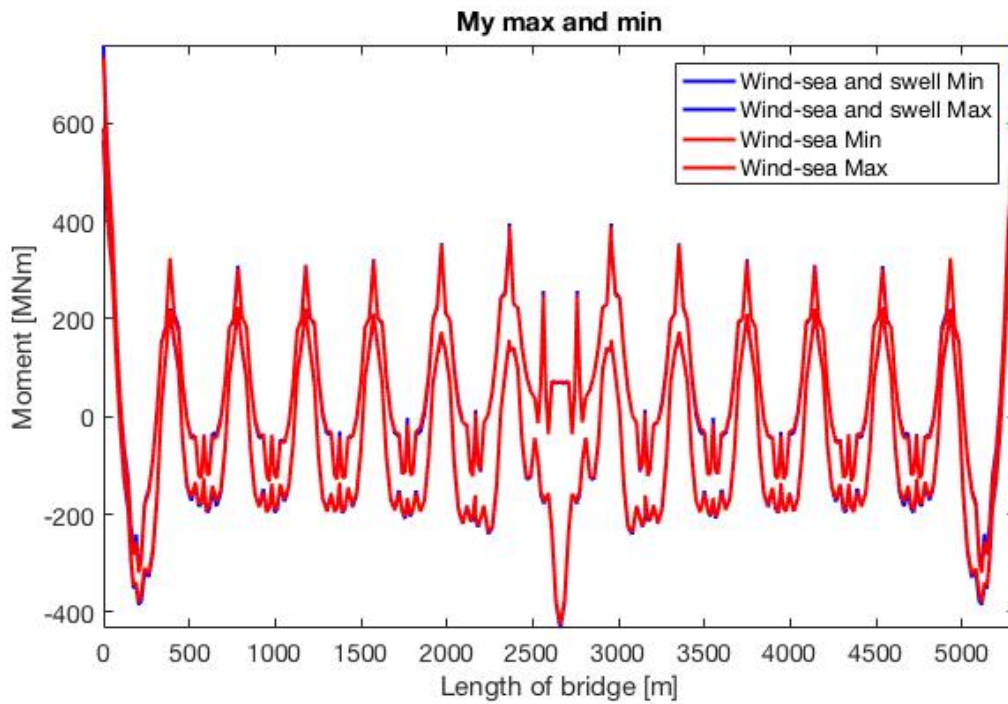
Figure 7.34: Maximum and minimum envelopes of moment about y-axis (My) for 3h wind-sea (red lines) and 3h wind-sea and swell (blue lines).
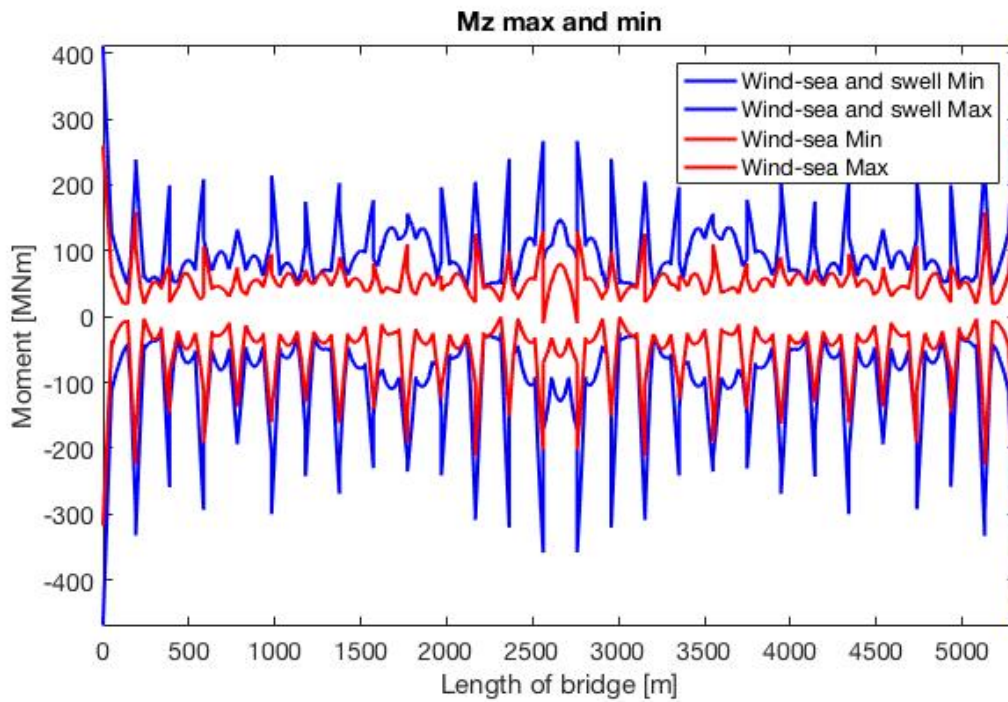
Figure 7.35: Maximum and minimum envelopes of moment about z-axis (Mz) for 3h wind-sea (red lines) and 3h wind-sea and swell (blue lines).

7.4.4 Stress in Cross-sections

The stress over the cross-sections are summarized in figure 7.18 for only wind-sea and 7.19 for wind-sea and swell.

Table 7.18: Maximum and minimum stress from wind-sea calculated at 8 points around cross-section of main tube.

	Stress summary outer tube - all lines, element 1, end 1 [MPa]									
	First 150 m		First 150 -1000 m		Middle part		Last 150-1000 m		Last 150 m	
	Max	Min	Max	Min	Max	Min	Max	Min	Max	Min
Point 1	2,635	-0,624	1,666	-0,672	2,312	-1,049	1,866	-0,598	0,435	-0,669
Point 2	-1,960	-5,380	2,857	-2,910	2,617	-3,654	3,138	-3,163	1,554	-3,541
Point 3	-3,613	-6,121	3,759	-3,932	2,811	-4,733	3,769	-3,942	2,212	-4,658
Point 4	-2,268	-5,793	2,725	-3,410	2,083	-3,937	2,745	-3,640	1,681	-3,309
Point 5	2,154	-2,635	0,896	-1,666	1,333	-2,312	1,317	-1,866	0,708	-0,435
Point 6	5,380	1,960	2,910	-2,857	3,654	-2,617	3,163	-3,138	3,541	-1,554
Point 7	6,121	3,613	3,932	-3,759	4,733	-2,811	3,942	-3,769	4,658	-2,212
Point 8	5,793	2,268	3,410	-2,725	3,937	-2,083	3,640	-2,745	3,309	-1,681

Table 7.19: Maximum and minimum stress from wind-sea and swell calculated at 8 points around cross-section of main tube.

	Stress summary outer tube - all lines, element 1, end 1 [MPa]									
	First 150 m		First 150 -1000 m		Middle part		Last 150-1000 m		Last 150 m	
	Max	Min	Max	Min	Max	Min	Max	Min	Max	Min
Point 1	3,897	-3,419	2,762	-1,983	3,892	-2,910	3,138	-2,425	1,217	-1,444
Point 2	-1,075	-6,270	3,747	-3,467	3,445	-4,596	3,534	-4,176	1,759	-4,045
Point 3	-3,587	-6,316	3,880	-3,918	2,818	-4,811	3,879	-3,908	2,313	-4,648
Point 4	-1,377	-6,677	3,171	-3,971	2,668	-5,359	3,092	-4,713	1,916	-3,828
Point 5	3,419	-3,897	1,983	-2,762	2,910	-3,892	2,425	-3,138	1,444	-1,217
Point 6	6,270	1,075	3,467	-3,747	4,596	-3,445	4,176	-3,534	4,045	-1,759
Point 7	6,316	3,587	3,918	-3,880	4,811	-2,818	3,908	-3,879	4,648	-2,313
Point 8	6,677	1,377	3,971	-3,171	5,359	-2,668	4,713	-3,092	3,828	-1,916

From tables over stress-extremals in cross-sections, the axial bending stress is seen to increase with the application of the swell wave.

Chapter 8

Discussion

8.1 Modal Analysis

In this section, resulting eigenfrequencies from analytical methods and from Riflex are discussed. Comparisons to reference results are also discussed.

8.1.1 Bridge

From the basic equation for eigenfrequency, for instance 4.46, it is known that for the eigenfrequency to be larger, either the stiffness has to be larger or the mass has to be smaller. Considering the first mode which is significantly different between the two analytical methods estimating the frequency, seen in table 7.1, the assumed shape function is perhaps not so good, or the relationship between the mass and the stiffness is different. For the modes from 2 to 10, the frequencies coincide well. From this it can be concluded that the assumption on the shape function used for the Generalized Modal Analysis is valid for the modes 2-10.

The eigenfrequencies resulting from the Generalized Modal Analysis (from equation 4.46, seen in table 7.2) are not found in the usual increasing order, and they have a "random" appearance of frequencies. The mode shape with the lowest energy will appear first, and this has always the longest period. It can be seen that frequency number 4 has the longest period and hence the lowest energy. According to the method of Generalized Modal Analysis, this frequency will appear first. The fact that the vertical frequencies appear in the "random order" is a result of the calculations done, and the effect of concentrated mass and stiffness points in the formula.

The difference in frequencies between analytical and computed methods can be explained by the assumptions in the analytical methods. By comparing calculated eigenperiods for a simple straight and curved beam from equations 4.29 and 4.30, it is found that for this case, the eigenperiod is larger for a straight beam, than for a curved beam. Therefore it is reasonable to assume that the actual eigenperiod for this curved SFTB is smaller than what calculated analytically, as these analytical methods are developed

for straight beams. A curved beam will have a smaller period than a straight beam as the arch shape makes it more stiff.

Differences can also be explained by that compared to simplified methods, the program has information about all components of the SFTB, including the cross-over tubes, bracings and parts of main tubes with larger cross-sections due to the lay-bys. This gives a different mass and stiffness distribution for the resulting calculation. Hence, the program is able to calculate frequencies for the specific, detailed model, while the analytical methods only give approximated frequencies.

The computed values for the bridge in table 7.3 correspond well with the eigenfrequencies of the reference model from 3D Float from table 3.9, but are in general, a little higher. The first vertical mode is found at mode no 11, with a period of 5.3s, while the first reference vertical mode is at period 4.8s. This is only a 10 % difference. The reference eigenmode no 3 looks a lot like the computed eigenmode no 4. The value of the eigenperiods are both at about 23s, with only a 0.3 % difference.

After the ten first computed eigenfrequencies in table 7.3, the frequencies increases very slowly, compared to the reference results. This may be due to a difference in the number of elements used for the different parts in the two analyses. In the reference analysis, the bridge was modelled a little different than in this thesis. The span of the bridge, the horizontal radius and the number of tether groups were different. Also the reference bridge was modelled only with a T9.5 cross-section, and not with the T12.5 for the parts with emergency lay-bys. All these factors will influence the mass and stiffness, which is what the eigenfrequency is dependent on.

The effect on including the local response of the tethers can be seen in appendix C.2.1. If more elements are used for the tethers, coupled frequencies are found. This means that also the tethers are excited and combined with response from the bridge giving a very complex response. It is seen that the number of eigenfrequencies found before reached a specific value decreases with the decrease in number of elements for the tethers. For instance, 331 frequencies were needed, before reaching what seems to be the first vertical mode of 5.3s, compared to only 11 frequencies for the run with 1 element per tether.

8.1.2   Tether

The frequencies and plots of the analysed tether in figures 7.15 - 7.18 seem reasonable, as the analytical results coincide very well with the computed results.

As the result in figure 7.14 of the equation for a beam with tension gives very similar results to the equation for a stretched wire with tension, it is judged that the tension in the beam is dominant in the calculation of the periods. This is probably due to the length of the tether, as this will decrease the importance of the term involving the bending stiffness of the beam, as seen in equation 4.31. It is also noted that the equation 4.31 gives accurate enough results for this case, even though the boundary conditions are different than what is meant for the equation. This is also due to the length of the tethers, as the mode shape will only be affected by the boundary conditions

very close to the ends. For the rest of the length, the effect of the boundary conditions will be less significant.

8.1.3 Sensitivity Studies

In figures 7.19 and 7.20 it is observed that with an increasing density of the material comes a decreasing net buoyancy of the bridge, resulting in a decreasing tension in the tethers. From the parameter analysis with varying length of the tethers shown in figure 7.21, it can be observed that the eigenfrequency decreases with an increasing length. From these results, it is seen that the response is in accordance with theory from section 4.6.

8.2 VIV Response

In this section, comparison between expected VIV response found from DNV GL VIV Response Models are compared to response found from analyses in Vivana.

8.2.1 Bridge

Vivana calculated the VIV in-line response amplitude of the bridge to be 0.86 m. This is only 86 % of what was estimated by the DNV GL model. The calculated acceleration of $5.67 \cdot 10^{-3}$ is well within the requirements of maximum horizontal accelerations. Hence, VIV at a 100y return period will not be a problem for accelerations, according to results from Vivana.

The two methods estimating the maximum moment from VIV does not coincide and give a difference in results of 34 %. These calculations are only to be considered a first estimate of the moment, as they both are based on approximated methods. For later estimations, results would be improved if Vivana gave the moment directly as part of the output. However, the moments obtained can be used in a first comparance to moments from waves.

8.2.2 Tether

From Vivana, the amplitude responses were 3.6 cm for the tether with a 14.5 MN tension and 7.5 cm for the 10.5 MN tension, both excited at the first frequency. This is respectively, 64 % and 89 % lower than what estimated from the DNV GL model. No cross-flow VIV was predicted. From these results, it is found to be a small risk of the tethers arranged in one tether group colliding, even under extreme conditions, due to the low amplitudes compared to the 12.5 m distance between tethers. However, only one tether was analysed, and the coupling of several tethers close to each other were not studied.

By looking at the different results between the two tethers of different tensions, it is seen that decreasing the tension in the tether, gives a higher in-line amplitude. The effect of the tension is not included in the DNV GL models, and this is seen to be a relevant parameter.

8.2.3 Varying Current

In the figures for IL and CF amplitudes for a varying reduced velocity, figures 7.25 - 7.27, only response in mode 1 is included. For larger current scalings, the response jumps to higher modes, and this also lowers the reduced velocity. Therefore it is experienced that it is difficult to obtain amplitude response for the last section of the graph.

The damping ratio, ζ_T, is in general difficult to predict for a structure, and therefore, also the stability parameter, K_{Sd}, is difficult to calculate. The estimation still resulted in an amplitude response giving conservative results. As seen in figures 7.25 and 7.26 the DNV GL IL model is in general overestimated and therefore give conservative results. The decrease in the amplitude around a reduced velocity of 3 for the bridge in figure 7.25 is an unexpected response and the reason for this is unknown. As only one frequency is included in the plots, the decrease should not be a result of the damping, as this is frequency-dependent. From conversation with co-supervisor Svein Sævik, the response in general looks good and as expected from previous similar work. Previously it has been found that Vivana usually gives about 80 % of what the DNV GL models predict. This correspond well with results in this thesis.

Amplitude results for the tether in cross-flow (figure 7.27) are not inside the maximum prediction for the given reduced velocities. The amplitudes are higher than predicted for the same reduced velocities. This could be critical in a real life situation, as the DNV GL model predicts too low response for the case. The decrease in the amplitude around a reduced velocity of 7 is probably due to the frequency being disturbed by the other frequencies that are excited at the same time.

In general the tube experienced a lower in-line VIV response amplitude from Vivana than the tethers. This may be because of the horizontal stiffness from the tethers holding the tube back in place, giving smaller horizontal motion amplitudes than the tethers.

8.2.4 Limitations of Vivana

Vivana should be further improved, if analysis on major structures are to be analysed for conventional use. The program is not made for working with many lines of a structure. The results in the post-processor are plotted for the structure as a whole, with the lines not in order. So processing of the results is hard when one have a large structure with many lines, as one can not choose what parts of the structure to study results from.

Vivana does also not include the fact that the velocity is reduced for the tube in the wake of the other (Passano, 2017). This is noticed as the current velocity applied for nodes on the two tubes are the same. In reality, the tube laying in the shadow of the

other, will experience a smaller current, according to equations 4.3 and 4.5. Therefore, an identical amplitude and snapshots of the downstream tube can be found from the results. The effect of this could have been included in a first estimate by reducing the drag force on the second cylinder accordingly. However, a complete CFD analysis, or even an experimental analysis would most probably yield more reliable results.

8.3 Dynamic Analyses

This section discusses the results from the dynamic wave analysis and compares results to reference results.

The vertical motion is seen to be less responsive to the inclusion of swell waves, compared to the horizontal motion, as seen from figures 7.28, 7.29 and 7.30. This may be due to a different set of mode shapes contributing in the vertical direction, giving smaller vertical displacements. Also there is a higher stiffness in the vertical direction due to the tethers. It is seen in figures 7.31 and 7.32 that the tension in the tethers is not increased significantly with the addition of swell. It is hence concluded that the low vertical motion is a result of different mode shapes acting in the vertical direction. This results in lower amplitudes for the vertical motion.

8.3.1 Displacements

When comparing the results from the Riflex analysis of swell waves (blue lines), with the reference results from 3D Float, appendix B.3.1, the maximum and minimum value of the axial and horizontal displacement correspond well, at around 0.2m for the axial and 0.8m for the horizontal displacement. The trend over the axial translation is largest on the sides of the bridge, and smallest in the middle, seen in both the reference results and Riflex results. It is logical that the axial displacement is largest on the sides, as the load is applied 90 degrees onto the middle part of the bridge. Due to the curvature of the bridge, the displacement will therefore be more axial on the sides, where the axial component of the load is larger.

The maximum horizontal displacement is seen at the middle of the bridge for the Riflex model. This is not the case for the reference model. Also, they do not have the same amount of half waves. This is a result of a different set of contributing mode shapes excited by the load case.

There is a significant peak in the middle of the bridge for the vertical displacement of the Riflex model. From the static results in appendix C.1.2, this is also seen for the symmetric model. While for the unsymmetric model, appendix C.1.1, there is no such peak. Consequently, the peak is found to be due to the two cross-over tubes with lay-by that are placed on the two middle mooring points, and that have a larger net buoyancy than the cross-over tubes without lay-by. The trend for the rest of the vertical displacement is the varying buoyancy between the tubes and the cross-over tubes. This is seen for both the reference model and the Riflex model. We can see from appendix B.3.1 that the reference results for the vertical translation envelope, is largest

at the area where the tethers are the longest. This is due to the elasticity of the tethers. As the Riflex model has a constant length of the tethers, this trend is correspondingly not seen here. The maximum displacement is about 10x larger for the Riflex model than for the reference model. This comes from the previously discussed larger net buoyancy of the bridge at the middle with the two cross-over tubes with lay-by. Disregarding the middle of the bridge, the displacement is only about 2-3x larger than for the reference model.

8.3.2 Forces and Moments

Comparing the axial forces from Riflex in figures 7.33 with the reference model in appendix B.3.1, the max value is about half the value of the reference model of 300 MN. The maximum force in the Riflex model is seen to be at the middle of the bridge, where the buoyancy is the largest.

The moment about the z-axis in figure 7.35 has maximum values around 200 MNm at the middle part and around 400 MNm at the supports. The minimum values have a slightly higher absolute value. The reference results have a similar behaviour, but are shifted about 100-150 MNm in the negative direction, for both the maximum values and the minimum values. The reference model has a stable moment between the ends and the middle of bridge, while the Riflex model has a larger difference. This may be due to softer constraints used at the supports for the reference model.

The moment about the y-axis in figure 7.34 has maximum values around 300-400 MNm at the middle part of the bridge and about 700 MNm at the ends. The moment at the support does not vary much and the minimum value is about the same as the maximum value. For the middle of the bridge, the minimum value is around -200 MNm and -400 at the point of the largest buoyancy. The reference results has maximum values around 200 MNm for the middle part of the bridge and minimum values around -200 MNm. At the supports, the reference moment is varying between 600 and -600 MNm. It is noted that the reference moment varies more along the whole bridge, while the Riflex moment varies only significantly for the points where the cross-over tubes have larger buoyancy.

8.3.3 Tether Tension

From the envelopes of the tether tension it is seen that there will never be pressure or slack in the tethers at the load conditions analysed. Compared to the reference results, the Riflex model has a larger maximum tension. This is due to a larger net buoyancy of the whole bridge.

8.3.4 Stress in Cross-sections

The stresses are from the dynamic analysis including weight and buoyancy. The reference results in appendix B.3.2 have included also current in their load case and it is therefore difficult to compare with Riflex results, not including current. Also, the

reference results are a combination of static and dynamic analysis multiplied with a load factor. It is then expected that the results will be higher in magnitude for the reference model.

There is in general smaller axial bending stresses reported for the Riflex model and the environment conditions used in this thesis, as seen in tables 7.18 and 7.19. The stress is seen to increase with the application of the swell wave. The stresses are seen to be higher than the tensile strength of the concrete, defined in table 3.3. This support the need for reinforcement and pre-stressing of the concrete by steel.

8.4 Significance of VIV

It is observed that the horizontal amplitude displacement is almost the same from waves and from VIV. When studying the response of the tube, it is seen that the 100y current gives VIV. Due to the nature of VIV being onset at specific current velocities, it is interesting to note at what return period for the velocity the VIV actually has its onset. It is seen in table 7.15 that for a current scale of 0.7 of the 100y return period, there is no in-line VIV. This velocity is 0.189 m/s. From table 3.8 with values of current velocities for different return periods, a current of 0.189 m/s corresponds to a 1y return period for the current at the depth. This implies that VIV wil occur more seldom than once a year. VIV is seen to occur at a current scale of 0.8, which yields a velocity of 0.216 m/s, which is less than the 10y current velocity. By assuming the relationship between the return periods as linear, the exact return period can be found by interpolation. This velocity is interpolated to have a return period of 7.16 years. Return periods for found VIV amplitude responses can be seen in table 8.1.

Table 8.1: Return periods for found VIV response.

Current scale [-]	Current velocity [m/s]	Return period [year]	Amplitude [m]
0.7	0.189	1	0
0.8	0.216	7.16	0.227
1	0.27	100	0.858

The maximum moment about the z-axis from waves are found to lay between 300 and 400 MNm. The estimated maximum moment from VIV is about 100 MNm, which is significantly smaller than the moment from waves. VIV can still be of a concern due to fatigue. Fatigue for tethers are seen to be very small and it is expected they will not experience significant damage. The tube however, is not analysed for fatigue, and this could be done in a further analysis. An SN curve for the tube with a concrete material would need to be established. It would be interesting to see how the concrete material responded to fatigue.

Waves will always be present, and will induce moments and stresses at all times. VIV however, will only be onset for current velocities that happen, statistically one time every 7 years and higher. The amplitude is at this return period only 22 cm, and it is expected that the moments will be smaller than what calculated for the 100y VIV. It can be discussed how crucial this is and for how long periods this will happen. It is important that the tube is designed to have frequencies that give small reduced

velocities, to avoid larger VIV response than anticipated here. Important to recall is the tandem effect that is not included, which may give different VIV response.

8.5   Discussion of Parameters Used

The assumption for the bracing being rectangular, in the calculation of drag force, added mass and torsional stiffness, can be discussed. However, the analysis done is a global analysis, so the use of more accurate values for these parameters, would probably not affect the results so much. This also goes for the cross-over tubes, on the assumption for rectangular cross-section, with no walls inside.

The drag coefficient from the wind tunnel test report could have been used for the main cross-sections, T9.5 and T12.5. This would give a higher response from current and waves. However, during the work it was decided on using the values given during supervision by Tore Søreide.

The use of the E-modulus for the concrete can be discussed as the effect of the pre-tension of reinforcement of the concrete are not included. This would in reality stiffen the material and make it less probable to give the actual response.

More sets of wave conditions could have been used in order to gain knowledge about the most extreme load case realistic for the area. More runs including more of the swell sea states given in section 3.6.1 could have been conducted.

The current velocity analysed for VIV is assumed as the maximum current to be expected during a 100y period. The current will in usual cases be lower than this, and the response correspondingly lower.

Chapter 9

Conclusive Remarks

The conclusive remarks can be summarized as

- The computed eigenfrequencies for the Riflex model are in general a little higher than the computed frequencies for the reference model by 3D Float. This is a result of a slightly different mass and stiffness distributions used and the number of elements for the parts.

- Resulting eigenfrequencies from sensitivity studies with a varying length of and tension in tethers correspond well with known theory.

- The onset for in-line VIV for the bridge is at a current velocity with a return period of 7 years. Moments resulting from VIV from a 100y return period current are reported to be about 25 % compared to moments from wave analysis. The VIV-analysis is simplified due to limitations of software used, and the validity of the results are therefore limited.

- In-line VIV for tethers is not of a critical response due to a high fatigue life. Amplitude response is seen to decrease with increasing tension in tether.

- No cross-flow VIV is reported for the 100y current for both the tube and the tether.

- Results from Vivana is about 80 % of the prediction of in-line amplitudes by the DNV GL model. This is in correspondence with previous similar analysis. Cross-flow results for different reduced velocities compared to DNV GL-predictions are not corresponding, and are therefore not as expected for the tether analysed.

- DNV GL gives conservative amplitudes for in-line motion for the present case.

- Adding swell to the wave analysis gives a significant increase in horizontal response compared to wind-sea for the current depth. Due to the depth of SFTBs, the swell waves are in general expected to be significant. The trends in the response found coincide well with reference results, when considering differences in the models used.

- Tension in tethers are always positive under the extreme 100y dynamic load conditions used.

- The concrete will need sufficient reinforcement/pre-stressing to withstand the stresses reported in the cross-sections.

Chapter 10

Recommendations for Further Work

- A fatigue analysis of the tube would be interesting to perform. Relevant material parameters for concrete for the SN curve would need to be established.

- An experimental VIV test of the two tubes in tandem would be interesting to study. The in-line VIV on both the tubes could be measured to see the difference in VIV between the tubes.

- More wave analyses can be conducted including more of the swell range relevant for the site. Also the effect of wave direction can be studied. Other directions for waves and current can be applied in further analyses. Current can also be included in a dynamic analysis to see if the stress extremals are more similar to the reference stresses.

- To make the comparison to the reference results more reliable, a new model exactly equal to the reference model can be made and analysed. For this to happen, the company have to make available more detailed information about their analysis. This was not available to the author.

- For the tethers, VIV-analysis could be conducted for scales of the velocities between 0.5 and 1, to collect information about at what specific current velocity VIV would be onset for the tethers.

Bibliography

Bergen Byleksikon. Nordhordalandsbrua. `http://www.bergenbyarkiv.no/bergenbyleksikon/arkiv/1424098`. Accessed 2016-12-10.

Blevins, R. D. (1977). *Flow-induced vibration.* Nav Nostrand Reinhold Company.

Blevins, R. D. (2005). Forces on and stability of a cylinder in a wake. *Journal of Offshore Mechanics and Arctic Engineering.*

Broer.no. Bergøysundbrua. `http://broer.no/bro/index.php?ID=40`. Accessed 2016-12-10.

Det Norske Veritas (2006). *Recommended Practice DNV-RP-F105 Free Spanning Pipelines.* Høvik.

Det Norske Veritas (2014). *Environmental Conditions and Environmental Loads.* Høvik.

Dr. techn. Olav Olsen (2016). 12149 bjornafjorden. 12149-03-gb-r-50000-1/02 concept 50000. hydrodynamic analysis 3d float. Technical report, Dr. techn. Olav Olsen.

Faltinsen, O. M. (1990). *Sea Loads on Ships and Offshore Structures.* Cambridge University Press, Cambridge, UK.

Hansen, S. O. (2015). Aerodynamic testing of tunnel cross-sectional shapes. Technical report, Svend Ole Hansen ApS, Copenhagen.

Huse, E. (1993). Interaction in deep-sea riser arrays. In *Offshore Technology Conference.*

Irgens, F. Formelsamling mekanikk. Trondheim.

Jakobsen, B., Larssen, R. M., Egseth, G., Karlsrud, K., and Birkeli, L. (2013). Various sft concepts for crossing wide and deep fjords. In *Proceedings of the sixth symposium on Strait Crossings 2013*, Bergen, Norway. Norwegian Public Road Administration.

Kawade, P. A. B. and Meghe, M. S. P. Submerged floating tunnel. `http://www.engineeringcivil.com/submerged-floating-tunnel.html`. Accessed 2017-06-01.

Kenny, J. P. and Ltd, P. (1993). Evaluation of vortex shedding frequency and dynamic span response. Technical report, Health and Safety Executive. Offshore Technology Information.

Kerr, A. D. (1964). Elastic and viscoelastic foundation models. *Journal of Applied Mechanics.*

Langen, I. and Sigbjörnsson, R. (1979). *Dynamic Analysis of Structures*. Tapir, Trondheim, Norway.

Larsen, C. M. (2015). Marin dynamikk. Institutt for marin teknikk, NTNU.

Larsen, C. M. (2016). Vortex induced vibrations. Power Point Lecture Notes from course TMR4305, lectured fall 2016.

Leira, B. (2017). Conversation with supervisor Leira.

Marintek. *RIFLEX 4.8.2 Theory Manual*. Marintek.

Marintek. *RIFLEX 4.8.2 User Guide*. Marintek.

Moan, T. (2003). *TMR 4190 Finite Element Modelling and Analysis of Marine Structures*. Department of Marine Technology, NTNU, Trondheim, Norway.

Passano, E. (2017). E-mail correspondance with Passano.

Passano, E., Larsen, C. M., Lie, H., and Wu, J. *Vivana Theory Manual Release 4.6 rev.0*. Marintek.

Pettersen, B. (2007). *Marin teknikk 3 - Hydrodynamikk*. Department of Marine Technology.

Reinertsen and Dr. techn. Olav Olsen (2013). Mulighetsstudie for kryssing av sognefjorden. neddykket rørbru. Technical report, Reinertsen and Dr. techn. Olav Olsen.

Reinertsen, Dr. techn. Olav Olsen, and Norconsult (2015a). Bjørnafjord submerged floating tube bridge. design basis. revision 03. Technical report, Dr. techn. Olav Olsen, Norconsult, Reinertsen.

Reinertsen, Dr. techn. Olav Olsen, and Norconsult (2015b). Bjørnafjord submerged floating tube bridge. design brief. Technical report, Dr. techn. Olav Olsen, Norconsult, Reinertsen.

Reinertsen, Dr. techn. Olav Olsen, and Norconsult (2016a). Bjørnafjord submerged floating tube bridge. k3/k4 design basis. revision 04. Technical report, Dr. techn. Olav Olsen, Norconsult, Reinertsen.

Reinertsen, Dr. techn. Olav Olsen, and Norconsult (2016b). Bjørnafjord submerged floating tube bridge. k3/k4 technical report. Technical report, Dr. techn. Olav Olsen, Norconsult, Reinertsen.

Skorpa, L. (2013). Crossing of deep and wide fjords on the western coast of norway with fixed connections. In *Proceedings of the sixth symposium on Strait Crossings 2013*, Bergen, Norway. Norwegian Public Road Administration.

Statens Vegvesen. Europaveg E39 Rogfast. `http://www.vegvesen.no/Europaveg/e39rogfast`. Accessed 2017-05-25.

Statens Vegvesen. Ferjefri e39 rørbro - teknologi for fremtiden. `http://www.vegvesen.no/_attachment/1087799/binary/1072528?fast_title=9+E39+Bj\T1\ornafjorden-R\T1\orbru.pdf`.

Statens Vegvesen. Fjordkryssing - Bjørnafjorden. `http://www.vegvesen.no/Europaveg/e39stordos/fjordkryssing-bjornafjorden`. Accessed 2017-05-25.

Statens Vegvesen. Stor bransjeinteresse for ferjefri e39. Webstite. `http://www.vegvesen.no/vegprosjekter/ferjefriE39/Nyhetsarkiv/stor-bransjeinteresse-for-ferjefri-e39`. Accessed 2017-04-30.

Statens Vegvesen (2016a). The submerged floating tube bridge (sftb) teknologidagene – trondheim september 2016. PowerPoint on Internet `http://www.vegvesen.no/_attachment/1545426/binary/1135142?fast_title=13+R\T1\orbru.pdf`.

Statens Vegvesen (2016b). Tether stabilized sftb. general view. Drawing set. Reinertsen and Dr. techn. Olav Olsen and Norconsult.

Store Norske Leksikon. Bergøysundet bru. Accessed 2016-12-10.

Søreide, T. and Brekke, H. (1989). *Handbok for forenklet analyse av flytebruer*. A.R. Reinertsen.

Timoshenko, S., Young, D., and W. Weaver, J. (1974). *Vibration Problems in Engineering*. John Wiley & Sons, Inc., fourth edition edition.

U. Evang, N. P. R. A. (1996). A submerged floating tunnel across the høgsfjord - a pilot project. dream or reality. In *International Conference Submerged Floating Tunnels 1996*, Sandnes, Norway. Norwegian Public Road Administration.

Underskog. E39 Nordhordalandsbrua. `https://underskog.no/bilde/1432284_e39-nordhordlandsbrua`. Accessed 2016-12-10.

User:Waldir. File:bridge types.svg. Photo taken from `https://commons.wikimedia.org/w/index.php?curid=3238712`. By User:Waldir - self-made, based on an image in Brochure SIJLAB, CC BY-SA 3.0, Accessed 2016-12-15.

Wallis, S. Strait crossings conference report. links across the waters. `http://www.tunneltalk.com/Strait-Crossings-Jan10-Conference-report.php`.

Appendix A

Information about concept

A.1 Magnified drawings

The following contain magnified drawings from the Assessment Study.

A.1.1 Cross-over tubes
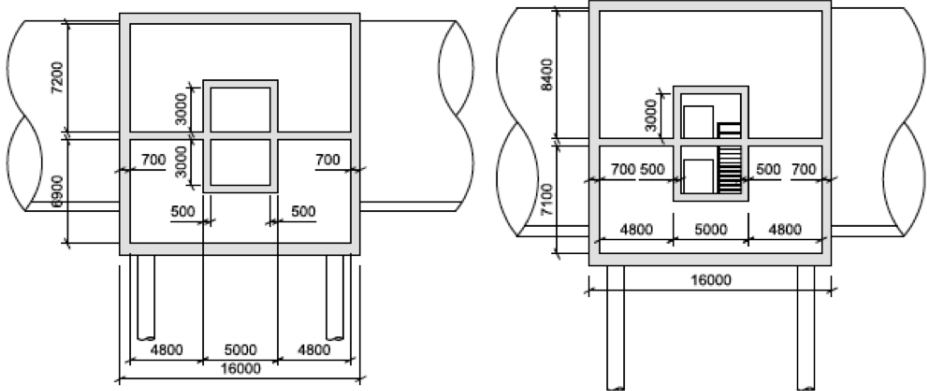
Figure A.1: Cross-tubes seen from along cross-tube (Statens Vegvesen, 2016b)
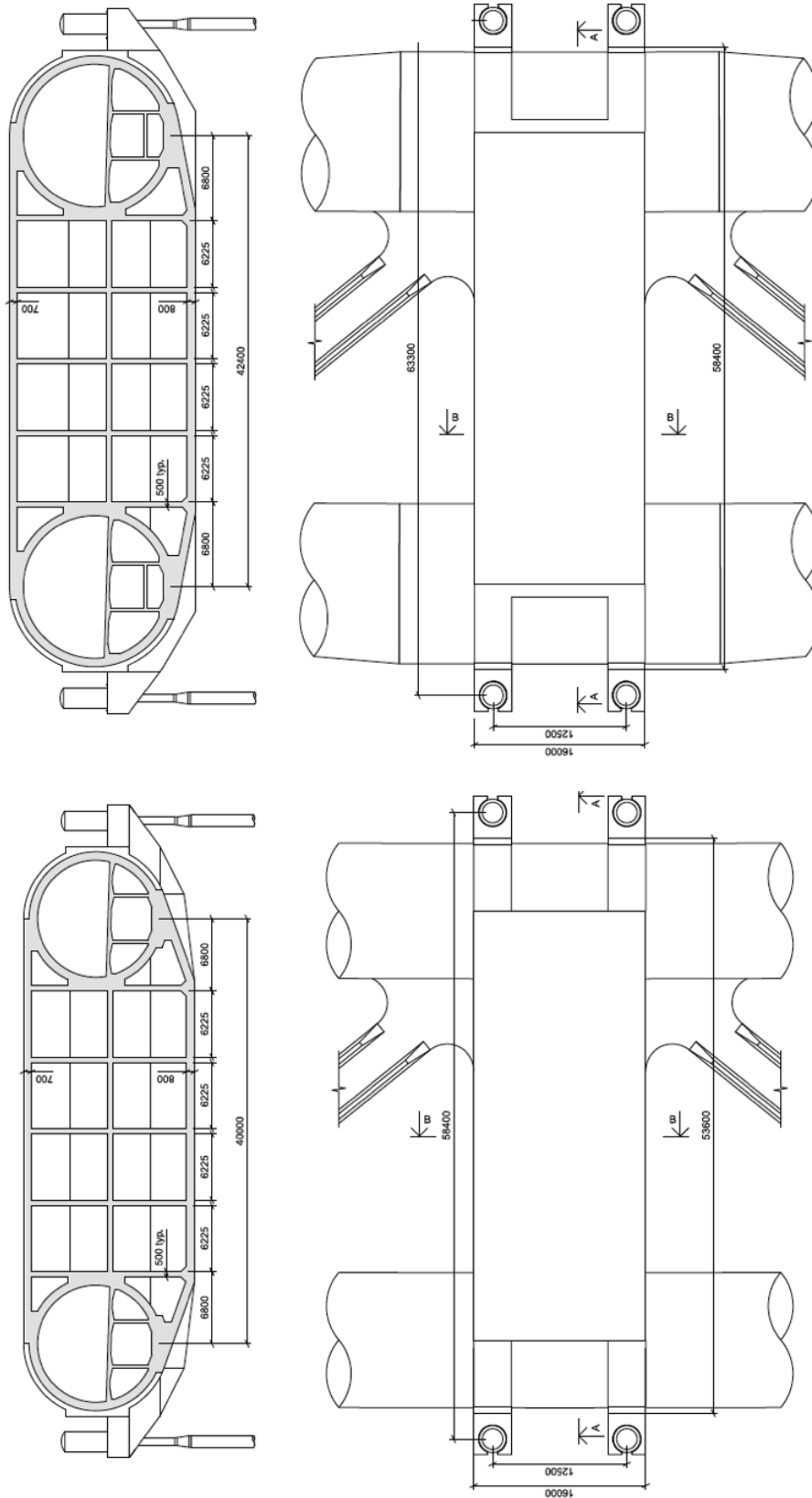
Figure A.2: Cross-tubes T12.5 (upper) and T9.5 (lower) seen from along bridge (left) and above (right). (Statens Vegvesen, 2016b)

A.1.2 Main tubes
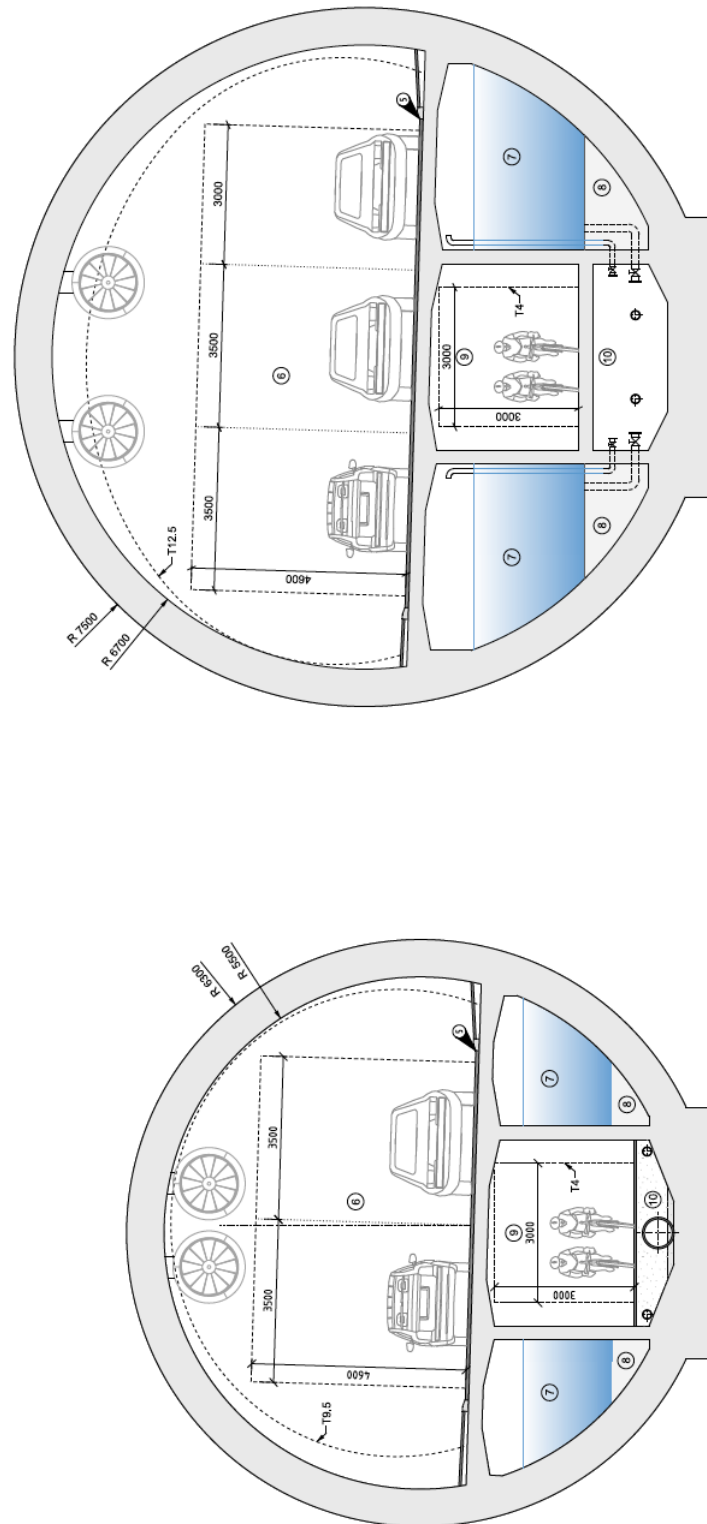
Figure A.3: Upper: Cross-section T12.5. Lower: Cross-section T9.5. (Statens Vegvesen, 2016b)

A.1.3 Bracings
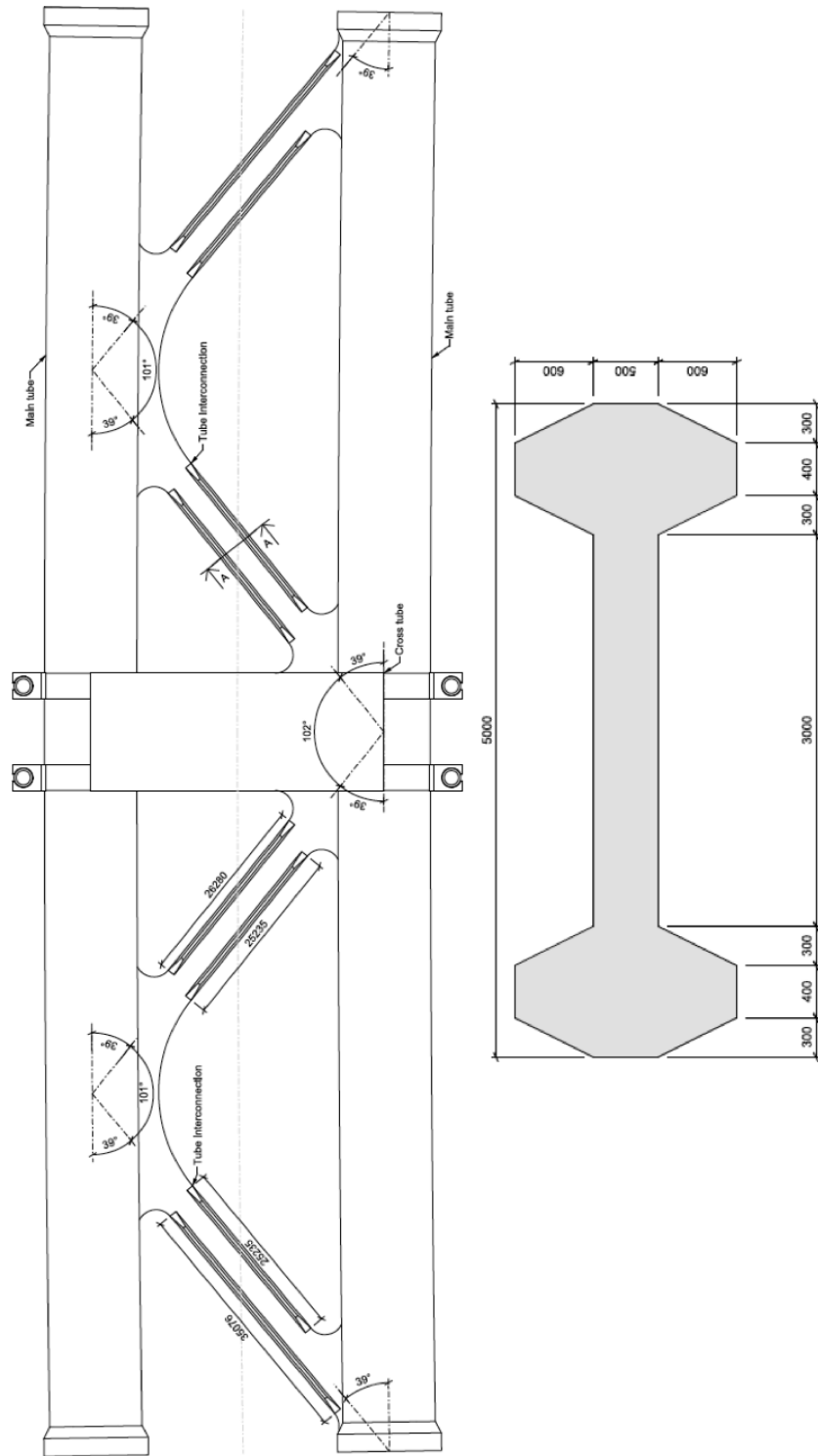
Figure A.4: Arrangement and cross-section of bracings. (Statens Vegvesen, 2016b)

A.1.4 SFTB horizontal alignment
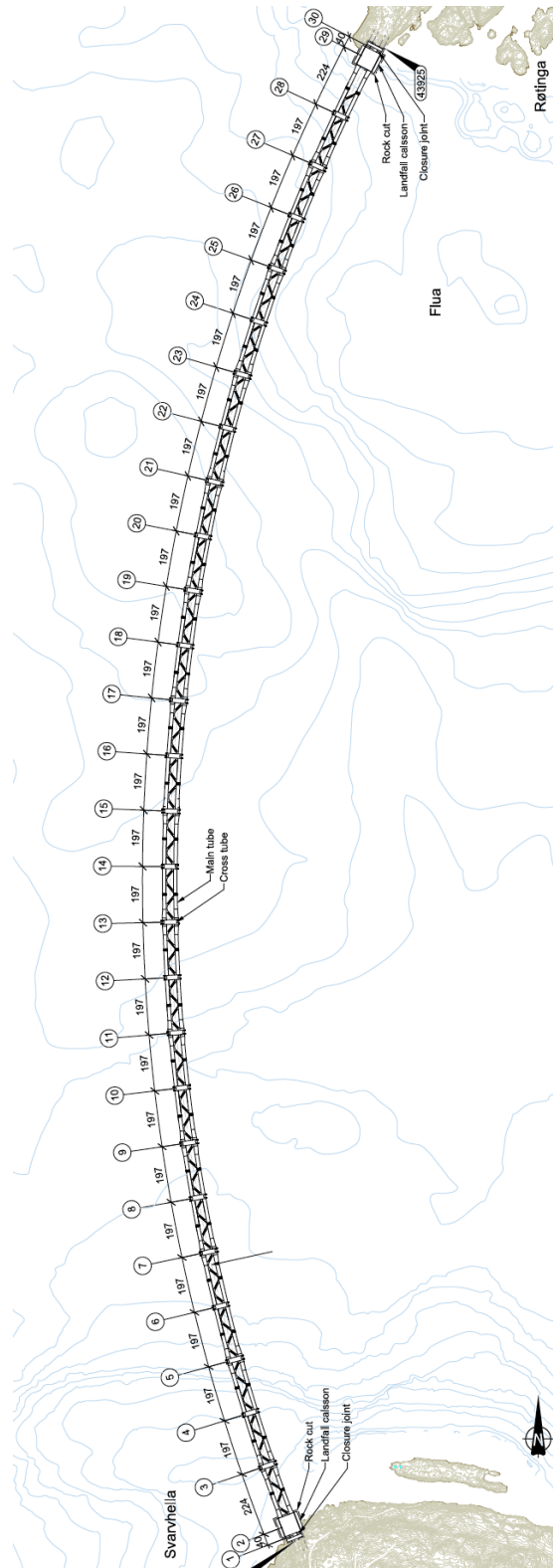
Figure A.5: SFTB seen from above (Statens Vegvesen, 2016b)

A.1.5 SFTB vertical alignment
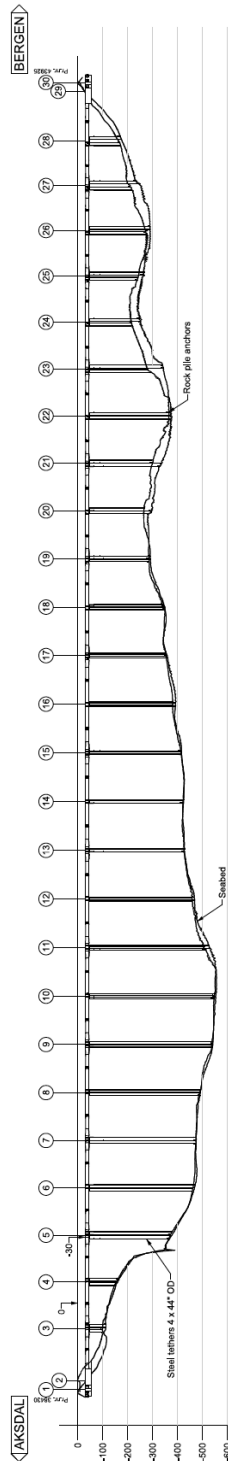
Figure A.6: SFTB seen from the side showing the sea bottom. (Statens Vegvesen, 2016b)

A.2 Additional information

The following pages contain information about the tether mooring, the rock anchorages and the landfalls and are taken from Reinertsen et al. (2016b).

7.3.5 Tether mooring

Since the axial stiffness of the mooring is governing the tether dimensions, the utilization of the tethers is moderate, and thus a lower material grade compared to offshore tethers are proposed. This will also reduce the interface loads as these are dictated by the tether breaking strength. The tether configuration (per mooring) is selected as follows:

— No. of tethers : 4
— Tether outer diameter : 1 118 mm (44 in.)
— Wall thickness : 38 mm (1.5 in.)
— Cross-sectional area : 0.129 m²
— Tether resistance $F_{t,Rd}$: 27 MN (Grade S235)
— Nominal pre-tension : 10.5/11.0 MN (without/with lay-by)

The tether assembly comprises, a top connector, the tether string and a bottom connector. The tether string is fabricated into a single pipe with quasi neutral buoyancy (submerged weight ~9 kg/m). The complete tether assembly is shown in Figure 7-36.
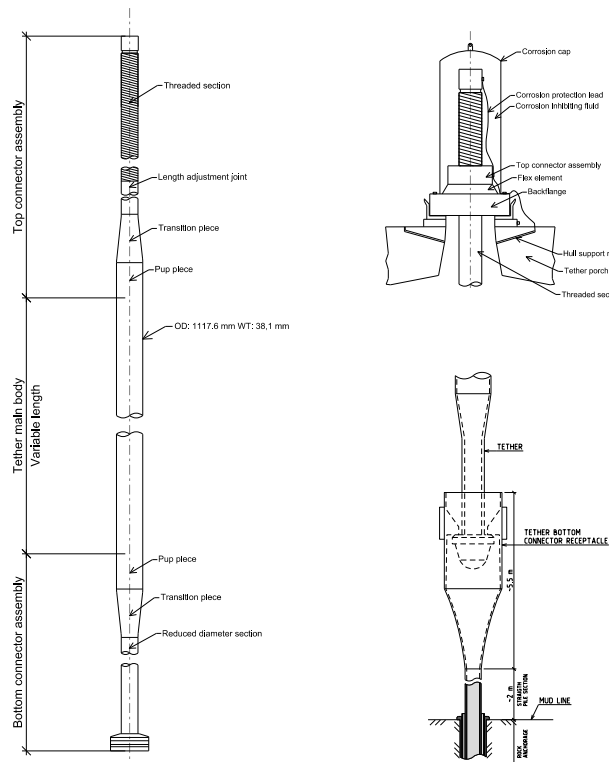
> *Figure 7-36: Complete tether assembly.*

The tether assembly will be based on already available systems. As the pre-tension, the dynamic load range and sway offsets are significantly smaller for the SFTB than compared to common offshore applications, simplification for cost reduction is possible. Unlike a tension leg platform, having a maximum horizontal offset of about 1/10 the water depth, the SFTB

will have an offset angle less than 0.2°. As the requirement for angular range is small, the costly flex elements in the top and bottom connectors can be greatly simplified.

The tethers will be installed with porch side entry both at the tube tether porches and the bottom connector receptacle. Side entry will warrant access for ROV inspection and possibility for replacement of the complete tether assembly. The tether body is protected by a coating of arc-sprayed aluminum and overlay of epoxy paint. This forms part of an overall SFTB corrosion protection and monitoring system which also includes the steel rock anchor.

For further details regarding structural design of tethers, reference is made to sub-report 12149-OO-R-019 *Bjørnafjord submerged floating tube bridge – Structural design of tethers* [13].

7.3.6   Rock anchorages

Due to the variable depth and soil conditions along the fjord crossing, several alternative foundation concepts were considered during in the first project phase [16]. The alternative foundation concepts studied are shown in Figure 7-37. Gravity based foundation with a steel caisson stabilized by rock dump was found technically feasible along most of the bridge. The drilled and grouted rock anchors (piles) was proposed in the steep rock areas, mainly at the north end of the SFTB crossing, to avoid complex and costly underwater blasting and seabed preparations.
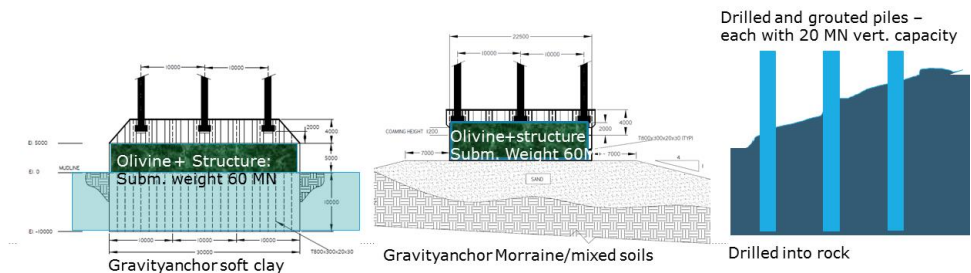
> *Figure 7-37:* Alternative tether foundation concepts.

Following the feasibility evaluation, a cost assessment was carried out considering all aspects related to engineering, procurement/fabrication and installation. Due to the relatively large dimensions and amount of solid ballast material required, the gravity foundations became costly and triggered the study considering drilled and grouted rock anchors for all tethers (Figure 7-38). The study conducted in the subsequent phase, involving expert personnel from offshore drilling, geotechnical engineering as well as jacket and TLP design, investigated the merits and challenges associated with utilizing drilled and grouted rock anchors as tether foundations.
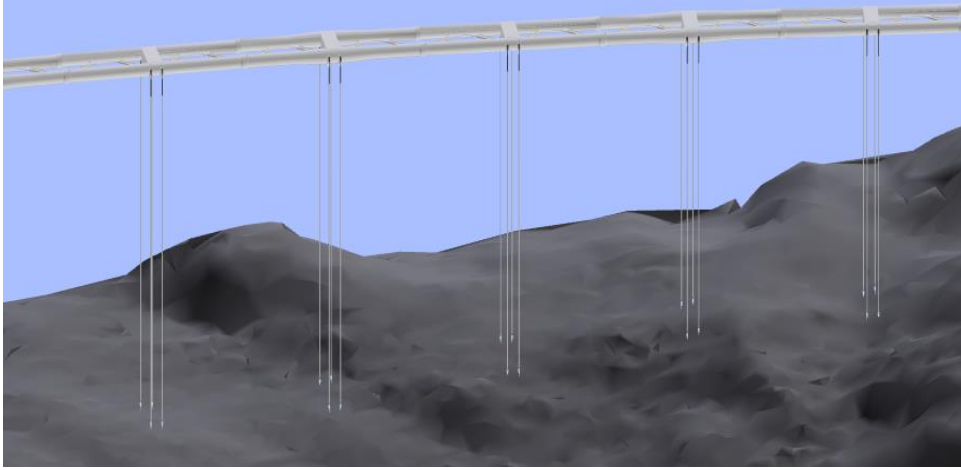
> *Figure 7-38:* Overview of tether stabilized tube bridge.

The study concludes that carefully designed drilled and grouted rock anchors can provide a promising solution for a consistent, safe and cost-effective foundation solution for the tether stabilized SFTB concept either as a complement or complete substitution of the gravity anchors. The tether dynamics from the SFTB is very low (typically +/- 1 MN, with an extreme range of less than 20 MN) all acting vertically, which is considered less severe compared to for example offshore jacket piles subject to substantial reversed loading. Moreover, no technical feasibility issues related to drilling tools, grout design and application or rock anchor installation or tether interfaces have been found. The study including a proposal for a tether rock anchor concept is described in sub-report 12149-OO-R-301 *Bjørnafjord submerged floating tube bridge - Drilled and grouted rock anchors for tethers* [17]. It is noted that Vegdirektoratet upon a principle review has acknowledged the tether rock anchor solution and encouraged further development.

A schematic of the proposed tether rock anchor concept is illustrated Figure 7-39 below. The tether load-carrying element (rock anchor) is proposed to be a seamless, thick walled pipe which is drilled and grouted sufficiently deep into the bedrock to ensure ample tensile load capacity. A round steel rod (solid), commonly used onshore, was also considered, but due to reduced yield strength capacity with thickness and challenges with joining the sections, sufficient tensile strength was not achieved based on off-the-shelf dimensions (350 mm).

Since the seabed may be uneven and have sediment deposits, casings (hollow concentric pipes) are pre-installed through the sediments and drilled into the first approx. 5 meters into the bedrock. These casings will not be included in the structural capacity calculations for the tether rock anchors, but will be used to aid the drilling process and also to provide an annulus for grouting. The grouting between the casings and the anchors will provide corrosion protection to the load carrying rock anchor. The rock anchor is welded to complete length (from 40 - 100 m) and fitted with the tether bottom connector receptacle prior to installation. The tether bottom connector interface is typically placed some 4 meters above the seabed, suitable for installation and future inspections. The exposed part of the tether rock anchor will be thoroughly cathodically protected in compliance with the corrosion protection of the tether itself. The rock anchor part below mudline will be grouted on the inside and outside.
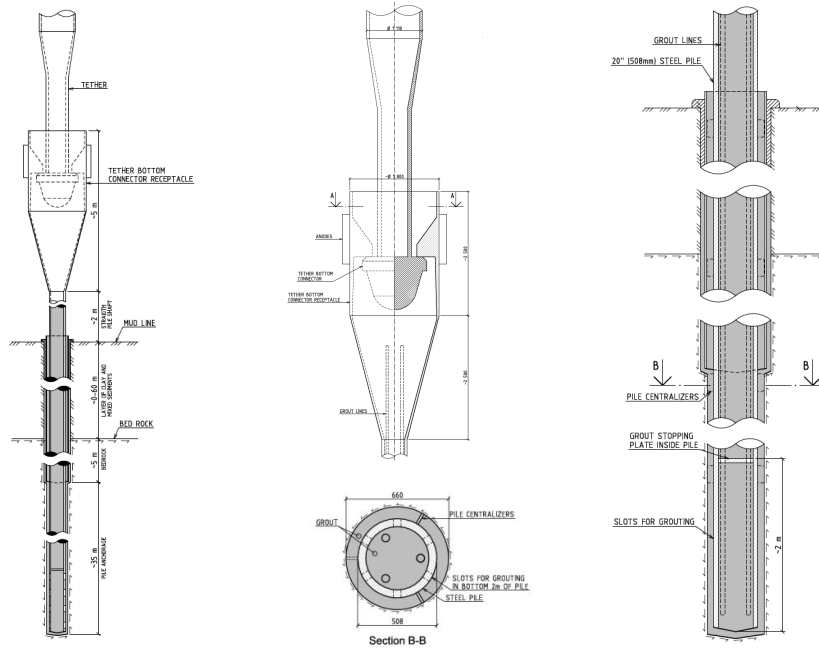
> *Figure 7-39: Tether rock anchor overview and tether interface.*

The rock anchor and tether interface is shown in Figure 7-39. A simplified, but proven, interface to bottom connector suitable for the SFTB is proposed in replacement for the RotoLatch concept commonly used on TLP foundation piles. This has side entry and is therefore easier to inspect. A locking device is applied after tether installation.

For the purpose of this study, preliminary sizing of a rock anchor and drilling depth based on tentative assumptions for rock volumes and grouting strength, the following tether rock anchor configuration is proposed:

— Outer diameter: 508 mm
— Wall thickness: 50.8 mm
— Steel quality API 5L X 65 PSL 2 / L450 N/Q (420 MPa)
— Weight in air: 570 kg/m
— Delivery lengths – will be welded to complete pile length 40-100 m
— The anchor axial yield capacity $T_{yield} = \sigma_{yield} \times A = 420 \times 0.072 = 30$ MN (slightly stronger than tether capacity)
— Weld bead included along entire pile length

The bed rock under the sediments (if any) is likely to be uneven. At present, it is therefore considered to drill the casing about to 5 m into the bed rock to ensure a proper seal is establish over the entire length of the tether pile below the sea bed. The drilling and installation of the anchors is proposed performed by the drilling vessel.

7.3.7 Landfalls

A general description of the landfalls and the substructure arrangement is given in Sec. 7.1.7. The interface axis between hard rock tunnel and submerged floating tube bridge is defined by the tunnel entrance. Its location is determined by the length and the position of the support caisson. In lack of detailed information about the geological condition, the caisson is set 10 m back from the start of the seabed slope. As the tunnel entrances are within dry land, the overburden thickness is ample for both rock tunnels.

The footprint dimensions B x L of the support caisson are determined by the demand for on-bottom weight to 83.4 x 71 m.
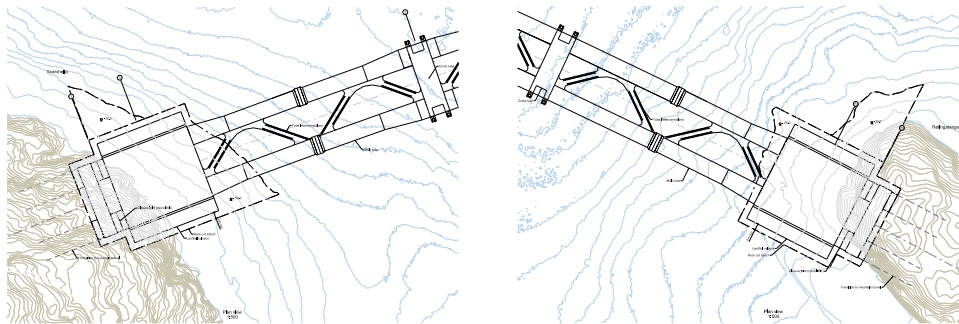
> *Figure 7-40: Plan layout of landfall at Svarvhella in south (left) and Røtingatangen in north (right).*
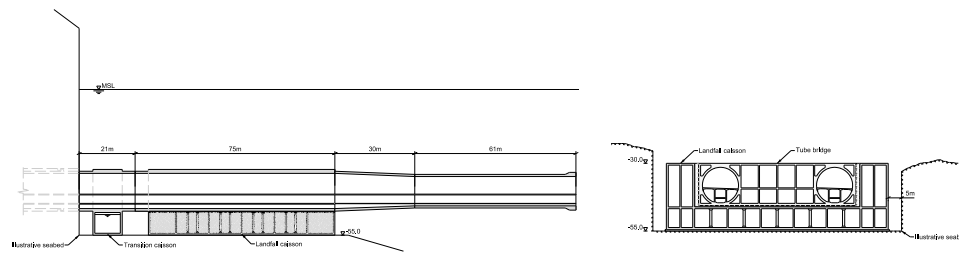
> *Figure 7-41: Landfall arrangement at Svarvhella (longitudinal and transverse section).*

> *Table 7-6: Trenching volumes (solid)*

Excavation		South landfall	North landfall	Total
Overburden	m³	26 000	24 000	50 000
Rock	m³	430 000	325 000	755 000

Appendix B

Reference Results

B.1 Static - Structural Self-weight

The following pages contain information about the reference results and are taken from Reinertsen et al. (2016b) and Dr. techn. Olav Olsen (2016).
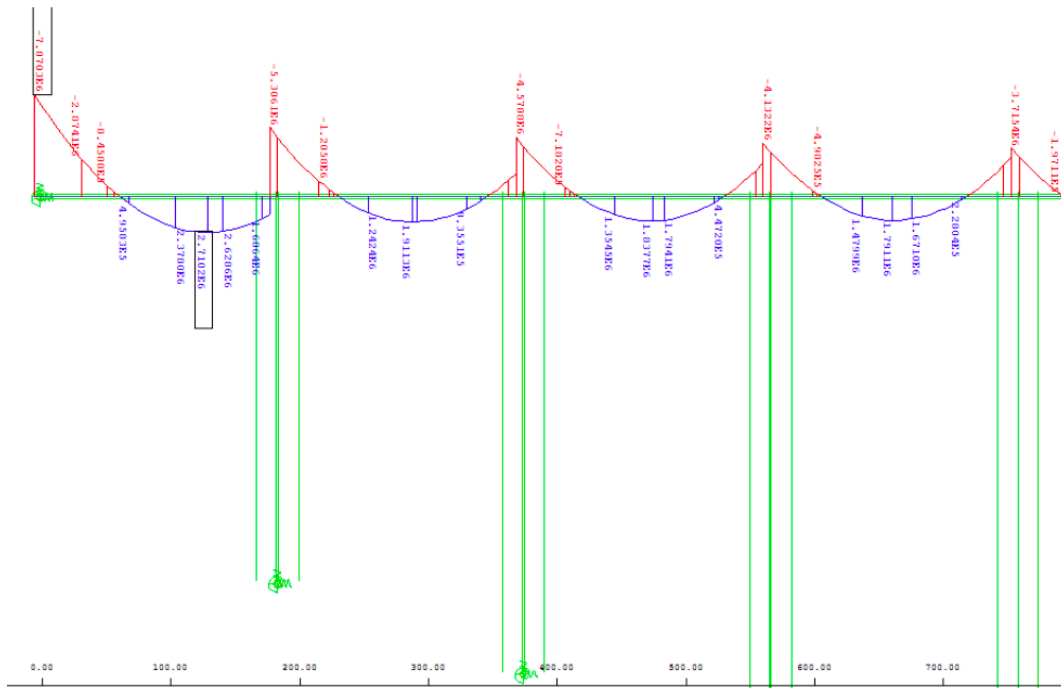
Figure B.1: Static self weight

B.2 Eigenvalue Analysis

3.1 Eigenmode plots in xy- xz- and yz- planes

In this chapter the modes given in Table 3.0.0.1 are plotted in the xy-, xz-, and the yz- planes. The modes are normalized, however the amplitude is magnified by a factor of 1000.

3.1.0.1 Mode-1

Freq=0.01544[Hz] T=64.75[s]
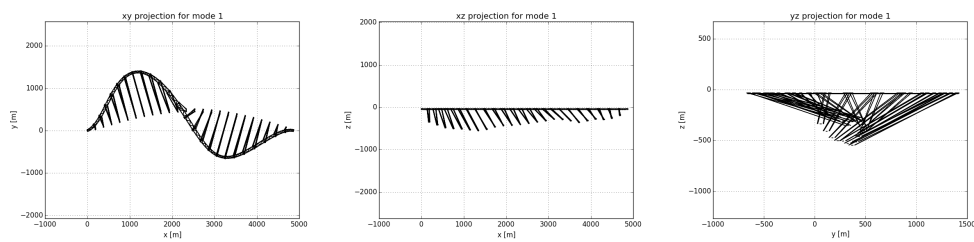
3.1.0.2 Mode-2

Freq=0.02968[Hz] T=33.69[s]
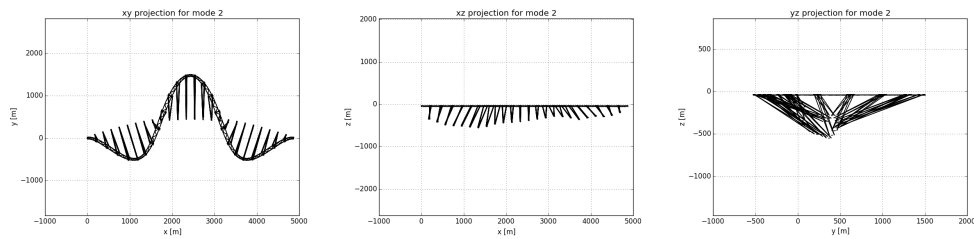
3.1.0.3 Mode-3

Freq=0.04401[Hz] T=22.72[s]

3.1.0.4 Mode-4

Freq=0.04897[Hz] T=20.42[s]
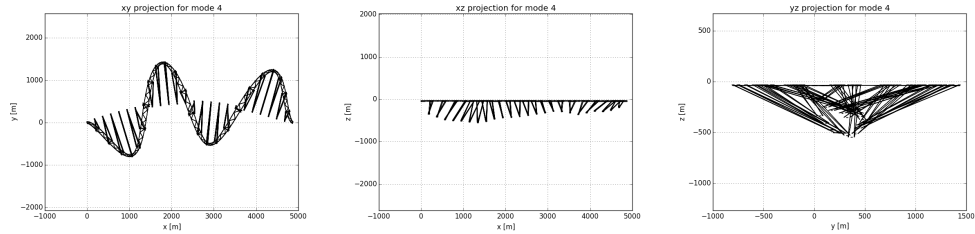
3.1.0.5 Mode-5

Freq=0.07141[Hz] T=14.0[s]
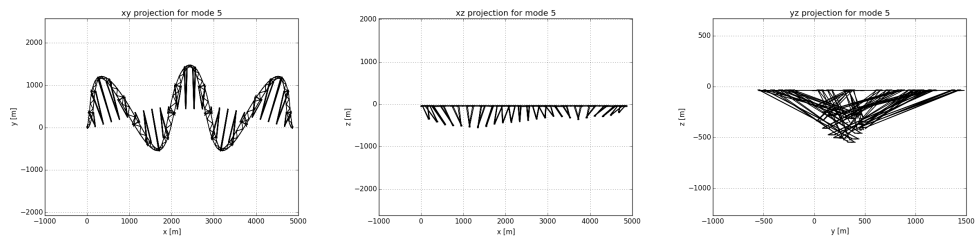
3.1.0.6 Mode-6

Freq=0.09758[Hz] T=10.25[s]
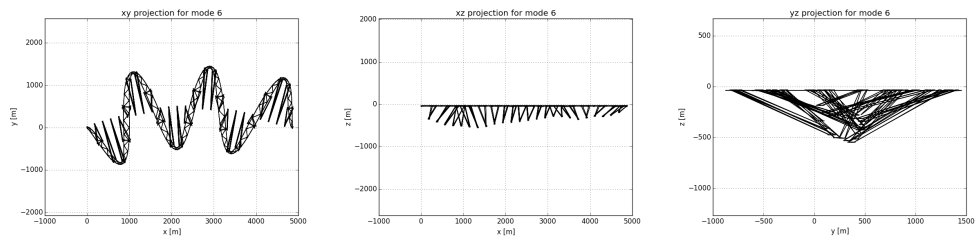
3.1.0.7 Mode-7

Freq=0.1259[Hz] T=7.942[s]
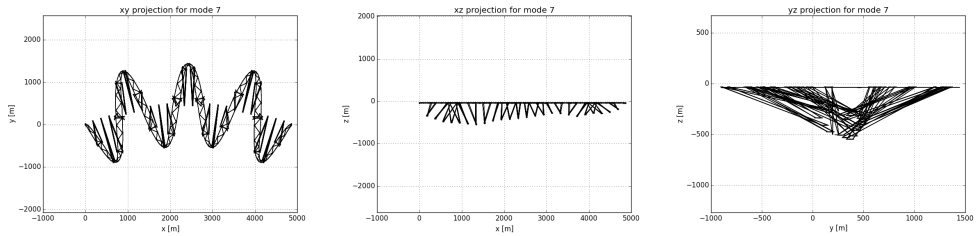
3.1.0.8 Mode-8

Freq=0.1578[Hz] T=6.337[s]
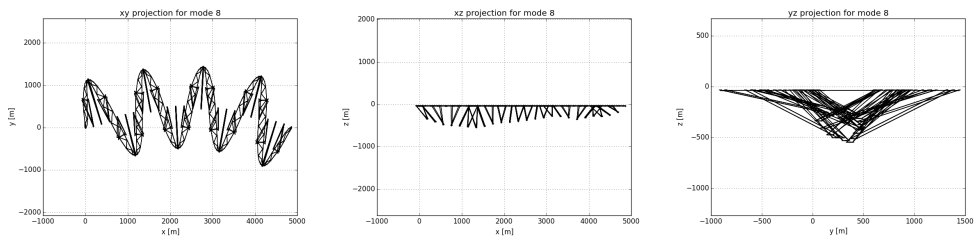
3.1.0.9 Mode-9

Freq=0.1899[Hz] T=5.266[s]

3.1.0.10 Mode-10

Freq=0.2082[Hz] T=4.804[s]
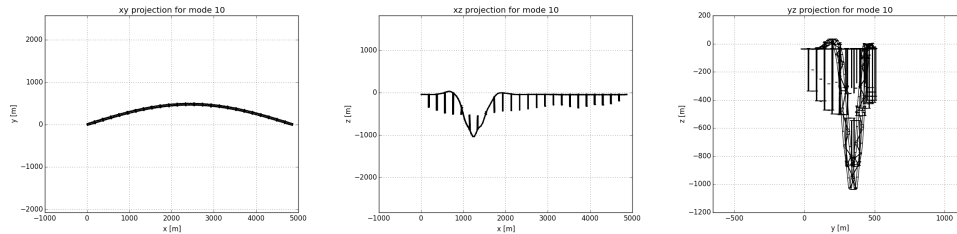
3.1.0.11 Mode-11

Freq=0.2133[Hz] T=4.688[s]
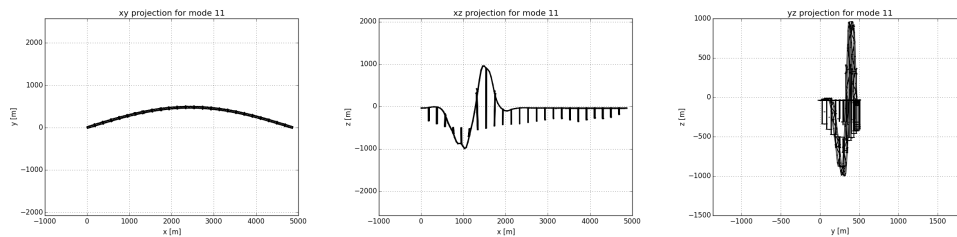
3.1.0.12 Mode-12

Freq=0.2166[Hz] T=4.617[s]
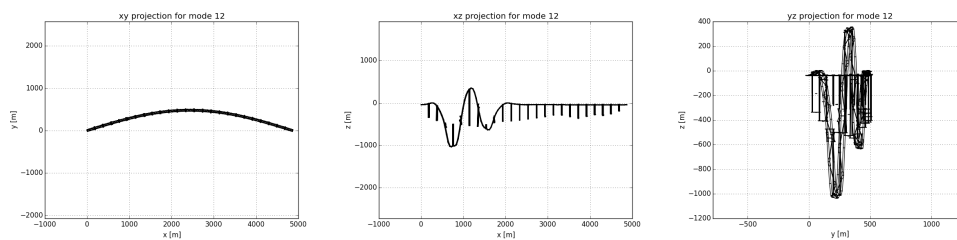
3.1.0.13   Mode-13

Freq=0.2263[Hz] T=4.419[s]
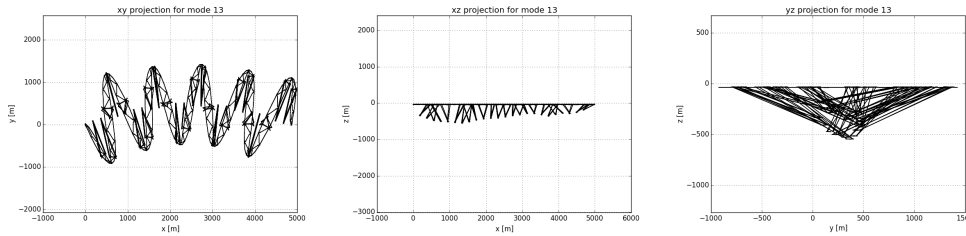
3.1.0.14   Mode-14

Freq=0.2288[Hz] T=4.371[s]
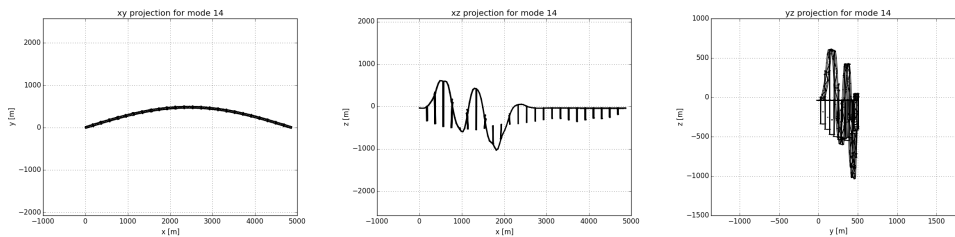
3.1.0.15   Mode-15

Freq=0.2325[Hz] T=4.3[s]

3.1.0.16 Mode-16

Freq=0.2379[Hz] T=4.204[s]
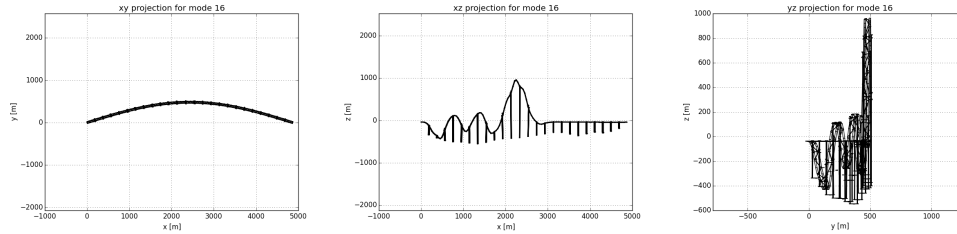
3.1.0.17 Mode-17

Freq=0.2407[Hz] T=4.155[s]
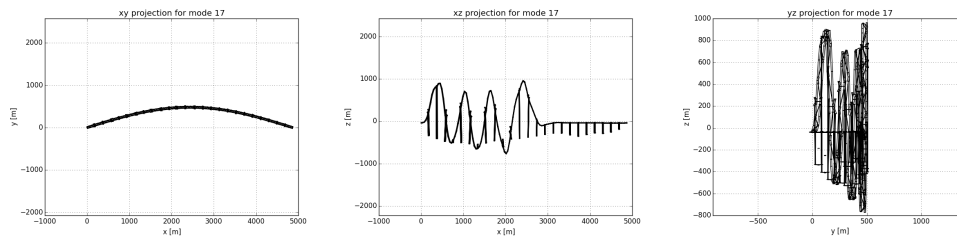
B.3   Dynamic Analysis

B.3.1   Envelopes

Envelopes of axial displacement, horizontal displacement, vertical displacement, axial forces, moment about y-axis, moment about z-axis and tether tension, is found, respectively.

Moment envelope in local y-direction for tube1pos1 over global x-direction

Force envelope in local x-direction for anchors over global x-direction
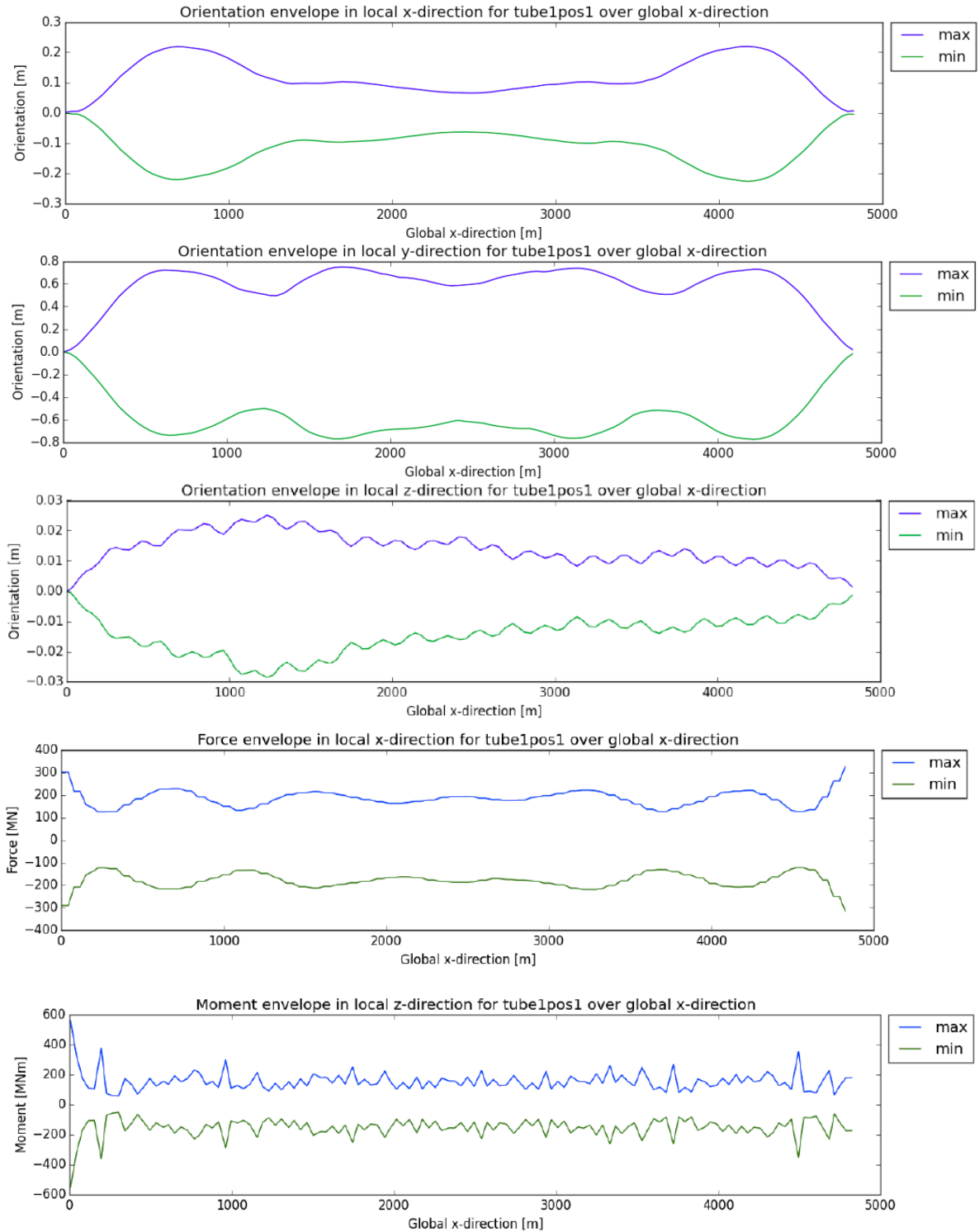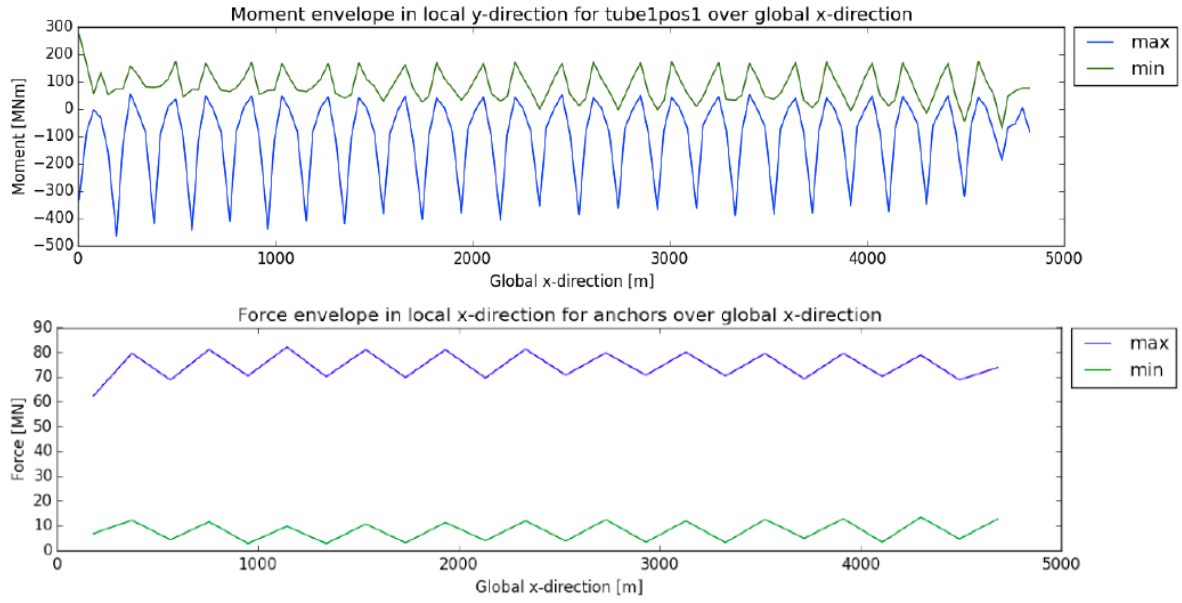
B.3.2 Stress Calculation Tube 1 position 1

5.0.1   Tube 1 position 1

Table 5.0.1.1: Stress-summary Tube 1 position 1 within first 100m of bridge

	Static [MPa]		Dynamic [MPa]		Combined [MPa]	
	Max	**Min**	**Max**	**Min**	**Max**	**Min**
Point 00	4.4409	-5.1101	4.78235	-4.69413	12.093	-12.621
Point 01	3.5977	-4.0959	7.57864	-7.43042	15.724	-15.985
Point 02	1.0566	-1.135	8.7655	-8.5689	15.081	-14.845
Point 03	2.6235	-1.9579	7.6154	-7.40256	14.808	-13.802
Point 04	3.5656	-3.0426	4.81093	-4.68495	11.263	-10.539
Point 05	2.5507	-2.1994	3.1803	-3.11667	6.2135	-6.0155
Point 06	0.34176	-0.41195	2.53813	-2.50872	4.3875	-4.2438
Point 07	3.0923	-3.5845	3.17981	-3.11255	6.8616	-7.3251

Table 5.0.1.2: Stress-summary Tube 1 position 1 in between first 100m and 1000m of bridge

	Static [MPa]		Dynamic [MPa]		Combined [MPa]	
	Max	**Min**	**Max**	**Min**	**Max**	**Min**
Point 00	2.6897	-5.9423	3.72158	-3.56319	8.4846	-11.369
Point 01	1.981	-4.225	4.64437	-4.42497	9.2846	-10.961
Point 02	0.49081	-0.94523	5.08759	-4.86395	8.4263	-8.5446
Point 03	3.7163	-1.4735	4.58972	-4.43393	10.414	-8.4507
Point 04	4.9266	-2.1618	3.75288	-3.57689	10.207	-7.7361
Point 05	2.9729	-1.4292	3.03435	-2.93083	7.5142	-5.8168
Point 06	0.54105	-1.0474	3.12399	-3.13317	5.4671	-5.9232
Point 07	2.0013	-4.7321	3.02601	-2.97066	6.3341	-9.0914

Table 5.0.1.3: Stress-summary Tube 1 position 1 in middle part of bridge

	Static [MPa]		Dynamic [MPa]		Combined [MPa]	
	Max	**Min**	**Max**	**Min**	**Max**	**Min**
Point 00	2.8992	-5.7616	3.59529	-3.6218	8.3047	-10.95
Point 01	2.1835	-4.2987	4.82222	-4.86351	9.1631	-11.333
Point 02	0.53491	-1.0372	5.37737	-5.42235	8.827	-9.3831
Point 03	3.2844	-1.4336	4.78348	-4.8511	10.745	-8.6364
Point 04	4.6564	-2.1353	3.58371	-3.58365	9.6932	-7.7231
Point 05	3.0653	-1.4232	3.11103	-3.16707	7.4249	-5.7339
Point 06	0.62244	-1.105	3.01412	-3.082	5.136	-5.7038
Point 07	2.1927	-4.3021	3.13628	-3.1799	6.1502	-8.9104

Table 5.0.1.4: Stress-summary Tube 1 position 1 in between last 1000m and 100m of the bridge

	Static [MPa]		Dynamic [MPa]		Combined [MPa]	
	Max	Min	Max	Min	Max	Min
Point 00	2.6633	-5.133	3.54081	-3.48352	8.1911	-10.707
Point 01	2.0048	-3.8289	4.41105	-4.36861	8.9159	-10.819
Point 02	0.4481	-0.88077	4.7929	-4.73694	8.0205	-8.2349
Point 03	2.9619	-1.3868	4.42985	-4.3101	9.84	-8.283
Point 04	4.0767	-2.0431	3.56799	-3.44821	9.583	-7.5602
Point 05	2.6443	-1.407	3.94741	-3.8264	7.6354	-5.7365
Point 06	0.45231	-0.87015	4.4037	-4.28197	7.3939	-7.5348
Point 07	1.9489	-3.8752	3.96674	-3.83522	6.3387	-8.4221

Table 5.0.1.5: Stress-summary Tube 1 position 1 within last 100m of bridge

	Static [MPa]		Dynamic [MPa]		Combined [MPa]	
	Max	Min	Max	Min	Max	Min
Point 00	1.221	-0.98945	4.14937	-4.02581	7.86	-7.4307
Point 01	1.0046	-0.68391	5.04307	-4.88028	9.0735	-8.1126
Point 02	0.44057	-0.35106	5.42543	-5.24257	9.1213	-8.6903
Point 03	0.7362	-0.82554	5.07183	-4.89161	8.4831	-8.6521
Point 04	1.0189	-1.1176	4.19576	-4.03798	7.7321	-7.5784
Point 05	0.71334	-0.76383	3.55788	-3.42157	6.4059	-6.2383
Point 06	0.39119	-0.33274	3.31791	-3.16177	5.6998	-5.3916
Point 07	0.96318	-0.70677	3.55572	-3.41419	6.6035	-6.1695

XXIV

Appendix C

Extra Results from Analyses

C.1   Static

C.1.1   Unsymmetric Model

Buoyancy of 35 cm from static equilibrium, at maximum. Max located at point with lay-bys. Large volume gives large buoyancy.
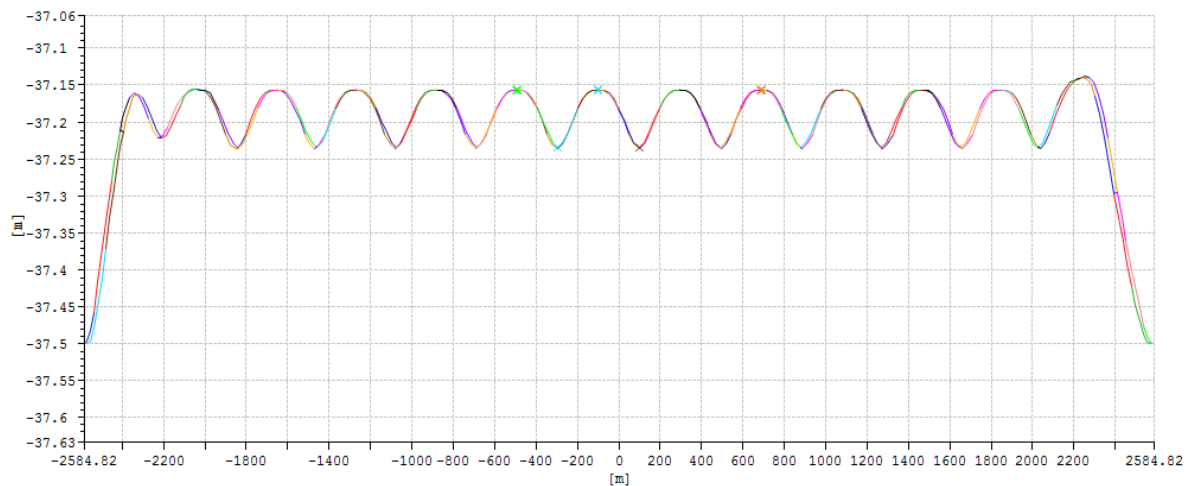
Figure C.1: Static equilibrium between mass and buoyancy for unsymmetrical model
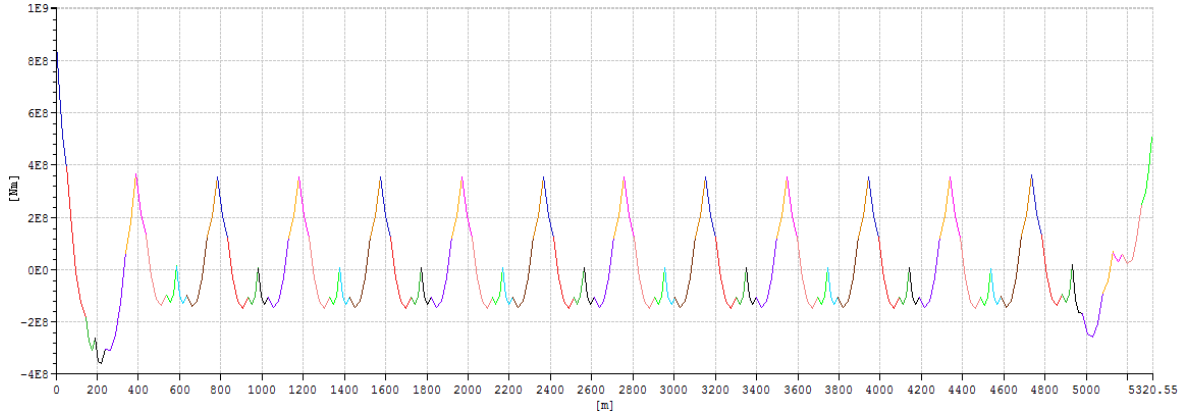
Figure C.2: Moment about Y-axis
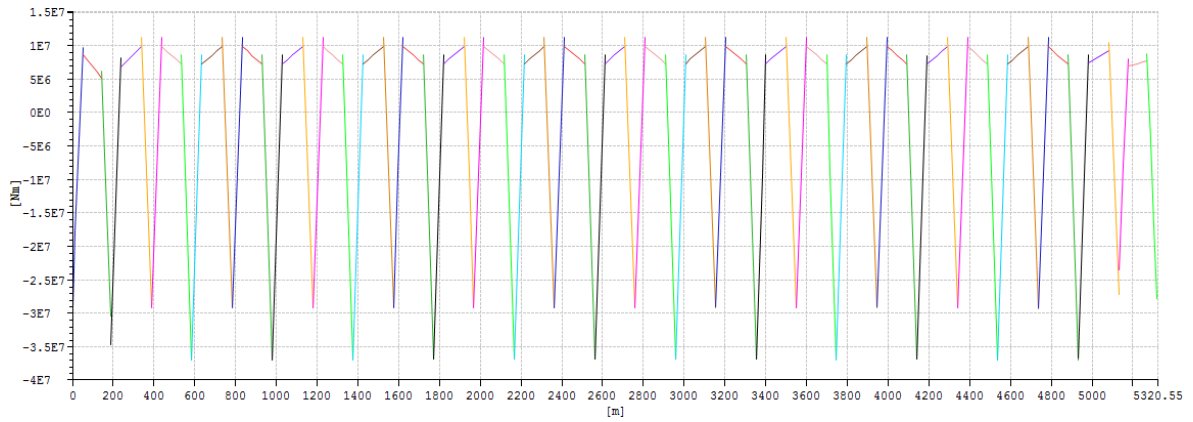
Figure C.3: Moment about Z-axis

C.1.2 Symmetric Model

The two mid cross-overs are with lay-bys (cross-over points 15 and 16, located at x=-98m and x = 98m). This gives the large buoyancy at the mid point. The cross-overs with lay-by have a larger buoyancy, 37 % vs 30 % for the cross-overs with no lay-by. There are 14 cross-over tubes with lay-by, and 12 cross-overs without lay-by. The trough represents the cross-overs without lay-by, while the crests represents the cross-overs with lay-by.
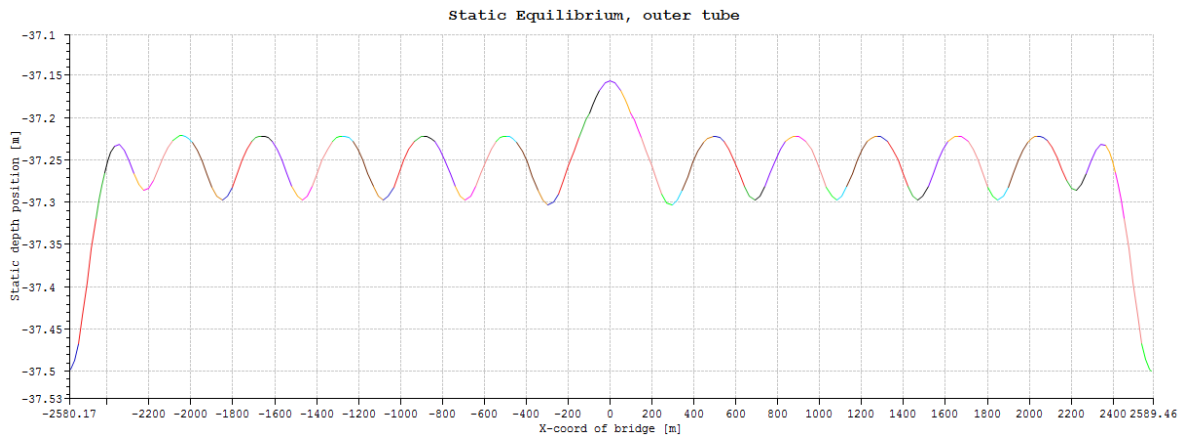
Figure C.4: Static equilibrium of symmetric model, outer tube
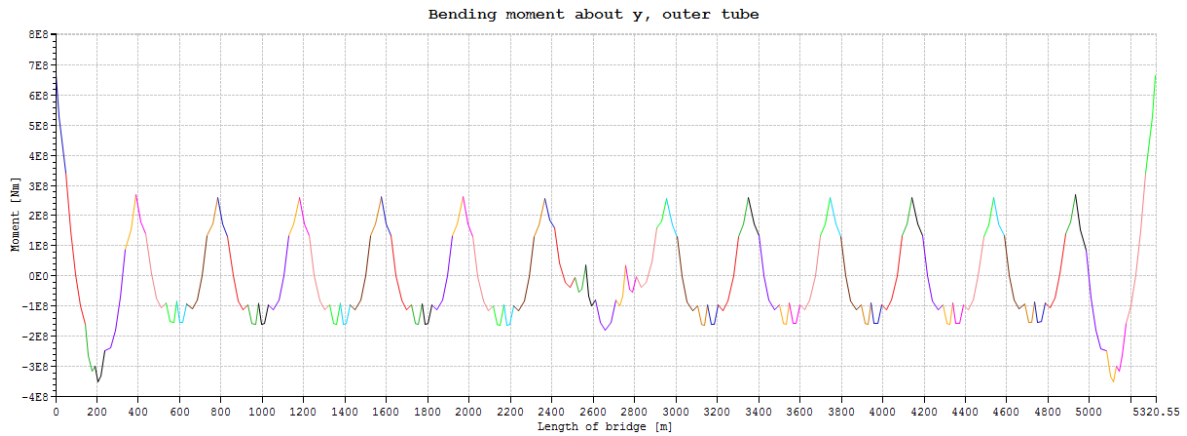
Figure C.5: Moment about Y-axis
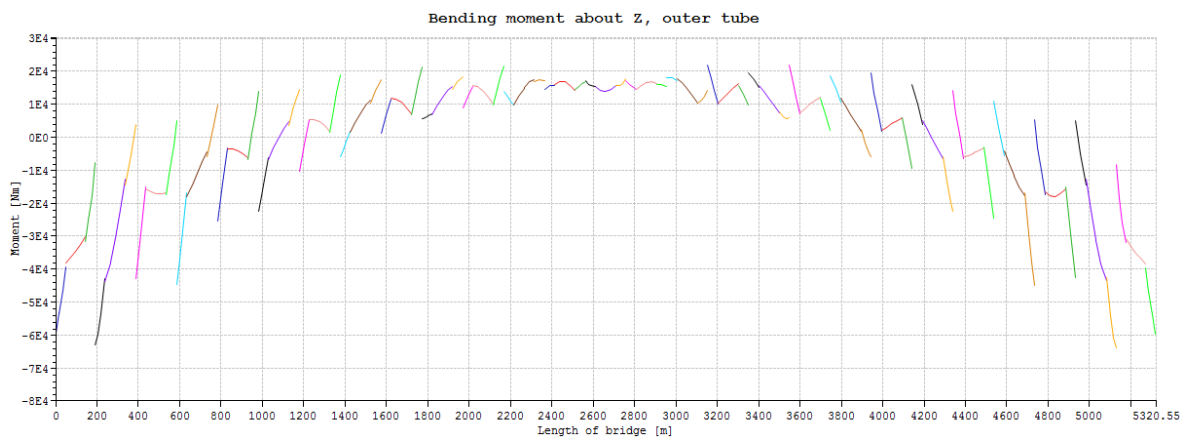
Figure C.6: Moment about Z-axis NB! Dobbelsjekk om riktig bilde

Tension in Tethers
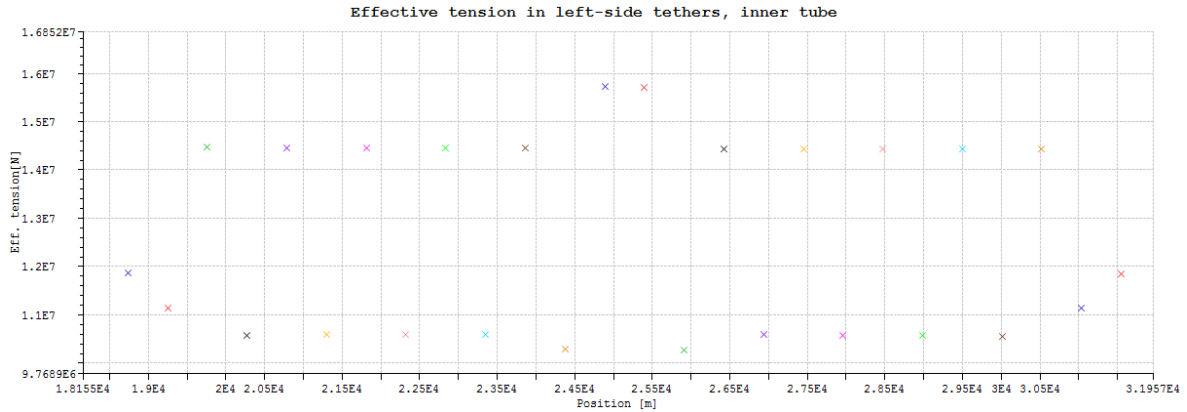
Figure C.7: Tension in tethers, left-side, inner tube

C.2 Eigenvalues from Riflex

C.2.1 Symmetric model - 10 elements for each tether

Firstly, the bridge is run eigenvalue analysis on with ten elements per tether. This gives a lot of frequencies. This is due to that also the tethers become excited, at different frequencies. Allowing both the bridge and tethers become excited allows for a very complex coupled dynamic response system, where the local frequencies hook on to the global response. The five first modes are seen in figures C.8 to C.12 Considering only the bridge, it looks like the first vertical eigenmode is seen at mode no 331, figure C.13. It has a period of 5.3 seconds. The second vertical mode seem to be no 447, as seen in figure C.14.
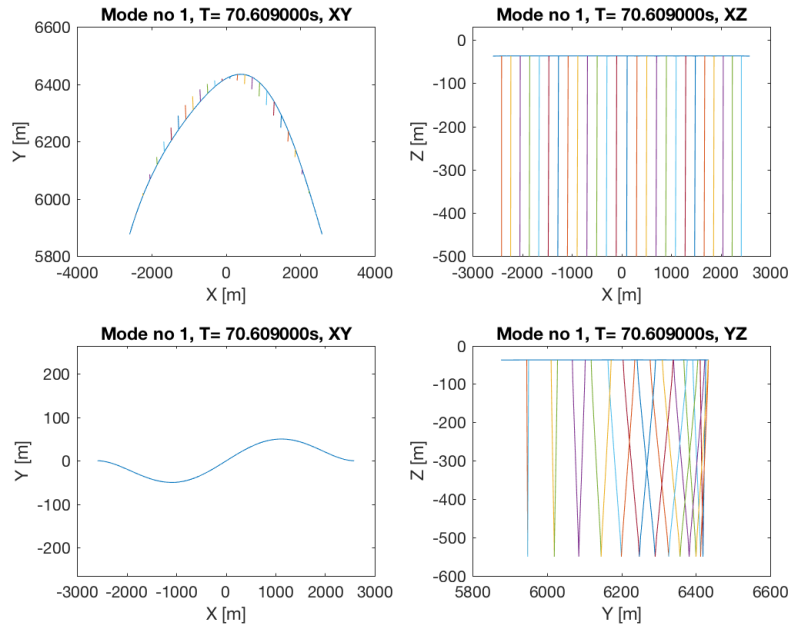
Figure C.8: Mode 1. 10 elements per tether
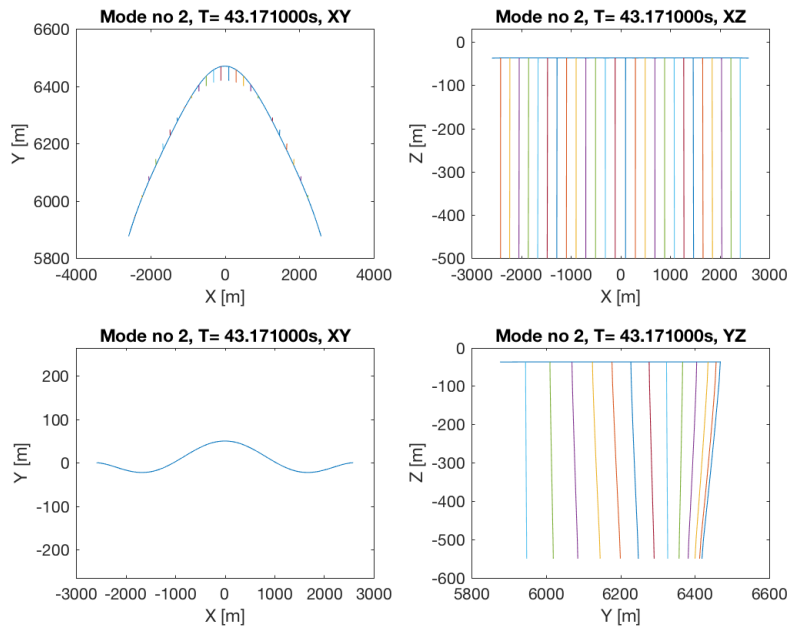
Figure C.9: Mode 2. 10 elements per tether
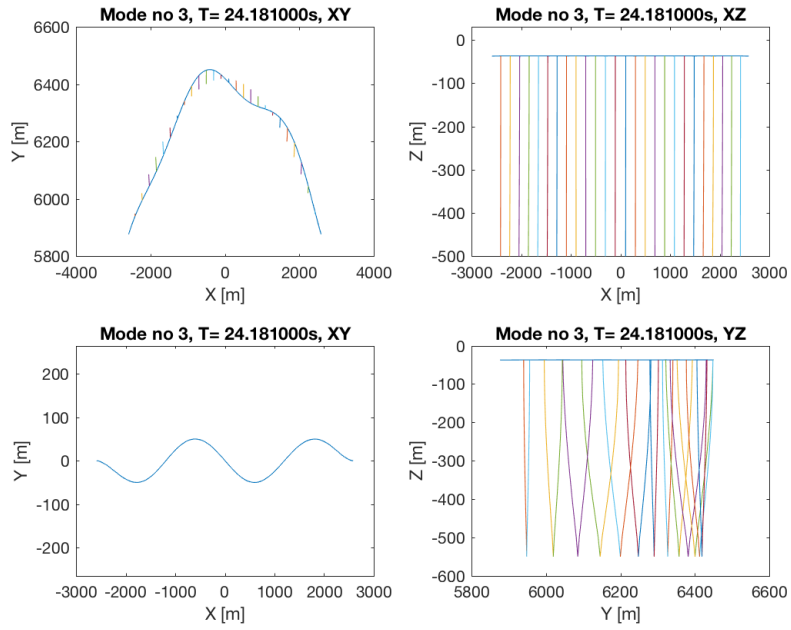
Figure C.10: Mode 3. 10 elements per tether
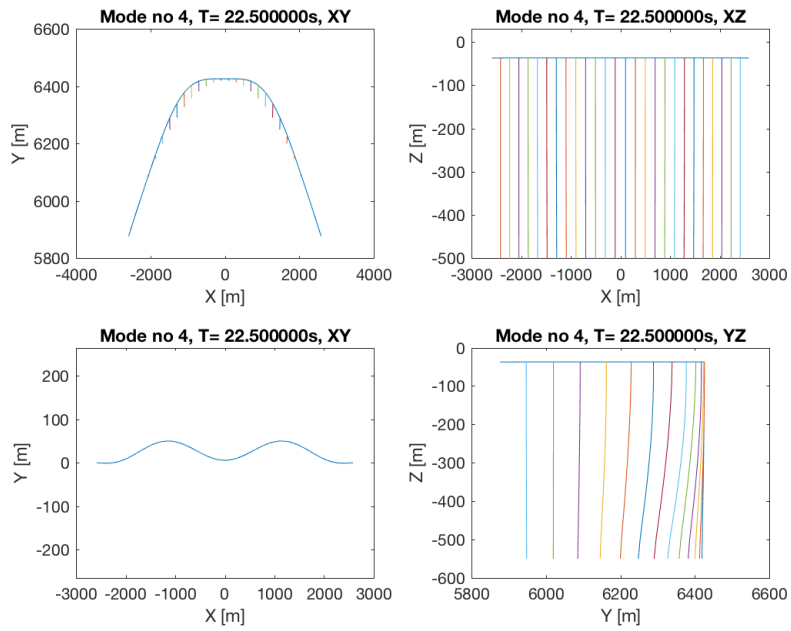
Figure C.11: Mode 4. 10 elements per tether
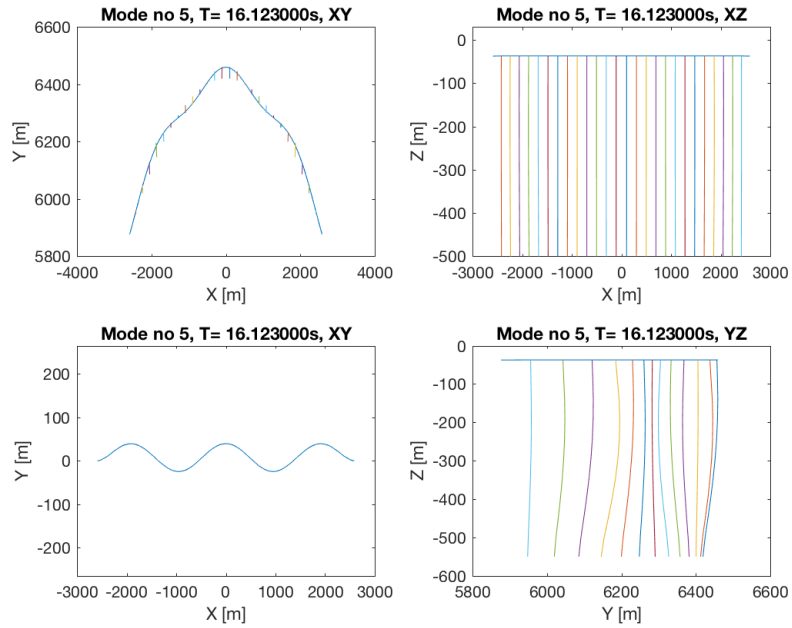
Figure C.12: Mode 5. 10 elements per tether
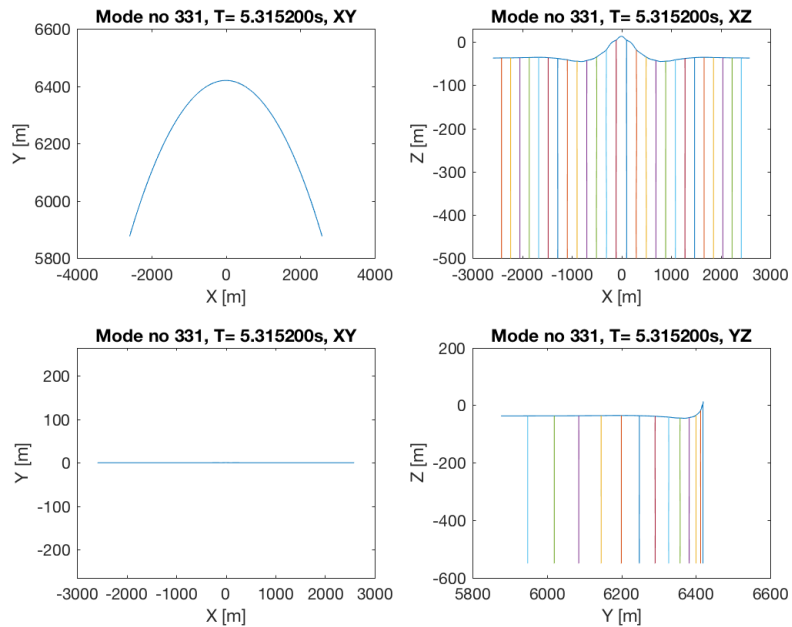
Figure C.13: Mode 331. 10 elements per tether. 1st vert. mode
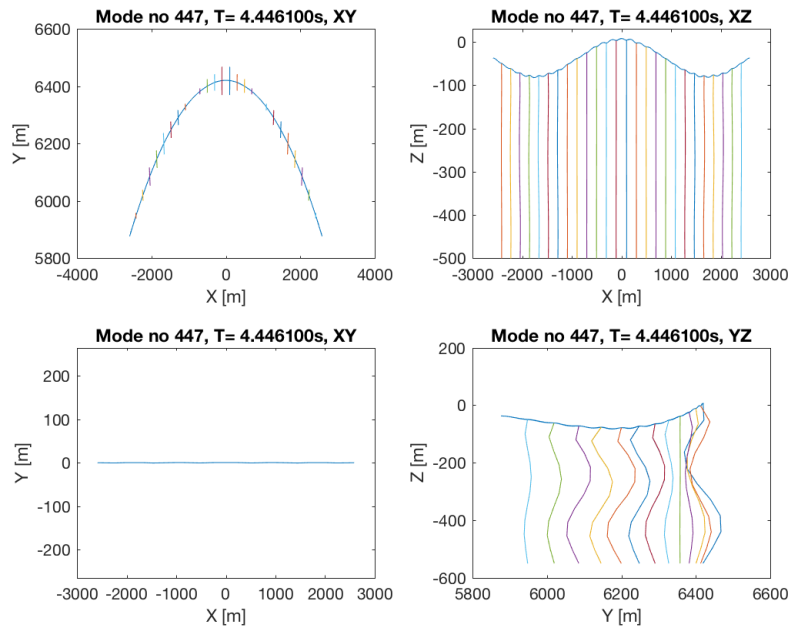
Figure C.14: Mode 447. 10 elements per tether. 2nd vert. mode

Appendix D

Calculation of properties

A number of structural parameters are calculated for input to Riflex. The axial-, bending- and torsional stiffnesses are calculated from the formulas in equations D.1, D.2, D.3 and D.4.

$$k_{axial} = EA \tag{D.1}$$

$$k_{bending,X} = EI_X \tag{D.2}$$

$$k_{bending,Y} = EI_Y \tag{D.3}$$

where Ix = Iy = $\frac{\pi r^4}{4}$ for a circular cylinder. For a rectangle, Ix = $\frac{bh3}{12}$, Iy = $\frac{hb3}{12}$. When calculating, the stiffness, also the walls in the cross-sections need to be included. This is done by the parallel axis theorem. When calculating the global stiffness for two tubes, also the parallel axis theorem is used, according to Ix = Ix + a^{2}A. See figure D.1 for reference on the parameters.

$$\frac{T}{\theta}_{\,torsional} = \frac{GJ}{L} \tag{D.4}$$

E is the elasticity modulus, I_Y and I_Z is the second moment of inertia about the Y and Z-axis. θ is the angle of twist in radians, T is the applied torque, L is the beam length,
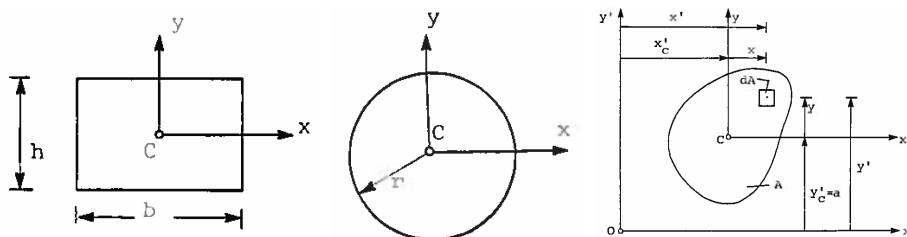
Figure D.1: Definition of cross-sections to be used for calculation of stiffness and the parallel axis theorem (Irgens)

G is the shear modulus of the material. The torsional constant J for a rectangle is

$$J_{\text{rectangle}} = \frac{1}{3}(1 - 0.6\frac{h}{b})bh^3 \text{ b } >= \text{ h}$$
(D.5)

while for a circular cylinder it is (Irgens)

$$J_{\text{circle}} = I_p = I_x + I_y = \frac{\pi r^4}{2}$$
(D.6)

The real stiffnesses would most probably be larger, as the road, and chambers for ballast also contributes to stiffness. This is not included in the analysis. The tube will be subject to a drag from the current. The velocity-independent quadratic drag force coefficient can be calculated according to equation 4.2, by dividing by velocity squared. The added mass for an arbitrary 2D shape is found from the equation D.7 (Det Norske Veritas, 2014) as

$$A_{22} = \rho_w A_{outer} C_A$$
(D.7)

where A_{outer} is the outer area of the shape. The quadratic drag force is calculated according to

$$F_{drag} = \frac{1}{2}C_D A_{proj}\rho_w$$
(D.8)

where $A_{\text{projected}}$ is the projected area for the current.

The mass moment of inertia (second moment of mass), is calculated from

$$I_x = \frac{mr^2}{2} \text{ for a thin solid disk}$$
(D.9)

$$I_x = \frac{m}{12}(h^2 + w^2) \text{ for a rectangular plate}$$
(D.10)

where m is the total mass of the body, r is the radius of the disk, and h and w is the height and width of the rectangle. The radius of gyration is calculated from

$$k = \sqrt{\frac{I_x}{m}}$$
(D.11)

where Ix is the mass moment of inertia and m is the total mass of the body.

Appendix E

MATLAB codes

E.1 Calculation of Supernodes for Bridge

```matlab
1  clc
2  clear
3  % Only including tether point 3 28  > 197*25 = 4925 m Centerline
4
5  %L_CL = 5495;        % Length of tunnel, centre line
6  r_CL = 6400;
7  L_CL = 4925;             % = 25 * 197 m ONLY points 3 26 TOTAL LENGTH = 5304
8  r_i = r_CL   20;         % Radii in curvature inner
9  r_o = r_CL + 20;         %Outer radius
10 L_i = r_i / r_CL * L_CL;
11 L_o = r_o / r_CL * L_CL;
12 %h = 740;             % sagitta
13
14 C_i = 2 * pi * r_i; % C_i = Total circumference inner
15 C_o = 2 * pi * r_o; % C_o = Total circumference outer
16
17 a = L_i / C_i * 360;  % Degrees in bridge, same for outer and inner
18 b0 = 90    (a / 2);     % Start position, first point (x,y)
19 b = a/25;               % Degrees between supernodes
20
21 CoordinatesXY_i = zeros(26,2);
22 CoordinatesXY_o = zeros(26,2);
23 for i = 1:26
24     CoordinatesXY_i(i,1) = r_i * cosd(b0 + b * (i 1));   %x
25     CoordinatesXY_i(i,2) = r_i * sind(b0 + b *(i 1));    %y
26     CoordinatesXY_o(i,1) = r_o * cosd(b0 + b * (i 1));   %x
27     CoordinatesXY_o(i,2) = r_o * sind(b0 + b *(i 1));    %y
28 end
29
30 i_Distance = sqrt((CoordinatesXY_i(1,1)   CoordinatesXY_i(2,1))^2 + (
       CoordinatesXY_i(1,2)   CoordinatesXY_i(2,2))^2)
31 o_Distance = sqrt((CoordinatesXY_o(1,1)   CoordinatesXY_o(2,1))^2 + (
       CoordinatesXY_o(1,2)   CoordinatesXY_o(2,2))^2)
32
33 %L_fjord = abs(CoordinatesXY(18,2)) +  CoordinatesXY(1,2);  % Length of
       crossing
34
```

```matlab
35  % Generating point 2
36  % inner2
37  arcLength_i = r_i / r_CL * 189.5;          % Inner arc length vs 224
38  arc_angle_i = 180 * arcLength_i / (pi*r_i); % Inner arc angle between
        points (same as outer)
39  angle_coord3_i = acosd(CoordinatesXY_i(26,1) / r_i ); % Polar angle
        coordinate of x y point
40  angle_coord2_i = angle_coord3_i + arc_angle_i; % New polar angle of new
        point
41  ix2 = r_i * cosd(angle_coord2_i);
42  iy2 = r_i * sind(angle_coord2_i);
43
44  % outer2
45  arcLength_o = r_o / r_CL * 189.5;
46  arc_angle_o = 180 * arcLength_o / (pi*r_o);
47  angle_coord3_o = acosd(CoordinatesXY_o(26,1) / r_o );
48  angle_coord2_o = angle_coord3_o + arc_angle_o;
49  ox2 = r_o * cosd(angle_coord2_o);
50  oy2 = r_o * sind(angle_coord2_o);
51
52  % Generating point 29
53  % inner29
54  angle_coord28_i = acosd(CoordinatesXY_i(1,1) / r_i );
55  angle_coord29_i = angle_coord28_i   arc_angle_i;
56  ix29 = r_i * cosd(angle_coord29_i);
57  iy29 = r_i * sind(angle_coord29_i);
58
59  % outer29
60  angle_coord28_o = acosd(CoordinatesXY_o(1,1) / r_o );
61  angle_coord29_o = angle_coord28_o   arc_angle_o;
62  ox29 = r_o * cosd(angle_coord29_o);
63  oy29 = r_o * sind(angle_coord29_o);
64
65  % Length between point 2 and 3. Should be around 224
66  i_Distance2_3 = sqrt((CoordinatesXY_i(26,1)    ix2)^2 + (CoordinatesXY_i
        (26,2)    iy2)^2)
67  o_Distance2_3 = sqrt((CoordinatesXY_o(26,1)    ox2)^2 + (CoordinatesXY_o
        (26,2)    oy2)^2)
68
69  % Bracing coordinates point 3 28  > 197*25 = 4925 m Centerline
70
71  br_b_i = a/100               % Degrees between supernodes for bracings 3 til
        28
72  br_b_o = a/100
73
74  br_CoordinatesXY_i = zeros(101,2);
75  br_CoordinatesXY_o = zeros(101,2);
76  for i = 1:101
77      br_CoordinatesXY_i(i,1) = r_i * cosd(b0 + br_b_i * (i 1));
78      br_CoordinatesXY_i(i,2) = r_i * sind(b0 + br_b_i *(i 1));
79      br_CoordinatesXY_o(i,1) = r_o * cosd(b0 + br_b_o * (i 1));
80      br_CoordinatesXY_o(i,2) = r_o * sind(b0 + br_b_o *(i 1));
81  end
82
83  %                              NB!!!
84  % For the inner circle, we only want every 4th point, starting from the
85  % 3rd line.
```

```
86  % For the outer circle, we want every 2nd point.
87
88  br_i_Distance = sqrt((br_CoordinatesXY_i(1,1)   br_CoordinatesXY_i(2,1))
        ^2 + (br_CoordinatesXY_i(1,2)   br_CoordinatesXY_i(2,2))^2)
89  br_o_Distance = sqrt((br_CoordinatesXY_o(1,1)   br_CoordinatesXY_o(2,1))
        ^2 + (br_CoordinatesXY_o(1,2)   br_CoordinatesXY_o(2,2))^2)
90
91  br_i_Distance_dia = sqrt((br_CoordinatesXY_i(99,1)   br_CoordinatesXY_o
        (100,1))^2 + (br_CoordinatesXY_i(99,2)   br_CoordinatesXY_o(100,2))^2)
92
93
94  % Generating braces between 2 and 3
95  % INNER RADIUS
96  arcLength_ibr = r_i / r_CL * 46; % 184/4. length of end elements are
        189,5 not 184, but ok.
97  arc_angle_ibr = 180 * arcLength_ibr / (pi*r_i);
98  angle_coord3br_i = acosd(br_CoordinatesXY_i(101,1) / r_i );
99  % Brace point 1 from mainpoint 3
100 angle_coord3_br1_i = angle_coord3br_i + arc_angle_ibr;
101 ix3_br1 = r_i * cosd(angle_coord3_br1_i);
102 iy3_br1 = r_i * sind(angle_coord3_br1_i);
103 % Brace point 2 from mainpoint 3
104 angle_coord3_br2_i = angle_coord3_br1_i + arc_angle_ibr;
105 ix3_br2 = r_i * cosd(angle_coord3_br2_i);
106 iy3_br2 = r_i * sind(angle_coord3_br2_i);
107 % Brace point 3 from mainpoint 3
108 angle_coord3_br3_i = angle_coord3_br2_i + arc_angle_ibr;
109 ix3_br3 = r_i * cosd(angle_coord3_br3_i);
110 iy3_br3 = r_i * sind(angle_coord3_br3_i);
111 % Brace point 4 from mainpoint 3
112 angle_coord3_br4_i = angle_coord3_br3_i + arc_angle_ibr;
113 ix3_br4 = r_i * cosd(angle_coord3_br4_i);
114 iy3_br4 = r_i * sind(angle_coord3_br4_i);
115
116 % OUTER RADIUS
117 arcLength_obr = r_o / r_CL * 46;
118 arc_angle_obr = 180 * arcLength_obr / (pi*r_o);
119 angle_coord3br_o = acosd(br_CoordinatesXY_o(101,1) / r_o );
120 % Brace point 1 from mainpoint 3
121 angle_coord3_br1_o = angle_coord3br_o + arc_angle_obr;
122 ox3_br1 = r_o * cosd(angle_coord3_br1_o);
123 oy3_br1 = r_o * sind(angle_coord3_br1_o);
124 % Brace point 2 from mainpoint 3
125 angle_coord3_br2_o = angle_coord3_br1_o + arc_angle_obr;
126 ox3_br2 = r_o * cosd(angle_coord3_br2_o);
127 oy3_br2 = r_o * sind(angle_coord3_br2_o);
128 % Brace point 3 from mainpoint 3
129 angle_coord3_br3_o = angle_coord3_br2_o + arc_angle_obr;
130 ox3_br3 = r_o * cosd(angle_coord3_br3_o);
131 oy3_br3 = r_o * sind(angle_coord3_br3_o);
132 % Brace point 4 from mainpoint 3
133 angle_coord3_br4_o = angle_coord3_br3_o + arc_angle_obr;
134 ox3_br4 = r_o * cosd(angle_coord3_br4_o);
135 oy3_br4 = r_o * sind(angle_coord3_br4_o);
136
137 % Generating braces between 28 and 29
138 % INNER RADIUS
```

```
139  angle_coord28br_i = acosd(br_CoordinatesXY_i(1,1) / r_i );
140  % Brace point 1 from mainpoint 3
141  angle_coord28_br1_i = angle_coord28br_i    arc_angle_ibr;
142  ix28_br1 = r_i * cosd(angle_coord28_br1_i);
143  iy28_br1 = r_i * sind(angle_coord28_br1_i);
144  % Brace point 2 from mainpoint 3
145  angle_coord28_br2_i = angle_coord28_br1_i    arc_angle_ibr;
146  ix28_br2 = r_i * cosd(angle_coord28_br2_i);
147  iy28_br2 = r_i * sind(angle_coord28_br2_i);
148
149  % Brace point 2 from mainpoint 3
150  angle_coord28_br3_i = angle_coord28_br2_i    arc_angle_ibr;
151  ix28_br3 = r_i * cosd(angle_coord28_br3_i);
152  iy28_br3 = r_i * sind(angle_coord28_br3_i);
153
154  % Brace point 2 from mainpoint 3
155  angle_coord28_br4_i = angle_coord28_br3_i    arc_angle_ibr;
156  ix28_br4 = r_i * cosd(angle_coord28_br4_i);
157  iy28_br4 = r_i * sind(angle_coord28_br4_i);
158
159  % OUTER RADIUS
160  angle_coord28br_o = acosd(br_CoordinatesXY_o(1,1) / r_o );
161  % Brace point 1 from mainpoint 3
162  angle_coord28_br1_o = angle_coord28br_o    arc_angle_obr;
163  ox28_br1 = r_o * cosd(angle_coord28_br1_o);
164  oy28_br1 = r_o * sind(angle_coord28_br1_o);
165  % Brace point 2 from mainpoint 3
166  angle_coord28_br2_o = angle_coord28_br1_o    arc_angle_obr;
167  ox28_br2 = r_o * cosd(angle_coord28_br2_o);
168  oy28_br2 = r_o * sind(angle_coord28_br2_o);
169
170  % Brace point 3 from mainpoint 3
171  angle_coord28_br3_o = angle_coord28_br2_o    arc_angle_obr;
172  ox28_br3 = r_o * cosd(angle_coord28_br3_o);
173  oy28_br3 = r_o * sind(angle_coord28_br3_o);
174  % Brace point 3 from mainpoint 3
175  angle_coord28_br4_o = angle_coord28_br3_o    arc_angle_obr;
176  ox28_br4 = r_o * cosd(angle_coord28_br4_o);
177  oy28_br4 = r_o * sind(angle_coord28_br4_o);
178
179  br23_i_Distance = sqrt((ix3_br3    ix3_br4)^2 + (iy3_br3    iy3_br4)^2)
180  br23_o_Distance = sqrt((ox3_br3    ox3_br4)^2 + (oy3_br3    oy3_br4)^2)
181  br23_i_Distance_dia = sqrt((ix3_br3    ox3_br4)^2 + (iy3_br3    oy3_br4)^2)
182
183  % TETHER CONFIGURATION
184  dist_midpoint_teth = 12.5 / 2; %Distance between tethers 12,5 m
185
186  arcLength_i_teth = r_i / r_CL * dist_midpoint_teth; % Inner length of arc
187  arc_angle_i_teth = 180 * arcLength_i_teth / (pi*r_i); % Inner arc angle
          between tether and midpoint
188  CoordinatesXY_tether_i_right = zeros(26,2);
189  CoordinatesXY_tether_i_left = zeros(26,2);
190
191  arcLength_o_teth = r_o / r_CL * dist_midpoint_teth; % Inner length of arc
          vs 8 in CL
192  arc_angle_o_teth = 180 * arcLength_i_teth / (pi*r_i); % Inner arc angle
          between tether and midpoint
```

```
193  CoordinatesXY_tether_o_right = zeros(26,2);
194  CoordinatesXY_tether_o_left = zeros(26,2);
195
196  for k = 1:26
197      %INNER
198      angle_coord_i_midpoint(k) = acosd(CoordinatesXY_i(k,1) / r_i );
199      angle_coord_i_teth_right(k) = angle_coord_i_midpoint(k) +
             arc_angle_i_teth;
200      angle_coord_i_teth_left(k) = angle_coord_i_midpoint(k)
             arc_angle_i_teth;
201      CoordinatesXY_tether_i_right(k,1) = r_i * cosd(
             angle_coord_i_teth_right(k) ); %x
202      CoordinatesXY_tether_i_right(k,2) = r_i * sind(
             angle_coord_i_teth_right(k) ); %y
203      CoordinatesXY_tether_i_left(k,1) = r_i * cosd(
             angle_coord_i_teth_left(k) ); %x
204      CoordinatesXY_tether_i_left(k,2) = r_i * sind(
             angle_coord_i_teth_left(k) ); %y
205
206      %                                   NB!!!!

207      %left and right is meant about the tethers laying left and right to
             the
208      %midpoint of the lay by.
209
210      %OUTER
211      angle_coord_o_midpoint(k) = acosd(CoordinatesXY_o(k,1) / r_o );
212      angle_coord_o_teth_right(k) = angle_coord_o_midpoint(k) +
             arc_angle_o_teth;
213      angle_coord_o_teth_left(k) = angle_coord_o_midpoint(k)
             arc_angle_o_teth;
214      CoordinatesXY_tether_o_right(k,1) = r_o * cosd(
             angle_coord_o_teth_right(k) ); %x
215      CoordinatesXY_tether_o_right(k,2) = r_o * sind(
             angle_coord_o_teth_right(k) ); %y
216      CoordinatesXY_tether_o_left(k,1) = r_o * cosd(
             angle_coord_o_teth_left(k) ); %x
217      CoordinatesXY_tether_o_left(k,2) = r_o * sind(
             angle_coord_o_teth_left(k) ); %y
218  end
219
220
221  % PLOT
222  figure()
223  plot(CoordinatesXY_i(:,1),CoordinatesXY_i(:,2), 'o')
224  hold on
225  plot(CoordinatesXY_o(:,1),CoordinatesXY_o(:,2), 'o')
226  hold on
227  plot(ix2, iy2, 'o')
228  hold on
229  plot(ox2, oy2, 'o')
230  hold on
231  plot(ix29, iy29, 'o')
232  hold on
233  plot(ox29, oy29, 'o')
234  xlabel('[m]')
235  ylabel('[m]')
```

```matlab
236
237  % PLOT
238  figure()
239  plot(CoordinatesXY_i(:,1),CoordinatesXY_i(:,2), 'o')
240  hold on
241  plot(CoordinatesXY_o(:,1),CoordinatesXY_o(:,2), 'o')
242  hold on
243  plot(br_CoordinatesXY_i(:,1),br_CoordinatesXY_i(:,2), 'g o')
244  hold on
245  plot(br_CoordinatesXY_o(:,1),br_CoordinatesXY_o(:,2), 'g o')
246  hold on
247  plot(ix2, iy2, 'o')
248  hold on
249  plot(ox2, oy2, 'o')
250  hold on
251  plot(ix29, iy29, 'o')
252  hold on
253  plot(ox29, oy29, 'o')
254  hold on
255  plot(ix3_br1, iy3_br1, 'g o')
256  hold on
257  plot(ix3_br2, iy3_br2, 'g o')
258  hold on
259  plot(ix3_br3, iy3_br3, 'g o')
260  hold on
261  plot(ix3_br4, iy3_br4, 'g o')
262  hold on
263  plot(ox3_br1, oy3_br1, 'g o')
264  hold on
265  plot(ox3_br2, oy3_br2, 'g o')
266  hold on
267  plot(ox3_br3, oy3_br3, 'g o')
268  hold on
269  plot(ox3_br4, oy3_br4, 'g o')
270  hold on
271  plot(ix28_br1, iy28_br1, 'g o')
272  hold on
273  plot(ix28_br2, iy28_br2, 'g o')
274  hold on
275  plot(ox28_br1, oy28_br1, 'g o')
276  hold on
277  plot(ox28_br2, oy28_br2, 'g o')
278  xlabel('[m]')
279  ylabel('[m]')
280
281
282  figure()
283  plot(CoordinatesXY_tether_i_right(:,1), CoordinatesXY_tether_i_right(:,2)
        , 'bo')
284  hold on
285  plot(CoordinatesXY_tether_i_left(:,1), CoordinatesXY_tether_i_left(:,2),
        'ro')
286  hold on
287  plot(CoordinatesXY_tether_o_right(:,1), CoordinatesXY_tether_o_right(:,2)
        , 'bo')
288  hold on
289  plot(CoordinatesXY_tether_o_left(:,1), CoordinatesXY_tether_o_left(:,2),
```

```matlab
          'ro')
290  hold on
291  plot(CoordinatesXY_i(:,1),CoordinatesXY_i(:,2), 'go')
292  hold on
293  plot(CoordinatesXY_o(:,1),CoordinatesXY_o(:,2), 'go')
294
295  % GATHERING COODINATES INNER TUBE
296  %br_CoordinatesXY_i(1,:) = [];
297  br_CoordinatesXY_i(1,:) = [];
298  br_CoordinatesXY_i(1,:) = [];
299  FinalCoord_i(:,1) = CoordinatesXY_i(:,1);
300  FinalCoord_i(:,2) = CoordinatesXY_i(:,2);
301
302  for i = 1:4:98
303      FinalCoord_i2((i+3)/4,:) = br_CoordinatesXY_i(i,:)
304  end
305  FinalCoord_i2(26,1) = ix3_br2; %only need inner number 2
306  FinalCoord_i2(26,2) = iy3_br2;
307  FinalCoord_i2(27,1) = ix28_br2; %only need inner number 2
308  FinalCoord_i2(27,2) = iy28_br2;
309
310  FinalCoord_i2(28,1) = ix3_br4; %only need inner number 2
311  FinalCoord_i2(28,2) = iy3_br4;
312  FinalCoord_i2(29,1) = ix28_br4; %only need inner number 2
313  FinalCoord_i2(29,2) = iy28_br4;
314
315  for i = 30:(29+26)
316      FinalCoord_i2(i,:) = CoordinatesXY_tether_i_left(i 29,:);
317  end
318  for i = 56:56+26 1
319      FinalCoord_i2(i,:) = CoordinatesXY_tether_i_right(i 55,:);
320  end
321
322  FinalCoord_i2(82,1) = ix2;
323  FinalCoord_i2(82,2) = iy2;
324  FinalCoord_i2(83,1) = ix29;
325  FinalCoord_i2(83,2) = iy29;
326
327  for i = 27:27+83 1
328      FinalCoord_i(i,:) = FinalCoord_i2(i 26,:)
329  end
330
331  % GATHERING COODINATES OUTER TUBE
332  br_CoordinatesXY_o(1,:) = [];
333  FinalCoord_o(:,1) = CoordinatesXY_o(:,1);
334  FinalCoord_o(:,2) = CoordinatesXY_o(:,2);
335
336  for i = 1:2:100
337      FinalCoord_o2((i+1)/2,:) = br_CoordinatesXY_o(i,:)
338  end
339  FinalCoord_o2(51,1) = ox3_br1;
340  FinalCoord_o2(51,2) = oy3_br1;
341  FinalCoord_o2(52,1) = ox28_br1;
342  FinalCoord_o2(52,2) = oy28_br1;
343  FinalCoord_o2(53,1) = ox3_br3;
344  FinalCoord_o2(53,2) = oy3_br3;
345
```

```matlab
346  for i = 54:(54+26) 1
347      FinalCoord_o2(i,:) = CoordinatesXY_tether_o_left(i 53,:);
348  end
349  for i = 80:80+26 1
350      FinalCoord_o2(i,:) = CoordinatesXY_tether_o_right(i 79,:);
351  end
352
353  FinalCoord_o2(106,1) = ox2;
354  FinalCoord_o2(106,2) = oy2;
355  FinalCoord_o2(107,1) = ox29;
356  FinalCoord_o2(107,2) = oy29;
357  FinalCoord_o2(108,1) = ox28_br3;
358  FinalCoord_o2(108,2) = oy28_br3;
359  %FinalCoord_o2(109,1) = ox28_br4;
360  %FinalCoord_o2(109,2) = oy28_br4;
361  %FinalCoord_o2(110,1) = ox28_br1;
362  %FinalCoord_o2(110,2) = oy28_br1;
363
364  for i = 27:27+108 1
365      FinalCoord_o(i,:) = FinalCoord_o2(i 26,:)
366  end
367
368  figure()
369  plot(FinalCoord_i(:,1),FinalCoord_i(:,2), 'ro')
370  hold on
371  plot(FinalCoord_o(:,1),FinalCoord_o(:,2), 'bo')
```

E.2 Calculation of Cross-sectional Parameters

```matlab
1   clc
2   clear
3   % If Ix,Iy; Ix = Iy, Iy =Iz.
4
5   % T 9.5
6   t95_Iy_test_2 = (pi * 6.3^4)/4   (pi*5.5^4)/4 + ((1/12 *10.761*0.4^3) +
        0.4*10.761*(0.471+0.2)^2) + 2*((1/12 * 0.3*4.5^3) +
        0.3*4.5*(0.471+0.4+(4.5/2))^2)
7   t95_Iz_test_2 = (pi * 6.3^4)/4   (pi*5.5^4)/4 + ((1/12 *10.761^3 * 0.4) +
        0) + 2*((1/12 * 0.3^3*4.5) + 0.3*4.5*(2+(0.3/2))^2)
8
9   % T 12.5
10  t125_Iy_test = (pi * 7.5^4)/4   (pi*6.7^4)/4 + ((1/12 *13.217*0.4^3) +
        0.4*13.217*(0.9+0.2)^2) + 2*((1/12 * 0.3*4.5^3) +
        0.3*4.5*(0.9+0.4+(4.5/2))^2) + (((1/12)*4*0.3^3) +
        0.3*4*(0.9+0.4+2.9+(0.3/2))^2)
11  t125_Iz_test = (pi * 7.5^4)/4   (pi*6.7^4)/4 + ((1/12 *13.217^3 * 0.4) +
        0) + 2*((1/12 * 0.3^3*4.5) + 0.3*4.5*(2+(0.3/2))^2) + ((1/12)*4^3*0.3
        + 0)
12
13  % Bracing
14  br_Ix_test = 5*0.5^3/12 + ((1/12)*0.4*0.6^3 + 0.6*0.7*((0.5/2)+(0.6/2))
        ^2)*4
15  br_Iy_test = 5^3*0.5/12 + ((1/12)*0.4^3*0.6 + 0.6*0.7*((5/2) 0.3 0.2)^2)
        *4
16
17  %Cross tube without lay by
```

```
18  cross_nolb_Ix_test = (16*16.1^3)/12    ((1/12)*4.8*6.9^3 +
       4.8*6.9*((0.5/2)+(6.9/2))^2)*2    ((1/12)*4.8*7.2^3+4.8*7.2*((0.5/2)
       +(7.2/2))^2)*2    ((1/12)*5*4.1^3 + 5*3.9*((0.5/2)+3+(3.9/2))^2)
       ((1/12)*5*4.2^3 + 5*4.2*((0.5/2)+3+(4.2/2))^2)    ((1/12)*4*2.5^3 +
       4*2.5*((0.5/2) + (2.5/2))^2)*2
19  cross_nolb_Iy_test = (16^3*16.1)/12    ((1/12)*4.8^3*6.9 + 4.8*6.9*((5/2)
       +(0.5/2)+(4.8/2))^2)*2    ((1/12)*4.8^3*7.2 + 4.8*7.2*((5/2)+(0.5/2)
       +(4.8/2))^2)*2    ((1/12)*5^3*3.9 + 0)    ((1/12)*5^3*4.2 + 0)    ((1/12)
       *4^3*2.5 + 0)*2
20
21  %Cross tube with lay by
22  cross_lb_Ix_test = (16*17.5^3)/12    ((1/12)*4.8*7.1^3 + 4.8*7.1*((0.5/2)
       +(7.1/2))^2)*2    ((1/12)*4.8*8.4^3+4.8*8.4*((0.5/2)+(8.4/2))^2)*2
       ((1/12)*5*4.1^3 + 5*4.1*((0.5/2)+3+(4.1/2))^2)    ((1/12)*5*5.4^3 +
       5*5.4*((0.5/2)+3+(5.4/2))^2)    ((1/12)*4*2.5^3 + 4*2.5*((0.5/2) +
       (2.5/2))^2)*2
23  cross_lb_Iy_test = (16^3*17.5)/12    ((1/12)*4.8^3*7.1 + 4.8*7.1*((5/2)
       +(0.5/2)+(4.8/2))^2)*2    ((1/12)*4.8^3*8.4 + 4.8*8.4*((5/2)+(0.5/2)
       +(4.8/2))^2)*2    ((1/12)*5^3*4.1 + 0)    ((1/12)*5^3*5.4 + 0)    ((1/12)
       *4^3*2.5 + 0)*2
24
25
26  % Tether
27  teth_D = 1.1176;
28  teth_R = teth_D/2;
29  teth_t = 0.038; % 38mm
30  teth_r = teth_R teth_t;
31
32  teth_Ix = pi * (teth_R^4    teth_r^4) / 4;
33  teth_Iy = teth_Ix;
```

E.3   Modal Analysis

```
1   % Modal Analysis
2   clc
3   clear
4
5   %for n = 1:10
6   % SHAPE FUNCTION IN SWAY
7   n=3; % mode no
8   L = 5304;
9   syms x
10  K = (n + 1/2)*pi    (( 1)^n / cosh((n+(1/2))*pi));
11  betax = K * x/L;
12  betax_L = K*(x L)/L;
13  betax_l = K*(x+L)/L;
14  alpha = sin(K)/(( 1)^n   cos(K));
15
16  phi = exp( betax)    cos(betax) + alpha*sin(betax)    ( 1)^n * (exp(betax_L
       ) exp( betax_l)/(1+exp(2*K)));
17
18  %Normalizing of displacement curve
19  fun = matlabFunction( phi);
20  [x,fval] = fminbnd(fun, 0,L);
21  max =   fval; % Maximum value
22
```

```matlab
23  phi_norm = phi/max; % normalized displacement
24
25  %                    Modal mass in sway
26  m_dry = 120531.09; %kg/m
27  m_added = 144551.7466; %kg/m
28  m_tube = m_dry*2 + m_added*2;
29
30  m_teth = 1012.65 * 512.5; %kg. dry and added mass
31
32  % Modal mass tube
33  M_tube = int(m_tube * phi_norm^2, [0 L]);
34  Mapprox = double(M_tube);
35
36
37  % Modal mass tethers
38  for i = 1:26
39  u(i) = 189.5 + 197*(i 1); % Tether locations along length
40  end
41
42  teth(n) = 0;
43      for i = 1:26     % 26 moorings
44      betaxt = K * u(i)/L;
45      betax_Lt = K*(u(i) L)/L;
46      betax_lt = K*(u(i)+L)/L;
47      alpha = sin(K)/(( 1)^n   cos(K));
48
49      phi_teth(i) = exp( betaxt)   cos(betaxt) + alpha*sin(betaxt)   ( 1)^n
              * (exp(betax_Lt) exp( betax_lt)/(1+exp(2*K)));
50
51      teth(n) = teth(n) + phi_teth(i)^2; % Summation of tether points
52      end
53
54  total_teth(n) = 1/3 * m_teth * teth(n); % 1/3 fra integrering   ok
55
56  M_total(n) = Mapprox + total_teth(n); % Modal mass in sway
57
58  % HEAVE
59  M_heave(n) = Mapprox + (m_teth * teth(n));
60
61  %                    Modal Stiffness in sway
62
63  phi_ddiff = diff(phi_norm, 2); % two times differentiation
64
65  %figure()
66  figure('units','centimeters','position',[10 5 55 15]);
67  displ = subplot(1,2,1);
68  fplot(phi_norm, [0 L], 'Linewidth',3) % Plots displacement curve,
      normalized
69  title('Displacement curve mode 3')
70  ylabel('Phi')
71  xlabel('X coordinate [m]')
72  %set(findall(gca, 'Type', 'Line'),'LineWidth',5);
73  set(gca,'fontsize',24)
74
75  curv = subplot(1,2,2);
76  fplot(phi_ddiff, [0 L], 'Linewidth',3) % Plots curvatue
77  title('Curvature curve mode 3')
```

```
78   ylabel('d^2/dx^2 Phi')
79   xlabel('X coordinate [m]')
80   % set(gcf, 'Visible', 'off')
81   %set([displ curv],'LineWidth',4)
82   %displ(1).LineWidth = 2;
83   set(gca,'fontsize',24)
84   saveas(displ,sprintf('Modal_anal_displ_curv3.png'))
85
86   E = 30*10^9; %GPa tube
87   Iz = (572.58 + 20^2*37.2)*2; %mm^4
88   K_tube(n) = E*Iz * int(phi_ddiff^2, [0 L]); % Modal stiffness tube
89   Kapprox(n) = double(K_tube(n)); %Nm2 * (m^1)^2 * m  > Nm ?
90
91   k_teth = 4 * 11*10^6 / 512.5; % Four (4) tethers per mooring! N/m
92   K_teth(n) = k_teth * teth(n); % N/m * m2 > Nm ?
93   K_total(n) = Kapprox(n) + K_teth(n); %Modal stiffness in sway
94
95   % HEAVE
96   Iy = 551.40 * 2;
97   K_tube_heave(n) = E*Iy * int(phi_ddiff^2, [0 L]); % Modal stiffness tube
98   Kapprox_heave(n) = double(K_tube_heave(n)); %Nm2 * (m^1)^2 * m  > Nm ?
99
100  Es = 2.07*10^11;
101  As = 0.129;
102  lt = 512.5;
103  k_teth_vert = 4 * Es * As / lt; % 4 tethers in one group
104  k_teth_total_vert(n) = k_teth_vert * teth(n);
105
106  K_total_heave(n) = Kapprox_heave(n) + k_teth_total_vert(n);
107
108  %end
109  % Curvature unit: m^1
110
111  % Sway   horizontal
112  w = sqrt(K_total./M_total); % angular frequency
113  T = 2*pi ./ w; % period    s
114
115  % Heave   vertical
116  w_heave = sqrt(K_total_heave./M_heave); % angular frequency
117  T_heave = 2*pi./w_heave; % period    s
118
119  fid = fopen('freqs_to_latex_modal.txt','w+');
120  for i = 1:10
121      fprintf(fid, '%.03f & %.03f \\\\ \n', w(i), T(i));
122  end
123  fprintf(fid, 'vert');
124  for i = 1:10
125      fprintf(fid, '     %.03f & %.03f \\\\ \n', w_heave(i), T_heave(i));
126  end
127  fclose(fid)
```

E.4 Calculation of Frequencies for Beam on Elastic Foundation

```
1   clc
```

```matlab
clear

L = 5304;
m_dry = 120531.09; %kg/m
m_added = 144551.7466; %kg/m
m_tube = m_dry*2 + m_added*2;
m_teth = 1012.65 * 512.5; %kg
m_tot = m_tube + (26 * 4 * m_teth);
E = 30*10^9; %GPa tube
Iz = (572.58 + 20^2*37.2)*2; %mm^4
Iy = 551.40*2; %m^4 Vertical stiffness

for i = 1:10
ki = (1+0.5)*pi/L;
ls = 512.5; %m length tether

kf_hor = 26 * 4 * 10*10^6 /ls /L;

Es = 210*10^9; %GPa steel tether
As = 0.129; %m^2

kf_vert = 26 * 4 * Es*As/ls/ L;

p_hor(i) = sqrt(((((i + 0.5)*pi)/L)^4 * E*Iz/m_tube) + kf_hor / m_tube);
p_vert(i) = sqrt(((((i + 0.5)*pi)/L)^4 * E*Iy/m_tube) + kf_vert / m_tube)
    ;

T_vert(i) = 2*pi/p_vert(i);
T_hor(i) = 2*pi/p_hor(i);

end

fid = fopen('freqs_to_latex_timoshenko.txt','w+');
for i = 1:10
    fprintf(fid, '      %.03f & %.03f \\\\ \n', p_hor(i), T_hor(i));
end
fprintf(fid, 'vert');
for i = 1:10
    fprintf(fid, '      %.03f & %.03f \\\\ \n', p_vert(i), T_vert(i));
end
fclose(fid)
```

E.5   Plotting of Bridge Modes

```matlab
%          STATIC DISPLACEMENT AND EIGENFREQUENCY POST PROCESSOR
clc
clear
%         Before running, check
%   Correct static fil
%   Correct eigmod fil
%   Correct eigfreq fil
%   Correct number of nodes, number of frequencies, start and endpoint
    for reading of excel document

Numfreqs = 100;
NumNodes_tube = 5;
```

```matlab
12  NumNodes_teth = 2; %11
13
14  %         READING COORDINATES FOR BRIDGE: X, Y, Z
15  [dataXY, textXY] = xlsread('Static_XY_symm_0417','B1:F242'); %
        Static_XY_config_symmetric_Max5nodes.xlsx', 'B1:F242');
16  [dataXZ, textXZ] = xlsread('Static_XZ_symm_0417','B1:F242'); %
        Static_XZ_config_symmetric_Max5nodes.xlsx', 'B1:F242');
17  Length_XY = length(dataXY);
18  Length_XZ = length(dataXZ);
19
20  NumRepeatX = 3;
21  NumRepeatY = 3;
22  NumRepeatZ = 3;
23
24  for i = 1:3:Length_XY
25       x(i,1:NumNodes_tube) = dataXY(i,1:NumNodes_tube); % Sets x values
26  end
27  for i = 2:3:Length_XY
28      y(i,1:NumNodes_tube) = dataXY(i,1:NumNodes_tube); % Sets y values
29  end
30  for i = 2:3:Length_XZ
31      z(i,1:NumNodes_tube) = dataXZ(i,1:NumNodes_tube); % Sets z values
32  end
33
34  y(1,:) = []; % Deletes first row
35  z(1,:) = []; % Deletes first row
36
37  x1 = zeros((Length_XY + 1)/NumRepeatX,4);
38  for i = 1:NumRepeatX:Length_XY + 1
39      for j = 1:NumNodes_tube
40      x1((i+2)/3,j) = x(i,j); % Makes new matrix without rows not needed
41      end
42  end
43  y1 = zeros((Length_XY + 1)/NumRepeatY,4);
44  for i = 1:NumRepeatY:Length_XY + 1
45      for j = 1:NumNodes_tube
46      y1((i+2)/3,j) = y(i,j); % Makes new matrix without rows not needed
47      end
48  end
49  z1 = zeros((Length_XZ + 1)/NumRepeatZ,4);
50  for i = 1:NumRepeatZ:Length_XZ + 1
51      for j = 1:NumNodes_tube
52      z1((i+2)/3,j) = z(i,j); % Makes new matrix without rows not needed
53      end
54  end
55
56  x1_trans = transpose(x1); % Flips matrix about diagonal
57  coord_x = reshape(x1_trans,[],1); % Makes matrix into one column for
        easily plotting
58  y1_trans = transpose(y1); % Flips matrix about diagonal
59  coord_y = reshape(y1_trans,[],1); % Makes matrix into one column for
        easily plotting
60  z1_trans = transpose(z1); % Flips matrix about diagonal
61  coord_z = reshape(z1_trans,[],1); % Makes matrix into one column for
        easily plotting
62
63  %% Plot of the static equilibrium
```

```matlab
64  % figure ()
65  % XYplot = subplot (2 ,1 ,1);
66  % plot ( coord_x , coord_y )
67  % title (XYplot , 'XY equilibrium position ')
68  % ylabel (XYplot , 'Static position in Y [m]')
69  % XZplot = subplot (2 ,1 ,2);
70  % plot ( coord_x , coord_z )
71  % title (XZplot , 'XZ equilibrium position ')
72  % ylabel (XZplot , 'Static position in Z [m]')
73
74  %            List of eigenvalues , frequencies , periods
75  NumEig = Numfreqs ;
76  StartLineEig = 172; %Found in "Fulldocu" matrix
77  %StartLineVec1 = 309; %239;
78  %NumNodes = 192; %2093;
79  Startdocu = 1;
80  % Nodes until 192 for stamod2
81
82  file = fopen ( 'sima_eigmod_symm_0417 . res ');
83  tline = fgets ( file );
84  ix = 1;
85  while ischar ( tline )
86      Fulldocu{ix ,1} = tline ;
87      tline = fgets ( file );
88      ix = ix +1;
89  end
90  Enddocu = ix ;
91
92  for i = StartLineEig : ( StartLineEig+(NumEig 1) )
93      Eig_only{i ( StartLineEig 1) ,1} = Fulldocu{i };
94      Eig_only_split{i ( StartLineEig 1) ,:} = strsplit ( Eig_only{i (
          StartLineEig 1) ,1}, ' ');
95      eig (i ( StartLineEig 1) ,:) = Eig_only_split{i ( StartLineEig 1) ,1};
96      %num{i 179 ,:} = str2num ( eig{i 179 ,:});
97  end
98  Eigenfreqs = str2double ( eig );
99
100 Eigenvalue = Eigenfreqs (: ,3);
101 Circ_freq = Eigenfreqs (: ,4);          % Rad/s
102 NaturalPeriod = Eigenfreqs (: ,5);    % s
103 RelativeError = Eigenfreqs (: ,6);
104 Frequency = Circ_freq * 1/(2* pi);    % Hz
105 %
106
107 %        READING EIGENVALUES FOR BRIDGE
108 [ data_eigX , text_eigX ] = xlsread ( 'EigenX_symm_0417 ' , 'B1:F24299 '); %
        eigenfreqX_1000_symmetric . xlsx ', 'B1:F242999 '); %F12149 '); %F242999 ')
        ;%F97199 '); 400
109 [ data_eigY , text_eigY ] = xlsread ( 'EigenY_symm_0417 ' , 'B1:F24299 '); %F72899
        '); 300
110 [ data_eigZ , text_eigZ ] = xlsread ( 'EigenZ_symm_0417 ' , 'B1:F24299 '); %'B1:
        E12149 ');
111 %[ data_eigfreqs , text_eigfreqs ] = xlsread ( 'eigenfreqZ . xlsx ', 'A1:A12149 ')
        ;
112
113 Length_eigX = length ( data_eigX );
114 Length_eigY = length ( data_eigY );
```

```matlab
115  Length_eigZ = length(data_eigZ);
116
117  NumRepeat_eigX = 3*Numfreqs;
118  TotalNodes = 81;%CONSTANT. Total spaces for nodes. 405/numnodes
        %405;%245; %81; % For outer tube
119
120  %           X DISP
121  for i = 2:3:Length_eigX
122        eigX(i,1:NumNodes_tube) = data_eigX(i,1:NumNodes_tube); % Sets eig
            values
123  end
124  eigX(1,:) = []; % Deletes first row
125  eigenX = zeros((Length_eigX + 1)/3,NumNodes_tube);
126  for i = 1:3:Length_eigX + 1
127        for j = 1:NumNodes_tube
128        eigenX((i+2)/3,j) = eigX(i,j); % Makes new matrix without rows not
            needed
129        end
130  end
131  eigen_transX = transpose(eigenX); % Flips matrix about diagonal
132  %eigen_x = reshape(eigen_trans,[],1); % Makes matrix into one column for
        easily plotting
133  for j = 1:TotalNodes
134        eigen_transX(((1:NumNodes_tube)+NumNodes_tube*(j 1)), 1:Numfreqs) =
            eigen_transX(1:NumNodes_tube, ((1:Numfreqs)+Numfreqs*(j 1)));
135  end
136  eigen_transX(:,(Numfreqs+1):(Numfreqs*TotalNodes)) = []; % Deletes
        unneeded columns
137  eigenfrequenciesX = eigen_transX;
138
139  %           Y DISP
140  for i = 2:3:Length_eigY
141        eigY(i,1:NumNodes_tube) = data_eigY(i,1:NumNodes_tube); % Sets eig
            values
142  end
143  eigY(1,:) = []; % Deletes first row
144  eigenY = zeros((Length_eigY + 1)/3,NumNodes_tube);
145  for i = 1:3:Length_eigY + 1
146        for j = 1:NumNodes_tube
147        eigenY((i+2)/3,j) = eigY(i,j); % Makes new matrix without rows not
            needed
148        end
149  end
150  eigen_transY = transpose(eigenY); % Flips matrix about diagonal
151  %eigen_x = reshape(eigen_trans,[],1); % Makes matrix into one column for
        easily plotting
152  for j = 1:TotalNodes
153        eigen_transY(((1:NumNodes_tube)+NumNodes_tube*(j 1)), 1:Numfreqs) =
            eigen_transY(1:NumNodes_tube, ((1:Numfreqs)+Numfreqs*(j 1)));
154  end
155  eigen_transY(:,(Numfreqs+1):(Numfreqs*TotalNodes)) = []; % Deletes
        unneeded columns
156  eigenfrequenciesY = eigen_transY;
157
158  %           Z DISP
159  for i = 2:3:Length_eigZ
160        eigZ(i,1:NumNodes_tube) = data_eigZ(i,1:NumNodes_tube); % Sets eig
```

```matlab
          values
161 end
162 eigZ(1,:) = []; % Deletes first row
163 eigenZ = zeros((Length_eigZ + 1)/3,NumNodes_tube);
164 for i = 1:3:Length_eigZ + 1
165     for j = 1:NumNodes_tube
166     eigenZ((i+2)/3,j) = eigZ(i,j); % Makes new matrix without rows not
            needed
167     end
168 end
169 eigen_transZ = transpose(eigenZ); % Flips matrix about diagonal
170 %eigen_x = reshape(eigen_trans,[],1); % Makes matrix into one column for
        easily plotting
171 for j = 1:TotalNodes
172     eigen_transZ(((1:NumNodes_tube)+NumNodes_tube*(j 1)), 1:Numfreqs) =
            eigen_transZ(1:NumNodes_tube, ((1:Numfreqs)+Numfreqs*(j 1)));
173 end
174 eigen_transZ(:,(Numfreqs+1):(Numfreqs*TotalNodes)) = []; % Deletes
        unneeded columns
175 eigenfrequenciesZ = eigen_transZ;
176
177 %              T E T H E R
178 %        READING COORDINATES: X, Y, Z
179 [dataXY, textXY] = xlsread('Static_XY_symm_teth_0417.xlsx', 'B1:L77');
180 [dataXZ, textXZ] = xlsread('Static_XZ_symm_teth_0417.xlsx', 'B1:L77');
181 Length_XZ = length(dataXZ);
182 Length_XY = length(dataXY);
183
184 NumRepeatX = 3;
185 NumRepeatY = 3;
186 NumRepeatZ = 3;
187
188 for i = 1:3:Length_XZ
189     x(i,1:NumNodes_teth) = dataXZ(i,1:NumNodes_teth); % Sets x values
190 end
191 for i = 2:3:Length_XY
192     y(i,1:NumNodes_teth) = dataXY(i,1:NumNodes_teth); % Sets y values
193 end
194 for i = 2:3:Length_XZ
195     z(i,1:NumNodes_teth) = dataXZ(i,1:NumNodes_teth); % Sets z values
196 end
197
198 z(1,:) = []; % Deletes first row
199 y(1,:) = []; % Deletes first row
200
201 coord_x_teth = zeros((Length_XZ + 1)/NumRepeatX,NumNodes_teth);
202 for i = 1:NumRepeatX:Length_XZ + 1
203     for j = 1:NumNodes_teth
204     coord_x_teth((i+2)/3,j) = x(i,j); % Makes new matrix without rows not
            needed
205     end
206 end
207 coord_y_teth = zeros((Length_XY + 1)/NumRepeatY,NumNodes_teth);
208 for i = 1:NumRepeatY:Length_XY + 1
209     for j = 1:NumNodes_teth
210     coord_y_teth((i+2)/3,j) = y(i,j); % Makes new matrix without rows not
            needed
```

```matlab
211         end
212   end
213   coord_z_teth = zeros((Length_XZ + 1)/NumRepeatZ,NumNodes_teth);
214   for i = 1:NumRepeatZ:Length_XZ + 1
215       for j = 1:NumNodes_teth
216       coord_z_teth((i+2)/3,j) = z(i,j); % Makes new matrix without rows not
                needed
217       end
218   end
219
220   %         READING EIGENVALUES of TETHERS outer ,
221   [data_eigXYZ, text_eigX] = xlsread('EigenXYZ_symm_teth_0417.xlsx','B1:
          C23399'); %L233999'); %C11699'); %L233999');
222
223   Length_eigXYZ = length(data_eigXYZ);
224
225   NumRepeat_eigX = 3*Numfreqs;
226
227   %           X DISP
228   for i = 2:9:Length_eigXYZ
229       eigX_teth(i,1:NumNodes_teth) = data_eigXYZ(i,1:NumNodes_teth); %
                Sets eig values
230   end
231   eigX_teth(1,:) = []; % Deletes first row
232   eigenX_teth = zeros((Length_eigXYZ + 1)/9,NumNodes_teth);
233   for i = 1:9:Length_eigXYZ + 1
234       for j = 1:NumNodes_teth
235       eigenX_teth((i+8)/9,j) = eigX_teth(i,j); % Makes new matrix without
                rows not needed
236       end
237   end
238   % eigenX_teth contains all 1000 frequencies in X for all 26 tethers
          >26*1000
239
240   %           Y DISP
241   for i = 5:9:Length_eigXYZ
242       eigY_teth(i,1:NumNodes_teth) = data_eigXYZ(i,1:NumNodes_teth); %
                Sets eig values
243   end
244   eigY_teth(1,:) = []; % Deletes first row
245   eigY_teth(1,:) = []; % Deletes first row
246   eigY_teth(1,:) = []; % Deletes first row
247   eigY_teth(1,:) = []; % Deletes first row
248   eigenY_teth = zeros((Length_eigXYZ + 1)/9,NumNodes_teth);
249   for i = 1:9:Length_eigXYZ + 1
250       for j = 1:NumNodes_teth
251       eigenY_teth((i+8)/9,j) = eigY_teth(i,j); % Makes new matrix without
                rows not needed
252       end
253   end
254   % eigenX contains all 1000 frequencies in X for all 26 tethers  >26*1000
255
256   %           Z DISP
257   for i = 8:9:Length_eigXYZ
258       eigZ_teth(i,1:NumNodes_teth) = data_eigXYZ(i,1:NumNodes_teth); %
                Sets eig values
259   end
```

```matlab
260  eigZ_teth(1,:) = []; % Deletes first row
261  eigZ_teth(1,:) = []; % Deletes first row
262  eigZ_teth(1,:) = []; % Deletes first row
263  eigZ_teth(1,:) = []; % Deletes first row
264  eigZ_teth(1,:) = []; % Deletes first row
265  eigZ_teth(1,:) = []; % Deletes first row
266  eigZ_teth(1,:) = []; % Deletes first row
267  eigenZ_teth = zeros((Length_eigXYZ + 1)/9,NumNodes_teth);
268  for i = 1:9:Length_eigXYZ + 1
269      for j = 1:NumNodes_teth
270      eigenZ_teth((i+8)/9,j) = eigZ_teth(i,j); % Makes new matrix without
              rows not needed
271      end
272  end
273  % eigenX contains all 1000 frequencies in X for all 26 tethers  >26*1000
274
275  %        NORMALIZING EIGENMODES
276  for i = 1:Numfreqs
277  MaxX(1,i) = max(abs(eigenfrequenciesX(:,i)));
278  MaxY(1,i) = max(abs(eigenfrequenciesY(:,i)));
279  MaxZ(1,i) = max(abs(eigenfrequenciesZ(:,i)));
280  end
281  end_norm = (Length_eigXYZ 8)/9 + 1;
282  for i = 1:end_norm %26000
283  MaxX_teth(i,1) = max(abs(eigenX_teth(i,:)));
284  MaxY_teth(i,1) = max(abs(eigenY_teth(i,:)));
285  MaxZ_teth(i,1) = max(abs(eigenZ_teth(i,:)));
286  end
287
288  for i = 1:Numfreqs%1000 % Finds the largest value within each frequency
        between all 26 tethers
289  MaxModeXteth(i,1) = MaxX_teth(i,1);
290  MaxModeYteth(i,1) = MaxY_teth(i,1);
291  MaxModeZteth(i,1) = MaxZ_teth(i,1);
292      for j = 1:Numfreqs:26*Numfreqs %26000
293      if MaxX_teth(j+(i 1),1) > MaxModeXteth(i,1)
294          MaxModeXteth(i,1) = MaxX_teth(j+(i 1),1); %Largest in X
295      end
296      if MaxY_teth(j+(i 1),1) > MaxModeYteth(i,1)
297          MaxModeYteth(i,1) = MaxY_teth(j+(i 1),1); %Largest in Y
298      end
299      if MaxZ_teth(j+(i 1),1) > MaxModeZteth(i,1)
300          MaxModeZteth(i,1) = MaxZ_teth(j+(i 1),1); %Largest in Z
301      end
302      end
303  end
304
305  MaxMode(1,:) = MaxX(1,:);
306  MaxMode(2,:) = MaxY(1,:);
307  MaxMode(3,:) = MaxZ(1,:);
308  MaxMode(4,:) = MaxModeXteth(:,1);
309  MaxMode(5,:) = MaxModeYteth(:,1);
310  MaxMode(6,:) = MaxModeZteth(:,1);
311
312  % for j = 1:1000:26000
313  % for i = 1:26
314  %      MaxMode(4+(i 1),:) = MaxX_teth(i,1);
```

```matlab
315  % end
316
317  for i = 1:Numfreqs
318      MaxMode_tot(1,i) = max(abs(MaxMode(:,i)));
319  end
320
321  for i = 1:Numfreqs
322  eigenfrequenciesXNORM(:,i) = eigenfrequenciesX(:,i) ./ MaxMode_tot(1,i);
323  eigenfrequenciesYNORM(:,i) = eigenfrequenciesY(:,i) ./ MaxMode_tot(1,i);
324  eigenfrequenciesZNORM(:,i) = eigenfrequenciesZ(:,i) ./ MaxMode_tot(1,i);
325  end
326
327  for i = 1:Numfreqs%1000
328      for j = 1:Numfreqs:26*Numfreqs%end_norm %1300;%26000
329          eigfreq_teth_XNORM(i+(j 1),:) = eigenX_teth(i+(j 1),:) ./
                  MaxMode_tot(1,i);
330          eigfreq_teth_YNORM(i+(j 1),:) = eigenY_teth(i+(j 1),:) ./
                  MaxMode_tot(1,i);
331          eigfreq_teth_ZNORM(i+(j 1),:) = eigenZ_teth(i+(j 1),:) ./
                  MaxMode_tot(1,i);
332      end
333  end
334
335  %
336  % % % %        PLOTS
337  % scalefactor = 50;
338  % for i = 1:10 %Numfreqs    Defines which frequencies to plot
339  % figure()
340  % eigXYplot = subplot(2,2,1);
341  % plot((coord_x+eigenfrequenciesXNORM(:,i)*scalefactor), coord_y+(
        eigenfrequenciesYNORM(:,i)*scalefactor));
342  % % hold on
343  % % for j = 1:Numfreqs:end_norm %26000
344  % %         plot(coord_x_teth((j+(Numfreqs 1))/Numfreqs,:)+
        eigfreq_teth_XNORM(j+(i 1),:)*scalefactor, coord_y_teth((j+(Numfreqs
        1))/Numfreqs,:)+eigfreq_teth_YNORM(j+(i 1),:)*scalefactor)
345  % %         hold on
346  % %     end
347  % % % hold on
348  % % % plot(coord_x, coord_y)
349  % title(eigXYplot, sprintf('Mode no %i, T= %fs, XY',i, NaturalPeriod(i)))
350  % ylabel(eigXYplot,'Y [m]')
351  % xlabel(eigXYplot,'X [m]')
352  % %axis([ 3000 3000  265 265])
353  %
354  % eigXZplot = subplot(2,2,2);
355  % plot((coord_x+eigenfrequenciesXNORM(:,i)*scalefactor), coord_z+(
        eigenfrequenciesZNORM(:,i)*scalefactor));
356  % % hold on
357  % % plot(coord_x, coord_z)
358  % % hold on
359  % % for j = 1:Numfreqs:end_norm %26000
360  % %         plot(coord_x_teth((j+(Numfreqs 1))/Numfreqs,:)+
        eigfreq_teth_XNORM(j+(i 1),:)*scalefactor, coord_z_teth((j+(Numfreqs
        1))/Numfreqs,:)+eigfreq_teth_ZNORM(j+(i 1),:)*scalefactor)
361  % %         hold on
362  % %     end
```

```matlab
363  % title(eigXZplot, sprintf('Mode no %i, T= %fs, XZ',i, NaturalPeriod(i)))
364  % ylabel(eigXZplot,'Z [m]')
365  % xlabel(eigXZplot,'X [m]')
366  % axis([ 3000 3000 500 30])
367  %
368
369  % eigXY2plot = subplot(2,2,3);
370  % plot((coord_x+eigenfrequenciesXNORM(:,i)*scalefactor), (
          eigenfrequenciesYNORM(:,i)*scalefactor));
371  % hold on
372  % % for j = 1:Numfreqs:end_norm %26000
373  % %        plot(coord_x_teth((j+(Numfreqs 1))/Numfreqs,:)+
          eigfreq_teth_XNORM(j+(i 1),:)*scalefactor, coord_y_teth((j+(Numfreqs
          1))/Numfreqs,:)+eigfreq_teth_YNORM(j+(i 1),:)*scalefactor)
374  % %        hold on
375  % %    end
376  %
377  % % hold on
378  % % plot(coord_x, coord_y)
379  % title(eigXY2plot, sprintf('Mode no %i, T= %fs, XY',i, NaturalPeriod(i))
          )
380  % ylabel(eigXY2plot,'Y [m]')
381  % xlabel(eigXY2plot,'X [m]')
382  % axis([ 3000 3000 265 265])
383  %
384  % eigXZ2plot = subplot(2,2,4);
385  % plot((coord_y+eigenfrequenciesYNORM(:,i)*scalefactor), coord_z+(
          eigenfrequenciesZNORM(:,i)*scalefactor));
386  % % hold on
387  % % plot(coord_x, coord_z)
388  % % hold on
389  % % for j = 1:Numfreqs:end_norm %26000
390  % %        plot(coord_y_teth((j+(Numfreqs 1))/Numfreqs,:)+
          eigfreq_teth_YNORM(j+(i 1),:)*scalefactor, coord_z_teth((j+(Numfreqs
          1))/Numfreqs,:)+eigfreq_teth_ZNORM(j+(i 1),:)*scalefactor)
391  % %        hold on
392  % %    end
393  % title(eigXZ2plot, sprintf('Mode no %i, T= %fs, YZ',i, NaturalPeriod(i))
          )
394  % ylabel(eigXZ2plot,'Z [m]')
395  % xlabel(eigXZ2plot,'Y [m]')
396  % %axis([ 3000 3000 500 30])
397  %
398  % % set(gcf, 'Visible', 'off')
399  % % saveas(eigXZplot,sprintf('Sym_mode_no%iT%fs_teth_11elem.png',i,
          NaturalPeriod(i)))
400  % end
401
402  % % %      PLOTS 3 in row
403  scalefactor = 50;
404  for i = 1:15 %Numfreqs   Defines which frequencies to plot
405  %figure('Mode%i',i)
406  figure('units','centimeters','InnerPosition',[1 1 70 15]);% 'position',[1
          1 45 15]);
407  eig1plot = subplot(1,3,1); %subplot(number of plots in row,number of
          plots in column,which is active);
408  plot((coord_x+eigenfrequenciesXNORM(:,i)*scalefactor), (
```

```
            eigenfrequenciesYNORM(:,i)*scalefactor), 'Linewidth',3);
409  hold on
410  for  j = 1:Numfreqs:end_norm %26000
411          plot(coord_x_teth((j+(Numfreqs 1))/Numfreqs,:)+eigfreq_teth_XNORM
                (j+(i 1),:)*scalefactor, eigfreq_teth_YNORM(j+(i 1),:)*
                scalefactor, 'Linewidth',3)
412          hold on
413      end
414  title(eig1plot, sprintf('XY Projection of mode %i',i))
415  ylabel(eig1plot,'Y [m]')
416  xlabel(eig1plot,'X [m]')
417  axis([ 3000 3000  300  300])
418  set(gca,'fontsize',24)
419
420
421  eig2plot = subplot(1,3,2);
422  plot((coord_x+eigenfrequenciesXNORM(:,i)*scalefactor), (
        eigenfrequenciesZNORM(:,i)*scalefactor), 'Linewidth',3);
423  hold on
424  for  j = 1:Numfreqs:end_norm %26000
425          plot(coord_x_teth((j+(Numfreqs 1))/Numfreqs,:)+eigfreq_teth_XNORM
                (j+(i 1),:)*scalefactor, coord_z_teth((j+(Numfreqs 1))/
                Numfreqs,:)+37.5+eigfreq_teth_ZNORM(j+(i 1),:)*scalefactor, '
                Linewidth',3)
426          hold on
427      end
428  title(eig2plot, sprintf('XZ Projection of mode %i',i ))
429  ylabel(eig2plot,'Z [m]')
430  xlabel(eig2plot,'X [m]')
431  axis([ 3000 3000  550 scalefactor+2])
432  set(gca,'fontsize',24)
433
434
435  eig3plot = subplot(1,3,3);
436  plot((coord_y+eigenfrequenciesYNORM(:,i)*scalefactor), (
        eigenfrequenciesZNORM(:,i)*scalefactor), 'Linewidth',3);
437  hold on
438  for  j = 1:Numfreqs:end_norm %26000
439          plot(coord_y_teth((j+(Numfreqs 1))/Numfreqs,:)+eigfreq_teth_YNORM
                (j+(i 1),:)*scalefactor, coord_z_teth((j+(Numfreqs 1))/
                Numfreqs,:)+37.5+eigfreq_teth_ZNORM(j+(i 1),:)*scalefactor, '
                Linewidth',3)
440          hold on
441      end
442  title(eig3plot, sprintf('YZ Projection of mode %i',i))
443  ylabel(eig3plot,'Z [m]')
444  xlabel(eig3plot,'Y [m]')
445  axis([5800 6500  550 +scalefactor+2])
446  set(gca,'fontsize',24)
447
448  set(gcf, 'Visible', 'off')
449  saveas(eig1plot,sprintf('Sym_mode_%i_teth_0417.png',i))
450  end
451
452  fid = fopen('freqs_to_latex.txt','w+');
453  for i = 1:25
454      fprintf(fid, '%i &  %.03f & %.03f & %i & %.03f & %.03f \\\\ \n', i,
```

```
                Frequency(i), NaturalPeriod(i), i+25, Frequency(i+25),
                NaturalPeriod(i+25));
455  end
456  fprintf(fid, 'T9.5 reduced velocity \n');
457  for i = 1:50
458      Vr = (0.41*0.7)/(Frequency(i) * 12.6);
459      fprintf(fid, '%i & %.03f & %.03f \\\\ \n', i, Frequency(i), Vr);
460  end
461  fprintf(fid, 'Tether reduced velocity \n');
462  for i = 1:22
463      Vr = (0.41*0.7)/(Frequency(i) * 1.1176);
464      Vr2 = (0.41*0.7)/(Frequency(i+22) * 1.1176);
465      fprintf(fid, '%i & %.03f & %.03f & %i & %.03f & %.03f \\\\ \n', i,
                Frequency(i), Vr, i+22, Frequency(i+22), Vr2);
466  end
467  fclose(fid)
468
469  % for i = 1:26 %1000 % Plots tethers 1 26 for frequency no j
470  %     figure()
471  %     for j = 1:1000:26000
472  %         plot(coord_x((j+999)/1000,:)+eigenX_teth(j+(i 1),:)*2000000,
        coord_z_teth((j+999)/1000,:)+eigenZ(j+(i 1),:)*2000000)
473  %         hold on
474  %     end
475  % end
```

E.6 Plotting of Envelopes from Dynamic Analysis

```
1   %%%%%%% PLOTTING OF ENVELOPES %%%%%%%
2   %         MOMENTS AND DISPLCEMENTS
3   clc
4   clear
5
6   NumNodes_tube = 5; % max value for all lines
7   NumElements = 8; % max value for all lines
8   NumElementsForce = 4; % max value for all lines
9   % Forces are calculated at the middle of each element > 3 element give 3
10  % points
11  % Moments are calculated one time for each end of each element > 3
        elements give 6
12  % points
13  % Displacements are calculated at the nodes > 4 nodes give 4 points
14
15  %   o           o
16  % This is 1 element with 2 nodes
17  %   o           o           o
18  % This is 2 elements with 3 nodes
19
20  %         READING COORDINATES FOR BRIDGE: X, Y, Z
21  [dataXY, textXY] = xlsread('Tp4_5_6_envelopes_MYmin',1,'B1:I971');
22  [dataXZ, textXY] = xlsread('Tp4_5_6_envelopes_MYmax',1,'B1:I971');
23  [dataXYz, textXY] = xlsread('Tp4_5_6_envelopes_MZmin',1,'B1:I971');
24  [dataXZz, textXY] = xlsread('Tp4_5_6_envelopes_MZmax',1,'B1:I971');
25  [dataAxFmn, textXY] = xlsread('Tp4_5_6_envelopes_AxFmin',1,'B1:I971');
26  [dataAxFmx, textXY] = xlsread('Tp4_5_6_envelopes_AxFmax',1,'B1:I971');
27  [dataXmx, textXY] = xlsread('Tp4_5_6_envelopes_Xmax','Ark1','B1:I971');
```

```
28  [dataXmn, textXY] = xlsread('Tp4_5_6_envelopes_Xmin',1,'B1:I971');
29  [dataYmx, textXY] = xlsread('Tp4_5_6_envelopes_Ymax',1,'B1:I971');
30  [dataYmn, textXY] = xlsread('Tp4_5_6_envelopes_Ymin',1,'B1:I971');
31  [dataZmx, textXY] = xlsread('Tp4_5_6_envelopes_Zmax',1,'B1:I971');
32  [dataZmn, textXY] = xlsread('Tp4_5_6_envelopes_Zmin',1,'B1:I971');
33
34  % SWELL INCLUDED
35  [S14dataXY, textXY] = xlsread('Tp4_5_6_SWELL14_envelopes_MYmin',1,'B1:
        I971');
36  [S14dataXZ, textXY] = xlsread('Tp4_5_6_SWELL14_envelopes_MYmax',1,'B1:
        I971');
37  [S14dataXYz, textXY] = xlsread('Tp4_5_6_SWELL14_envelopes_MZmin',1,'B1:
        I971');
38  [S14dataXZz, textXY] = xlsread('Tp4_5_6_SWELL14_envelopes_MZmax',1,'B1:
        I971');
39  [S14dataAxFmn, textXY] = xlsread('Tp4_5_6_SWELL14_envelopes_AxFmin',1,'B1
        :I971');
40  [S14dataAxFmx, textXY] = xlsread('Tp4_5_6_SWELL14_envelopes_AxFmax',1,'B1
        :I971');
41  [S14dataXmx, textXY] = xlsread('Tp4_5_6_SWELL14_envelopes_Xmax','Ark1','
        B1:I971');
42  [S14dataXmn, textXY] = xlsread('Tp4_5_6_SWELL14_envelopes_Xmin',1,'B1:
        I971');
43  [S14dataYmx, textXY] = xlsread('Tp4_5_6_SWELL14_envelopes_Ymax',1,'B1:
        I971');
44  [S14dataYmn, textXY] = xlsread('Tp4_5_6_SWELL14_envelopes_Ymin',1,'B1:
        I971');
45  [S14dataZmx, textXY] = xlsread('Tp4_5_6_SWELL14_envelopes_Zmax',1,'B1:
        I971');
46  [S14dataZmn, textXY] = xlsread('Tp4_5_6_SWELL14_envelopes_Zmin',1,'B1:
        I971');
47
48  [S15dataXY, textXY] = xlsread('Tp4_5_6_SWELL15_envelopes_MYmin',1,'B1:
        I971');
49  [S15dataXZ, textXY] = xlsread('Tp4_5_6_SWELL15_envelopes_MYmax',1,'B1:
        I971');
50  [S15dataXYz, textXY] = xlsread('Tp4_5_6_SWELL15_envelopes_MZmin',1,'B1:
        I971');
51  [S15dataXZz, textXY] = xlsread('Tp4_5_6_SWELL15_envelopes_MZmax',1,'B1:
        I971');
52  [S15dataAxFmn, textXY] = xlsread('Tp4_5_6_SWELL15_envelopes_AxFmin',1,'B1
        :I971');
53  [S15dataAxFmx, textXY] = xlsread('Tp4_5_6_SWELL15_envelopes_AxFmax',1,'B1
        :I971');
54  [S15dataXmx, textXY] = xlsread('Tp4_5_6_SWELL15_envelopes_Xmax','Ark1','
        B1:I971');
55  [S15dataXmn, textXY] = xlsread('Tp4_5_6_SWELL15_envelopes_Xmin',1,'B1:
        I971');
56  [S15dataYmx, textXY] = xlsread('Tp4_5_6_SWELL15_envelopes_Ymax',1,'B1:
        I971');
57  [S15dataYmn, textXY] = xlsread('Tp4_5_6_SWELL15_envelopes_Ymin',1,'B1:
        I971');
58  [S15dataZmx, textXY] = xlsread('Tp4_5_6_SWELL15_envelopes_Zmax',1,'B1:
        I971');
59  [S15dataZmn, textXY] = xlsread('Tp4_5_6_SWELL15_envelopes_Zmin',1,'B1:
        I971');
60
```

```
61  Length_XY = length(dataXY);
62  Length_XZ = length(dataXZ);
63
64  NumRepeatX = 3;
65  NumRepeatY = 3;
66  NumRepeatZ = 3;
67
68  for i = 1:3:Length_XY
69       x(i,1:NumElements) = dataXY(i,1:NumElements); % Sets x values
70  end
71  for i = 2:3:Length_XY
72      y(i,1:NumElements) = dataXY(i,1:NumElements); % Sets y values
73  end
74  for i = 2:3:Length_XZ
75      z(i,1:NumElements) = dataXZ(i,1:NumElements); % Sets y values
76  end
77  for i = 2:3:Length_XY
78      AxFmn(i,1:NumElementsForce) = dataAxFmn(i,1:NumElementsForce); % Sets
             y values
79  end
80  for i = 2:3:Length_XZ
81      AxFmx(i,1:NumElementsForce) = dataAxFmx(i,1:NumElementsForce); % Sets
             y values
82  end
83
84  for i = 1:3:Length_XZ
85      Fcoord(i,1:NumElementsForce) = dataAxFmx(i,1:NumElementsForce); %
             Sets y values
86  end
87  for i = 2:3:Length_XY
88      yz(i,1:NumElements) = dataXYz(i,1:NumElements); % Sets y values
89  end
90  for i = 2:3:Length_XZ
91      zz(i,1:NumElements) = dataXZz(i,1:NumElements); % Sets y values
92  end
93
94  % X
95  for i = 2:3:Length_XZ
96      Xmx(i,1:NumNodes_tube) = dataXmx(i,1:NumNodes_tube); % Sets y values
97  end
98  for i = 2:3:Length_XZ
99      Xmn(i,1:NumNodes_tube) = dataXmn(i,1:NumNodes_tube); % Sets y values
100 end
101
102 % COORD DISPL
103 for i = 1:3:Length_XZ
104     coord_xdispl(i,1:NumNodes_tube) = dataXmx(i,1:NumNodes_tube); % Sets
             y values
105 end
106 % Y
107 for i = 2:3:Length_XZ
108     Ymx(i,1:NumNodes_tube) = dataYmx(i,1:NumNodes_tube); % Sets y values
109 end
110 for i = 2:3:Length_XZ
111     Ymn(i,1:NumNodes_tube) = dataYmn(i,1:NumNodes_tube); % Sets y values
112 end
113 % Z
```

```matlab
114  for i = 2:3:Length_XZ
115      Zmx(i,1:NumNodes_tube) = dataZmx(i,1:NumNodes_tube); % Sets y values
116  end
117  for i = 2:3:Length_XZ
118      Zmn(i,1:NumNodes_tube) = dataZmn(i,1:NumNodes_tube); % Sets y values
119  end
120
121  % INCLUDED SWELL
122  for i = 2:3:Length_XY
123      S14y(i,1:NumElements) = S14dataXY(i,1:NumElements); % Sets y values
124  end
125  for i = 2:3:Length_XZ
126      S14z(i,1:NumElements) = S14dataXZ(i,1:NumElements); % Sets y values
127  end
128  for i = 2:3:Length_XY
129      S14AxFmn(i,1:NumElementsForce) = S14dataAxFmn(i,1:NumElementsForce);
             % Sets y values
130  end
131  for i = 2:3:Length_XZ
132      S14AxFmx(i,1:NumElementsForce) = S14dataAxFmx(i,1:NumElementsForce);
             % Sets y values
133  end
134
135  for i = 2:3:Length_XY
136      S14yz(i,1:NumElements) = S14dataXYz(i,1:NumElements); % Sets y values
137  end
138  for i = 2:3:Length_XZ
139      S14zz(i,1:NumElements) = S14dataXZz(i,1:NumElements); % Sets y values
140  end
141
142  % X
143  for i = 2:3:Length_XZ
144      S14Xmx(i,1:NumNodes_tube) = S14dataXmx(i,1:NumNodes_tube); % Sets y
             values
145  end
146  for i = 2:3:Length_XZ
147      S14Xmn(i,1:NumNodes_tube) = S14dataXmn(i,1:NumNodes_tube); % Sets y
             values
148  end
149
150  % Y
151  for i = 2:3:Length_XZ
152      S14Ymx(i,1:NumNodes_tube) = S14dataYmx(i,1:NumNodes_tube); % Sets y
             values
153  end
154  for i = 2:3:Length_XZ
155      S14Ymn(i,1:NumNodes_tube) = S14dataYmn(i,1:NumNodes_tube); % Sets y
             values
156  end
157  % Z
158  for i = 2:3:Length_XZ
159      S14Zmx(i,1:NumNodes_tube) = S14dataZmx(i,1:NumNodes_tube); % Sets y
             values
160  end
161  for i = 2:3:Length_XZ
162      S14Zmn(i,1:NumNodes_tube) = S14dataZmn(i,1:NumNodes_tube); % Sets y
             values
```

```matlab
163  end
164
165  %Tp=15 SWELL
166  for i = 2:3:Length_XY
167      S15y(i,1:NumElements) = S15dataXY(i,1:NumElements); % Sets y values
168  end
169  for i = 2:3:Length_XZ
170      S15z(i,1:NumElements) = S15dataXZ(i,1:NumElements); % Sets y values
171  end
172  for i = 2:3:Length_XY
173      S15AxFmn(i,1:NumElementsForce) = S15dataAxFmn(i,1:NumElementsForce);
             % Sets y values
174  end
175  for i = 2:3:Length_XZ
176      S15AxFmx(i,1:NumElementsForce) = S15dataAxFmx(i,1:NumElementsForce);
             % Sets y values
177  end
178
179  for i = 2:3:Length_XY
180      S15yz(i,1:NumElements) = S15dataXYz(i,1:NumElements); % Sets y values
181  end
182  for i = 2:3:Length_XZ
183      S15zz(i,1:NumElements) = S15dataXZz(i,1:NumElements); % Sets y values
184  end
185
186  % X
187  for i = 2:3:Length_XZ
188      S15Xmx(i,1:NumNodes_tube) = S15dataXmx(i,1:NumNodes_tube); % Sets y
             values
189  end
190  for i = 2:3:Length_XZ
191      S15Xmn(i,1:NumNodes_tube) = S15dataXmn(i,1:NumNodes_tube); % Sets y
             values
192  end
193
194  % Y
195  for i = 2:3:Length_XZ
196      S15Ymx(i,1:NumNodes_tube) = S15dataYmx(i,1:NumNodes_tube); % Sets y
             values
197  end
198  for i = 2:3:Length_XZ
199      S15Ymn(i,1:NumNodes_tube) = S15dataYmn(i,1:NumNodes_tube); % Sets y
             values
200  end
201  % Z
202  for i = 2:3:Length_XZ
203      S15Zmx(i,1:NumNodes_tube) = S15dataZmx(i,1:NumNodes_tube); % Sets y
             values
204  end
205  for i = 2:3:Length_XZ
206      S15Zmn(i,1:NumNodes_tube) = S15dataZmn(i,1:NumNodes_tube); % Sets y
             values
207  end
208
209  y(1,:) = []; % Deletes first row
210  z(1,:) = []; % Deletes first row
211  yz(1,:) = []; % Deletes first row
```

```matlab
212  zz(1,:) = []; % Deletes first row
213  AxFmn(1,:) = []; % Deletes first row
214  AxFmx(1,:) = []; % Deletes first row
215  Xmx(1,:) = []; % Deletes first row
216  Xmn(1,:) = []; % Deletes first row
217  Ymx(1,:) = []; % Deletes first row
218  Ymn(1,:) = []; % Deletes first row
219  Zmx(1,:) = []; % Deletes first row
220  Zmn(1,:) = []; % Deletes first row
221
222  S14y(1,:) = []; % Deletes first row
223  S14z(1,:) = []; % Deletes first row
224  S14yz(1,:) = []; % Deletes first row
225  S14zz(1,:) = []; % Deletes first row
226  S14AxFmn(1,:) = []; % Deletes first row
227  S14AxFmx(1,:) = []; % Deletes first row
228  S14Xmx(1,:) = []; % Deletes first row
229  S14Xmn(1,:) = []; % Deletes first row
230  S14Ymx(1,:) = []; % Deletes first row
231  S14Ymn(1,:) = []; % Deletes first row
232  S14Zmx(1,:) = []; % Deletes first row
233  S14Zmn(1,:) = []; % Deletes first row
234
235  S15y(1,:) = []; % Deletes first row
236  S15z(1,:) = []; % Deletes first row
237  S15yz(1,:) = []; % Deletes first row
238  S15zz(1,:) = []; % Deletes first row
239  S15AxFmn(1,:) = []; % Deletes first row
240  S15AxFmx(1,:) = []; % Deletes first row
241  S15Xmx(1,:) = []; % Deletes first row
242  S15Xmn(1,:) = []; % Deletes first row
243  S15Ymx(1,:) = []; % Deletes first row
244  S15Ymn(1,:) = []; % Deletes first row
245  S15Zmx(1,:) = []; % Deletes first row
246  S15Zmn(1,:) = []; % Deletes first row
247
248  x1 = zeros((Length_XY + 1)/NumRepeatX,4);
249  for i = 1:NumRepeatX:Length_XY + 1
250      for j = 1:NumElements
251      x1((i+2)/3,j) = x(i,j); % Makes new matrix without rows not needed
252      end
253  end
254  y1 = zeros((Length_XY + 1)/NumRepeatY,4);
255  for i = 1:NumRepeatY:Length_XY + 1
256      for j = 1:NumElements
257      y1((i+2)/3,j) = y(i,j); % Makes new matrix without rows not needed
258      end
259  end
260  z1 = zeros((Length_XZ + 1)/NumRepeatZ,4);
261  for i = 1:NumRepeatZ:Length_XZ + 1
262      for j = 1:NumElements
263      z1((i+2)/3,j) = z(i,j); % Makes new matrix without rows not needed
264      end
265  end
266  y1z = zeros((Length_XY + 1)/NumRepeatY,4);
267  for i = 1:NumRepeatY:Length_XY + 1
268      for j = 1:NumElements
```

```matlab
269        y1z((i+2)/3,j) = yz(i,j); % Makes new matrix without rows not needed
270        end
271  end
272  z1z = zeros((Length_XZ + 1)/NumRepeatZ,4);
273  for i = 1:NumRepeatZ:Length_XZ + 1
274        for j = 1:NumElements
275        z1z((i+2)/3,j) = zz(i,j); % Makes new matrix without rows not needed
276        end
277  end
278  AxFmx1 = zeros((Length_XY + 1)/NumRepeatY,4);
279  for i = 1:NumRepeatY:Length_XY + 1
280        for j = 1:NumElementsForce
281        AxFmx1((i+2)/3,j) = AxFmx(i,j); % Makes new matrix without rows not
                needed
282        end
283  end
284  AxFmn1 = zeros((Length_XZ + 1)/NumRepeatZ,4);
285  for i = 1:NumRepeatZ:Length_XZ + 1
286        for j = 1:NumElementsForce
287        AxFmn1((i+2)/3,j) = AxFmn(i,j); % Makes new matrix without rows not
                needed
288        end
289  end
290  Fcoord1 = zeros((Length_XZ + 1)/NumRepeatZ,4);
291  for i = 1:NumRepeatZ:Length_XZ + 1
292        for j = 1:NumElementsForce
293        Fcoord1((i+2)/3,j) = Fcoord(i,j); % Makes new matrix without rows not
                needed
294        end
295  end
296
297  % X
298  Xmx1 = zeros((Length_XZ + 1)/NumRepeatZ,4);
299  for i = 1:NumRepeatZ:Length_XZ + 1
300        for j = 1:NumNodes_tube
301        Xmx1((i+2)/3,j) = Xmx(i,j); % Makes new matrix without rows not
                needed
302        end
303  end
304  Xmn1 = zeros((Length_XZ + 1)/NumRepeatZ,4);
305  for i = 1:NumRepeatZ:Length_XZ + 1
306        for j = 1:NumNodes_tube
307        Xmn1((i+2)/3,j) = Xmn(i,j); % Makes new matrix without rows not
                needed
308        end
309  end
310  % COORD DISPL
311  X11 = zeros((Length_XZ + 1)/NumRepeatZ,4);
312  for i = 1:NumRepeatZ:Length_XZ + 1
313        for j = 1:NumNodes_tube
314        X11((i+2)/3,j) = coord_xdispl(i,j); % Makes new matrix without rows
                not needed
315        end
316  end
317  % Y
318  Ymx1 = zeros((Length_XZ + 1)/NumRepeatZ,4);
319  for i = 1:NumRepeatZ:Length_XZ + 1
```

```matlab
320        for j = 1:NumNodes_tube
321            Ymx1((i+2)/3,j) = Ymx(i,j); % Makes new matrix without rows not
                   needed
322        end
323    end
324    Ymn1 = zeros((Length_XZ + 1)/NumRepeatZ,4);
325    for i = 1:NumRepeatZ:Length_XZ + 1
326        for j = 1:NumNodes_tube
327            Ymn1((i+2)/3,j) = Ymn(i,j); % Makes new matrix without rows not
                   needed
328        end
329    end
330    % Z
331    Zmx1 = zeros((Length_XZ + 1)/NumRepeatZ,4);
332    for i = 1:NumRepeatZ:Length_XZ + 1
333        for j = 1:NumNodes_tube
334            Zmx1((i+2)/3,j) = Zmx(i,j); % Makes new matrix without rows not
                   needed
335        end
336    end
337    Zmn1 = zeros((Length_XZ + 1)/NumRepeatZ,4);
338    for i = 1:NumRepeatZ:Length_XZ + 1
339        for j = 1:NumNodes_tube
340            Zmn1((i+2)/3,j) = Zmn(i,j); % Makes new matrix without rows not
                   needed
341        end
342    end
343
344    % SWELL
345    S14y1 = zeros((Length_XY + 1)/NumRepeatY,4);
346    for i = 1:NumRepeatY:Length_XY + 1
347        for j = 1:NumElements
348            S14y1((i+2)/3,j) = S14y(i,j); % Makes new matrix without rows not
                   needed
349        end
350    end
351    S14z1 = zeros((Length_XZ + 1)/NumRepeatZ,4);
352    for i = 1:NumRepeatZ:Length_XZ + 1
353        for j = 1:NumElements
354            S14z1((i+2)/3,j) = S14z(i,j); % Makes new matrix without rows not
                   needed
355        end
356    end
357    S14y1z = zeros((Length_XY + 1)/NumRepeatY,4);
358    for i = 1:NumRepeatY:Length_XY + 1
359        for j = 1:NumElements
360            S14y1z((i+2)/3,j) = S14yz(i,j); % Makes new matrix without rows not
                   needed
361        end
362    end
363    S14z1z = zeros((Length_XZ + 1)/NumRepeatZ,4);
364    for i = 1:NumRepeatZ:Length_XZ + 1
365        for j = 1:NumElements
366            S14z1z((i+2)/3,j) = S14zz(i,j); % Makes new matrix without rows not
                   needed
367        end
368    end
```

```matlab
369  S14AxFmx1 = zeros((Length_XY + 1)/NumRepeatY,4);
370  for i = 1:NumRepeatY:Length_XY + 1
371      for j = 1:NumElementsForce
372      S14AxFmx1((i+2)/3,j) = S14AxFmx(i,j); % Makes new matrix without rows
             not needed
373      end
374  end
375  S14AxFmn1 = zeros((Length_XZ + 1)/NumRepeatZ,4);
376  for i = 1:NumRepeatZ:Length_XZ + 1
377      for j = 1:NumElementsForce
378      S14AxFmn1((i+2)/3,j) = S14AxFmn(i,j); % Makes new matrix without rows
             not needed
379      end
380  end
381
382  % X
383  S14Xmx1 = zeros((Length_XZ + 1)/NumRepeatZ,4);
384  for i = 1:NumRepeatZ:Length_XZ + 1
385      for j = 1:NumNodes_tube
386      S14Xmx1((i+2)/3,j) = S14Xmx(i,j); % Makes new matrix without rows not
             needed
387      end
388  end
389  S14Xmn1 = zeros((Length_XZ + 1)/NumRepeatZ,4);
390  for i = 1:NumRepeatZ:Length_XZ + 1
391      for j = 1:NumNodes_tube
392      S14Xmn1((i+2)/3,j) = S14Xmn(i,j); % Makes new matrix without rows not
             needed
393      end
394  end
395
396  % Y
397  S14Ymx1 = zeros((Length_XZ + 1)/NumRepeatZ,4);
398  for i = 1:NumRepeatZ:Length_XZ + 1
399      for j = 1:NumNodes_tube
400      S14Ymx1((i+2)/3,j) = S14Ymx(i,j); % Makes new matrix without rows not
             needed
401      end
402  end
403  S14Ymn1 = zeros((Length_XZ + 1)/NumRepeatZ,4);
404  for i = 1:NumRepeatZ:Length_XZ + 1
405      for j = 1:NumNodes_tube
406      S14Ymn1((i+2)/3,j) = S14Ymn(i,j); % Makes new matrix without rows not
             needed
407      end
408  end
409  % Z
410  S14Zmx1 = zeros((Length_XZ + 1)/NumRepeatZ,4);
411  for i = 1:NumRepeatZ:Length_XZ + 1
412      for j = 1:NumNodes_tube
413      S14Zmx1((i+2)/3,j) = S14Zmx(i,j); % Makes new matrix without rows not
             needed
414      end
415  end
416  S14Zmn1 = zeros((Length_XZ + 1)/NumRepeatZ,4);
417  for i = 1:NumRepeatZ:Length_XZ + 1
418      for j = 1:NumNodes_tube
```

```matlab
419        S14Zmn1((i+2)/3,j) = S14Zmn(i,j); % Makes new matrix without rows not
                needed
420        end
421   end
422
423
424   % Tp = 15 Swell
425   S15y1 = zeros((Length_XY + 1)/NumRepeatY,4);
426   for i = 1:NumRepeatY:Length_XY + 1
427        for j = 1:NumElements
428        S15y1((i+2)/3,j) = S15y(i,j); % Makes new matrix without rows not
                needed
429        end
430   end
431   S15z1 = zeros((Length_XZ + 1)/NumRepeatZ,4);
432   for i = 1:NumRepeatZ:Length_XZ + 1
433        for j = 1:NumElements
434        S15z1((i+2)/3,j) = S15z(i,j); % Makes new matrix without rows not
                needed
435        end
436   end
437   S15y1z = zeros((Length_XY + 1)/NumRepeatY,4);
438   for i = 1:NumRepeatY:Length_XY + 1
439        for j = 1:NumElements
440        S15y1z((i+2)/3,j) = S15yz(i,j); % Makes new matrix without rows not
                needed
441        end
442   end
443   S15z1z = zeros((Length_XZ + 1)/NumRepeatZ,4);
444   for i = 1:NumRepeatZ:Length_XZ + 1
445        for j = 1:NumElements
446        S15z1z((i+2)/3,j) = S15zz(i,j); % Makes new matrix without rows not
                needed
447        end
448   end
449   S15AxFmx1 = zeros((Length_XY + 1)/NumRepeatY,4);
450   for i = 1:NumRepeatY:Length_XY + 1
451        for j = 1:NumElementsForce
452        S15AxFmx1((i+2)/3,j) = S15AxFmx(i,j); % Makes new matrix without rows
                not needed
453        end
454   end
455   S15AxFmn1 = zeros((Length_XZ + 1)/NumRepeatZ,4);
456   for i = 1:NumRepeatZ:Length_XZ + 1
457        for j = 1:NumElementsForce
458        S15AxFmn1((i+2)/3,j) = S15AxFmn(i,j); % Makes new matrix without rows
                not needed
459        end
460   end
461
462   % X
463   S15Xmx1 = zeros((Length_XZ + 1)/NumRepeatZ,4);
464   for i = 1:NumRepeatZ:Length_XZ + 1
465        for j = 1:NumNodes_tube
466        S15Xmx1((i+2)/3,j) = S15Xmx(i,j); % Makes new matrix without rows not
                needed
467        end
```

```matlab
468    end
469    S15Xmn1 = zeros((Length_XZ + 1)/NumRepeatZ,4);
470    for i = 1:NumRepeatZ:Length_XZ + 1
471        for j = 1:NumNodes_tube
472        S15Xmn1((i+2)/3,j) = S15Xmn(i,j); % Makes new matrix without rows not
                needed
473        end
474    end
475
476    % Y
477    S15Ymx1 = zeros((Length_XZ + 1)/NumRepeatZ,4);
478    for i = 1:NumRepeatZ:Length_XZ + 1
479        for j = 1:NumNodes_tube
480        S15Ymx1((i+2)/3,j) = S15Ymx(i,j); % Makes new matrix without rows not
                needed
481        end
482    end
483    S15Ymn1 = zeros((Length_XZ + 1)/NumRepeatZ,4);
484    for i = 1:NumRepeatZ:Length_XZ + 1
485        for j = 1:NumNodes_tube
486        S15Ymn1((i+2)/3,j) = S15Ymn(i,j); % Makes new matrix without rows not
                needed
487        end
488    end
489    % Z
490    S15Zmx1 = zeros((Length_XZ + 1)/NumRepeatZ,4);
491    for i = 1:NumRepeatZ:Length_XZ + 1
492        for j = 1:NumNodes_tube
493        S15Zmx1((i+2)/3,j) = S15Zmx(i,j); % Makes new matrix without rows not
                needed
494        end
495    end
496    S15Zmn1 = zeros((Length_XZ + 1)/NumRepeatZ,4);
497    for i = 1:NumRepeatZ:Length_XZ + 1
498        for j = 1:NumNodes_tube
499        S15Zmn1((i+2)/3,j) = S15Zmn(i,j); % Makes new matrix without rows not
                needed
500        end
501    end
502
503
504
505    % Coord for moment, force
506    x1_trans = transpose(x1); % Flips matrix about diagonal
507    coord_x = reshape(x1_trans,[],1); % Makes matrix into one column for
            easily plotting
508
509    y1_trans = transpose(y1); % Flips matrix about diagonal
510    Mymin = reshape(y1_trans,[],1); % Makes matrix into one column for easily
                plotting
511    z1_trans = transpose(z1); % Flips matrix about diagonal
512    Mymax = reshape(z1_trans,[],1); % Makes matrix into one column for easily
                plotting
513
514    y1_transz = transpose(y1z); % Flips matrix about diagonal
515    Mzmin = reshape(y1_transz,[],1); % Makes matrix into one column for
            easily plotting
```

```matlab
516  z1_trans = transpose(z1z); % Flips matrix about diagonal
517  Mzmax = reshape(z1_trans,[],1); % Makes matrix into one column for easily
         plotting
518
519  Axfmx1_transz = transpose(AxFmx1); % Flips matrix about diagonal
520  Axmax = reshape(Axfmx1_transz,[],1); % Makes matrix into one column for
         easily plotting
521  Axfmn1_transz = transpose(AxFmn1); % Flips matrix about diagonal
522  Axmin = reshape(Axfmn1_transz,[],1); % Makes matrix into one column for
         easily plotting
523  % COORD force
524  Fcoord_trans = transpose(Fcoord1); % Flips matrix about diagonal
525  Fcoord_x = reshape(Fcoord_trans,[],1); % Makes matrix into one column for
         easily plotting
526
527
528  % COORD for DISPL
529  Xdispl_trans = transpose(X11); % Flips matrix about diagonal
530  coord_xdispl1 = reshape(Xdispl_trans,[],1); % Makes matrix into one
         column for easily plotting
531
532  Xmx_trans = transpose(Xmx1); % Flips matrix about diagonal
533  Xmax = reshape(Xmx_trans,[],1); % Makes matrix into one column for easily
         plotting
534  Xmn_trans = transpose(Xmn1); % Flips matrix about diagonal
535  Xmin = reshape(Xmn_trans,[],1); % Makes matrix into one column for easily
         plotting
536  Ymx_trans = transpose(Ymx1); % Flips matrix about diagonal
537  Ymax = reshape(Ymx_trans,[],1); % Makes matrix into one column for easily
         plotting
538  Ymn_trans = transpose(Ymn1); % Flips matrix about diagonal
539  Ymin = reshape(Ymn_trans,[],1); % Makes matrix into one column for easily
         plotting
540  Zmx_trans = transpose(Zmx1); % Flips matrix about diagonal
541  Zmax = reshape(Zmx_trans,[],1); % Makes matrix into one column for easily
         plotting
542  Zmn_trans = transpose(Zmn1); % Flips matrix about diagonal
543  Zmin = reshape(Zmn_trans,[],1); % Makes matrix into one column for easily
         plotting
544
545
546  % SWELL
547  S14y1_trans = transpose(S14y1); % Flips matrix about diagonal
548  S14Mymin = reshape(S14y1_trans,[],1); % Makes matrix into one column for
         easily plotting
549  S14z1_trans = transpose(S14z1); % Flips matrix about diagonal
550  S14Mymax = reshape(S14z1_trans,[],1); % Makes matrix into one column for
         easily plotting
551
552  S14y1_transz = transpose(S14y1z); % Flips matrix about diagonal
553  S14Mzmin = reshape(S14y1_transz,[],1); % Makes matrix into one column for
         easily plotting
554  S14z1_transz = transpose(S14z1z); % Flips matrix about diagonal
555  S14Mzmax = reshape(S14z1_trans,[],1); % Makes matrix into one column for
         easily plotting
556
557  S14Axfmx1_transz = transpose(S14AxFmx1); % Flips matrix about diagonal
```

```matlab
558  S14Axmax = reshape(S14Axfmx1_transz,[],1); % Makes matrix into one column
         for easily plotting
559  S14Axfmn1_transz = transpose(S14AxFmn1); % Flips matrix about diagonal
560  S14Axmin = reshape(S14Axfmn1_transz,[],1); % Makes matrix into one column
         for easily plotting
561
562  S14Xmx_trans = transpose(S14Xmx1); % Flips matrix about diagonal
563  S14Xmax = reshape(S14Xmx_trans,[],1); % Makes matrix into one column for
         easily plotting
564  S14Xmn_trans = transpose(S14Xmn1); % Flips matrix about diagonal
565  S14Xmin = reshape(S14Xmn_trans,[],1); % Makes matrix into one column for
         easily plotting
566  S14Ymx_trans = transpose(S14Ymx1); % Flips matrix about diagonal
567  S14Ymax = reshape(S14Ymx_trans,[],1); % Makes matrix into one column for
         easily plotting
568  S14Ymn_trans = transpose(S14Ymn1); % Flips matrix about diagonal
569  S14Ymin = reshape(S14Ymn_trans,[],1); % Makes matrix into one column for
         easily plotting
570  S14Zmx_trans = transpose(S14Zmx1); % Flips matrix about diagonal
571  S14Zmax = reshape(S14Zmx_trans,[],1); % Makes matrix into one column for
         easily plotting
572  S14Zmn_trans = transpose(S14Zmn1); % Flips matrix about diagonal
573  S14Zmin = reshape(S14Zmn_trans,[],1); % Makes matrix into one column for
         easily plotting
574
575  % Tp = 15 Swell
576  S15y1_trans = transpose(S15y1); % Flips matrix about diagonal
577  S15Mymin = reshape(S15y1_trans,[],1); % Makes matrix into one column for
         easily plotting
578  S15z1_trans = transpose(S15z1); % Flips matrix about diagonal
579  S15Mymax = reshape(S15z1_trans,[],1); % Makes matrix into one column for
         easily plotting
580
581  S15y1_transz = transpose(S15y1z); % Flips matrix about diagonal
582  S15Mzmin = reshape(S15y1_transz,[],1); % Makes matrix into one column for
         easily plotting
583  S15z1_trans = transpose(S15z1z); % Flips matrix about diagonal
584  S15Mzmax = reshape(S15z1_trans,[],1); % Makes matrix into one column for
         easily plotting
585
586  S15Axfmx1_transz = transpose(S15AxFmx1); % Flips matrix about diagonal
587  S15Axmax = reshape(S15Axfmx1_transz,[],1); % Makes matrix into one column
         for easily plotting
588  S15Axfmn1_transz = transpose(S15AxFmn1); % Flips matrix about diagonal
589  S15Axmin = reshape(S15Axfmn1_transz,[],1); % Makes matrix into one column
         for easily plotting
590
591  S15Xmx_trans = transpose(S15Xmx1); % Flips matrix about diagonal
592  S15Xmax = reshape(S15Xmx_trans,[],1); % Makes matrix into one column for
         easily plotting
593  S15Xmn_trans = transpose(S15Xmn1); % Flips matrix about diagonal
594  S15Xmin = reshape(S15Xmn_trans,[],1); % Makes matrix into one column for
         easily plotting
595  S15Ymx_trans = transpose(S15Ymx1); % Flips matrix about diagonal
596  S15Ymax = reshape(S15Ymx_trans,[],1); % Makes matrix into one column for
         easily plotting
597  S15Ymn_trans = transpose(S15Ymn1); % Flips matrix about diagonal
```

```matlab
598  S15Ymin = reshape(S15Ymn_trans,[],1); % Makes matrix into one column for
        easily plotting
599  S15Zmx_trans = transpose(S15Zmx1); % Flips matrix about diagonal
600  S15Zmax = reshape(S15Zmx_trans,[],1); % Makes matrix into one column for
        easily plotting
601  S15Zmn_trans = transpose(S15Zmn1); % Flips matrix about diagonal
602  S15Zmin = reshape(S15Zmn_trans,[],1); % Makes matrix into one column for
        easily plotting
603
604
605  repeat = length(Mymin)/4;
606  Mymin(1:repeat,2) = Mymin(repeat+1:repeat*2,:);
607  Mymin(1:repeat,3) = Mymin(repeat*2+1:repeat*3,1);
608  Mymin(1:repeat,4) = Mymin(repeat*3+1:repeat*4,1);
609  Mymin(repeat+1:length(Mymin),:) = [];
610
611  Mymax(1:repeat,2) = Mymax(repeat+1:repeat*2,:);
612  Mymax(1:repeat,3) = Mymax(repeat*2+1:repeat*3,1);
613  Mymax(1:repeat,4) = Mymax(repeat*3+1:repeat*4,1);
614  Mymax(repeat+1:length(Mymax),:) = [];
615
616  repeatForce = length(Axmin)/4
617  Axmin(1:repeatForce,2) = Axmin(repeatForce+1:repeatForce*2,:);
618  Axmin(1:repeatForce,3) = Axmin(repeatForce*2+1:repeatForce*3,1);
619  Axmin(1:repeatForce,4) = Axmin(repeatForce*3+1:repeatForce*4,1);
620  Axmin(repeatForce+1:length(Axmin),:) = [];
621
622  Axmax(1:repeatForce,2) = Axmax(repeatForce+1:repeatForce*2,:);
623  Axmax(1:repeatForce,3) = Axmax(repeatForce*2+1:repeatForce*3,1);
624  Axmax(1:repeatForce,4) = Axmax(repeatForce*3+1:repeatForce*4,1);
625  Axmax(repeatForce+1:length(Axmax),:) = [];
626
627  Mzmin(1:repeat,2) = Mzmin(repeat+1:repeat*2,:);
628  Mzmin(1:repeat,3) = Mzmin(repeat*2+1:repeat*3,1);
629  Mzmin(1:repeat,4) = Mzmin(repeat*3+1:repeat*4,1);
630  Mzmin(repeat+1:length(Mzmin),:) = [];
631
632  Mzmax(1:repeat,2) = Mzmax(repeat+1:repeat*2,:);
633  Mzmax(1:repeat,3) = Mzmax(repeat*2+1:repeat*3,1);
634  Mzmax(1:repeat,4) = Mzmax(repeat*3+1:repeat*4,1);
635  Mzmax(repeat+1:length(Mzmax),:) = [];
636
637  repeatdispl = length(Xmax)/4;
638  Xmax(1:repeatdispl,2) = Xmax(repeatdispl+1:repeatdispl*2,:);
639  Xmax(1:repeatdispl,3) = Xmax(repeatdispl*2+1:repeatdispl*3,1);
640  Xmax(1:repeatdispl,4) = Xmax(repeatdispl*3+1:repeatdispl*4,1);
641  Xmax(repeatdispl+1:length(Xmax),:) = [];
642  Xmin(1:repeatdispl,2) = Xmin(repeatdispl+1:repeatdispl*2,:);
643  Xmin(1:repeatdispl,3) = Xmin(repeatdispl*2+1:repeatdispl*3,1);
644  Xmin(1:repeatdispl,4) = Xmin(repeatdispl*3+1:repeatdispl*4,1);
645  Xmin(repeatdispl+1:length(Xmin),:) = [];
646
647  Ymax(1:repeatdispl,2) = Ymax(repeatdispl+1:repeatdispl*2,:);
648  Ymax(1:repeatdispl,3) = Ymax(repeatdispl*2+1:repeatdispl*3,1);
649  Ymax(1:repeatdispl,4) = Ymax(repeatdispl*3+1:repeatdispl*4,1);
650  Ymax(repeatdispl+1:length(Ymax),:) = [];
651  Ymin(1:repeatdispl,2) = Ymin(repeatdispl+1:repeatdispl*2,:);
```

```matlab
652  Ymin(1:repeatdispl,3) = Ymin(repeatdispl*2+1:repeatdispl*3,1);
653  Ymin(1:repeatdispl,4) = Ymin(repeatdispl*3+1:repeatdispl*4,1);
654  Ymin(repeatdispl+1:length(Ymin),:) = [];
655
656  Zmax(1:repeatdispl,2) = Zmax(repeatdispl+1:repeatdispl*2,:);
657  Zmax(1:repeatdispl,3) = Zmax(repeatdispl*2+1:repeatdispl*3,1);
658  Zmax(1:repeatdispl,4) = Zmax(repeatdispl*3+1:repeatdispl*4,1);
659  Zmax(repeatdispl+1:length(Zmax),:) = [];
660
661  Zmin(1:repeatdispl,2) = Zmin(repeatdispl+1:repeatdispl*2,:);
662  Zmin(1:repeatdispl,3) = Zmin(repeatdispl*2+1:repeatdispl*3,1);
663  Zmin(1:repeatdispl,4) = Zmin(repeatdispl*3+1:repeatdispl*4,1);
664  Zmin(repeatdispl+1:length(Zmin),:) = [];
665
666
667  % SWELL
668  S14Mymin(1:repeat,2) = S14Mymin(repeat+1:repeat*2,:);
669  S14Mymin(1:repeat,3) = S14Mymin(repeat*2+1:repeat*3,1);
670  S14Mymin(1:repeat,4) = S14Mymin(repeat*3+1:repeat*4,1);
671  S14Mymin(repeat+1:length(S14Mymin),:) = [];
672
673  S14Mymax(1:repeat,2) = S14Mymax(repeat+1:repeat*2,:);
674  S14Mymax(1:repeat,3) = S14Mymax(repeat*2+1:repeat*3,1);
675  S14Mymax(1:repeat,4) = S14Mymax(repeat*3+1:repeat*4,1);
676  S14Mymax(repeat+1:length(S14Mymax),:) = [];
677
678  S14Axmin(1:repeatForce,2) = S14Axmin(repeatForce+1:repeatForce*2,:);
679  S14Axmin(1:repeatForce,3) = S14Axmin(repeatForce*2+1:repeatForce*3,1);
680  S14Axmin(1:repeatForce,4) = S14Axmin(repeatForce*3+1:repeatForce*4,1);
681  S14Axmin(repeatForce+1:length(S14Axmin),:) = [];
682
683  S14Axmax(1:repeatForce,2) = S14Axmax(repeatForce+1:repeatForce*2,:);
684  S14Axmax(1:repeatForce,3) = S14Axmax(repeatForce*2+1:repeatForce*3,1);
685  S14Axmax(1:repeatForce,4) = S14Axmax(repeatForce*3+1:repeatForce*4,1);
686  S14Axmax(repeatForce+1:length(S14Axmax),:) = [];
687
688  S14Mzmin(1:repeat,2) = S14Mzmin(repeat+1:repeat*2,:);
689  S14Mzmin(1:repeat,3) = S14Mzmin(repeat*2+1:repeat*3,1);
690  S14Mzmin(1:repeat,4) = S14Mzmin(repeat*3+1:repeat*4,1);
691  S14Mzmin(repeat+1:length(S14Mzmin),:) = [];
692
693  S14Mzmax(1:repeat,2) = S14Mzmax(repeat+1:repeat*2,:);
694  S14Mzmax(1:repeat,3) = S14Mzmax(repeat*2+1:repeat*3,1);
695  S14Mzmax(1:repeat,4) = S14Mzmax(repeat*3+1:repeat*4,1);
696  S14Mzmax(repeat+1:length(S14Mzmax),:) = [];
697
698
699  S14Xmax(1:repeatdispl,2) = S14Xmax(repeatdispl+1:repeatdispl*2,:);
700  S14Xmax(1:repeatdispl,3) = S14Xmax(repeatdispl*2+1:repeatdispl*3,1);
701  S14Xmax(1:repeatdispl,4) = S14Xmax(repeatdispl*3+1:repeatdispl*4,1);
702  S14Xmax(repeatdispl+1:length(S14Xmax),:) = [];
703  S14Xmin(1:repeatdispl,2) = S14Xmin(repeatdispl+1:repeatdispl*2,:);
704  S14Xmin(1:repeatdispl,3) = S14Xmin(repeatdispl*2+1:repeatdispl*3,1);
705  S14Xmin(1:repeatdispl,4) = S14Xmin(repeatdispl*3+1:repeatdispl*4,1);
706  S14Xmin(repeatdispl+1:length(S14Xmin),:) = [];
707
708  S14Ymax(1:repeatdispl,2) = S14Ymax(repeatdispl+1:repeatdispl*2,:);
```

```
709  S14Ymax(1:repeatdispl,3) = S14Ymax(repeatdispl*2+1:repeatdispl*3,1);
710  S14Ymax(1:repeatdispl,4) = S14Ymax(repeatdispl*3+1:repeatdispl*4,1);
711  S14Ymax(repeatdispl+1:length(S14Ymax),:) = [];
712  S14Ymin(1:repeatdispl,2) = S14Ymin(repeatdispl+1:repeatdispl*2,:);
713  S14Ymin(1:repeatdispl,3) = S14Ymin(repeatdispl*2+1:repeatdispl*3,1);
714  S14Ymin(1:repeatdispl,4) = S14Ymin(repeatdispl*3+1:repeatdispl*4,1);
715  S14Ymin(repeatdispl+1:length(S14Ymin),:) = [];
716
717  S14Zmax(1:repeatdispl,2) = S14Zmax(repeatdispl+1:repeatdispl*2,:);
718  S14Zmax(1:repeatdispl,3) = S14Zmax(repeatdispl*2+1:repeatdispl*3,1);
719  S14Zmax(1:repeatdispl,4) = S14Zmax(repeatdispl*3+1:repeatdispl*4,1);
720  S14Zmax(repeatdispl+1:length(S14Zmax),:) = [];
721
722  S14Zmin(1:repeatdispl,2) = S14Zmin(repeatdispl+1:repeatdispl*2,:);
723  S14Zmin(1:repeatdispl,3) = S14Zmin(repeatdispl*2+1:repeatdispl*3,1);
724  S14Zmin(1:repeatdispl,4) = S14Zmin(repeatdispl*3+1:repeatdispl*4,1);
725  S14Zmin(repeatdispl+1:length(S14Zmin),:) = [];
726
727  % Tp = 15 Swell
728  S15Mymin(1:repeat,2) = S15Mymin(repeat+1:repeat*2,:);
729  S15Mymin(1:repeat,3) = S15Mymin(repeat*2+1:repeat*3,1);
730  S15Mymin(1:repeat,4) = S15Mymin(repeat*3+1:repeat*4,1);
731  S15Mymin(repeat+1:length(S15Mymin),:) = [];
732
733  S15Mymax(1:repeat,2) = S15Mymax(repeat+1:repeat*2,:);
734  S15Mymax(1:repeat,3) = S15Mymax(repeat*2+1:repeat*3,1);
735  S15Mymax(1:repeat,4) = S15Mymax(repeat*3+1:repeat*4,1);
736  S15Mymax(repeat+1:length(S15Mymax),:) = [];
737
738  S15Axmin(1:repeatForce,2) = S15Axmin(repeatForce+1:repeatForce*2,:);
739  S15Axmin(1:repeatForce,3) = S15Axmin(repeatForce*2+1:repeatForce*3,1);
740  S15Axmin(1:repeatForce,4) = S15Axmin(repeatForce*3+1:repeatForce*4,1);
741  S15Axmin(repeatForce+1:length(S15Axmin),:) = [];
742
743  S15Axmax(1:repeatForce,2) = S15Axmax(repeatForce+1:repeatForce*2,:);
744  S15Axmax(1:repeatForce,3) = S15Axmax(repeatForce*2+1:repeatForce*3,1);
745  S15Axmax(1:repeatForce,4) = S15Axmax(repeatForce*3+1:repeatForce*4,1);
746  S15Axmax(repeatForce+1:length(S15Axmax),:) = [];
747
748  S15Mzmin(1:repeat,2) = S15Mzmin(repeat+1:repeat*2,:);
749  S15Mzmin(1:repeat,3) = S15Mzmin(repeat*2+1:repeat*3,1);
750  S15Mzmin(1:repeat,4) = S15Mzmin(repeat*3+1:repeat*4,1);
751  S15Mzmin(repeat+1:length(S15Mzmin),:) = [];
752
753  S15Mzmax(1:repeat,2) = S15Mzmax(repeat+1:repeat*2,:);
754  S15Mzmax(1:repeat,3) = S15Mzmax(repeat*2+1:repeat*3,1);
755  S15Mzmax(1:repeat,4) = S15Mzmax(repeat*3+1:repeat*4,1);
756  S15Mzmax(repeat+1:length(S15Mzmax),:) = [];
757
758
759  S15Xmax(1:repeatdispl,2) = S15Xmax(repeatdispl+1:repeatdispl*2,:);
760  S15Xmax(1:repeatdispl,3) = S15Xmax(repeatdispl*2+1:repeatdispl*3,1);
761  S15Xmax(1:repeatdispl,4) = S15Xmax(repeatdispl*3+1:repeatdispl*4,1);
762  S15Xmax(repeatdispl+1:length(S15Xmax),:) = [];
763  S15Xmin(1:repeatdispl,2) = S15Xmin(repeatdispl+1:repeatdispl*2,:);
764  S15Xmin(1:repeatdispl,3) = S15Xmin(repeatdispl*2+1:repeatdispl*3,1);
765  S15Xmin(1:repeatdispl,4) = S15Xmin(repeatdispl*3+1:repeatdispl*4,1);
```

```matlab
766  S15Xmin( repeatdispl+1:length (S15Xmin) ,:) = [];
767
768  S15Ymax(1:repeatdispl ,2) = S15Ymax( repeatdispl+1:repeatdispl *2 ,:);
769  S15Ymax(1:repeatdispl ,3) = S15Ymax( repeatdispl*2+1:repeatdispl *3 ,1);
770  S15Ymax(1:repeatdispl ,4) = S15Ymax( repeatdispl*3+1:repeatdispl *4 ,1);
771  S15Ymax( repeatdispl+1:length (S15Ymax) ,:) = [];
772  S15Ymin(1:repeatdispl ,2) = S15Ymin( repeatdispl+1:repeatdispl *2 ,:);
773  S15Ymin(1:repeatdispl ,3) = S15Ymin( repeatdispl*2+1:repeatdispl *3 ,1);
774  S15Ymin(1:repeatdispl ,4) = S15Ymin( repeatdispl*3+1:repeatdispl *4 ,1);
775  S15Ymin( repeatdispl+1:length (S15Ymin) ,:) = [];
776
777  S15Zmax(1:repeatdispl ,2) = S15Zmax( repeatdispl+1:repeatdispl *2 ,:);
778  S15Zmax(1:repeatdispl ,3) = S15Zmax( repeatdispl*2+1:repeatdispl *3 ,1);
779  S15Zmax(1:repeatdispl ,4) = S15Zmax( repeatdispl*3+1:repeatdispl *4 ,1);
780  S15Zmax( repeatdispl+1:length (S15Zmax) ,:) = [];
781
782  S15Zmin(1:repeatdispl ,2) = S15Zmin( repeatdispl+1:repeatdispl *2 ,:);
783  S15Zmin(1:repeatdispl ,3) = S15Zmin( repeatdispl*2+1:repeatdispl *3 ,1);
784  S15Zmin(1:repeatdispl ,4) = S15Zmin( repeatdispl*3+1:repeatdispl *4 ,1);
785  S15Zmin( repeatdispl+1:length (S15Zmin) ,:) = [];
786
787
788  for i = 1:repeat
789      MyMIN(i ,1) = min(Mymin(i ,:));
790  end
791  for i = 1:repeat
792      MyMAX(i ,1) = max(Mymax(i ,:));
793  end
794  for i = 1:repeat
795      MzMIN(i ,1) = min(Mzmin(i ,:));
796  end
797  for i = 1:repeat
798      MzMAX(i ,1) = max(Mzmax(i ,:));
799  end
800  for i = 1:repeatForce
801      AxMAX(i ,1) = max(Axmax(i ,:));
802  end
803  for i = 1:repeatForce
804      AxMIN(i ,1) = min(Axmin(i ,:));
805  end
806
807  for i = 1:repeatdispl
808      XMIN(i ,1) = min(Xmin(i ,:));
809  end
810  for i = 1:repeatdispl
811      XMAX(i ,1) = max(Xmax(i ,:));
812  end
813
814  for i = 1:repeatdispl
815      YMIN(i ,1) = min(Ymin(i ,:));
816  end
817  for i = 1:repeatdispl
818      YMAX(i ,1) = max(Ymax(i ,:));
819  end
820  for i = 1:repeatdispl
821      ZMIN(i ,1) = min(Zmin(i ,:));
822  end
```

```matlab
823  for i = 1:repeatdispl
824      ZMAX(i,1) = max(Zmax(i,:));
825  end
826
827  % SWELL
828  for i = 1:repeat
829      S14MyMIN(i,1) = min(S14Mymin(i,:));
830  end
831  for i = 1:repeat
832      S15MyMIN(i,1) = min(S15Mymin(i,:));
833  end
834  for i = 1:repeat
835      SMyMIN(i,1) = min(S15MyMIN(i,1),S14MyMIN(i,1));
836  end
837
838  for i = 1:repeat
839      S14MyMAX(i,1) = max(S14Mymax(i,:));
840  end
841  for i = 1:repeat
842      S14MzMIN(i,1) = min(S14Mzmin(i,:));
843  end
844  for i = 1:repeat
845      S14MzMAX(i,1) = max(S14Mzmax(i,:));
846  end
847  for i = 1:repeatForce
848      S14AxMAX(i,1) = max(S14Axmax(i,:));
849  end
850  for i = 1:repeatForce
851      S14AxMIN(i,1) = min(S14Axmin(i,:));
852  end
853
854  for i = 1:repeatdispl
855      S14XMIN(i,1) = min(S14Xmin(i,:));
856  end
857  for i = 1:repeatdispl
858      S14XMAX(i,1) = max(S14Xmax(i,:));
859  end
860
861  for i = 1:repeatdispl
862      S14YMIN(i,1) = min(S14Ymin(i,:));
863  end
864  for i = 1:repeatdispl
865      S14YMAX(i,1) = max(S14Ymax(i,:));
866  end
867  for i = 1:repeatdispl
868      S14ZMIN(i,1) = min(S14Zmin(i,:));
869  end
870  for i = 1:repeatdispl
871      S14ZMAX(i,1) = max(S14Zmax(i,:));
872  end
873
874  % Tp = 15
875  for i = 1:repeat
876      S15MyMAX(i,1) = max(S15Mymax(i,:));
877  end
878  for i = 1:repeat
879      S15MzMIN(i,1) = min(S15Mzmin(i,:));
```

```matlab
880  end
881  for i = 1:repeat
882      S15MzMAX(i,1) = max(S15Mzmax(i,:));
883  end
884  for i = 1:repeatForce
885      S15AxMAX(i,1) = max(S15Axmax(i,:));
886  end
887  for i = 1:repeatForce
888      S15AxMIN(i,1) = min(S15Axmin(i,:));
889  end
890
891  for i = 1:repeatdispl
892      S15XMIN(i,1) = min(S15Xmin(i,:));
893  end
894  for i = 1:repeatdispl
895      S15XMAX(i,1) = max(S15Xmax(i,:));
896  end
897
898  for i = 1:repeatdispl
899      S15YMIN(i,1) = min(S15Ymin(i,:));
900  end
901  for i = 1:repeatdispl
902      S15YMAX(i,1) = max(S15Ymax(i,:));
903  end
904  for i = 1:repeatdispl
905      S15ZMIN(i,1) = min(S15Zmin(i,:));
906  end
907  for i = 1:repeatdispl
908      S15ZMAX(i,1) = max(S15Zmax(i,:));
909  end
910
911  for i = 1:repeat
912      SMyMAX(i,1) = max(S15MyMAX(i,1),S14MyMAX(i,1));
913  end
914  for i = 1:repeat
915      SMzMAX(i,1) = max(S15MzMAX(i,1),S14MzMAX(i,1));
916  end
917  for i = 1:repeat
918      SMzMIN(i,1) = min(S15MzMIN(i,1),S14MzMIN(i,1));
919  end
920  for i = 1:repeatForce
921      SAxMAX(i,1) = max(S15AxMAX(i,1),S14AxMAX(i,1));
922  end
923  for i = 1:repeatForce
924      SAxMIN(i,1) = min(S15AxMIN(i,1),S14AxMIN(i,1));
925  end
926
927  for i = 1:repeatdispl
928      SXMAX(i,1) = max(S15XMAX(i,1),S14XMAX(i,1));
929  end
930  for i = 1:repeatdispl
931      SXMIN(i,1) = min(S15XMIN(i,1),S14XMIN(i,1));
932  end
933  for i = 1:repeatdispl
934      SYMAX(i,1) = max(S15YMAX(i,1),S14YMAX(i,1));
935  end
936  for i = 1:repeatdispl
```

```matlab
937       SYMIN( i ,1 )  =  min(S15YMIN( i ,1 ) ,S14YMIN( i ,1 ) ) ;
938  end
939  for  i  =  1: repeatdispl
940       SZMAX( i ,1 )  =  max(S15ZMAX( i ,1 ) ,S14ZMAX( i ,1 ) ) ;
941  end
942  for  i  =  1: repeatdispl
943       SZMIN( i ,1 )  =  min(S15ZMIN( i ,1 ) ,S14ZMIN( i ,1 ) ) ;
944  end
945
946  % Deleting NaN to obtain continuing lines in plot
947  coord_x (any( isnan ( coord_x ) , 2) , :) = [] ; % Deletes all NaN in column
948  MzMAX( any( isnan (MzMAX) , 2) , :) = [] ; % Deletes all NaN in column
949  MzMIN( any( isnan (MzMIN) , 2) , :) = [] ; % Deletes all NaN in column
950  MyMAX( any( isnan (MyMAX) , 2) , :) = [] ; % Deletes all NaN in column
951  MyMIN( any( isnan (MyMIN) , 2) , :) = [] ; % Deletes all NaN in column
952  Fcoord_x (any( isnan ( Fcoord_x ) , 2) , :) = [] ; % Deletes all NaN in column
953  AxMAX( any( isnan (AxMAX) , 2) , :) = [] ; % Deletes all NaN in column
954  AxMIN( any( isnan (AxMIN) , 2) , :) = [] ; % Deletes all NaN in column
955
956  %SWELL
957  SMzMAX( any( isnan (SMzMAX) , 2) , :) = [] ; % Deletes all NaN in column
958  SMzMIN( any( isnan (SMzMIN) , 2) , :) = [] ; % Deletes all NaN in column
959  SMyMAX( any( isnan (SMyMAX) , 2) , :) = [] ; % Deletes all NaN in column
960  SMyMIN( any( isnan (SMyMIN) , 2) , :) = [] ; % Deletes all NaN in column
961  SAxMAX( any( isnan (SAxMAX) , 2) , :) = [] ; % Deletes all NaN in column
962  SAxMIN( any( isnan (SAxMIN) , 2) , :) = [] ; % Deletes all NaN in column
963
964  a  =  length (MzMAX) ;
965  b  =  length (AxMAX) ;
966
967  % figure ()
968  % plot ( coord_x (1: a ) , MyMIN,  'Linewidth ' ,2)
969  % hold on
970  % plot ( coord_x (1: a ) , MyMAX,  'Linewidth ' ,2)
971  % title ( 'My max and min ' , 'FontSize ' ,18)
972  % xlabel ( 'Length of bridge [m] ' , 'FontSize ' ,18) ; %, 'FontWeight ' , 'bold ' , '
        Color ' , 'r ')
973  % ylabel ( 'Moment [Nm] ' , 'FontSize ' ,18) ; %, 'FontWeight ' , 'bold ' , 'Color ' , 'r ')
974  % axis ([0  max( coord_x ) min(MyMIN) max(MyMAX) ])
975  % figure ()
976  % plot ( coord_x (1: a ) , MzMIN,  'Linewidth ' ,2)
977  % hold on
978  % plot ( coord_x (1: a ) , MzMAX,  'Linewidth ' ,2)
979  % title ( 'Mz max and min ' , 'FontSize ' ,18)
980  % xlabel ( 'Length of bridge [m] ' , 'FontSize ' ,18) ; %, 'FontWeight ' , 'bold ' , '
        Color ' , 'r ')
981  % ylabel ( 'Moment [Nm] ' , 'FontSize ' ,18) ; %, 'FontWeight ' , 'bold ' , 'Color ' , 'r ')
982  % axis ([0  max( coord_x ) min(MzMIN) max(MzMAX) ])
983  % figure ()
984  % plot ( Fcoord_x (1: b ) , AxMIN,  'Linewidth ' ,2)
985  % hold on
986  % plot ( Fcoord_x (1: b ) , AxMAX,  'Linewidth ' ,2)
987  % title ( 'Axial Force max and min ' , 'FontSize ' ,18)
988  % xlabel ( 'Length of bridge [m] ' , 'FontSize ' ,18) ; %, 'FontWeight ' , 'bold ' , '
        Color ' , 'r ')
989  % ylabel ( 'Force [Nm] ' , 'FontSize ' ,18) ; %, 'FontWeight ' , 'bold ' , 'Color ' , 'r ')
990  % axis ([0  max( coord_x ) min(AxMIN) max(AxMAX) ])
```

```
991
992
993 % figure ()
994 % plot(coord_xdispl1(1:repeatdispl), XMIN, 'Linewidth',3)
995 % hold on
996 % plot(coord_xdispl1(1:repeatdispl), XMAX, 'Linewidth',3)
997 % title('X max and min')
998 % xlabel('Length of bridge [m]','FontSize',18); %,'FontWeight','bold','
          Color','r')
999 % ylabel('Axial Displacement of bridge [m]','FontSize',18); %,'FontWeight
          ','bold','Color','r')
1000 % axis([0 max(coord_xdispl1) min(XMIN) max(XMAX)])
1001 % figure ()
1002 % plot(coord_xdispl1(1:repeatdispl), YMIN, 'Linewidth',3)
1003 % hold on
1004 % plot(coord_xdispl1(1:repeatdispl), YMAX, 'Linewidth',3)
1005 % title('Y max and min')
1006 % xlabel('Length of bridge [m]','FontSize',18); %,'FontWeight','bold','
          Color','r')
1007 % ylabel('Horizontal Displacement of bridge [m]','FontSize',18); %,'
          FontWeight','bold','Color','r')
1008 % axis([0 max(coord_xdispl1) min(YMIN) max(YMAX)])
1009 % figure ()
1010 % plot(coord_xdispl1(1:repeatdispl), ZMIN, 'Linewidth',3)
1011 % hold on
1012 % plot(coord_xdispl1(1:repeatdispl), ZMAX, 'Linewidth',3)
1013 % title('Z max and min')
1014 % xlabel('Length of bridge [m]','FontSize',18); %,'FontWeight','bold','
          Color','r')
1015 % ylabel('Vertical Displacement of bridge [m]','FontSize',18); %,'
          FontWeight','bold','Color','r')
1016 % axis([0 max(coord_xdispl1) min(ZMIN) max(ZMAX)])
1017
1018
1019 %%%% SWELL %%%%
1020 figure ()
1021 plot(coord_x(1:a), SMyMIN/10^6,'b', 'Linewidth',2)
1022 hold on
1023 plot(coord_x(1:a), SMyMAX/10^6,'b', 'Linewidth',2)
1024 hold on
1025 plot(coord_x(1:a), MyMIN/10^6, 'r', 'Linewidth',2)
1026 hold on
1027 plot(coord_x(1:a), MyMAX/10^6, 'r', 'Linewidth',2)
1028 title('My max and min','FontSize',18)
1029 xlabel('Length of bridge [m]','FontSize',18); %,'FontWeight','bold','
          Color','r')
1030 ylabel('Moment [MNm]','FontSize',18); %,'FontWeight','bold','Color','r')
1031 legend('Wind sea and swell Min', 'Wind sea and swell Max', 'Wind sea Min'
          , 'Wind sea Max');
1032 set(gca,'fontsize',14)
1033 axis([0 max(coord_x) min(SMyMIN/10^6) max(SMyMAX/10^6)])
1034 figure ()
1035 plot(coord_x(1:a), SMzMIN/10^6,'b', 'Linewidth',2)
1036 hold on
1037 plot(coord_x(1:a), SMzMAX/10^6,'b', 'Linewidth',2)
1038 hold on
1039 plot(coord_x(1:a), MzMIN/10^6,'r', 'Linewidth',2)
```

```matlab
1040  hold on
1041  plot(coord_x(1:a), MzMAX/10^6,'r', 'Linewidth',2)
1042  title('Mz max and min','FontSize',18)
1043  xlabel('Length of bridge [m]','FontSize',18); %,'FontWeight','bold','
          Color','r')
1044  ylabel('Moment [MNm]','FontSize',18); %,'FontWeight','bold','Color','r')
1045  legend('Wind sea and swell Min', 'Wind sea and swell Max', 'Wind sea Min'
          , 'Wind sea Max');
1046  set(gca,'fontsize',14)
1047  axis([0 max(coord_x) min(SMzMIN/10^6) max(SMzMAX/10^6)])
1048  figure()
1049  plot(Fcoord_x(1:b), SAxMIN./10^6,'b', 'Linewidth',2)
1050  hold on
1051  plot(Fcoord_x(1:b), SAxMAX./10^6,'b', 'Linewidth',2)
1052  hold on
1053  plot(Fcoord_x(1:b), AxMIN./10^6,'r', 'Linewidth',2)
1054  hold on
1055  plot(Fcoord_x(1:b), AxMAX./10^6,'r', 'Linewidth',2)
1056  title('Axial Force max and min','FontSize',18)
1057  xlabel('Length of bridge [m]','FontSize',18); %,'FontWeight','bold','
          Color','r')
1058  ylabel('Force [MN]','FontSize',18); %,'FontWeight','bold','Color','r')
1059  axis([0 max(coord_x) min(SAxMIN/10^6) max(SAxMAX/10^6)])
1060  legend('Wind sea and swell Min', 'Wind sea and swell Max', 'Wind sea Min'
          , 'Wind sea Max');
1061  set(gca,'fontsize',14)
1062
1063
1064  figure()
1065  plot(coord_xdispl1(1:repeatdispl), SXMIN,'b', 'Linewidth',3)
1066  hold on
1067  plot(coord_xdispl1(1:repeatdispl), SXMAX,'b', 'Linewidth',3)
1068  hold on
1069  plot(coord_xdispl1(1:repeatdispl), XMIN,'r', 'Linewidth',3)
1070  hold on
1071  plot(coord_xdispl1(1:repeatdispl), XMAX,'r', 'Linewidth',3)
1072  title('X max and min')
1073  xlabel('Length of bridge [m]','FontSize',18); %,'FontWeight','bold','
          Color','r')
1074  ylabel('Axial Displacement of bridge [m]','FontSize',18); %,'FontWeight
          ','bold','Color','r')
1075  axis([0 max(coord_xdispl1) min(SXMIN) max(SXMAX)])
1076  legend('Wind sea and swell Min', 'Wind sea and swell Max', 'Wind sea Min'
          , 'Wind sea Max');
1077  set(gca,'fontsize',14)
1078  figure()
1079  plot(coord_xdispl1(1:repeatdispl), SYMIN,'b', 'Linewidth',3)
1080  hold on
1081  plot(coord_xdispl1(1:repeatdispl), SYMAX,'b', 'Linewidth',3)
1082  hold on
1083  plot(coord_xdispl1(1:repeatdispl), YMIN,'r', 'Linewidth',3)
1084  hold on
1085  plot(coord_xdispl1(1:repeatdispl), YMAX,'r', 'Linewidth',3)
1086  title('Y max and min')
1087  xlabel('Length of bridge [m]','FontSize',18); %,'FontWeight','bold','
          Color','r')
1088  ylabel('Horizontal Displacement of bridge [m]','FontSize',18); %,'
```

```matlab
        FontWeight','bold','Color','r')
1089  axis([0 max(coord_xdispl1) min(SYMIN) max(SYMAX)])
1090  legend('Wind sea and swell Min', 'Wind sea and swell Max', 'Wind sea Min'
        , 'Wind sea Max');
1091  set(gca,'fontsize',14)
1092  figure()
1093  plot(coord_xdispl1(1:repeatdispl), SZMIN,'b', 'Linewidth',3)
1094  hold on
1095  plot(coord_xdispl1(1:repeatdispl), SZMAX,'b', 'Linewidth',3)
1096  hold on
1097  plot(coord_xdispl1(1:repeatdispl), ZMIN,'r', 'Linewidth',3)
1098  hold on
1099  plot(coord_xdispl1(1:repeatdispl), ZMAX,'r', 'Linewidth',3)
1100  title('Z max and min')
1101  xlabel('Length of bridge [m]','FontSize',18); %,'FontWeight','bold','
        Color','r')
1102  ylabel('Vertical Displacement of bridge [m]','FontSize',18); %,'
        FontWeight','bold','Color','r')
1103  axis([0 max(coord_xdispl1) min(SZMIN) max(SZMAX)])
1104  legend('Wind sea and swell Min', 'Wind sea and swell Max', 'Wind sea Min'
        , 'Wind sea Max');
1105  set(gca,'fontsize',14)
```